Nanofibrous Membranes Obtained by Electrospinning for Bone Tissue Engineering and Wound Dressing Applications

A thesis submitted to obtain the degree of doctor,
presented by

Javier Aragón Fernández

Zaragoza, 2019

Nanofibrous Membranes Obtained by Electrospinning for Bone Tissue Engineering and Wound Dressing Applications

A thesis

Prepared in the framework of Erasmus Mundus Doctorate in Membrane Engineering (EUDIME) to obtain multiple Doctoral degrees issue by

Universidad de Zaragoza, Departamento de Ingeniería Química y Tecnología del Medio Ambiente

Departamento de Ingeniería Química y Tecnologías del Medio Ambiente
Universidad Zaragoza

Università della Calabria, Istituto per la Tecnologia delle Membrane (ITM)

Universidade Nova de Lisboa, Facultade de Ciência e Tecnologia

Supervisors:

Dr. Silvia Irusta Alderete, Associate Research Professor, Departamento de Ingeniería Química y Tecnología del Medio Ambiente, Universidad de Zaragoza, Spain

Dr. Loredana De Bartolo, Senior Researcher, Istituto per la Tecnologia delle Membrane, Italy

Dr. Ana Isabel Aguiar-Ricardo, Full Professor, Faculdade de Ciências e Tecnologia of Universidade Nova de Lisboa, Portugal

To my family for their love, compression,

and unconditional support.

List of abbreviations

ACS	Absorbable collagen sponge
ACN	Acetonitrile
AIC	Akaike information crite
BSA-FITC	Albumin–fluorescein isothiocyanate conjugate
ALP	Alkaline phosphatase
NH_4OH	Ammonium hydroxide solution
$(NH_4)_2SO_4$	Ammonium sulfate
RGD	Arginine–glycine–aspartate
AES	Artificial exudates solutions
Bis-GMA	Bis-glycidyl dimethacrylate
BMA	Bone marrow aspirate
BMSCs	Bone marrow stromal cells
BMP	Bone morphogenetic protein
BMP2	Bone morphogenetic protein 2
BMP7	Bone morphogenetic protein 7
BSA	Bovine serum albumin
$CaCO_3$	Calcium carbonate
$CaCl_2.2H_2O$	Calcium chloride dihydrate
CP	Calcium phosphate
CF	Carbon fibers
CNF	Carbon nanofibres
CNT	Carbon nanotubes
CRV	Carvacrol
CARG	Compound annual growth rate
DMB	Demineralized bone matrix
DCM	Dichloromethane
DMSO	Dimethyl sulfoxide
DMEN	Dulbecco's modification of eagle medium
DPBS	Dulbecco's phosphate-buffered saline
EHDA	Electrospraying or electrohydrodynamic atomization
EE	Encapsulation efficiency
EDX	Energy dispersive x-ray
ETOH	Ethanol absolute
EthD-1	Ethdium homodimer-1
ECM	Extracellular matrix
FBS	Fetal bovine serum
FTIR	Fourier transform infrared
GF	Glass fibers
HPLC	High-performance liquid chromatography

HDFs	Human dermal fibroblasts
HOBs	Human osteoblasts
HA	Hydroxyapatite
KF	Kevlar fiber
MSCS	Mesenchymal stem cells
MBC	Minimum bactericidal concentration
MIC	Minimum inhibitory concentration
MVTR	Moisture vapor transmission rate
MTT	3-(3,4-dimethylthiazol-2-yl)-2,5-diphenyltetrazoliumbromide
DMF	N,n-dimethylformamide
Han	Nanohydroxyapatite
NDS	Normal donkey serum
NHOst	Normal human osteoblasts
OGM	Osteoblast growth medium
OCN	Osteocalcin
OPN	Osteopontin
PBS	Phosphate-buffered saline
H_3PO_4	Phosphoric acid
PAG	Poly aldehyde guluronate
PGA	Poly glycolic acid
PLA	Poly lactic acid
PAA	Poly acrylic acid
PBT	Poly butylene terephthalate
P(DLLA-CL)	Poly(d,l-lactide/-caprolactone)
PEEK	Poly(ether-ether-ketone)
PEI	Poly(ether-imide)
PELA	Poly(ethylene oxide)-b-poly(lactic acid) block copolymer
PET	Poly ethylene terephthalate
PEG	Poly ethyleneglycol
PLGA	Poly lactide-co-glycolic acid
PLLA	Poly l-lactic acid
PPF	Poly propylene fumarate
PVA	Poly vinyl alcohol
PCL	Poly ε-caprolactone
PA12	Polyamide 12
PE	Polyethylene
PMMA	Polymethyl methacrylate
PP	Polypropylene
PSU	Polysulfone
PU	Polyurethane
PVAc	Polyvinyl acetate

CH_3COOK	Potassium acetate
rhBMP-2	Recombinant human bone morphogenetic protein 2
rhBMP-7	Recombinant human bone morphogenetic protein 7
RH	Relative humidity
RFP	Rifampicin
SEM	Scanning electron *microscope*
SBF	Simulated body fluid
SWCNT	Single-wall carbon nanotubes
NaCl	Sodium chloride
SDS	Sodium dodecyl sulfate
NaOH	Sodium hydroxide
$NaNO_2$	Sodium nitrate
SD	Standard deviation
SSR	Sum of the squared residuals
TGA	Thermogravimetric analysis
3D	Three-dimensional
TGF-β	Transforming growth factor-beta
TEM	Transmission electron microscope
β-TCP	Tricalcium phosphate
TCP	Tricalciumphosphate
TRIS	Tris(hydroxymethyl)aminomethane
TSA	Trypticasein soy agar
TSB	Trypticasein soy broth
2D	Two-dimensional
UTS	Ultimate tensile strengths
UHMWPE	Ultra-high molecular weight polyethylene
FDA	US food and drug administration
XRD	X-ray diffraction

INDEX

Summary and Objectives

The current Doctoral Thesis work has been performed under a co-supervision agreement between University of Zaragoza (Home University), University of Calabria (Host University) and Faculty of Sciences and Technology of the NOVA University of Lisbon (FCT NOVA) (Host University). This research has been carried out inside the Erasmus Mundus Doctorate in Membrane Engineering program (EUDIME), (FPA 2011-0014), funded by the European Union.

This thesis focused mainly on the use of the electrospinning technique to produce different kind of membranes for biomedical applications. In particular, it described the synthesis and production of inorganic and organic nanoparticles to be used as fillers or as carriers (drug delivery system) as well as the production of electrospun nanofibrous membranes. This work was carried out within the Institute of Nanoscience of Aragon (INA), specifically in the Nanostructured Films and Particles (NFP) group under the supervision of the Professor Silvia Irusta and Dr Gracia Mendoza. Also an important part of the physico-chemical characterization was done at INA.

The study of different biological signals and the use of specific techniques for membrane characterization were acquired at the University of Calabria under the supervision of Dr. Loredana De Bartolo in the Institute on Membrane Technology of the National Research Council of Italy (ITM-CNR). On the other hand, the mobility carried out at the Faculty of Sciences and Technology (FCT NOVA) of Universidade NOVA (FCT NOVA) under the supervision of Professor Ana Isabel Aguiar-Ricardo, allowed a total characterization of two asymmetric membranes following different International Standards to accomplish testing for primary wound dressing.

The development of novel membranes loaded with morphogenetic proteins or antibiotic are of great interest in the field of bone tissue engineering. To promote the cellular viability and extracellular matrix production, electrospun membranes with enhanced porosity and micro-scale pores could be beneficial since increased porosity and pore size can provide a three-dimensional (3D) environment that not only facilitates cell seeding/diffusion but also provides better diffusion of nutrients and waste throughout the membranes. The addition of calcium phosphate ceramics has been extensively investigated to fabricate highly porous membranes to bone

tissue engineering due to their close similar composition of bone, including excellent biocompatibility, osteoinductive and osteoconductive properties. A homogeneous distribution of the bone morphogenetic protein-loaded particles along the entire membrane could be ensuring a continuous release of the growth factor to provide the necessary biochemical cues for bone repair and regeneration.

Antibiotic-loaded membranes may provide drug targeted and sustained release, avoiding the long-term oral and intravenous systematic multidrug administration, which implies toxic side effects, low delivery to the target site and low patient adherence to the treatment. Therefore, membranes loaded with antibiotics can overcome the drawbacks of the traditional therapy sustaining enhanced osteogenic properties for the successful regeneration of the bone.

Another interesting biomedical application of electrospun membranes is the fabrication of efficient smart dressings for the treatment of wounds. A rapid wound healing requires developing appropriate membranes with interconnected pores that allow the oxygen diffusion and transport of metabolic waste, as well as an adequate pore size to prevent rapid dehydration and bacteria penetration. A high absorption capacity and adequate water vapor transmission will be necessary to keep a moist environment in the wound bed. Besides, if the electrospun membrane has some bactericidal properties will be better for the healing process.

The main goal of this thesis was the development of fibrous membranes by electrospinning with the appropriate characteristics to be used in bone tissue engineering or as wound dressing materials. To achieve this target, several specific objectives were defined, which are described in **Chapters II** to **V.**

The thesis was divided in the following sections:

- **CHAPTER I**, is an introduction where the concepts of biomaterials, scaffolds and tissue engineering and the main target of drug delivery systems are described. The chapter includes the classification of biomaterials according to the origin of the materials and tissue engineering is also described as well as all the factors that must be taken into account to develop and properly apply a wound dressing are discussed. Different kind of techniques used in the literature to produce scaffolds or membranes for

bone tissue engineering and wound dressings are mentioned, focusing on the use of electrospinning and electrospray to produce them.

- **CHAPTER II**, focuses on the development of enhanced 3D membranes able to promote efficient bone regeneration together with targeted antibiotic release to prevent bacteria colonization. The aim of this work was to synthesize and characterize a drug delivery system consisting of polycaprolactone (PCL) electrospun nanofibers decorated with rifampicin (RFP) loaded into poly(lactic-coglicolic acid) (PLGA) particles. This material would promote bone repair avoiding the impairment of the membrane mediated by infection. The bactericidal ability of the synthesized electrospun material was assessed *In vitro* against gram positive (*Staphylococcus aureus*) and gram negative (*Escherichia coli*) bacteria, as well as its cytocompatibility in human osteoblasts 3D cultures. These results are included in the accepted article entitled ***"Composite scaffold obtained by electro-hydrodynamic technique for infection prevention and treatment in bone repair".*** Javier Aragon, Sergio Feoli, Gracia Mendoza, Silvia Irusta. International Journal of Pharmaceutics.

- **CHAPTER III**, describes the synthesis and characterization of core-shell membranes of PCL and polyvinyl acetate (PVAc) obtained by electrospinning. The fibers were loaded with synthetic hydroxyapatite nanoparticles (HAn) to increase the bioactivity of the materials. The prepared membranes were then treated by laser ablation to create desired microscale topographical features in order to favor cell adhesion and growth.

All prepared membranes exhibited a three-dimensional network structure with interconnected pores; the laser treatment has modified the structural characteristics of the membrane causing an increase the cell viability and cell density. The materials biocompatibility is affected by the structural properties of the membranes, indeed smaller micropore sizes favor cell adhesion and proliferation. These results are published in the article entitled ***"Laser-treated electrospun fibers loaded with nano-hydroxyapatite for bone tissue engineering".*** Javier Aragon, Nuria Navascues, Gracia Mendoza, Silvia Irusta. International Journal of Pharmaceutics 525,112–122, 2017. DOI:10.1016/j.ijpharm.2017.04.022.

- **CHAPTER IV**, refers to the development of a composite electrospun membrane of PCL or PCL/PVAc core–shell fibers loaded with synthetic HAn. These fibers were decorated with bone morphogenetic

protein 2 (BMP2) loaded in/into PLGA particles via simultaneous electrospraying and coaxial electrospinning. The aim of this study was to evaluate the structural and physico-chemical properties and biodegradation processes of the newly developed membranes assessing their ability to address the architectural, biochemical, and functional features of bone tissue. For this purpose, the membrane bioactivity was tested by culturing human osteoblasts on the membranes and by monitoring cell viability up to 4 weeks. The *In vitro* osteogenic activity of cells seeded onto the membranes was evaluated by assessing alkaline phosphatase (ALP) activity and the expression of osteogenic proteins osteocalcin (OCN) and osteopontin (OPN). These results are published in the article "***Polymeric electrospun scaffolds for bone morphogenetic protein 2 delivery in bone tissue engineering*".** Javier Aragón, Simona Salerno, Loredana De Bartolo, Silvia Irusta and Gracia Mendoza. Journal of Colloid and Interface Science, 531 (2018) 126–137. DOI:10.1016/j.jcis.2018.07.029.

- **CHAPTER V**, describes the synthesis of an antimicrobial wound dressing material, with appropriate mechanical resistance avoiding rapid dehydration and absorbing exudates. PCL/PVAc asymmetric membranes loaded with carvacrol (CRV) were prepared by electrospinning and electrospraying simultaneously. The membranes consist of two layers: the first is an electrospun PCL sheet, the second a PVAc sheet that would be in contact with the skin releasing the antimicrobial compound. The use of different solvents results in different morphologies for the PVAc-CRV layer. The membranes exhibit mechanical properties with strain to failure values that are in the range of human skin, being adequate to be deposited over a wound surface. The samples present Water Vapor Transmission (WVTR) values in the required range to keep good moisture balance with water loss from the wound at the optimal rate. In the first week, more than 60 % of the loaded CRV was released while after three weeks membranes released between 85 to 100 % of the loaded CRV through a Fickian diffusion and diffusion due to polymer relaxation. The synthesized membranes are potential candidates to be used for wound dressing applications. The manuscript summing up these results has been submitted to a scientific journal and is currently under review.

- **GENERAL CONCLUSIONS**, summarizes the conclusions of the thesis work.

- **APPENDIX 1,** describes the main characterization techniques and the methods to evaluate different properties according to the possible applications.

- **APPENDIX 2,** summarizes the articles published and the participation in scientific forums during the thesis period.

Resumen y Objetivos

Esta tesis doctoral se ha realizado dentro del marco de un acuerdo de co-tutela entre la Universidad de Zaragoza (Universidad de origen), la Universidad de Calabria (Universidad anfitriona) y la Facultad de Ciencias y Tecnología de la Universidad NOVA de Lisboa (FCT NOVA) (Universidad anfitriona). El trabajo de investigación se ha llevado a cabo dentro del programa de Doctorado en Ingeniería de Membranas Erasmus Mundus (EUDIME), (FPA 2011-0014), financiado por la Unión Europea.

La tesis se centró principalmente en el uso de la técnica de electrohilado para producir diferentes tipos de membranas que puedan ser utilizadas en distintas aplicaciones biomédicas. Se sintetizaron y produjeron nanopartículas orgánicas e inorgánicas para ser utilizadas como relleno o como portadores (sistema de administración de fármacos), así como membranas nanofibrosas electrohiladas. Este trabajo se llevó a cabo en el Instituto de Nanociencia de Aragón (INA), específicamente en el grupo de *Nanostructured Films and Particles* (NFP) bajo la supervisión de la profesora Silvia Irusta y la Dra. Gracia Mendoza. Una parte importante de la caracterización físico-química se realizó en el INA.

El estudio de diferentes señales biológicas y el uso de técnicas especificad de caracterización de membranas fue realizado en la Universidad de Calabria bajo la supervisión de la Dra. Loredana De Bartolo en el Instituto de Tecnología de Membranas perteneciente al Consejo Naional de Investigación de Italia (ITM-CNR). Por otra parte, la movilidad realizada en la Facultad de Ciencias y Tecnología (FCT NOVA) de la Universidade NOVA (FCT NOVA) bajo la supervisión de la profesora Ana Isabel Aguiar-Ricardo, permitió realizar una caracterización completa de dos membranas asimétricas siguiendo diferentes Normas Internacionales que establecen diferentes ensayos a realizar en apósitos primarios utilizados en heridas.

El desarrollo de nuevas membranas cargadas con proteínas morfogenéticas o antibióticos es de gran interés en el campo de la ingeniería de tejidos óseos. El uso de membranas electrohiladas con una microporosidad mejorada puede ser beneficiosas para mejorar la viabilidad celular debido a que una alta porosidad junto a la presencia de microporos puede proporcionar un entorno tridimensional (3D) que no solamente facilita la siembra y difusión celular sino también proporciona una mejor

difusión de los nutrientes y residuos a través de la membrana. La adición de cerámica de fosfato de calcio ha sido ampliamente investigada para fabricar membranas altamente porosas para la ingeniería de tejidos óseos debido a que presentan una composición muy similar al hueso, poseen excelentes propiedades de biocompatibilidad, osteoinductivas y osteoconductoras. Partículas cargadas con proteínas morfogenéticas de hueso distribuidas homogéneamente en las membranas podrían asegurar una liberación continua del factor de crecimiento proporcionando de esta forma las señales bioquímicas necesarias para la reparación y regeneración ósea.

Las membranas cargadas con antibióticos pueden proporcionar una liberación sostenida del fármaco en el sitio de interés, evitando una administración múltiple de fármacos por vía oral o intravenosa durante largos periodos de tiempo, lo que puede implicar efectos secundarios de toxicidad, niveles ineficaces en la zona de interés y disminuyendo el número de pacientes que aceptan estos tratamientos. Por lo tanto, las membranas cargadas con antibióticos pueden superar los inconvenientes de la terapia tradicional manteniendo propiedades osteogénicas mejoradas para la regeneración exitosa del hueso.

Otra aplicación biomédica interesante de las membranas electrohiladas es la fabricación de apósitos inteligentes eficientes para el tratamiento de heridas. Para lograr una curación rápida de la herida es necesario desarrollar membranas apropiadas con poros interconectados que permiten la difusión de oxígeno y el transporte de residuos metabólicos así como un tamaño de poro adecuado capaces de prevenir la deshidratación rápida y la penetración de bacterias. Para mantener un ambiente húmedo en el lecho de la herida se necesita una alta capacidad de absorción y una adecuada transmisión de vapor de agua. Además, si la membrana electrohilada presenta propiedades bactericidas facilitará el proceso de curación.

El objetivo principal de esta tesis fue el desarrollo mediante electrohilado de membranas fibrosas con las características apropiadas para ser utilizadas en la ingeniería de tejidos óseos o como apósito para heridas. En los **Capítulos II** al **V** se plantean una serie de objetivos específicos con el fin de cumplir el objetivo principal.

Este documento de tesis se dividió en las siguientes secciones:

- **CAPÍTULO I,** es una introducción donde se describen los conceptos de biomateriales, *scaffolds*, ingeniería de tejidos y el objetivo principal de los sistemas de liberación de fármacos. Este capítulo incluye la clasificación de los biomateriales según el origen de los materiales y se describe además la ingeniería de tejidos así como también se los factores que deben tenerse en cuenta para desarrollar y aplicar adecuadamente los apósitos para heridas. Se mencionan las diferentes técnicas utilizadas en la literatura haciendo énfasis en el uso de electrohilado y electropulverización para producir *scaffolds* o membranas para su uso en la ingeniería del tejido óseo y como apósitos para heridas.

- **CAPÍTULO II,** se enfoca en el desarrollo y mejora de membranas 3D capaces de promover una eficiente regeneración ósea junto con la liberación de antibióticos dirigidos para prevenir la colonización de bacterias. El objetivo de este trabajo fue sintetizar y caracterizar un sistema de liberación de fármacos que consiste en nanofibras electrohiladas de policaprolactona (PCL) decoradas con partículas de poli (ácido láctico-coglicólico) (PLGA) cargadas con rifampicina (RFP). Este material favorecería la reparación ósea evitando el deterioro de las membranas provocado por una infección. Se realizó la evaluación *In vitro* de la capacidad bactericida del material electrohilado sintetizado contra bacterias gram positivas (*Staphylococcus aureus*) y gram negativas (*Escherichia coli*), así como su citocompatibilidad en cultivos 3D con osteoblastos humanos. Estos resultados han sido incluidos en un artículo aceptado titulado ***"Composite scaffold obtained by electro-hydrodynamic technique for infection prevention and treatment in bone repair".*** Javier Aragon, Sergio Feoli, Gracia Mendoza, Silvia Irusta. International Journal of Pharmaceutics, 2018.

- **CAPÍTULO III,** se describe la síntesis y caracterización de membranas con estructura de núcleo-corona de PCL y acetato de polivinilo (PVAc) obtenidas por electrohilado. Las fibras se cargaron con nanopartículas de hidroxiapatita sintética (HAn) para aumentar la bioactividad de los materiales. Las membranas desarrolladas se trataron con ablación láser para crear características topográficas deseadas a nivel micrométrico con el objetivo de favorecer la adhesión y crecimiento celular.

Todas las membranas obtenidas presentaron una estructura de poros tridimensionalmente interconectados y el tratamiento con láser provocó un aumento en la viabilidad y densidad celular. Además, el aumento en la

biocompatibilidad de las membranas sugiere que los microporos pequeños favorecen la adhesión y proliferación celular. Estos resultados fueron publicados en el artículo titulado ***"Laser-treated electrospun fibers loaded with nano-hydroxyapatite for bone tissue engineering"*.** Javier Aragon, Nuria Navascues, Gracia Mendoza, Silvia Irusta. International Journal of Pharmaceutics 525,112–122, 2017. DOI:10.1016/j.ijpharm.2017.04.022.

- **CAPÍTULO IV,** se refiere al desarrollo de una *membrana* electrohilada compuesta por fibras con estructura de núcleo-corona de PCL o PCL/PVAc cargado con HAn sintética. Estas fibras se decoraron con partículas de PLGA cargadas con proteína morfogenética ósea 2 (BMP2) mediante el uso simultaneo de electrohilado coaxial y electropulverización. El objetivo de este trabajo fue evaluar las propiedades estructurales y físico-químicas así como el proceso de biodegradación de las nuevas membranas desarrolladas y su capacidad para abordar las características arquitectónicas, bioquímicas y funcionales del tejido óseo. Para esto, se probó la bioactividad de la membrana mediante el cultivo de osteoblastos humanos sobre ellos y se monitoreo de la viabilidad celular durante 4 semanas. Se evaluó la actividad osteogénica *In vitro* de las células sembradas sobre las membranas determinando la actividad de la fosfatasa alcalina (ALP) y la expresión de osteocalcina (OCN) y osteopontina (OPN) como proteínas osteogénicas. Estos resultados fueron publicados en el artículo titulado "***Polymeric electrospun scaffolds for bone morphogenetic protein 2 delivery in bone tissue engineering*".** Javier Aragón, Simona Salerno, Loredana De Bartolo, Silvia Irusta and Gracia Mendoza. Journal of Colloid and Interface Science, 531 (2018) 126–137. DOI:10.1016/j.jcis.2018.07.029.

- **El CAPÍTULO V,** describe la síntesis de un apósito antimicrobiano para heridas, con una resistencia mecánica adecuada que es capaz de absorber exudados y evitar la deshidratación rápida de una herida. Se prepararon membranas asimétricas de PCL/PVAc cargadas con carvacrol (CRV) mediante el uso simultáneo de electrohilado y electropulverización. Las membranas constan de dos capas; la primera es una capa de PCL electrohilado; la segunda, una lámina de PVAc que estaría en contacto con la piel liberando a su vez el compuesto antimicrobiano. Se demostró que el uso de diferentes disolventes pueden dar lugar a la obtención de diferentes morfologías de la capa PVAc-CRV. Los valores obtenidos de elongación máxima de las membranas son adecuados para ser utilizados como apósitos para heridas ya que están en el mismo rango reportado de elongaciones en la

piel humana. Las membranas presentan una tasa óptima de Transmisión de vapor de agua (WVTR) con valores que se encuentran en el rango requerido para mantener un buen balance entre humedad y pérdida de agua en la herida. En la primera semana, se liberó más del 60 % del CRV cargado, mientras que después de tres semanas, las membranas liberaron entre el 85 y el 100 % del CRV cargado mediante la contribución de un proceso de difusión de tipo Fickiano y la relajación delas cadenas poliméricas. Las membranas sintetizadas son candidatas potenciales para ser utilizadas como apósitos para heridas. El manuscrito que resume estos resultados se envió a una revista científica y está bajo revisión.

- **CONCLUSIONES GENERALES,** resume las conclusiones del trabajo de tesis.

- **APÉNDICE 1,** describe las principales técnicas de caracterización y los métodos para evaluar diferentes propiedades en función de las posibles aplicaciones.

- **APÉNDICE 2,** resume los artículos publicados y la participación en foros científicos durante el período de tesis.

Sommario e Obiettivi

La presente tesi di dottorato è stata svolta in base ad un accordo di co-supervisione tra l'Università di Saragozza (Università di appartenenza), l'Università della Calabria (Università ospitante) e la Facoltà di Scienze e Tecnologia dell'Università NOVA di Lisbona (FCT NOVA) (Università ospitante). Questa ricerca è stata condotta all'interno del programma *Erasmus Mundus Doctorate in Membrane Engineering (EUDIME)*, (FPA 2011-0014), finanziato dall'Unione Europea.

Questa tesi è incentrata principalmente sull'uso della tecnica di elettrofilatura per produrre diversi tipi di membrane per applicazioni biomediche. In particolare è descritta la sintesi e la produzione di nanoparticelle inorganiche e organiche da utilizzare come fillers o vettori (sistema di somministrazione di farmaci) e produzione di membrane nanofibrose elettrofilate. Questo lavoro è stato condotto all'interno *dell'Institute of Nanoscience of Aragon* (INA), in particolare nel gruppo *Nanostructured Films and Particles* (NFP) sotto la supervisione della Professoressa Silvia Irusta e della dott.ssa Gracia Mendoza. All'interno dello stesso istituto INA si è svolta una parte importante di caratterizzazione chimico-fisica.

Lo studio di diversi segnali biologici e l'uso di tecniche specifiche per la caratterizzazione delle membrane è stato effettuato presso l'Università della Calabria sotto la supervisione della dott.ssa Loredana De Bartolo presso l'Istituto per la Tecnologia delle Membrane del Consiglio Nazionale delle Ricerche (ITM-CNR). Infine, la mobilità svolta presso la Facoltà di Scienze e Tecnologia (FCT NOVA) dell'Università NOVA (FCT NOVA) sotto la supervisione della prof.ssa Ana Isabel Aguiar-Ricardo, ha permesso una caratterizzazione completa di due membrane asimmetriche in accordo a diversi standard internazionali sull'esecuzione dei test per il trattamento primario di una ferita.

Lo sviluppo di nuove membrane caricate con proteine morfogenetiche o antibiotici sono di grande interesse nel campo dell'ingegneria del tessuto osseo. Le membrane elettrofilate con una maggiore porosità e pori su scala micrometrica potrebbero essere utili per promuovere la vitalità cellulare e la produzione di matrice extracellulare. Infatti un incremento della porosità e della dimensione dei pori potrebbe fornire un ambiente tridimensionale che

favorisce il piastramento e la distribuzione cellulare all'interno della membrane promuovendo il trasporto diffusivo di nutrienti e prodotti di rifiuto. L'uso di composti ceramici di fosfato di calcio è stato ampiamente studiato per la realizzazione di membrane altamente porose utili per l'ingegneria del tessuto osseo poiché essi presentano una composizione chimica simile al tessuto osseo, un'eccellente biocompatibilità e proprietà osteoinduttive ed osteoconduttive. Particelle caricate con la proteina morfogenetica ossea distribuite omogeneamente nell'intero membrana potrebbero garantire un rilascio continuo del fattore di crescita, che rappresenta uno stimolo biochimico necessario per la riparazione e la rigenerazione ossea.

Le membrane caricate con antibiotici possono fornire un rilascio mirato e prolungato di farmaci, evitando la somministrazione a lungo termine per via orale ed endovenosa, che implica effetti collaterali tossici, una bassa erogazione al sito target e una bassa risposta al trattamento da parte del paziente. Queste membrane potrebbero superare gli svantaggi della terapia tradizionale sostenendo un incremento dell'osteogenicità che è importante per la rigenerazione ossea.

Un'altra interessante applicazione biomedica delle membrane elettrofilate è la realizzazione di medicazioni intelligenti per il trattamento delle ferite della pelle. Una guarigione rapida delle ferite richiede lo sviluppo di membrane appropriate aventi pori interconnessi che consentano la diffusione dell'ossigeno e il trasporto dei rifiuti metabolici, nonché un'adeguata dimensione dei pori allo scopo di prevenire una rapida disidratazione e la penetrazione di batteri. Un'elevata capacità di assorbimento e una trasmissione adeguata del vapore acqueo saranno necessari per mantenere un ambiente umido nel sito della ferita. Inoltre, le proprietà battericide delle membrane miglioreranno il processo di guarigione.

L'obiettivo principale di questa tesi è lo sviluppo di membrane fibrose mediante elettrofilatura per applicazioni nell'ingegneria del tessuto osseo e per il trattamento di ferite a carico della pelle. A tal scopo sono stati definiti diversi obiettivi specifici descritti nei **Capitoli** da **II** a **V**.

La tesi è stata così articolata nelle seguenti sezioni:

- **CAPITOLO I,** è un'introduzione in cui vengono descritti i concetti di biomateriali, scaffold e ingegneria tissutale e l'obiettivo principale dei sistemi di somministrazione di farmaci. Il capitolo include la classificazione dei biomateriali in base all'origine dei materiali. Viene inoltre descritta l'ingegneria tissutale elencando tutti i fattori per lo sviluppo e l'applicazione di trattamenti per le ferite della pelle. Sono stati menzionati diversi tipi di tecniche utilizzate in letteratura per produrre scaffold o membrane per l'ingegneria del tessuto osseo e le medicazioni delle ferite, concentrandosi sull'uso di electrospinning ed electrospray.

- **CAPITOLO II** è focalizzato sullo sviluppo di strutture 3D innovative in grado di promuovere una rigenerazione ossea efficiente rilasciando nello stesso tempo antibiotici allo scopo di prevenire la colonizzazione batterica. Lo scopo di questo lavoro è stato quello di sintetizzare e caratterizzare un sistema di somministrazione di farmaci costituito da nanofibre elettrofilate di policaprolattone (PCL) decorate con particelle di acido poli(lattico-co-glicolico) (PLGA) caricate con rifampicina (RFP). Questo materiale promuoverebbe la riparazione ossea evitando il danneggiamento della membrana a causa dell'infezione. Le proprietà antibatteriche del materiale sintetizzato mediante elettrofilatura sono state valutate *In vitro* contro batteri Gram positivi (Staphylococcus aureus) e Gram negativi (Escherichia coli), mentre le caratteristiche dicitocompatibilità sono state testate adoperando colture di osteoblasti umani. Questi risultati sono stati accettati per pubblicare nell'articolo ***"Composite scaffold obtained by electro-hydrodynamic technique for infection prevention and treatment in bone repair".*** Javier Aragon, Sergio Feoli, Gracia Mendoza, Silvia Irusta. International Journal of Pharmaceutics, 2018.

- **CAPITOLO III,** descrive la sintesi e la caratterizzazione della membrana core-shell di PCL e polivinilacetato (PVAc) ottenute per elettrospinning. Le fibre sono state caricate con nanoparticelle di idrossiapatite sintetica (HAn) allo scopo di aumentare la bioattività dei materiali. Le membrane preparate sono state quindi trattate mediante ablazione con laser per creare le caratteristiche topografiche su microscala desiderata al fine di favorire l'adesione e la crescita delle cellule.

Tutte le membrane realizzate mostrano una struttura tridimensionale con pori interconnessi ed il trattamento laser ha modificato le caratteristiche strutturali delle membrane provocando un aumento della vitalità e della

densità cellulare. La biocompatibilità delle membrane è fortemente influenzata dalle sue proprietà strutturali infatti la diminuzione della dimensione dei pori risulta in un aumento dell'adesione e della proliferazione cellulare. Questi risultati sono stati pubblicati nell'articolo "***Laser-treated electrospun fibers loaded with nano-hydroxyapatite for bone tissue engineering***". Javier Aragon, Nuria Navascues, Gracia Mendoza, Silvia Irusta. *International Journal of Pharmaceutics* 525, 12-122, 2017. DOI: 10.1016 / j.ijpharm.2017.04.022.

- **CAPITOLO IV,** si riferisce allo sviluppo di un'impalcatura elettrofilata composita di fibre core-shell PCL o PCL / PVAc caricate con HAn sintetico. Queste fibre sono state decorate con la proteina morfogenetica ossea 2 (BMP2) caricata in particelle di PLGA mediante elettrofiltrazione simultanea ed elettrofilatura coassiale. Lo scopo di questo lavoro è stato quello di valutare le proprietà strutturali e fisico-chimiche nonchè i processi di biodegradazione delle membrane sviluppate investigando la loro capacità di mimare le caratteristiche architettoniche, biochimiche e funzionali del tessuto osseo. A tale scopo, la bioattività delle membrane è stata testata effettuando colture di osteoblasti umani e monitorando la vitalità cellulare fino a 4 settimane. L'attività osteogenica *In vitro* delle cellule coltivate sulle membrane è stata valutata determinando l'attività della fosfatasi alcalina (ALP) e l'espressione di proteine osteogeniche come l'osteocalcina (OCN) e l'osteopontina (OPN). Questi risultati sono stati pubblicati nell'articolo ***"Polymeric electrospun scaffolds for bone morphogenetic protein 2 delivery in bone tissue engineering***". Javier Aragón, Simona Salerno, Loredana De Bartolo, Silvia Irusta e Gracia Mendoza. *Journal of Colloid and Interface Science*, 531 (2018) 126-137. DOI: 10.1016 / j.jcis.2018.07.029.

- **CAPITOLO V,** descrive la sintesi di un materiale per la medicazione delle ferite con attività antimicrobiche edun'adeguata resistenza meccanica che evita la rapida disidratazione e l'assorbimento degli essudati. Le membrane asimmetriche PCL / PVAc caricate con carvacrolo (CRV) sono state preparate mediante elettrospinning e elettrospray simultaneamente. Le membrane sono costituite da due strati: il primo è un foglio elettrofilato di PCL; il secondo, un foglio di PVAc che durante il contatto con il tessuto epidermico dovrebbe rilasciare il composto antimicrobico. L'uso di diversi solventi determina morfologie differenti per lo strato PVAc-CRV. Le membranes presentano delle proprietà mecchaniche con valori di deformazione fino a rottura che sono nello stesso range di

quello che si trova nella pelle umana, perciò possono essere considerati adeguati per essere depositati sulla superficie di una ferita. I campioni presentano valori di trasmissione del vapore acqueo (WVTR) nell'intervallo richiesto per mantenere un'umidità adeguata con perdita di acqua dalla ferita ad una velocità ottimale. Nella prima settimana, oltre il 60 % del CRV caricato è stato rilasciato mentre dopo tre settimane le membrane hanno rilasciato tra l'85 e il 100 % del CRV caricato attraverso una diffusione di Fick e una diffusione dovuta al rilassamento del polimero. Le membrane sintetizzate sono potenzialmente candidabili per applicazioni come la medicazione di ferite. Il manoscritto che riassume questi risultati è stato presentato a una rivista scientifica ed è in fase di revisione.

- **CONCLUSIONI GENERALI,** riassume le conclusioni del lavoro di tesi.

- **APPENDICE 1,** descrive le principali tecniche di caratterizzazione ed i metodi per valutare le diverse proprietà in base alle possibili applicazioni.

- **APPENDICE 2**, riassume gli articoli pubblicati e la partecipazione a forum scientifici durante il periodo della tesi.

Resumo e Objetivos

O presente trabalho de Tese de Doutoramento foi realizado sob um acordo de co-supervisão entre a Universidade de Saragoça (Universidade de Origem), a Universidade da Calábria (Universidade Anfitriã) e a Faculdade de Ciências e Tecnologia da Universidade NOVA de Lisboa (FCT NOVA) (Universidade Anfitriã). Esta investigação foi realizada no âmbito do programa de Doutoramento Erasmus Mundus em Engenharia das Membranas (EUDIME), (FPA 2011-0014), financiado pela União Europeia.

Esta tese enfocou principalmente no uso da técnica de eletrofiação para produzir diferentes tipos de membranas para aplicações biomédicas. Em particular, descreve a síntese e a produção de nanopartículas inorgânicas e orgânicas para serem utilizadas como cargas ou como transportadores (sistema de libertação de fármacos), bem como a produção de membranas nanofibrosas eletrofuncionais. Este trabalho foi realizado no Instituto de Nanociência de Aragon (INA), especificamente no grupo de *Nanostructured Films and Particles* (NFP) sob a supervisão da Professora Silvia Irusta e da Doutora Gracia Mendoza. Também uma parte importante da caracterização físico-química foi feita no INA.

O estudo de diferentes sinais biológicos e o uso de técnicas específicas para a caracterização de membranas foram adquiridos na Universidade da Calábria sob a supervisão da Doutora Loredana de Bartolo no Institute on Membrane Technology (ITM). Por outro lado, a mobilidade realizada na Faculdade de Ciências e Tecnologia (FCT NOVA) da Universidade NOVA (FCT NOVA), sob a supervisão da Professora Ana Isabel Aguiar-Ricardo, permitiu uma caracterização total de duas membranas assimétricas seguindo diferentes Normas Internacionais para realizar testes de curativos primários.

O desenvolvimento de novos scaffolds carregados com proteínas morfogenéticas ou antibióticos é de grande interesse no campo da engenharia de tecidos ósseos. Para promover a viabilidade celular e a produção de matriz extracelular, os suportes elétricos com poros de micro-incrustação ou porosidade aumentada podem ser benéficos, pois o aumento da porosidade e do tamanho dos poros podem proporcionar um ambiente tridimensional (3D) que não apenas facilita a disseminação e difusão celular mas também melhora a difusão de nutrientes e resíduos em todos os andaimes. A adição de cerâmica de fosfato de cálcio tem sido extensivamente

investigada para fabricar estruturas de suporte altamente porosas para engenharia de tecido ósseo devido à semelhança da composição do osso, incluindo excelentes propriedades de biocompatibilidade, osteoindutoras e osteocondutoras. Uma distribuição homogênea das partículas carregadas de proteína óssea morfogenética ao longo de todo o arcabouço poderia assegurar uma libertação contínua do fator de crescimento para fornecer as pistas bioquímicas necessárias para o reparo e a regeneração óssea.

Suportes carregados com antibióticos podem fornecer uma libertação direcionada e sustentada, evitando a administração sistêmica por via oral e intravenosa de múltiplos fármacos a longo prazo, o que implica efeitos colaterais tóxicos, baixa entrega ao local alvo e baixa adesão do paciente ao tratamento, bem como propriedades para a regeneração bem sucedida do osso.

Outra aplicação biomédica interessante das membranas electrospun é a fabricação de curativos inteligentes eficazes para o tratamento de feridas. Uma rápida cicatrização das feridas requer o desenvolvimento de membranas apropriadas com poros interconectados para evitar desidratação rápida e penetração de bactérias. Uma alta capacidade de absorção e uma transmissão adequada de vapor de água serão necessárias para manter um ambiente úmido no leito da ferida. Além disso, se a membrana electrospun tiver algumas propriedades bactericidas, será melhor para o processo de cicatrização.

O objetivo principal desta tese foi o desenvolvimento de membranas fibrosas por eletrofiação com as características adequadas para uso em engenharia de tecido ósseo ou como material de curativo. Para atingir esses objetivos, vários objetivos específicos foram definidos, descritos nos **Capítulos II** a **V**.

Este documento foi dividido nas seguintes seções:

- **CAPÍTULO I,** é uma introdução onde são descritos os conceitos de biomateriais, scaffolds e engenharia de tecidos e o principal alvo dos sistemas de libertação de drogas. Também é descrita a classificação de biomateriais e engenharia de tecidos de acordo com a origem dos materiais e todos os fatores a ter em conta para desenvolver e aplicar corretamente um curativo. Diferentes tipos de técnicas usadas na literatura para produzir scaffolds ou membranas para engenharia de tecidos ósseos e curativos foram

mencionados, com foco no uso de eletrofiação e eletropulverização para produzi-lo.

- **CAPÍTULO II,** enfoca no desenvolvimento de andaimes 3D aprimorados capazes de promover uma regeneração óssea eficiente, juntamente com a libertação de antibióticos direcionados para evitar a colonização de bactérias. O objetivo deste trabalho foi sintetizar e caracterizar um sistema de libertação de fármaco constituído por nanofibras de eletrofun policaprolactona (PCL) decoradas com partículas de poli (ácido láctico-coglicólico) (PLGA) carregadas com rifampicina (RFP). Este material promoveria a reparação óssea evitando o comprometimento da estrutura mediada pela infecção. A capacidade bactericida do material sintetizado foi avaliada *In vitro* contra bactérias Gram positivas (Staphylococcus aureus) e Gram negativas (Escherichia coli), bem como a sua citocompatibilidade foi avaliada em culturas 3D de osteoblastos humanos. Estes resultados foram aceitos para publicação no artigo intitulado ***"Composite scaffold obtained by electro-hydrodynamic technique for infection prevention and treatment in bone repair".*** Javier Aragon, Sergio Feoli, Gracia Mendoza, Silvia Irusta. International Journal of Pharmaceutics, 2018.

- **CAPÍTULO III,** descreve a síntese e a caracterização de membranas de núcleo-casca de PCL e acetato de polivinila (PVAc) obtidas por eletrofiação. As fibras foram carregadas com nanopartículas de hidroxiapatita sintética (HAn) para aumentar a bioatividade dos materiais. Os andaimes preparados foram tratados por ablação a laser para criar características topográficas em microescala de modo a favorecer a adesão e crescimento celular.

Todas as membranas obtidas exibiram uma estrutura de rede de poros interconectados tridimensionalmente e o tratamento com laser causou um aumento na viabilidade celular e na densidade celular. Além disso, um aumento na biocompatibilidade dos scaffolds sugere que tamanhos menores de microporos favorecem a adesão e a proliferação celular. Estes resultados estão publicados no artigo intitulado ***"Laser-treated electrospun fibers loaded with nano-hydroxyapatite for bone tissue engineering".*** Javier Aragon, Nuria Navascues, Gracia Mendoza, Silvia Irusta. *International Journal of Pharmaceutics* 525,112–122, 2017. DOI:10.1016/j.ijpharm.2017.04.022.

- **CAPÍTULO IV,** refere-se ao desenvolvimento de um andaime de eletropneio compósito de fibras de núcleo-casca PCL ou PCL PVAc

carregadas com HAn sintético. Estas fibras foram decoradas com partículas de PLGA carregadas com proteína morfogenética óssea 2 (BMP2) por eletropulverização e eletrofiação coaxial simultaneamente. O objetivo deste trabalho foi avaliar as propriedades estruturais e físico-químicas e os processos de biodegradação dos novos scaffolds desenvolvidos e a sua capacidade de abordar as características arquitetônicas, bioquímicas e funcionais do tecido ósseo. Para este propósito, a bioatividade do andaime foi testada cultivando osteoblastos humanos nos andaimes e monitorando a viabilidade celular durante 4 semanas. A atividade osteogênica *In vitro* de células semeadas nos arcabouços foi avaliada pela atividade da fosfatase alcalina (ALP) e a expressão das proteínas osteogênicas osteocalcina (OCN) e osteopontina (OPN). Estes resultados estão publicados no artigo "***Polymeric electrospun scaffolds for bone morphogenetic protein 2 delivery in bone tissue engineering*".** Javier Aragón, Simona Salerno, Loredana De Bartolo, Silvia Irusta and Gracia Mendoza. *Journal of Colloid and Interface Science,* 531 (2018) 126–137. DOI:10.1016/j.jcis.2018.07.029.

- **CAPÍTULO V,** descreve a síntese de um material antimicrobiano para curativos, com resistência mecânica adequada, evitando a rápida desidratação e absorvendo exsudatos. As membranas assimétricas de PCL/PVAc carregadas com carvacrol (CRV) foram preparadas simultaneamente por electrospinning e electropulverização. As membranas consistem em duas camadas; a primeira é uma folha de PCL electrospun; a segunda é uma folha de PVAc que estaria em contato com a pele libertando o composto antimicrobiano. O uso de diferentes solventes resulta em diferentes morfologias para a camada PVAc-CRV. Os valores de tensão para falha estão na faixa da pele humana, sendo adequados para serem depositados sobre a superfície da ferida. As amostras apresentam valores de Transmissão de Vapor de Água (WVTR) na faixa necessária para manter um bom equilíbrio de humidade com a perda de água da ferida na taxa ideal. Na primeira semana, mais de 60 % do CRV carregado foi libertado, enquanto após três semanas as membranas libertaram entre o 85 e o 100 % do CRV carregado através de difusão e difusão de Fick, devido ao relaxamento do polímero. Membranas sintetizadas são potenciais candidatos a serem usadas em aplicações de curativos. O manuscrito que resume estos resultados foi submetido a uma revista científica e está atualmente em revisão.

- **CONCLUSÕES GERAIS,** resume as conclusões do trabalho de tese.

- **APÊNDICE 1,** descreve as principais técnicas de caracterização e os métodos para avaliar diferentes propriedades de acordo com as possíveis aplicações.

- **APÊNDICE 2,** resume os artigos publicados e a participação em fórums científicos durante o período da tese.

CHAPTER I

Introduction

INDEX

I.1 Biomaterials

The loss of a body part or an organ generates, besides the loss of function, social and psychological disorders. This has determined not only the interest of finding new materials, but constantly new technologies are developed to improve them and provide materials that meet the most modern requirements in this field. For more than a century, efforts have been devoted to find materials with the appropriate characteristics to solve the problems related to the reconstruction of tissues and organs injured due to aging diseases or due to trauma from accidents or falls (1–4).

The widespread definition of biomaterials was suggested by the American National Institute of Health, "biomaterial is any substance or combination of substances, other than drugs, synthetic or natural in origin, which can be used for any period of time, which augments or replaces partially or totally any tissue, organ or function, in order to maintain or improve the quality of life of the individual" (1).

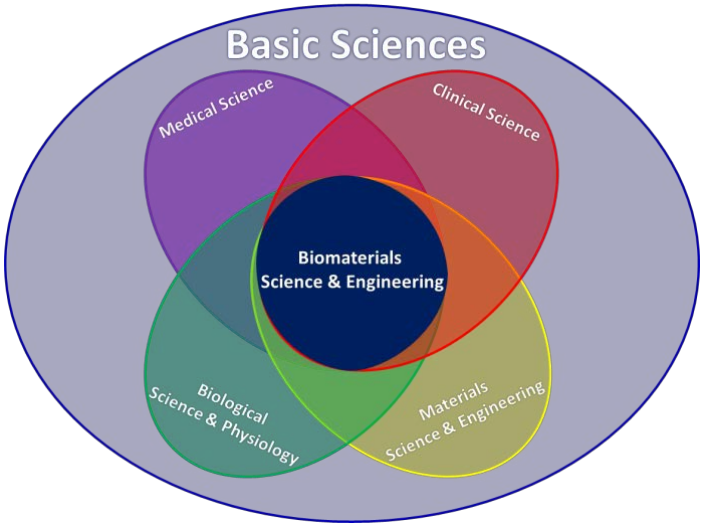

Figure I.1. Main disciplines that integrate the biomaterials sciences and engineering. Modified from von Recum and LaBerge (7).

Gold and ivory were the first materials used by Egyptians and Romans as biomaterials for replacements of cranial defects (1). Amniotic membrane (innermost layer of the placenta) was the first biological material documented for its use as a surgical material in skin transplantation with

better results when compared to xenograft or cadaveric coverings (5). Polymethyl methacrylate (PMMA) is a non-degradable polyacrylate and was one of the first polymers accepted to be used in orthopedics applications in the mid-1950s (6). The tissue biocompatibility of this polymer became further apparent when Plexiglas fragments were accidentally implanted in eyes and other body tissues of World War II fighter pilots during aircraft crashes (6).

The advance in modern medicine has implied the increase in human life and, thus, a greater use of biomaterials. Nowadays, biomaterials play an essential role in medicine facilitating healing and reestablishing the main functions of tissues after injury or disease. The modern field of biomaterials combines not only chemistry, physics, biology and medicine and also recent influences from materials science, regenerative medicine and tissue engineering (Figure I.1) (7).

Biomaterials science and engineering is an interdisciplinary research field that requires knowledge from different areas, which are mentioned in Table I.1.

Table I.1. Disciplines involved in the development of biomaterials.

Discipline	***Essential Knowledge***
Basic Science	Physics, chemistry and Biology.
Materials Science and Engineering	Structure, property, relationship of synthetic and biological materials including metals, ceramics, polymers, composites, body tissues, design and prototype development, applied mechanics, thermodynamics, etc.
Medical Science	Composition of human body (cells, tissues, organs and systems), anatomy, physiology, pharmacology, immunology and pathology with some biochemistry, microbiology, molecular biology, genetics, etc.
Clinical Science	Clinical specialties, among which are: surgery, orthopedics, maxillofacial, plastic and reconstructive surgery, dentistry, ophthalmology, neurosurgery, obstetrics and gynecology, cardiovascular surgery, veterinary medicine, etc.

The global market of biomaterials was around 70 billion of USD in 2016 and is expected to reach about 150 Billion of USD by 2021 with a compound annual growth rate (CAGR) of 16.0% (8). According to their applications, the biomaterials market is sectioned into cardiovascular, orthopedic, ophthalmology, dental, plastic surgery, wound healing, tissue engineering, neurological/central nervous system, and other applications (8).

I.1.1 Biomaterial classification

Biomaterials can be classified according to the nature of the material, being the most important groups: ceramics, metals, polymers and composites. They can be defined either as passive biomaterials (generally remain neutral in their biological environment and have no inherent power of action) or active biomaterials (able to interact with their environment and may even become an integral part of the body) with different bioactivity (9).

I.1.1.1 Metallic biomaterials

Metallurgic industry is able to produce a large number of metals and alloys, but only a few are biocompatible and long-term successful as an implant material. The combination of high mechanical strength and fracture toughness makes metals more suitable for load-bearing applications compared with ceramics or polymeric materials. At the beginning, metallic implants were developed to be used mainly in bone repair (internal fracture fixation of long bones), playing a major role in most orthopedic devices, including temporal and permanent devices (e.g. bone plates, pins, screws and total joint replacements) (10). The main methods to obtain them are by casting, forging, pressing, rolling and machining. Afterwards, the metallic implants developed were used not only in orthopedic surgery, but also in dental and orthodontic practice, including tooth fillings and roots. Currently, several researches point to the use of metallic biomaterials in application of nonconventional reconstructive surgery of hard tissues/organs (NiTi shape memory alloys as vascular stents) and to develop new magnesium-based alloys for bone tissue engineering and regeneration (10).

Chen and Thouas summarized the current status and clinical applications of the four classes of metallic biomaterial (10): ***Stainless steels, Co-based and Ti-based alloys*** are routinely applied in: temporary devices

(fracture plates, screws, hip nails, etc.); stem and cup of total hip replacements with cobalt–chromium-molybdenum or ceramic femoral heads; total joint replacements (wrought alloys); dentistry castings and other permanent devices (nails, pacemakers). The last category corresponds to "***Miscellaneous***" and within there are different alloys such as ***tantalum alloys,*** used as a radiographic marker and wire sutures for plastic surgery and neurosurgery, both approved by the US Food and Drug Administration (FDA); ***magnesium alloys,*** that have been reported in different papers as a biodegradable orthopedic implants and ***nickel-titanium alloys*** (known as Nitinol), which have been FDA approved for different applications: orthodontic dental archwires, vascular stents, vena cava filter, intracranial aneurysm clips, catheter guide wires, orthopedic staples and contractile artificial muscles for an artificial heart.

Despite all its advantages for bone repair current metallic biomaterials present limitations or disadvantages, among which can be highlighted (11):

- ✓ possible release of toxic metallic ions and/or particles through corrosion or wear processes, reducing biocompatibility, leading to the beginning of the inflammatory cascades and triggering tissue loss
- ✓ the elastic moduli are not well matched with that of natural bone tissue, producing stress shielding effects reducing the remodeling and stimulations of new bone growth, compromising the implant stability
- ✓ are essentially neutral *in vivo*, remaining as permanent fixtures, causing a second surgical procedure after the tissue has healed sufficiently to remove them safely, such are the cases of plates, screws and pins used to secure serious fractures.

I.1.1.2 Ceramic biomaterials

Ceramic materials are composed of inorganic, non-metallic substances crystalline, semi-crystalline or non-crystalline (amorphous compounds), glasses and glass-ceramics (partially crystallized glasses).

Ceramic biomaterials (Table I.2) can be categorized according with the interactions or attachment between material and host tissue (bioinert or

bioactive). Furthermore, the bioactive ceramics may be divided as resorbable or non-resorbable and they may be manufactured either in granulates, as coatings, porous or dense in bulk form (12).

Ceramic biomaterials have been widely used to repair the skeletal system, comprising bone, joints and teeth and to augment both hard and soft tissue (13). Additionally, these materials have been used as carriers for enzymes, antibodies, antigens and as microinjectable delivery system for radioactive isotopes for in situ treatment of tumors. They are also used for eyeglasses, diagnostic instruments, chemical ware, thermometers, tissue culture flasks and fiber optics for endoscopy (12). In dentistry, ceramics are used as restorative materials (including inlays and onlays), in gold-porcelain crowns, glass-filled ionomer cements, multi-unit bridges and dentures (1,12).

The main methods of manufacturing ceramic biomaterials are plasma spraying, liquid phase sintering (vitrified), hydrothermal synthesis and solid state sintering (12).

In addition, the main advantages of the use of ceramic biomaterials are their high biocompatibility, high resistance to compression, lower wear rates, resistance to corrosion, chemical inertness, release of very low concentrations of 'inert' wear particles, low thermal and electrical conductivity, easy obtaining and low production costs (13,14). Its main disadvantages are associated with the low impact resistance and the difficulties in processing specific geometric forms (14).

Table I.2. Types of Ceramic biomaterials (12).

Interaction with host tissue	*Properties*	*Implant–Tissue Response*	*Ceramic*
Bioinert	Non-toxic material, dense or non-porous and biologically inactive (nearly inert)	A fibrous tissue of variable thickness is formed and adhered by growth into surface irregularities by cementing the device into the tissues or by press-fitting into a defect	Aluminum oxide (single crystal and polycrystalline) Zirconia (13)
	Non-toxic material, porous (pore diameter between 50-150μm) and biologically inactive (nearly inert)	An ingrown occurs that mechanically attaches the tissue to the material	Aluminum oxide (polycrystalline) Hydroxyapatite-coated porous metals
Bioactive	Non-toxic material biologically active, dense or non-porous, glasses and glass-ceramics with a reactive surface	They connect directly by chemical bonding with the tissue forming an interfacial bond	Bioactive glasses Bioactive glass-ceramics Hydroxyapatite (HA)
	Non-toxic resorbable material biologically active, dense, non-porous or porous able to dissolve in biological environment	The surrounding tissue replaces it slowly	Calcium sulfate Tricalcium phosphate Calcium–phosphate salts

I.1.1.3 Polymeric biomaterials

Polymers are the biomaterials most used in medicine because they show several unique properties which make them useful in a wide range of applications, such as hard and soft tissue replacements, orthopedics, dental or cardiovascular devices. The polarity, stiffness and organization of the polymeric chains into very interesting architectures are the main characteristics of polymeric biomaterials. These materials are often mechanically weaker than other classes of biomaterials (metals and ceramics), because they are linked by secondary interactions, such as hydrogen bonding, dipole-dipole interactions and London forces. Nonetheless, they can exhibit physical behavior more similar to native tissue (15).

Polymeric biomaterials can be classified regarding its origin in natural or synthetic. Biodegradability is considered the main characteristic of natural polymers, but synthetic polymers are more available and usually have a more cost-effective fabrication compared with the obtaining of natural polymers (16). Many researchers consider that natural polymers are showing increasing applications in the area of bone replacement and hard tissue augmentation but its availability and cost of obtaining is its main disadvantage (16). Among the most used natural polymers, it can be found: collagen, chitosan, alginate, starch, cellulose, hyaluronic acid, elastin, keratin, silk, etc. (17,18) . Some of them are highly desirable to induce rapid bone colonization since they can provide a template for biomimetic apatite formation (18).

The main methods to process synthetic polymers are thermally induced phase separation, porogen leaching/solvent casting, electrospinning, gas foaming, rapid prototyping or 3D printing are some of the methods used to process synthetic polymers (19). Synthetic polymers such as, poly(ε-caprolactone) (PCL), poly lactic acid (PLA), poly glycolic acid (PGA) and their copolymers, e.g. poly(lactide-co-glycolic acid) (PLGA) have been widely used to create 3D constructs for bone regeneration due to its biocompatibility and their tailorable biodegradation (19,20).

In 2016, Teo and collaborators reported a list of synthetic polymers approved by the FDA (Table I.3), commonly used as medical implants (16).

Table I.3. Synthetic polymers approved by FDA for biomedical applications (16).

Synthetic Polymer	***Biomedical Applications***
Polyethylene	Anesthesiology, Cardiovascular, Otolaryngology, Gastroenterology, Urology, Hematology, Pathology, Neurology, Ophthalmic and Orthopedic
Polytetrafluorethylene	Anesthesiology, Cardiovascular, Gastroenterology, Urology, General Surgery, Plastic Surgery, Hematology, Pathology, Neurology and Ophthalmic
Polyamide	Anesthesiology, Cardiovascular, Gastroenterology, Urology, Hematology, Pathology, Neurology General Surgery, Plastic Surgery and Ophthalmic
Polypropylene	Cardiovascular, Gastroenterology, Urology, General Surgery, Plastic Surgery, Obstetric and Gynecologic
Polyethylene terephthalate	Cardiovascular, General Surgery and Plastic Surgery
Polydimethylsiloxane	Cardiovascular, Otolaryngology, Gastroenterology, Urology, General Surgery, Plastic Surgery and Neurology
Polyhydroxyalkanoates	Cardiovascular, Gastroenterology, Urology, Neurology and Orthopedic
Polymethylmethacrylate	Dental and Ophthalmic
Liquid crystal polymer	Otolaryngology and Neurology
Silicone	Otolaryngology, Gastroenterology, Urology, General Surgery, Plastic Surgery, Obstetric and Gynecologic
Parylene	Otolaryngology, Neurology
Polyimides	Neurology
Polyether Ether Ketone	Orthopedic
Polyurethane	Obstetric and Gynecologic

Despite all their advantages and applications, polymeric biomaterials present low mechanical resistance and some of them are easily biodegradable. These two properties must be taken into account when developing a new biomaterial (14).

I.1.1.4 Composite biomaterials

Composite materials were defined by William in the Dictionary of Biomaterials, as a "structural material made of two or more distinctly different materials, where each component contributes positively to the final properties" (21). In our body, many tissues are considered "composite" with an additional complexity due to their hierarchical structure, such as extracellular matrix (ECM), tendons, ligaments, skin, and bone, among others (22). Generally, composite biomaterials are associated to combinations of two or more components from the basic biomaterials classes, metals, ceramic and polymers, rather than a combination of materials within the same class (21). Distribution, content and interaction of the constituent materials together with their physical, chemical and mechanical properties, have a strong repercussion on the final properties of the composite biomaterials (22).

Composite biomaterials usually consist of one or more discontinuous phases (commonly known as filler or reinforcing material) embedded within a continuous phase (known as matrix). The principal functions of the filler are to increase the mechanical properties and bioactivity and change the physical and chemical properties. Ceramic and glass particles as well as carbon, polymer and glass fibers have been the main reinforcing materials used in composite biomaterials (Table I.4).

Most composite biomaterials used in biomedical applications have a polymeric matrix (Table I.5), that can be bio absorbable or not. Ceramic and metallic matrices composites are used mainly in non-biomedical applications, only a few composite biomaterials have a ceramic matrix, such as calcium phosphate bone cements (22).

Table I.4. Advantages/Disadvantage of reinforcing materials (22).

Reinforcing materials	Main properties	Disadvantage
Carbon fiber	Lightweight, flexible; high strength; and high tensile modulus	Poor shear strength and may be fragile
Polymer fibers	Biocompatibility, biodegradation; high strength and fatigue resistance; controlled release	Poor mechanical properties
Ceramic	Biocompatibility; bioactivity; reinforce polymers	Poor shear strength and may be fragile
Glasses	High strength-to-weight ratio; good dimensional stability; good resistance to heat, cold, moisture; and corrosion; good electrical insulation properties; ease of fabrication and relatively low cost	Poor shear strength

Table I.5. Some biomedical composite systems used and its applications (22).

Matrix/Reinforcement	***Applications***
Epoxy resin/CF	External fixator
Epoxy resins/CF; PMMA/CF; PSU/CF; PP/CF, PE/CF; PBT/CF; PEEK/CF; PEEK/GF; PLLA/HA; PLLA/PLLA fibers and PGA/PGA fiber	Bone fracture fixation plates, pins, screws
PMMA/HA particles; PMMA/Glass beads; Calcium phosphate/aramid fibers, CF, GF, PLGA fibers and PMMA/UHMWPE fiber	Bone cement
PU/Bioglass; PSU/Bioglass; PEEK/CF; Hydrogels/PET fibers and PLA/PLA fibers/CP	Spine surgery, bone substitute
Bis-GMA/inorganic particles	Dental cements and other dental applications
PEEK/CF	Acetabular cups
PEI/CF-GF; PEEK/CF and CF/PA12	Hip prostheses stem
PE/HA particles	Bone replacement, substitute
Poly(propylene fumarate)/TCP; PEG-PBT/HA PLGA/HA fibers; P(DLLA-CL)/HA particles and Starch/HA particles	Bone filling, regeneration
Hydrogels/PET and Polyolefins/UHMWPE fiber	Tendons and ligaments
PELA/Polyurethane fiber	Vascular grafts
Epoxy resins/CF, GF, KF	Prosthetic limbs

Bis-GMA: Bis-glycidyl dimethacrylate; CF: carbon fibers; CP: calcium phosphate; GF: glass fibers; KF: Kevlar fiber; PA12: polyamide 12; PBT: poly(butylene terephthalate); P(DLLA-CL): poly(D,L-lactide/-caprolactone); PE: polyethylene; PEEK: poly(ether-ether-ketone); PEG: poly(ethyleneglycol); PEI: poly(ether-imide); PELA: poly(ethylene oxide)-b-poly(lactic acid) block copolymer; PET: poly(ethylene terephthalate); PLLA: poly(L-lactic acid); PP: polypropylene; PSU: polysulfone; PU: polyurethane; TCP: tricalciumphosphate; UHMWPE: ultra-high molecular weight polyethylene.

I.2 Drug delivery system

Drug delivery systems are focused on enhancing the therapeutic effect of an active molecule at a specific target site, controlling drug release and protecting it under physiological conditions. Toxic and ineffective dose levels are unwanted effects from systemic delivery that can be avoided with the use of these systems (Figure I.2) (23–26). The goal of controlled release systems is to prevent the variability of dose levels and maintain an appropriate therapeutic dose for the desired time.

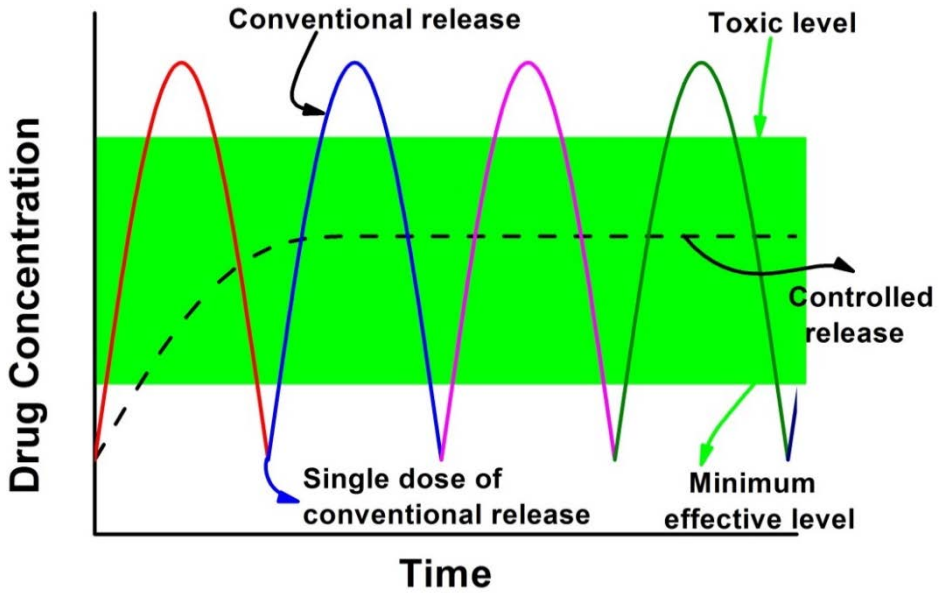

Figure I.2. Drug levels from conventional and controlled drug delivery. Modified from Kohrs *et al.* (24).

Drug controlled release is associated with different phenomena such as diffusion, swelling, degradation, erosion and dissolution, it depends mainly on composition and structure of the vehicles used and drug distribution. The most used materials to develop controlled release systems are polymers (natural or synthetic), ceramics (calcium phosphate including hydroxyapatite), glass (bioglass), metals, and metal alloys (24).

Hydrophilic drugs release from polymer materials are controlled by Fickian or non-Fickian diffusion and erosion process. When the polymers reach the

rubbery state (above glass transition temperature) the surrounding medium can penetrate allowing dissolution and subsequent diffusion of the drug.

On the other hand, hydrophobic drugs are released by erosion process. *In vivo* erosion or degradation (biological environment) can be passive (by hydrolysis) or active (by enzymes) producing surface or bulk erosion. Surface erosion is considered ideal for several drug delivery applications, because the drug release is usually correlated with the expected erosion rate. In bulk erosion the drug is released in three stages (24):

1. Burst release (drug located on the surface)
2. Drug release during the initial biodegradation process
3. Release of residual drug during complete biodegradation

In addition, the controlled release systems can be sensitive to certain stimuli (responsive drug delivery systems), such as pH and temperature.

The main applications of drug delivery systems are transdermal, topical, gastrointestinal, nasal, mucoadhesive, parenteral, and implantable carrier systems. Kohrs *et al.* (24) summarizes the major advantages and disadvantages for the different applications (TABLE I.6).

The active compounds used in wound management have evolved in parallel to the pharmaceutical agents and wound dressings used as drug delivery systems. New generation of wound dressings that incorporate new active compounds is in continue development. Hydrocolloids, hydrogels, alginates, polyurethane foam/films, and silicone gels are widely used as wound dressing to deliver active molecules (27).

Active compounds loaded in wound dressings play an active role in the wound healing process, as debriding or cleansing agents to eliminate necrotic tissue. Wound dressing loaded with antimicrobial agents prevents or treats infection to aid tissue regeneration (27). When growth factors are loaded into wound dressings, several processes (migration, cell division, differentiation, protein expression, and enzyme production) could be activated at different phases of wound healing (inflammatory, proliferation and migratory phases) (27–29).

Table I.6. Advantages and disadvantages of common drug delivery approaches (24).

Approach	Advantages	Disadvantages
Transdermal/topical	1. Sustained delivery 2. Avoids first-pass metabolism 3. Reduced dosing frequency 4. Steady absorption 5. Noninvasive	1. Possible skin reaction 2. Delayed drug action 3. Variability in drug absorbance rates due to application location 4. Adhesion failure
Gastrointestinal	1. Convenient 2. Simple design 3. Safest administration route 4. Low cost	1. Gastric retention time 2. Requires high levels of gastric liquid and food 3. Drugs with solubility and stability issues in highly acidic environment cannot be used 4. First-pass metabolism
Nasal	1. Rapid absorption 2. Quick drug action 3. Avoids first-pass metabolism	1. Possible nasal irritation 2. Potential toxicity of absorption enhancers 3. Difficult to halt after administration

Table I.6. Continued		
Mucoadhesive	1. Prolonged residence times 2. Localization of treatment 3. High drug flux at absorbing tissues 4. Avoids first-pass metabolism	1. Potential for damage to mucosa 2. Patient discomfort
Parenteral	1. Highest bioavailability 2. Immediate physiological response 3. Avoids first-pass metabolism 4. Dosing control	1. Pain 2. Potential injection site infection 3. Patient aversion to needles 4. Difficult to halt after administered
Implantable	1. Eliminates need for patient compliance 2. Avoids first-pass metabolism 3. Potential for zero-order release	1. Invasive 2. Limited loading capacity 3. Biocompatibility considerations 4. Surgical removal at therapy termination 5. Possible device failure and drug dumping

Vitamins (A, C, E) and mineral supplements (copper and zinc) are other active compounds involved in the wound healing process that can be released from the dressings. The dressings most employed with this kind of active molecules are oil-based liquid emulsions, creams, ointments, gauze, and silicone gel sheets (27).

Drug delivery systems with long-term therapeutic properties and high clinical efficacy have a growing interest in tissue engineering to release bioactive molecules (mainly growth factors). Growth factors can be incorporated within the scaffold, in order to induce biological signals that favor the formation of new tissue (23,30).

I.3 Wound dressing materials

Human skin is the most susceptible tissue to suffer an injury because is the largest and most external organ of the human body. Skin is about 15% of the total body weight and it has an average surface area of 1.6-2 m^2 (30). A "wound" is commonly known when the normal skin structure is broken or destroyed, but not only includes lacerations or tears in the skin layer with exposure of the subcutaneous tissue (an open wound), also contusions from blunt objects (a closed wound). In pathology, wounds are restricted to cases in which the trauma sustained by skin structures has penetrated through the epidermis and inflicted damage on the dermis (31).

Wounds can be classified based on several criteria (32):

a) Severity. In accordance with the amount of damage tissue, the involvement of muscle, bone, nerve and whether the infection is present. These wounds are usually caused by trauma (burn and ulcer wounds), pressure sores, abrasions and iatrogenic wounds, such as skin graft donor sites and dermabrasions.

b) Morphology and thickness. Depending on the layers involved, wounds can be superficial wounds (only the epidermis is involved); partial-thickness wounds (epidermis and dermis and involved); and full-thickness wounds (involve the subcutaneous fat or deeper tissue).

c) Surgical. According to the degree of contamination, i.e., clean, clean-contaminated, contaminated and infected, as per the USA National Research Council

d) Aetiology. Based on the cause of wound formation, wounds are classified as pressure ulcers, neuropathic ulcers, vascular ulcers (arterial and venous) and burns.

e) Wounds with and without tissue loss (skin, muscle, bone, tendon).

The physiological process of normal wound healing requires skin restoration via re-epithelialization and collagen formation (2,33). Several type of dressing are widely used to protect the wound, to increase the speed and quality of wound healing.

The main characteristic of a wound dressing is to provide the optimum conditions for wound healing and, at the same time, offer protection to the wound from invasion by pathogenic microorganisms and further trauma (33). It is also essential that the dressing does not integrate into the tissue and can be detached without causing any trauma to the wound surface during dressing changes (34).

The obtaining of an ideal dressing is very complicated because it not only must take into account the characteristics of each type of wound, but also should mimic the properties and functions of human skin (35):

- ✓ Protecting the organism from its environment even while maintaining it in uninterrupted communication with the environment;
- ✓ Preventing body fluid from escaping and external fluids from penetrating;
- ✓ Thermoregulation;
- ✓ Synthesis (vitamin D and melanin)
- ✓ Storage (lipids, melanin and water);
- ✓ Resistance to mechanical stress;
- ✓ Absorption;

- ✓ Excretion; etc.)

To select an appropriate wound dressing, it is necessary to take into account multiple factors, based on their functional and performance characteristics (27).

- ✓ Debridement (wound cleansing): Enhances the migration of leukocytes into the wound bed and supports the accumulation of enzymes. Necrotic tissue, foreign bodies and particles prolong the inflammatory phase and serve as a medium for bacterial growth.

- ✓ Provide or maintain a moist wound environment: Prevents desiccation and cell death, enhances epidermal migration, promotes angiogenesis and connective tissue synthesis, and supports autolysis *via* the rehydration of desiccated tissue.

- ✓ Absorption. Removal of blood and excess exudate: In chronic wounds there is an excess of exudate, containing tissue-degrading enzymes, which block the proliferation and activity of cells, and break down extracellular matrix materials and growth factors, thus delaying wound healing. The excess of exudate can also macerate the surrounding skin.

- ✓ Gaseous exchange (water vapor and air): Permeability to water vapor controls the management of exudate. Low tissue oxygen levels stimulate angiogenesis. Raised tissue oxygen stimulates epithelialization and fibroblasts growing.

- ✓ Prevent infection: protect the wound from bacterial invasion. Infection prolongs the inflammatory phase and delays collagen synthesis, inhibits epidermal migration and induces additional tissue damage.

- ✓ Provision of thermal insulation: Normal tissue temperature improves the blood flow to the wound bed and enhances epidermal migration.

- ✓ Low adherence. Protects the wound from trauma: Adherent dressings may be painful and difficult to remove, and cause further tissue damage.

- ✓ Cost effective low frequency of dressing change: Dressing comparisons based on treatment costs rather than unit or pack costs should be made (cost-benefit-ratio). Although many dressings are more expensive than traditional materials, the more rapid response to treatment may save considerably on the total cost.

Global wound dressings market was estimated to be valued at 6.3 billion of USD in 2016, and is expected to grow at a CAGR of 6.0% from 2016 to 2021, to reach around 8.5 Billion of USD by 2021 (36). Advanced wound dressings segment registered the largest market share in 2015 and it is expected to grow at a CAGR of 6.9%. Increasing knowledge regarding wound care management, the high growth potential of emerging economies, and the increasing number of acquisitions by key companies have opened up a wide range of opportunities for the growth of this market in upcoming years (36).

In the estimated global prevalence by wound type according to the report from MedMarket Diligence, LLC, it is expected that the most frequent injuries in the world in 2020 will be surgical wounds (about 450 million of people), followed by diabetic ulcers (more than 60 million of people), venous ulcers (about 40 million of people), pressure ulcers and lacerations (more than 20 million of people) and burn wounds (about 10 million of people) (37). This indicates the importance of developing new wound dressings for the efficient treatment of these types of wounds.

I.3.1 Wound dressing classification

Traditionally, wound dressings are classified based on its nature or action as: passive products (gauze and tulle dressings, which is the largest market segment); interactive products (polymeric films and foams recommended for low exuding wounds, which are mostly transparent, permeable to water vapor and oxygen but impermeable to bacteria); and bioactive products (dressings constructed from material which has endogenous activity or dressings able to act as a drug delivery system of bioactive compounds in wound healing) (38).

In 1999, wound dressing categories were reclassified by the FDA as follow (38):

- ✓ ***Nonresorbable Gauze/Sponge Dressing for External Use:*** sterile or nonsterile device, to be placed directly on a patient's wound to absorb exudates.

- ✓ ***Hydrophilic Wound Dressing:*** non-resorbable materials with ***hydrophilic*** properties available in sterile or nonsterile form, to cover a wound and absorb exudates.

- ✓ ***Occlusive Wound Dressing:*** non-resorbable material sterile or nonsterile with or without an adhesive backing, intended to cover a wound, to provide or support a moist wound environment and to allow the exchange of gases such as oxygen and water vapor through the device.

- ✓ ***Hydrogel Wound and Burn Dressing:*** non-resorbable matrix sterile or nonsterile made of hydrophilic polymers or other material in combination with at least a 50 % of water, designed to cover a wound, to absorb wound exudates, to control bleeding or fluid loss, and to protect against abrasion, friction, desiccation and contamination.

- ✓ ***Interactive Wound and Burn Dressings:*** reduces the colonization count, exudates level, improves the wound bed moisture retention, improves the wound collagen matrix, removes cellular products and provides protection for the epithelializing bed.

At present, wound dressing market offers more than 3,000 of dressing products registered to suit the needs according to the condition of the wound (39) and according to the base of dressings, they can be divided into 8 main categories (Table I.7).

Table I.7. Wound dressing categories and its applications.

Dressing categories	*Main features*	*Applications*	*Disadvantages*
Gauze and Impregnated Gauze Dressings	Highly permeable and relatively non-occlusive, inexpensive, and used as a non-time or short-term use.	Secondary dressings commonly used for both infected and non-infected wounds of any size, shape, depth, or etiology.	Require more force to remove and may leave residue or lint in the wound bed.
Films	Flexible, permeable to water vapor and gas, but impermeable to bacteria and water.	Superficial wounds such as lacerations, abrasions, partial thickness wounds, sutured wounds, and graft donor sites with minimal drainage. They may also be used on granular wounds and areas of friction.	Not to be used on infected wounds, wounds with moderate to heavy drainage (little absorptive capabilities), or patients with fragile skin.
Hydrogels	Permeable to gas and water, provide moisture to dry wounds and absorbs a minimal amount of fluid, effective for softening eschars.	Available in sheets, gels, or impregnated gauzes are indicated for any thickness wounds with minimal or moderate drainage. They can decrease pain and provide padding to decrease shear forces.	Most hydrogels are almost non-adhesive, thus requiring a secondary dressing. Should not be used on infected wounds and on heavily draining wounds.

Table I.7. Continued			
Foams	Porous 3 layered polyurethane foams able to quickly and effectively draw the exudates deeply into the absorbent material and reliably hold it there. Hydrophobic outer layer prevents bacteria from penetrating. Middle absorption layer is devised to retain absorbed wound exudates. The inner contact layer is hydrophilic with specifically pores size.	Universally used on wounds with minimal to heavy exudates, because they are easy to place and provide thermal insulation. Foams dressing should be able to quickly and effectively extract the exudates deeply into the absorbent material and reliably keep it there. It should also provide soft cover to the wound site, in order to manage the wound environment.	Semipermeable foams are not indicated for dry or eschar covered wounds because it can adhere to the wound
Hydrocolloids	Hydrophilic colloidal particles with a strong film or a foam adhesive backing sheet provide thermal insulation. Impermeable to water, gas, and bacteria and therefore can be effective barriers against urine, stool, and pathogenic microorganisms.	Indicated for any thickness wounds, may be safely used on both granular and necrotic wounds. They should only be used with skin sealants on patients with good skin integrity.	Often leave residues after removal. Not appropriate for bleeding or heavily draining wounds. They are contraindicated for infected wounds and must be used with caution on immuno-compromised patients.

Table I.7. Continued			
Alginates and Hydrofibers	React with serum and wound exudates to form a hydrophilic gel to provide a moist wound environment. They are highly permeable and non-occlusive.	Ideal dressings for moderate to highly draining wounds (they can absorb up to 20 times their weight of exudates). Indicated for partial and full thickness draining wounds and can also be used for infected wounds.	They require a secondary dressing and are not indicated for dry or minimally draining wounds and on wounds with exposed tendon, capsule, or bone
Biological Dressings	Derived from natural tissues, such as skin or amnion. Generally, they provide and maintain moist wound environment that is conducive to regeneration and migration of fibroblasts and epithelial cells and act as a bacterial barrier to protect the wound from infection and fluid loss. Decrease the pain associated with open wounds. Some types may adhere firmly to the wound by vascular connections.	Temporary coverage of open and large wounds. Ideal skin substitute for use in acute and chronic wounds (40).	Low availability and high produce cost. (40) The most serious potential liability of biologic wound dressings is transmission of infection; however, the actual incidence of such transmission is extremely low.

Table I.7. Continued			
Composite Dressings and Adjunctives	Multiple layers and each layer is physiologically distinct. They usually have 3 layers: inner contact layer (is non adherent, preventing trauma to the wound bed), middle layer (absorbs moisture and wicks it away to prevent maceration yet maintaining a moist wound bed) and outer layer (commonly a semipermeable film, serves as a bacterial barrier).	Convenient for both partial and full thickness wounds. It can be used as primary or secondary dressings.	Less flexibility and more expensive (2).

As described above, each dressing variety has unique properties, which makes it suitable for different wound conditions. The disadvantage of a dressing for a specific type of wound may be beneficial for the treatment of another wound. Some of the commercial products are described in Table I.8 (38). However, there is still no superior product that heals chronic wounds like venous leg ulcers, diabetic wound and pressure ulcers which often fail to achieve complete healing. Hence, developing a dressing material that addresses the major interfering factors of normal healing process will help patients and wound care practitioners (2).

Table I.8. Some commercial dressing materials. Modified from Sharma (38).

Type	*Material*	*Dressing*	*Company*
Film	Silicone	Cica-Care	Smith & Nephew
		Mepiform®	Mölnlycke Health Care
	PU	Bioclusive®	Johnson & Johnson
		Mefilm®	Mölnlycke Health Care
		Mitraflex®	
		Omiderm®	Iatro Medical
		Opsite®	Smith & Nephew
		Spyrosorb®	BritCair
Form	Collagen/regenerated cellulose	Promogran	Johnson & Johnson
	Chitosan fibers	KytoCel®	Aspen Medical
	Chitosan	HemCon®	HemCon Medical Tech., Inc.
Film/form	Silicone/PU	Mepilex®	Mölnlycke Health Care
Film/pad/ foam	Hydrocolloid/acrylic	Tegaderm®	3M Health Care
Foam/film	PU	Biatain®	Coloplast
		PolyMem®	Ferris Mfg. Corp.
	PU containing silver	Contreet®	Coloplast
Form/pad/ granules	Chitosan	CeloxTM	Medtrade Products Ltd.

Table I.8. Continued			
Foam	Silicone	Cavi-careTM	Smith & Nephew
	PU	Allevyn®	
		Lyofoam®	
		Tielle®	
Deodorizing	Activated charcoal cloth with silver	Actisorb plus®	Johnson & Johnson
	Activated charcoal cloth	Carbonet®	Smith & Nephew
	Activated charcoal cloth with alginate	Kaltocarb®	ConvaTec
Bioactive	Hydrocolloid	Alione	Coloplast AS
		Comfeel Contour®	
		Cutinova Hydro	Smith & Nephew
		Tegasorb®	3M Health Care
		Biofilm	Biotrol
		Granuflex®	ConvaTec
		CombiDERM®	
		Duoderm®	
	Hydrocolloid paste	GranuGel® Paste	
	Hydrocolloid with honey	Mesitran®	Theo Manufacturing BV
	Hydrofiber	Aquacel®	ConvaTec
	Carboxymethyl cellulose	Versiva®	
	Hydrogel	Aquaform®	Aspen Medical
		Geliperm®	Geistlich Sons Ltd.
		Intrasite Gel®	Smith & Nephew
		Nu-Gel®	Johnson & Johnson
		Purilon Gel®	Coloplast Ltd.
		Sterigel®	Seton
		Vigilon	Bard
		Granugel®	ConvaTec

Table I.8. Continued			
Bioactive	Alginates	Kaltostat®	ConvaTec
		Algisite®	Smith & Nephew
		Algosteril®	Brothier
		Melgisorb	Mölnlycke Health Care
		SeaSorb®	Coloplast AS
		Sorbsan®	Pharma-Plast Ltd.
		Tegagel®	3M Health Care
		Tegagen®	
Traditional	Nonwoven polyester fabric	Mepore®	Mölnlycke Health Care
Pad	Chitosan	AquanovaTM	MedTrade Products Ltd.
Sponge/film	Chitin	Beschitin®	Unitika Medical Products
Beads	Polysaccharide	Debrisan®	Pharmacia and Upjohn Ltd.
		Iodosorb	Smith & Nephew
		Iodoflex	
Silver	High-density polyethylene mesh and nonwoven fabric of rayon and polyester	Acticoat	Smith & Nephew

I.4 Tissue engineering

One of the most devastating, costly and frequent problem in human health care is the loss or failure of an organ or tissue (41). Every year, millions of people suffer tissue loss or end stage organ failure. Tissue engineering is considered a new field dating from late-1980s, that benefits/takes advantage of the principles of engineering and biology to the development of functional substitutes for damaged tissue.

In 1988, tissue engineering was defined by Y.C. Fung as "an interdisciplinary field that applies the principles of engineering and the life sciences toward the development of biological substitutes that restore, maintain, or improve tissue function" (17).

In 1993, three general strategies were proposed for the creation of new tissue (41):

- ✓ Isolated cells or cell substitutes. It allows the replacement of only the affected cells and permits manipulation of cells before using them. Its limitations include failure of the cells used to maintain their function in the recipient and immunological rejection.

- ✓ Tissue-inducing substances. This approach not only depends on the large-scale production and purification of appropriate signal molecules, but also on the development of methods to deliver these molecules (growth factors, drugs or any bioactive ingredient) to their targets.

- ✓ Cells placed on or within matrices. The matrices are produced from natural or synthetic materials (commonly known as scaffolds). Immunological rejection may be prevented by using autologous cells or by immunosuppressive drugs. In this approach, it is possible to find open and closed system. In open systems, cells attached to matrices are implanted and become incorporated into the body. In closed systems, the cells are isolated from the body by a membrane that allows permeation of nutrients and wastes but prevents large entities such as antibodies or immune cells from destroying the transplant. These systems can be implanted or used as extracorporeal devices.

Twenty years later, some general strategies have been adopted to obtain new tissues, such as: use of autogenous (or autologous) cells sources; production of scaffolds for damaged target tissue; tissue culture systems; and use of substances that can induce the regeneration of damaged tissue (Figure I.3) (41–43). Among the main current research areas in tissue engineering, the engineering of bone, bone marrow, skin, nerves, cartilage, blood vessels, corneal epithelia, arteries, heart valves, and heart myocardium are the most relevant (44).

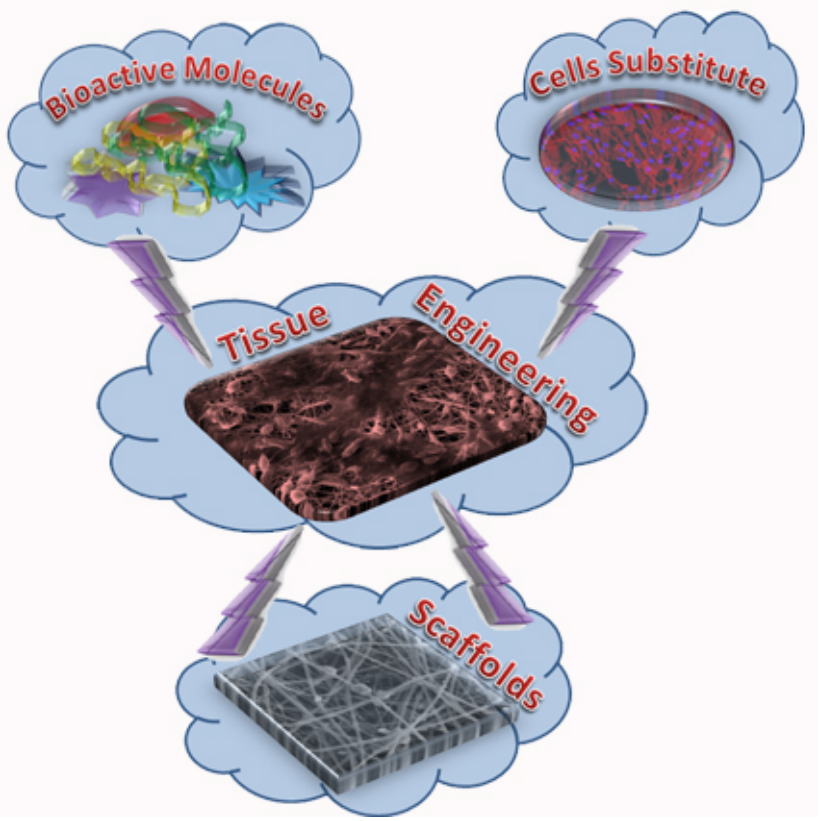

Figure I.3. Tissue engineering strategy currently used.

In the mid 80's, Dr. Joseph Vacanti proposed the idea "to design appropriate scaffoldings for cell delivery as opposed to seeding cells onto available naturally occurring scaffolds having physical and chemical properties that could not be manipulated". Dr. Vacanti worked intensely to generate functional tissue equivalents utilizing a branching network of synthetic biocompatible/biodegradable polymers configured as scaffolds seeded with viable cells (45). In 1999, the concept of scaffolds based on tissue engineering was defined in Williams Dictionary of Biomaterials as "a porous structure, usually polymeric, which serves as a substrate and guide for tissue regeneration (21).

Nowadays, a combination of biological and engineering requisites should be taken into account to design a scaffold for a specific application. The biocompatibility of the material used involves that the scaffold should not demonstrate immunogenicity or bring out an adverse inflammatory

response (46,47). A suitable degradation/tissue regeneration rate will be necessary to be sure, that mechanical properties and functionality of the scaffolds are not compromised. Bioresorbable scaffolds developed must also be sterilizable and degraded without significant cytotoxic, inflammatory or immunogenic degradation components. Scaffold design should take into account also bulk properties, porosity, pore diameter, surface area, chemical properties, micro and macro-environments to regulate cell adhesion, spreading, motility, survival, and differentiation (48).

In 2016, the global tissue engineering market size was valued at around USD 5 billion and according to a new report by Grand View Research, Inc., it is expected to reach USD 11.5 billion by 2022 with a CAGR about 13% (49). This market growth is supported by a growing potential of tissue engineering procedures in the treatment of tissue damages (50).

Factors such as rising geriatric population and lifestyle-oriented diseases are positively affecting the market growth of tissue engineering. Moreover, every year, around 1.3 million case of breast cancer are reported, over 1.5 million people are diagnosed with Parkinson's disease (49). More than 900 million surgeries are performed for bone reconstruction or replacement. Increasing cases of chronic diseases, road accidents, and trauma injuries are contributing to the growth of the development of tissue engineering (49). Among the various applications covered in the global tissue engineering market, orthopedics, musculoskeletal, and spine currently holds the highest 55 % revenue share in 2016 (49–51).

I.4.1 Bone tissue engineering

For more than a century, efforts have been devoted to find materials with the appropriate characteristics for the restoration of bone tissue in humans. Constantly, new technologies are developed to improve these materials and provide surgeons with biomaterials that meet the most modern requirements in this field. It is necessary to understand the properties and functions of bone tissue in order to develop successful materials for bone tissue engineering.

Bone tissue is a heterogeneous natural material composed of an inorganic part, an organic matrix and water. Inorganic content of bone ranges from 30 to 98 % dry weight, but most of the bones have approximately 60–70 % of the total bone/dry weight, depending upon site, species and stage of

development (52). In 1926, de Jong (53) found that X-ray diffraction patterns obtained from ground bone are similar to geologic hydroxyapatite [$Ca_5(PO_4)_3(OH)_2$]. The inorganic phase of bone tissue is commonly known as biological apatite. The main difference between them is the variety of substitutions and vacancies in the bone apatite nanocrystals, different Ca/P molar ratio and crystallinity (54) that result in different reabsorptions properties. Bone organic phase is formed mainly by a matrix of collagen type I (around 90 %), non-collagenous proteins (around 5 %), lipids (around 2 %) and water. Several families of non-collagenous proteins have been identified in the bone matrix: albumin, alpha 2-HS glycoprotein, osteocalcin, fibronectin, proteoglycans, osteopontin, osteonectin, thrombospondins, alkaline phosphatase, among others (55). All these proteins are closely linked to collagen and fulfil important functions in matrix organization, cell signaling, metabolism and mineralization. If noncollagenous proteins are extracted from the bone tissue, it cannot be re-mineralized (56). Lipids are fat soluble and plays an important function for cell, they surround the cell body and regulate the flux of signaling molecules and ions into and out of the cell (52). Water in our body has many functions and in the bone tissue is responsible for filling the pores, interacting with collagen fibrils and binding to mineral crystals.

Bone tissue is a complex organ and supports the living structures that give the body form and shape. Bones protect our vital organs and act as a reservoir for critical vitamins and nutrients, such as calcium, and also act as the levers and pivots that permit control for direction and range of movement (57). Bone tissue has an innate ability to remodel and regenerate itself and it is completely renewed every 10 years (58–60). The bone remodeling process is a homeostatic balance between bone deposition and bone resorption by osteoblasts and osteoclasts, respectively. The health and wellbeing of patients can be affected if serious complications occur during bone healing. When normal repair process becomes dysregulated or interrupted, or bone defects are too large, bone tissue is unable to completely heal without external intervention (57). Several investigating models suggest that during healing processes of the large bone defects only around 10 % of the defect is normally repaired in the studied period (no more than 12 weeks) (61). These large bone defects were originally defined as critical size defects (CSDs) (62,63).

In 2007, the "diamond concept" of bone tissue engineering was proposed and described by Giannoudis and collaborators, as a “standard tissue engineering approach to provide solutions for impaired fracture healing, bone restoration and regeneration”. This concept has become widely accepted and acknowledged in the field of bone tissue engineering (57,64,65).

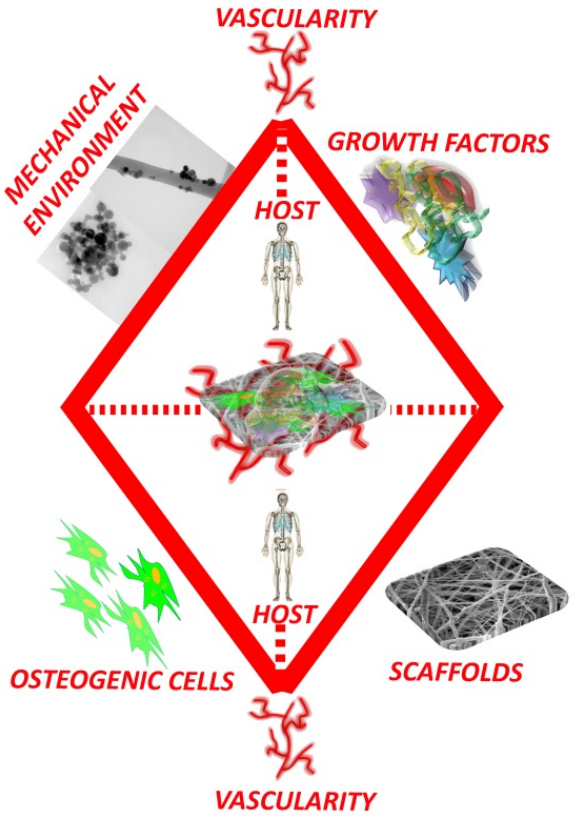

Figure I.4. Diamond model of bone fracture healing interactions. Modified from Giannoudis *et al.* (65).

Following the "diamond concept" (Figure I.4), to develop a functional bone graft substitute able to promote vascularization by bone tissue engineering, it is necessary to use a osteoconductive three-dimensional structure (scaffolds or matrix), usually composed by a natural or synthetic polymer loaded with bioactive molecules (such as growth factors, among others) and osteoinductive materials (such as calcium phosphate biomaterials). Furthermore, they can also act as mechanical reinforcement to increase the mechanical properties. Mesenchymal stem cells (MSCs) and/or

differentiated osteoblasts were also used to enhance fracture healing in a number of *In vitro* and *in vivo* studies (57,64,65).

The Department of Economic and Social Affairs (United Nations, Population Division) expects that people aged over 60 reach 2 billion worldwide in 2050 (66). This fact will bring an increase in the number of orthopedic surgeries, because this population is more prone to orthopedic ailments and the market is anticipated to witness a significant demand during the next 30 years. The global bone grafts and substitutes market is expected to reach around $4 billion by the period 2022-2025, registering a CAGR between 4 and 5% since 2015 (67–70).

Table I.9 shows some of the most successful commercially available bone tissue engineered scaffolds.

Table I.9. Some of the most successful commercially available bone tissue engineered products and its description. Modified from Bishop *et al.* (71).

Product	***Product description***	***Company***
Vertigraft® Allograft	Variety of structural allografts and an array of osteobiological properties, including, but not limited to, VG1 ALIF, VG2 PLIF, VG2 RAMP and VG2 TLIF.	DePuy Orthopaedics, Inc., Warsaw, IN, USA
Symphony® I/C Graft Chambers	Osteoinductive and osteoconductive product comprised of a mixture of allograft cancellous chips and DBM. Also contains naturally occurring cascade of BMP's and growth factors.	
Restore® Orthobiologic Soft Tissue Implant	Resorbable scaffold to reinforce weakened or damaged soft tissue repair including rotator cuff, patellar, Achilles, biceps, quadriceps and other tendons.	

Table I.9. Continued		
Optium DBM® System	Includes both Optium DBM® Gel and Putty. Both contain osteoinductive and osteoconductive properties.	DePuy Orthopaedics, Inc., Warsaw, IN, USA
Healos® Fx Injectable Bone Graft Replacement	An osteoconductive and easy to use bone graft replacement which provides a scaffold. It has potentially osteogenic properties when autologous bone marrow is added.	
OP-1 Implant	Osteoinductive and osteoconductive bone graft material consisting of collagen matrix, 1 g of Type I bovine collagen, 3.3 mg of rhBMP-7 and 2–3 cc of saline.	
Healos Bone Graft Replacement	Osteoconductive matrix comprised of cross-linked collagen fibers that are fully coated with hydroxyapatite. When combined with BMA, product provides an environment for osteoprogenitor cell attachment, proliferation, and differentiation.	
Conduit® TCP Granules	Osteoconductive synthetic porous ceramic graft material made of tricalcium phosphate which provides a scaffold for bone cell attachment.	
Infuse® bone graft	Solution containing rhBMP-2 and an ACS used to fill the LT-CAGE® lumbar tapered fusion device.	Medtronic Inc., Minneapolis, MN, USA
Actifuse	Silicate substituted calcium phosphate.	Baxter International Inc., Deerfield, IL, USA

Table I.9. Continued		
Vitoss	Bioactive glass and calcium phosphate.	Orthovita Inc. Malvern, PA, USA
OP-1® Putty	rhBMP-7, Type I bovine collagen matrix and putty additive carboxymethylcellulose sodium.	Olympus Biotech, Hopkinton, MA, USA

ACS: absorbable collagen sponge; BMA: bone marrow aspirate; DBM: demineralized bone matrix; BMP: bone morphogenetic protein; rhBMP-2 and rhBMP-7: recombinant human bone morphogenetic protein 2 and 7.

I.4.1.1 Classification of scaffolds in bone tissue engineering

Scaffolds used in bone tissue engineering must provide a stable mechanical environment and adequate degradation rate over a certain period of time in order to achieve optimal bone tissue ingrowth and regeneration. In 2013, Henkel and Hutmacher proposed a novel approach to design scaffolds-based bone tissue engineering (Figure I.5) (72).

Scaffolds designed for bone tissue engineering should provide a suitable microenvironment for the tissue regeneration capacity, promote the crucial steps in the organ maturation process and tissue remodeling (72). Scaffolds can be classified according to the nature of the material (metals, ceramic and polymer scaffolds with or without modifications). Polymeric scaffolds with modifications (addition of ceramics) are the most used in this field.

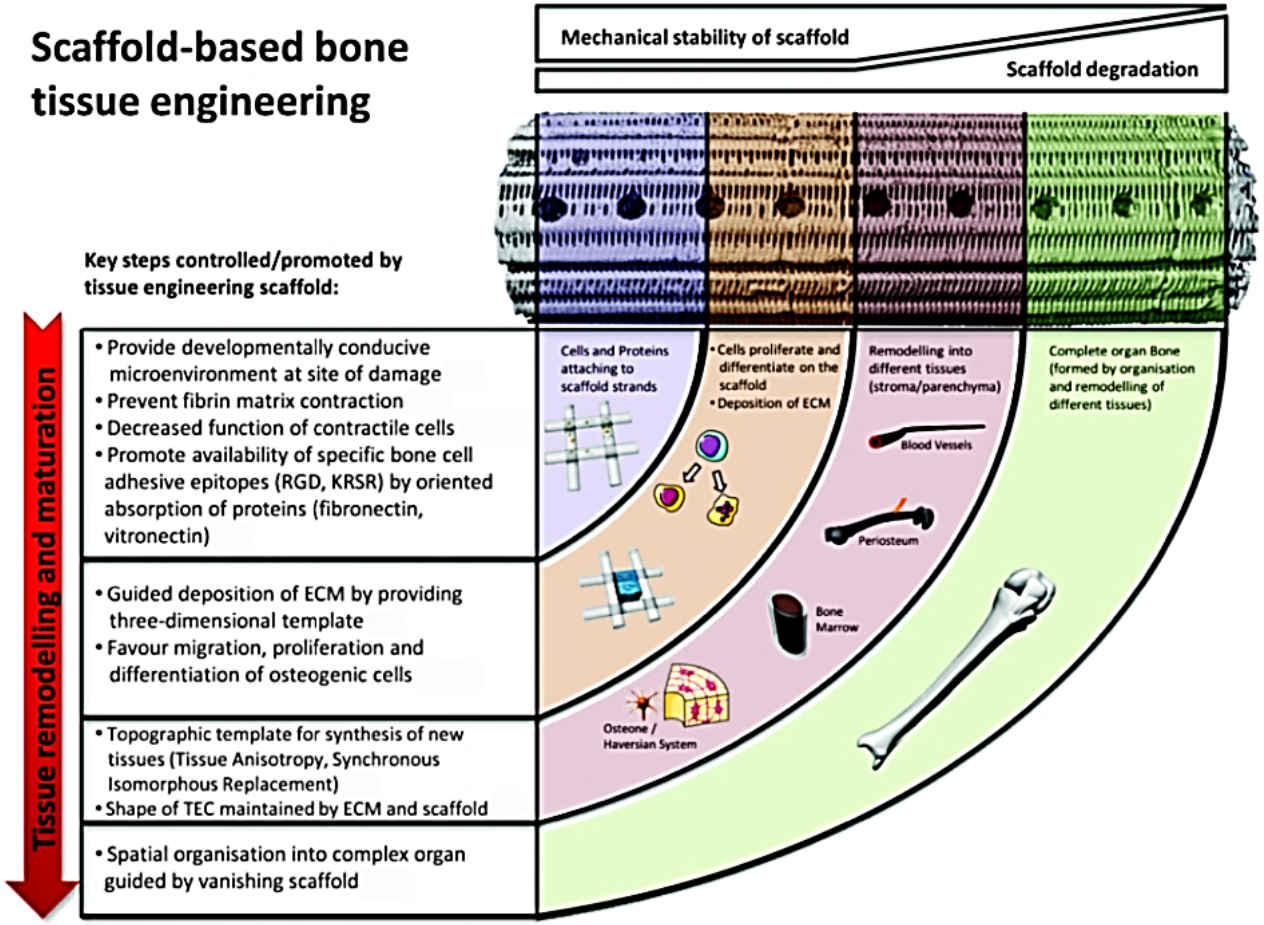

Figure I.5. Targeted design and application of scaffolds for bone tissue engineering. Images from Servier Medical Art, © 2013 SERVIER. All Rights Reserved (57,72).

I.4.1.1.1 Metallic scaffolds in bone tissue engineering

Metallic scaffolds act more like permanent implants than scaffolding. Pure metals like iron, magnesium, titanium, tantalum, zirconium and niobium, and different alloys such as, chrome-cobalt, magnesium-calcium, iron-magnesium, titanium-aluminum-vanadium, nickel-titanium and stainless steel, have been used. Clinical applications as well as their advantages and disadvantages are discussed in **I.1.1.1 section.**

I.4.1.1.2 Ceramic scaffolds in bone tissue engineering

Bio-ceramics practically mimic the bone tissue and provide a higher osteoblasts adherence and proliferation because solubility and surface topography have a significant influence in cell behavior compared to other materials. Calcium phosphate ceramics such as hydroxyapatite, tricalcium phosphate, biphasic and amorphous calcium phosphates have been greatly studied for bone tissue repair in the form of scaffolding or in combination with polymers or metals.

I.4.1.1.3 Polymeric scaffolds in bone tissue engineering

Several physiochemical characteristics (solubility, porosity, pore size, enzymatic reactions, biocompatibility and allergic response) are usually more controllable in polymeric materials used to design scaffolds. Natural polymer scaffolds could be tissue or cell derived that show osteoinductive properties. They are composed mainly by proteins (collagen, elastin, gelatin, keratin, fibrinogen and silk), polysaccharides (cellulose, glycosaminoglycans, amylose, chitin and dextran), polynucleotides (DNA, RNA) and extracellular matrix.

Table I.10. Most used polymeric scaffolds in bone repair. Modified from *Ghassemi et al.* (73).

Name	*Mechanical Properties*	*Modifications*	*Advantages*
		Synthetic polymers	
PLLA*	+++	- HA incorporation to enhance cell growth.	- biocompatible - biodegradable - support cell adhesion
PGA*	+++	- Alkaline hydrolysis for increasing cell replacement and cells biomaterials interaction improvement.	- biocompatible - biodegradable - support cell adhesion
PCL*	++	- High RGD concentration for increasing osteoblast attachment. - CNTs addition for mechanical properties, BMSCs proliferation and differentiation enhancement.	- biodegradable
PET*	+++	-	- highly biocompatible - biodegradable - impact resistance
PAG	+	-	- biocompatible
PAA*	+	-	- non-biodegradable
PBT*	++	-	- highly biocompatible - biodegradable - impact resistance
PLGA*	+	- HA incorporation for enhancing compressive strength. - Diamond nanoparticles incorporation for higher mechanical resistance. - Incorporation of CNTs for higher rate of cell attachment, proliferation, and differentiation.	- biodegradable - support cell adhesion

Table I.10. Continued			
PEG*	+	- RGD peptides for facilitating cell adhesion and spreading.	- biocompatible - steering cells into scaffolds - osmotic effects in body
PVA	+++	- CNT and CNF incorporation for higher concentration of ALP and mineralised matrix.	- Non-biodegradable - great resistance against organic solvents
PPF*	++	- Linked RGD peptides for osteoblast migration regulation.	- biocompatible - suitable physical properties and decomposition rate
PU	+	-	- variable degradability - injectable
Collagen (type I, II and III)	+	- Mixing with calcium for mechanical integrity increase. - Blending with PCL for mechanical improvement.	- biocompatible - biodegradable
Chitosan	-	- Nanocrystalline hydroxyapatite and SWCNT incorporation for mechanically and cytocompatibility enhancement.	- biocompatible - biodegradable

Table I.10. Continued			
		Natural polymers	
Chitin	+	-	- biocompatible - biodegradable
Alginate	+	- Addition of HA, calcium phosphate cements, bioglass and other natural and synthetic polymers for upgrading cell adhesion and mechanical properties.	- biocompatible - biodegradable - minimally invasive manner (gel-forming) - ease of chemical modification with adhesion ligands and controlled release of tissue induction factors (e.g., BMP, TGF-β)

Mechanical properties: +++ good, ++ average, + poor

RGD: Arginine–Glycine–Aspartate; CNTs: carbon nanotubes; BMSCs: bone marrow stromal cells; CNF: carbon nanofibres; ALP: alkaline phosphatase; SWCNT: single-wall carbon nanotubes

FDA approved: *

On the other hand, biocompatible and biodegradable synthetic polymers such as PCL, PLA and PGA have been the most utilized in bone tissue engineering for their excellent mechanical properties and its low cost of obtaining. But some polymers lose their compressive strength due to rapid degradation *in vivo* (poly(propylene fumarate), generating a local acidic environment which can cause adverse tissue responses. Table I.10 shows some of the most used polymeric scaffolds modified and their advantages.

I.5 Techniques to produce materials for biomedical applications

As previously mentioned, biomaterials may be designed and fabricated using all kind of materials: polymers, ceramics and metals, as well as their combinations (74). In the literature, there are diverse methods to produce biomaterials for medical applications, specifically for wound dressing applications and bone tissue engineering (74–76). Salerno and Netti summarized some of them (freeze drying, particles sintering, phase inversion, solid freeform fabrication, reverse templating, spraying, textiles, emulsion, gas foaming, bioprinting, microfluidic, self-assembly) (74).

The design of an appropriate biomaterial depends not only on its specific medical application but also on the characteristics of the particular patient. It is very difficult to describe specific characteristics to take into account in such developments, but any device used should be able to maintain its functionality during all the accurate time without rejection and safely.

On the other hand, to prepare 3D porous scaffolds, the most used methods are fiber bonding, compression molding, extrusion, high internal phase emulsion templating, emulsion freeze drying, solvent casting/particulate leaching, high pressure processing, superstructure engineering, supercritical fluid processing, gas foaming/particulate leaching, thermally induced phase separation, electrospinning and rapid prototyping (48,77).

Electrospinning is a versatile, simple, scalable and cost-effective spinning technique to produce scaffolds or membranes in form of fibers with a random orientation or with a certain degree of alignment (Figure I.6). Currently, several natural (hyaluronic acid, collagen, alginate, cellulose,

chitosan, gelatin, pullulan, zein, silk fibroin) or synthetic (polyamide, polycaprolactone, polylactic acid, poly (lactic-co-glycolic acid), polyvinyl alcohol, polyurethane, poly (ethylene-co-vinil alcohol), polystyreneetc, etc.) (78,79) polymers were electrospun and the fibers obtained by these technique have been used in various applications such as tissue engineering scaffolds, wound dressing and in numerous biomedical applications (4,78,79).

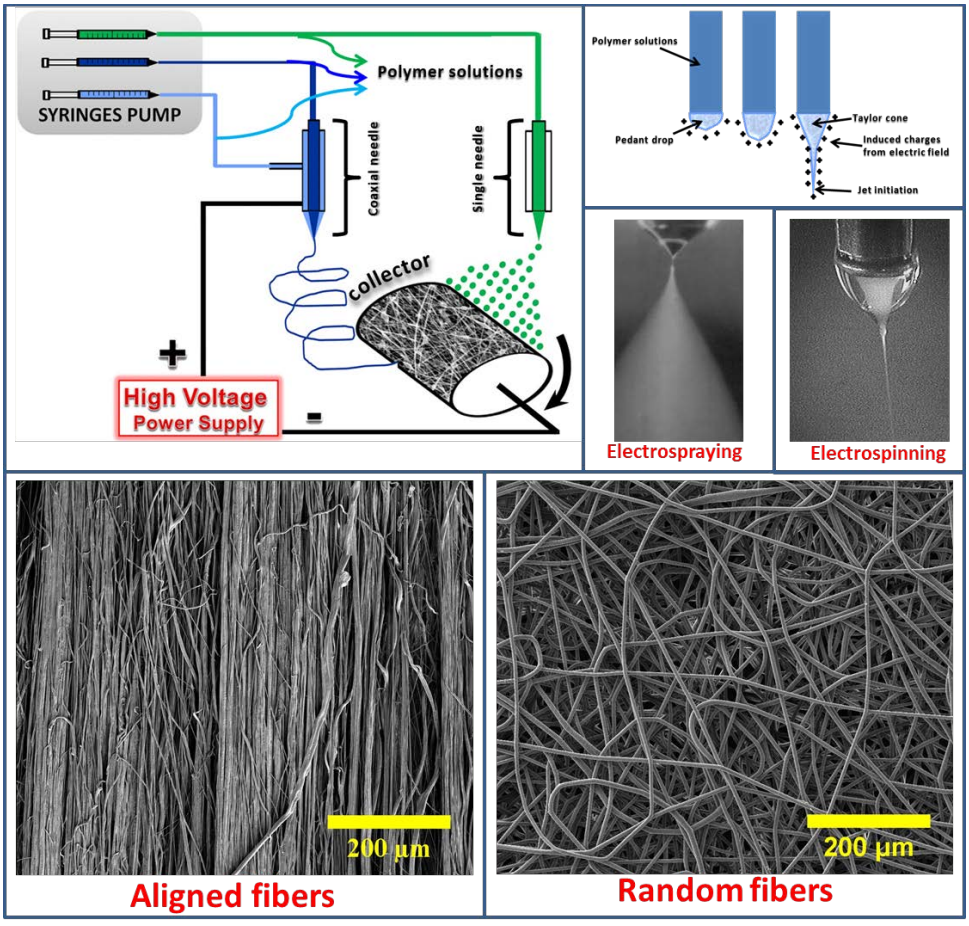

Figure I.6. Schematic diagram of a vertical set up of electrospinning apparatus.

Electrospinning technique is governed by electrostatic forces to produce fibers with different diameters from nanometer to micrometer (4,79). To produce an electrospun material polymer solutions are pumped through a needle under an electric field generated by a voltage source. When

the electric field applied to the needle reaches a critical value and the repulsive electrical forces overcome the surface tension forces, a Taylor cone is formed on the needle tip (Figure I.6) (79–83). Solvent evaporation of the polymers solution occurs between the needle tip and the collector, leaving a solid polymer in fiber form on the collector(4,79,84–88).

Several parameters must be taken into account to produce electrospun material, such as solution properties, process parameters, and environmental conditions (79,88,89). All of them affect the process in a different way, Table I.11 summarizes these effects.

Scaffolds obtained by electrospinning for bone tissue engineering have received special attention, due to its high porosity (> 90 % porosity) and its similarities with the structure and morphology of the native ECM (87). A successful delivery of differentiation and proliferation factors (growth factors, such as, BMP-2 and BMP-7) (90) with the electrospun structures composed by biodegradable polymer filled or impregnated with calcium phosphate could solve the exigency of bone tissue engineering (91).

On the other hand, electrospun membranes have shown a great capability for wound dressing due to the extremely high surface area, allowing adjustment of the wound moisture. The electrospun materials preserve the wound from bacterial infections due to their small pore size. The high porosity allows a good exchange of oxygen and water vapor (4,78,79,84–90,92–96). In the electrospinning process, it is also possible to load antibiotics and antimicrobial agents to obtain controlled delivery systems of one or multiple bioactive factors (23,79,90,96–101). Furthermore, these systems have the potential to be used as wound dressing materials, bone tissue engineering scaffolds, augmentation devices, and antimicrobial filters (2,32,36,39,78,102,103).

Micro and/or nanoparticles can be obtained by electrospraying technique, using the same equipment and governed by the same principle of electrospinning (Figure I.7) (89,90). Loaded and unloaded particles can be obtained in a single step process by electrospraying without the use of any surfactant (89,95,104,105). For this purpose, the polymer solution should fulfill certain characteristics related to flow rate, polymer concentration, viscosity, and polymer molecular weight. On the other hand, the use of highly volatile solvents together with the appropriate needle-collector distance could help the particles synthesis(95,105–107). Particles obtained by

electrospray have a higher encapsulate efficiency compared with other particles production technique (90,105).

Table I.11. Effects and results of different parameters on electrospun morphology (79,85).

Parameters	Effect on fiber morphology
Solution parameters	
Polymer concentration	Increase in polymer concentration produce an increase in fiber diameter.
Molecular weight (Mw) of polymer	Number of beads and droplets are reduced with high Mw.
Viscosity	Optimal viscosity range is needed to produce fibers. Viscosity, polymer concentration and Mw are strongly related.
Surface tension	Instability of jets is obtained when surface tension is high.
Conductivity/surface charge density	Decrease in conductivity induces an increase in fiber diameter.
Processing parameters	
Applied voltage	Increase in voltage cause a decrease in fiber diameter.
Feed rate/Flow rate	A decrease in flow rate generates a decrease in fiber diameter. Particles can be obtained if the flow decreases considerably.
Tip to collector distance	Too large and too small distance can generate beads formation. A minimum distance is necessary to facilitate the solvent evaporation and produce homogeneous fibers.
Ambient parameters	
Humidity	It must controlled. A high humidity can result in beads formations and small circular pores can appear on the surface of the fiber.
Temperature	Increase in temperature cause a decrease in fiber diameter.

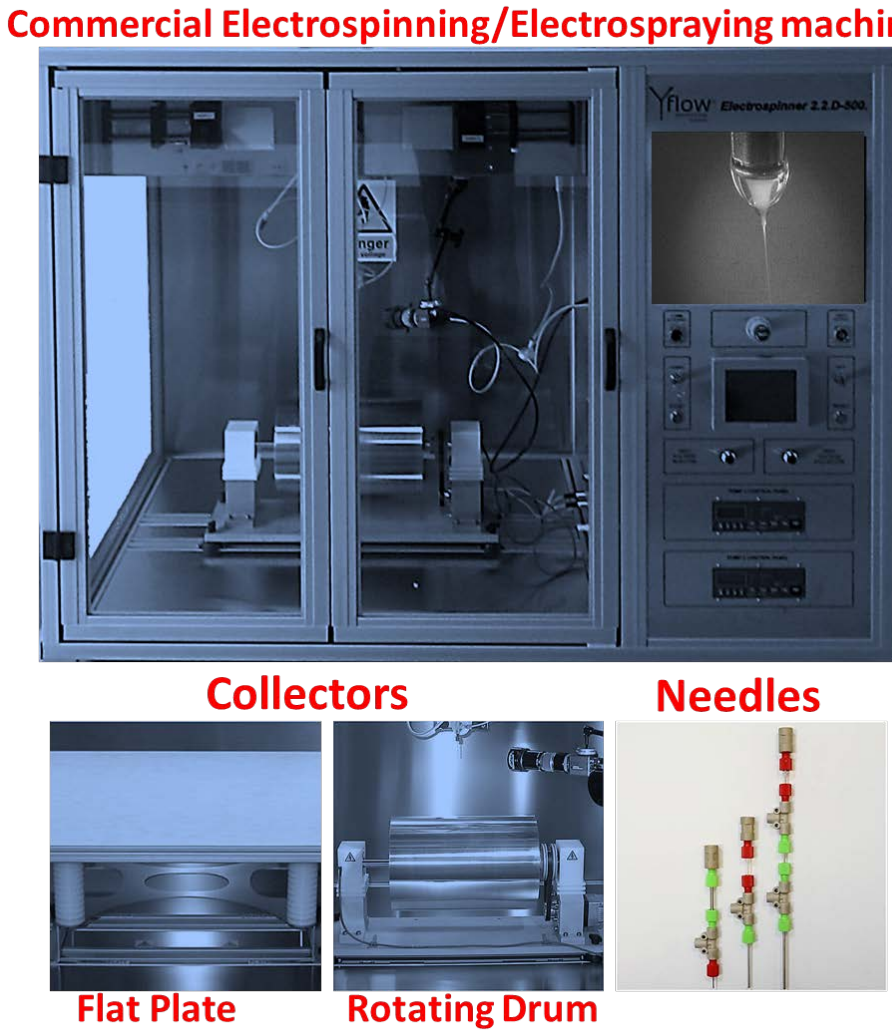

Figure I.7. Yflow 2.2.D-500 coaxial electrospinni ng machines R&D microencapsulation from Malaga Spain)

The use of single, coaxial or triaxial needles, as well as the simultaneous use of electrospinning/electrospraying techniques, allows the design of very specific biomaterials with core/shell and/or particle decorated fibers structures for bone tissue engineering or wound dressing applications (4,20,23,48,78,79,85–87,89,90,92,95,96,98–100,107–131,131–138).
Multiple materials such as drugs, biomolecules, essential oils or inorganic particles can be dissolved or dispersed in a polymer solution to obtain electrospun biomaterials (90).

References

1. Bergmann CP, Stumpf A. Biomaterials. In: Bergmann CP, editor. Dental Ceramics Microstructure, Properties and Degradation. Springer-Verlag Berlin Heidelberg; 2013. p. 84.

2. Dhivya S, Padma VV, Santhini E. Wound dressings – a review. BioMedicine. 2015;5(4):24–8.

3. Ratner B, Hoffman AS, Schoen FJ, Lemons JE. Biomaterials science : an introduction to materials in medicine. Third. Ratner B, Hoffman AS, Schoen FJ, Lemons JE, editors. Academic Press; 2013. 1573 p.

4. Uyar T, Kny E. Electrospun Materials for Tissue Engineering and Biomedical Applications: Research, Design and Commercialization. Electrospun Materials for Tissue Engineering and Biomedical Applications: Research, Design and Commercialization. 2017.

5. Davis JS. Skin transplantation with a review of 550 cases at the Johns Hopkins hospital. Johns Hopkins Med J. 1910;15:307–96.

6. Hacker MC, Krieghoff J, Mikos AG. Synthetic Polymers. In: Atala A, Lanza R, Nerem R, Mikos AG, editors. Principles of Regenerative Medicine. Third. Academic Press; 2019. p. 559–90.

7. Von Recum AF, Laberge M. Educational goals for biomaterials science and engeneering: perspective view. J Appl Biomater. 1995;6:137–44.

8. Biomaterials Market by Type of Materials (Metallic, Ceramic, Polymers, Natural) & Application (Cardiovascular, Orthopedic, Dental, Plastic Surgery, Wound Healing, Neurology, Tissue Engineering, Ophthalmology) - Global Forecast to 2021 [Internet]. MarketsandMarkets. 2016 [cited 2018 Jul 24]. Available from: https://www.marketsandmarkets.com/Market-Reports/biomaterials-393.html?gclid=CjwKCAjwspHaBRBFEiwA0eM3kXnsj7wpCUj3UMF-4SfNYz4shf_LOBeDjvto5uJAFl11Y5V0po5FNBoC_RUQAvD_BwE

9. Ducheyne P. Comprehensive Biomaterials II. 2nd ed. Ducheyne P, editor. Elsevier; 2017. 4858 p.

10. Chen Q, Thouas GA. Metallic implant biomaterials. Mater Sci Eng R Reports. Elsevier B.V.; 2015;87:1–57.

11. Staiger MP, Pietak AM, Huadmai J, Dias G. Magnesium and its alloys as orthopedic biomaterials: A review. Biomaterials. 2006;27(9):1728–34.

12. Hench LL, Best SM. Ceramics, Glasses, and Glass-Ceramics: Basic Principles. In: Ratner B, Hoffman AS, Schoen FJ, Lemons JE, editors. Biomaterials Science : An introduction to materials in medicine. Third. Academic Press; 2013. p. 128–51.

13. Huang J, Best S. Ceramic biomaterials for tissue engineering. In: Baccaccini AR, Ma PX, editors. Tissue Engineering Using Ceramics and Polymers. Second. Woodhead Publishing; 2014. p. 3–34.

14. Sáenz A, Rivera-Muñoz E, Brostow W, Castaño VM. Ceramic biomaterials: An introductory overview. J Mater Educ. 1999;21(5–6):297–306.

15. Heath DE, Cooper SL. POLYMERS: BASIC PRINCIPLES. In: Ratner B, Hoffman AS, Schoen FJ, Lemons JE, editors. Biomaterials science : an introduction to materials in medicine. Third. Academic Press; 2013. p. 64–111.

16. Teo AJT, Mishra A, Park I, Kim YJ, Park WT, Yoon YJ. Polymeric Biomaterials for Medical Implants and Devices. ACS Biomater Sci Eng. 2016;2(4):454–72.

17. Love B. Polymeric Biomaterials. In: Love B, editor. Biomaterials. Academic Press; 2017. p. 205–38.

18. He W, Benson R. Polymeric Biomaterials. In: Ebnesajjad S, editor. Plastics Design Library Handbook of Biopolymers and Biodegradable Plastics: Properties, Processing and Applications. William Andrew; 2013. p. 87–107.

19. Dubruel P, Van Vlierberghe S. Biomaterials for Bone Regeneration. Novel Techniques and Applications. Dubruel P, Van Vlierberghe S, editors. Woodhead Publishing; 2014. 502 p.

20. Boccaccini AR, Ma PX. Tissue Engineering Using Ceramics and Polymers. Second. Boccaccini AR, Ma PX, editors. Woodhead Publishing; 2014. 728 p.

21. Williams DF. The Williams Dictionary of Biomaterials. Williams DF, editor. Liverpool University Press; 1999. 343 p.

22. Migliaresi C. COMPOSITES. In: Ratner BD, Hoffman AS, Schoen FJ, Lemons JE, editors. Biomaterials Science An Introduction to Materials in Medicine. Third. Academic Press; 2013. p. 223–41.

23. Lühmann TC, Meinel L, Groll J, Dalton PD. 4.29 Electrospun Fibers for Drug Delivery ☆. In: Ducheyne P, editor. Comprehensive Biomaterials II. 2nd ed. Elsevier Ltd.; 2017. p. 527–48.

24. Kohrs NJ, Liyanage T, Venkatesan N, Najarzadeh A, Puleo DA. Drug Delivery Systems and Controlled Release. In: Narayan R, editor. Encyclopedia of Biomedical Engineering. Elsevier Inc.; 2019. p. 316–29.

25. Brannon-Peppas L. Biomaterials: Polymers in controlled drug delivery. Medical Plastics and Biomaterials Magazine [Internet]. 1997; Available from: https://www.mddionline.com/polymers-controlled-drug-delivery

26. Robinson JR, Lee VHL. Controlled drug delivery: Fundamentals and applications. Second. Robinson JR, Lee VHL, editors. New York: CRC Press; 1987. 744 p.

27. Boateng JS, Matthews KH, Stevens HNE, Eccleston GM. Wound healing dressings and drug delivery systems: A review. J Pharm Sci. 2008;97(8):2892–923.

28. Abdal-Hay A, Hamdy AS, Khalil KA, Lim JH. A novel simple one-step air jet spinning approach for deposition of poly(vinyl acetate)/hydroxyapatite composite nanofibers on Ti implants. Mater Sci Eng C. 2015;49:681–90.

29. Abdal-Hay A, Hamdy AS, Khalil KA, Lim JH. A novel simple one-step air jet spinning approach for deposition of poly(vinyl acetate)/hydroxyapatite composite nanofibers on Ti implants. Mater

Sci Eng C. 2015;49:681–90.

30. Paul W, Sharma CP. The Anatomy and Functions of Skin. In: Paul W, Sharma CP, editors. Advances in Wound Healing Materials : Science and Skin Engineering. Smithers Rapra Technology Ltd; 2015. p. 25–34.

31. Han S-K. Basics of Wound Healing. In: Han S-K, editor. Innovations and Advances in Wound Healing. Second Edi. Berlin, Heidelberg: Springer Berlin Heidelberg; 2016. p. 1–38.

32. Paul W, Sharma CP. Classification of Wound Dressing Products. In: Paul W, Sharma CP, editors. Advances in Wound Healing Materials : Science and Skin Engineering. Smithers Rapra Technology Ltd; 2015. p. 49–60.

33. Longaker MT, Gurtner GC, Werner S, Barrandon Y. Wound repair and regeneration. Nature. 2008;453(7193):314–21.

34. FDA. FDA Executive Summary: Classification of Wound Dressings Combined with Drugs. 2016;83. Available from: https://www.fda.gov/downloads/AdvisoryCommittees/CommitteesMeetingMaterials/MedicalDevices/MedicalDevicesAdvisoryCommittee/GeneralandPlasticSurgeryDevicesPanel/UCM518494.pdf

35. Montagn W, Parakkal PF. An Introduction to Skin. In: Montagn W, Parakkal PF, editors. THE STRUCTURE AND FUNCTION OF SKIN. Third Edit. New York and London: Academic Press; 1974. p. 1–17.

36. Wound Dressings Market by Type (Advanced Wound Dressings, Traditional Wound Dressings), Application (Surgical Wounds, Ulcers, Burns), End User (Inpatient Facilities, Outpatient Facilities) - Global Forecast to 2021 [Internet]. MarketsandMarkets. 2016 [cited 2018 Jul 24]. Available from: https://www.marketsandmarkets.com/Market-Reports/wound-dressings-market-123903496.html

37. Wound Management, Forecast 2016 to 2026. Report #S254 [Internet]. MedMarket Diligence, LLC. 2018 [cited 2018 Jul 27]. Available from: http://mediligence.com/s254/

38. Paul W, Sharma CP. Wound Management – An Introduction to Wound Healing. In: Advances in Wound Healing Materials : Science and Skin

Engineering. Smithers Rapra Technology Ltd; 2015. p. 1–14.

39. Han S-K. Interactive Wound Dressings. In: Han S-K, editor. Innovations and Advances in Wound Healing. Second Edi. Berlin, Heidelberg: Springer Berlin Heidelberg; 2016. p. 39–62.

40. Chern PL, Baum CL, Arpey CJ. Biologic dressings: Current applications and limitations in dermatologic surgery. Dermatologic Surg. 2009;35(6):891–906.

41. Langer R, Vacanti JP. Tissue Engineering. Sience. 1993;260(May):920–6.

42. Santos Jr. AR, de Carvalho Zavaglia CA. Tissue Engineering Concepts. Ref Modul Mater Sci Mater Eng Elsevier,. 2016;1–5.

43. Santos ARJ, Lombello CB, Genari SC. Technologies Applied to Stimulate Bone Regeneration. In: Davies J, editor. Tissue Regeneration From Basic Biology to Clinical Application. IntechOpen; 2012. p. 339–66.

44. Chiu LLY, Chu Z, Radisic M, Mozafari M. Tissue Engineering. Ref Modul Mater Sci Mater Eng. 2017;2:1–31.

45. Vacanti CA. The history of tissue engineering. J Cell Mol Med. 2006;10(3):569–76.

46. Anderson JM. Biocompatibility and the Relationship to Standards: Meaning and Scope of Biomaterials Testing. In: Comprehensive Biomaterials. Elsevier; 2011. p. 7–26.

47. Spector M. 4.1 The Concept of Biocompatibility. In: Comprehensive Biomaterials II. 2017. p. 1–6.

48. Singh M, Kasper FK, Mikos AG. Tissue Engineering Scaffolds. In: Ratner B, Hoffman A, Schoen F, Lemons J, editors. Biomaterials Science: An Introduction to Materials: Third Edition. Third Edit. Academic Press; 2013. p. 1138–59.

49. Tissue Engineering Market Size, Share & Trends Analysis Report By Application (Cord Blood & Cell Banking, Cancer, GI & Gynecology, Dental, Skin/Integumentary, Orthopedics), And Segment Forecasts, 2018 - 2025 [Internet]. Grand View Research. 2018 [cited 2018 Aug

7]. Available from: https://www.grandviewresearch.com/industry-analysis/tissue-engineering-and-regeneration-industry/methodology

50. Global Tissue Engineering Market Forecasts, 2017-2025 [Internet]. Bizwit Research. 2018 [cited 2018 Aug 7]. Available from: http://www.orbisresearch.com/reports/index/global-tissue-engineering-market-forecasts-2017-2025

51. Global Tissue Engineering Market by Manufacturers, Regions, Type and Application, Forecast to 2023 [Internet]. Global Info Research. 2018 [cited 2018 Aug 7]. p. 149. Available from: http://www.orbisresearch.com/reports/index/global-tissue-engineering-market-by-manufacturers-regions-type-and-application-forecast-to-2023

52. Boskey AL. Bone composition: relationship to bone fragility and antiosteoporotic drug effects. Bonekey Rep. Nature Publishing Group; 2013;2(September):1–11.

53. de Jong WF. La substance minérale dans les os. Recl des Trav Chim des Pays-Bas. 1926;45(6):445–8.

54. Young RA. Biological Apatite vs Hydroxyapatite at the Atomic Level. Clin Orthop Relat Res. 1975;113:249–62.

55. Young MF. Bone matrix proteins: their function, regulation, and relationship to osteoporosis. Osteoporos Int. 2003;14(S3):35–42.

56. Boskey AL. Mineralization of Bones and Teeth. Elements. 2007;3(6):385–91.

57. Baldwin J, Henkel J, Hutmacher DW. 6.3 Engineering the Organ Bone. In: Ducheyne P, editor. Comprehensive Biomaterials II. 2nd ed. Elsevier Ltd.; 2017. p. 54–74.

58. Spruyt D, Gillet C, Rasschaert J. Bone and Bone Marrow; Interactions. In: Huhtaniemi I, Martini L, editors. Reference Module in Biomedical Sciences. second. Academic Press; 2019. p. 31–9.

59. Clarke B. Normal bone anatomy and physiology. Clin J Am Soc Nephrol.

2008;3 Suppl 3:131–9.

60. Bartl R, Frisch B. Biology of Bone. In: Osteoporosis. second. Springer, Berlin, Heidelberg; 2009. p. 7–28.

61. Cowan CM, Soo C, Ting K, Wu B. Evolving Concepts in Bone Tissue Engineering. Curr Top Dev Biol. 2005;66:239–85.

62. Schmitz JP, Hollinger JO. The Critical Size Defect as an Experimental Model for Craniomandibulofacial Nonunions. Clin Orthop Relat Res. 1986;205:299–308.

63. Boyan BD, Cohen DJ, Schwartz Z. 7.17 Bone Tissue Grafting and Tissue Engineering Concepts ☆. In: Ducheyne P, editor. Comprehensive Biomaterials II. 2nd ed. Elsevier Ltd.; 2017. p. 298–313.

64. Giannoudis P V., Einhorn TA, Marsh D. Fracture healing: The diamond concept. Injury. 2007;38(Supplement 4):3–6.

65. Giannoudis P V., Einhorn TA, Schmidmaier G, Marsh D. The diamond concept - open questions. Injury. 2008;39(Supplement 2):5–8.

66. Bone Grafts and Substitutes Market Size, Share & Trends Analysis Report By Material Type (Natural, Synthetic), By Application Type (Spinal Fusion, Craniomaxillofacial, Long Bone), By Region, And Segment Forecasts, 2018 - 2025 [Internet]. Grand View Research, Inc. 2018 [cited 2018 Aug 10]. p. 87. Available from: https://www.grandviewresearch.com/industry-analysis/bone-grafts-substitutes-market

67. Global Bone Grafts and Substitutes Market Analysis & Trends - Industry Forecast to 2025 [Internet]. Research and Markets. 2017 [cited 2018 Aug 10]. p. 173. Available from: https://www.researchandmarkets.com/reports/4039804/global-bone-grafts-and-substitutes-market#rela3-992759

68. Bone Graft and Substitutes - Global Market Outlook (2016-2022) [Internet]. Research and Markets. 2017 [cited 2018 Aug 10]. Available from: https://www.researchandmarkets.com/reports/4335734/bone-graft-and-substitutes-global-market#rela3-4039804

69. Global Bone Graft and Substitute Market Insights, Opportunity, Analysis, Market Shares And Forecast 2017 – 2023 [Internet]. Research and Markets. 2017 [cited 2018 Aug 10]. p. 140. Available from: https://www.researchandmarkets.com/reports/4263768/global-bone-graft-and-substitute-market-insights#relb1-4039804

70. Bone Grafts and Substitutes Market by Product (Allografts, Bone Grafts Substitutes, and Cell-based Matrices), by Application (Spinal Fusion, Long Bone, Foot & Ankle, Craniomaxillofacial, Joint Reconstruction, and Dental Bone Grafting) - Global Opportunity [Internet]. Allied Market Research. 2016 [cited 2018 Aug 10]. p. 130. Available from: https://www.alliedmarketresearch.com/bone-graft-substitutes-market

71. Mishra R, Bishop T, Valerio I, Fisher J, Dean D. The potential impact of bone tissue engineering in the clinic. Regen Med. 2016;11(6):571–87.

72. Henkel J, Hutmacher DW. Design and fabrication of scaffold-based tissue engineering. BioNanoMaterials. 2013;14(3–4):171–93.

73. Ghassemi T, Shahroodi A, Ebrahimzadeh MH, Mousavian A, Movaffagh J, Moradi A. Current Concepts in Scaffolding for Bone Tissue Engineering. Arch bone Jt Surg. 2018;6(2):90–9.

74. Salerno A, Netti PA. 1 – Introduction to biomedical foams. In: Netti PA, editor. Biomedical Foams for Tissue Engineering Applications. Woodhead Publishing; 2014. p. 3–39.

75. Picheth GF, Pirich CL, Sierakowski MR, Woehl MA, Sakakibara CN, de Souza CF, et al. Bacterial cellulose in biomedical applications: A review. Int J Biol Macromol. Elsevier B.V.; 2017;104:97–106.

76. Aragon J, Navascues N, Mendoza G, Irusta S. Laser-treated electrospun fibers loaded with nano-hydroxyapatite for bone tissue engineering. Int J Pharm. 2017;525(1):112–22.

77. Aramwit P. 1 – Introduction to biomaterials for wound healing. Wound Healing Biomaterials. Elsevier Ltd; 2016. 3-38 p.

78. Miguel SP, Figueira DR, Simões D, Ribeiro MP, Coutinho P, Ferreira P,

et al. Electrospun polymeric nanofibres as wound dressings: A review. Colloids and Surfaces B: Biointerfaces. Elsevier; 2018. p. 60–71.

79. Bhardwaj N, Kundu SC. Electrospinning: A fascinating fiber fabrication technique. Biotechnol Adv. 2010;28(3):325–47.

80. Doshi J, Reneker DH. Electrospinning Process and Applications of Electrospun Fibers Jayesh. J Electrostat. 1995;35:151–60.

81. Formhals A. Process and apparatus for preparing artificial threads. US1975504, 1934.

82. Zeleny J. The Electrical Discharge from Liquid Points, and a Hydrostatic Method of Measuring the Electric Intensity at Their Surfaces. Phys Rev. American Physical Society; 1914 Feb;3(2):69–91.

83. Taylor GI. Electrically driven jets. Proc R Soc London A Math Phys Eng Sci. 1969 Dec 2;313(1515):453–75.

84. Stocco TD, Bassous NJ, Zhao S, Granato AEC, Webster TJ, Lobo AO. Nanofibrous scaffolds for biomedical applications. Nanoscale [Internet]. 2018;10(26):12228–55. Available from: http://xlink.rsc.org/?DOI=C8NR02002G

85. Ramakrishna S, Fujihara K, Teo W-E, Lim T-C, Ma Z. An introduction to Electrospinning and Nanofibers. Ramakrishna S, Fujihara K, Teo W-E, Lim T-C, Ma Z, editors. World Scientific Publishing Co. Pte. Ltd.; 2005. 382 p.

86. Bosworth LA, Downes S. Electrospinning for Tissue Regeneration [Internet]. 1 Edition. Bosworth LA, Downes S, editors. Electrospinning for Tissue Regeneration. Woodhead Pub; 2011. 409 p. Available from: http://www.sciencedirect.com/science/article/pii/B9781845697419500094

87. Min Ju Y, Lee J, Jin Lee S, Xu W. Tissue Engineering Scaffolding Using Electrospinning. In: Neves NM, editor. Electrospinning for Advanced Biomedical Applications and Therapies. Smithers Rapra Technology; 2012. p. 89–134.

88. Doshi J, Reneker DH. Electrospinning process and applications of

electrospun fibers. J Electrostat. Elsevier; 1995 Aug 1;35(2–3):151–60.

89. Soares RMD, Siqueira NM, Prabhakaram MP, Ramakrishna S. Electrospinning and electrospray of bio-based and natural polymers for biomaterials development. Mater Sci Eng C. Elsevier; 2018 Nov 1;92:969–82.

90. Wang M, Zhao Q. Electrospinning and Electrospray for Biomedical Applications. Encycl Biomed Eng. Elsevier; 2019 Jan 1;330–44.

91. Aragón J, Salerno S, Bartolo L De, Irusta S, Mendoza G. Polymeric electrospun scaffolds for bone morphogenetic protein 2 delivery in bone tissue engineering. J Colloid Interface Sci. 2018;

92. Stanger J, Tucker N, Staiger M. Report 190. Electrospinning. Smithers Rapra Technology; 2005.

93. Ramakrishna S, Fujihara K, Teo W, Yong T, Ramaseshan R. Electrospun nanofibers: solving global issues. Mater Today. 2006;9(3):40–50.

94. Ramakrishna S, Fujihara K, Teo W-E, Yong T, Ma Z, Ramaseshan R. Electrospun nanofibers: solving global issues. Mater Today. Elsevier; 2006 Mar 1;9(3):40–50.

95. Zamani M, Prabhakaran MP, Ramakrishna S. Advances in drug delivery via electrospun and electrosprayed nanomaterials. Int J Nanomedicine. Dove Press; 2013 Aug 9;8(1):2997–3017.

96. Wang L, Ryan AJ. Introduction to electrospinning. In: Bosworth LA, Downes S, editors. Electrospinning for tissue regeneration. Woodhead Pub; 2011. p. 1–33.

97. El-Naggar ME, Abdelgawad AM, Salas C, Rojas OJ. Curdlan in fibers as carriers of tetracycline hydrochloride: Controlled release and antibacterial activity. Carbohydr Polym. Elsevier Ltd.; 2016;154:194–203.

98. Huang ZM, He CL, Yang A, Zhang Y, Han XJ, Yin J, et al. Encapsulating drugs in biodegradable ultrafine fibers through co-axial electrospinning. J Biomed Mater Res - Part A. 2006;77(1):169–79.

99. Ulubayram K, Calamak S, Shahbazi R, Eroglu I. Nanofibers Based Antibacterial Drug Design, Delivery and Applications. Curr Pharm Des. 2015;21(15):1930–43.

100. Ali M, Yang F, Jansen J. Smart Drug Delivery Systems for Tissue Engineering. In: Wang Q, editor. Smart Materials for Tissue Engineering: Applications. The Royal Society of Chemistry; 2017. p. 505–28.

101. Gaikwad V V., Patil AB, Gaikwad M V. Scaffolds for drug delivery in tissue engineering. Int J Pharm Sci Nanotechnol. 2008;1(2):113–22.

102. Han SK. Innovations and Advances in Wound Healing. 2 Edition. Innovations and Advances in Wound Healing. Springer-Verlag Berlin Heidelberg; 2015. 1-38 p.

103. Paul W, Sharma CP. Wound-healing Dressings and Drug Delivery. In: Advances in Wound Healing Materials : Science and Skin Engineering. Smithers Rapra Technology Ltd; 2015. p. 81–102.

104. Gao Y, Zhao D, Chang MW, Ahmad Z, Li X, Suo H, et al. Morphology control of electrosprayed core-shell particles via collection media variation. Mater Lett. North-Holland; 2015 May 1;146:59–64.

105. Bock N, Dargaville TR, Woodruff MA. Electrospraying of polymers with therapeutic molecules : state of the art. Prog Polym Sci. Elsevier; 2012;37(11):1510–51.

106. Hao S, Wang Y, Wang B, Deng J, Zhu L, Cao Y. Formulation of porous poly(lactic-co-glycolic acid) microparticles by electrospray deposition method for controlled drug release. Mater Sci Eng C. 2014;39(1):113–9.

107. Luo CJ, Edirisinghe M. Core-liquid-induced transition from coaxial electrospray to electrospinning of low-viscosity poly(lactide- co -glycolide) sheath solution. Macromolecules. 2014;47(22):7930–8.

108. Song W, Yu X, Markel DC, Shi T, Ren W. Coaxial PCL/PVA electrospun nanofibers: Osseointegration enhancer and controlled drug release device. Biofabrication. 2013;5(3).

109. Li J, Feng H, He J, Li C, Mao X, Xie D, et al. Coaxial electrospun zein nanofibrous membrane for sustained release. J Biomater Sci Polym Ed. 2013;24(17):1923–34.

110. Raheja A, Chandra TS, Natarajan TS. Design of a low cost spinneret assembly for coaxial electrospinning. Appl Phys Lett. 2015;106(August 2016):254101.

111. Wei QL, Xu FY, Xu XJ, Geng X, Ye L, Zhang AY, et al. The multifunctional wound dressing with core-shell structured fibers prepared by coaxial electrospinning. Front Mater Sci. 2016;10(2):113–21.

112. Zhang L, Si T, Fischer AJ, Letson A, Yuan S, Roberts CJ, et al. Coaxial Electrospray of Ranibizumab-Loaded Microparticles for Sustained Release of Anti-VEGF Therapies. Jablonski MM, editor. PLoS One. Public Library of Science; 2015 Aug;10(8):e0135608.

113. Song W, Yu X, Markel DC, Shi T, Ren W. Coaxial PCL/PVA electrospun nanofibers: Osseointegration enhancer and controlled drug release device. Biofabrication. 2013 Sep;5(3):35006.

114. Song W, Yu X, Markel DC, Shi T, Ren W. Coaxial PCL/PVA electrospun nanofibers: osseointegration enhancer and controlled drug release device. Biofabrication. 2013 Sep;5(3):35006.

115. Wang Y, Wei Y, Zhang X, Xu M, Liu F, Ma Q, et al. PLGA/PDLLA core shell submicron spheres sequential release system: Preparation, characterization and promotion of bone regeneration *In vitro* and *in vivo*. Chem Eng J. 2015;273:490–501.

116. Aragon J, Navascues N, Mendoza G, Irusta S. Laser-treated electrospun fibers loaded with nano-hydroxyapatite for bone tissue engineering. Int J Pharm. 2017 Jun;525(1):112–22.

117. Yang JC, Lee SY, Tseng WC, Shu YC, Lu JC, Shie HS, et al. Formation of highly aligned, single-layered, hollow fibrous assemblies and the fabrication of large pieces of PLLA membranes. Macromol Mater Eng. 2012;297(2):115–22.

118. Ribeiro N, Sousa SR, Van Blitterswijk CA, Moroni L, Monteiro FJ. A biocomposite of collagen nanofibers and nanohydroxyapatite for bone

regeneration. Biofabrication. IOP Publishing; 2014;6(3).

119. Paletta JRJ, Mack F, Schenderlein H, Theisen C, Schmitt J, Wendorff JH, et al. Incorporation of osteoblasts (MG63) into 3D nanofibre matrices by simultaneous electrospinning and spraying in bone tissue engineering. Eur Cells Mater. 2011;21:384–95.

120. Pilehvar-Soltanahmadi Y, Akbarzadeh A, Moazzez-Lalaklo N, Zarghami N. An update on clinical applications of electrospun nanofibers for skin bioengineering. Artif cells, nanomedicine, Biotechnol. 2015;(January):1–15.

121. Murray E, Thompson BC, Sayyar S, Wallace GG. Enzymatic degradation of graphene/polycaprolactone materials for tissue engineering. Polym Degrad Stab. Elsevier Ltd; 2015;111:71–7.

122. Sridhar R, Lakshminarayanan R, Madhaiyan K, Amutha Barathi V, Lim KHC, Ramakrishna S. Electrosprayed nanoparticles and electrospun nanofibers based on natural materials: applications in tissue regeneration, drug delivery and pharmaceuticals. Chem Soc Rev. Royal Society of Chemistry; 2015;44(3):790–814.

123. Puhl S, Ilko D, Li L, Holzgrabe U, Meinel L, Germershaus O. Protein release from electrospun nonwovens: Improving the release characteristics through rational combination of polyester blend matrices with polidocanol. Int J Pharm. Elsevier B.V.; 2014;477(1–2):273–81.

124. Ambrosio L. Biomedical composites. Ambrosio L, editor. Woodhead Publishing; 2010. 648 p.

125. Wendorff JH, Agarwal S, Greiner A. Electrospinning Materials, Processing, and Applications. Wendorff JH, Agarwal S, Greiner A, editors. Wiley-VCH Verlag GmbH & Co. KGaA; 2012. 254 p.

126. Andreu V, Mendoza G, Arruebo M, Irusta S. Smart dressings based on nanostructured fibers containing natural origin antimicrobial, anti-inflammatory, and regenerative compounds. Materials (Basel). 2015;8(8):5154–93.

127. Unnithan AR, Gnanasekaran G, Sathishkumar Y, Lee YS, Kim CS.

Electrospun antibacterial polyurethane-cellulose acetate-zein composite mats for wound dressing. Carbohydr Polym. Elsevier Ltd.; 2014;102(1):884–92.

128. Hung WC, Lin LH, Tsen WC, Shie HS, Chiu HL, Yang TCK, et al. Permeation of biological compounds through porous poly(l-lactic acid) (PLLA) microtube array membranes (MTAMs). Eur Polym J. Elsevier Ltd; 2015;67:166–73.

129. Ou KL, Chen CS, Lin LH, Lu JC, Shu YC, Tseng WC, et al. Membranes of epitaxial-like packed, super aligned electrospun micron hollow poly(l-lactic acid) (PLLA) fibers. Eur Polym J. Elsevier Ltd; 2011;47(5):882–92.

130. Sarhan WA, Azzazy HME, El-Sherbiny IM. The effect of increasing honey concentration on the properties of the honey/polyvinyl alcohol/chitosan nanofibers. Mater Sci Eng C. Elsevier B.V.; 2016;67:276–84.

131. Alhusein N, Blagbrough IS, de Bank PA. Zein/polycaprolactone electrospun matrices for localised controlled delivery of tetracycline. Drug Deliv Transl Res. 2013;3(6):542–50.

132. Guarino V, Altobelli R, Cirillo V, Cummaro A, Ambrosio L. Additive electrospraying: A route to process electrospun scaffolds for controlled molecular release. Polym Adv Technol. 2015;26(12):1359–69.

133. Prabhakaran MP, Ghasemi-Mobarakeh L, Ramakrishna S. Electrospun Composite Nanofibers for Tissue Regeneration. J Nanosci Nanotechnol. 2011;11(4):3039–57.

134. Bosworth LA, Downes S. Electrospinning for tissue regeneration. Bosworth LA, Downes S, editors. Woodhead Pub; 2011. 409 p.

135. Kim TG, Lee DS, Park TG. Controlled protein release from electrospun biodegradable fiber mesh composed of poly(??-caprolactone) and poly(ethylene oxide). Int J Pharm. 2007;338(1–2):276–83.

136. Biomedical Textiles for Orthopaedic and Surgical Applications.

137. Lin J, Li C, Zhao Y, Hu J, Zhang LM. Co-electrospun nanofibrous membranes of collagen and zein for wound healing. ACS Appl Mater Interfaces. 2012;4(2):1050–7.

138. Allen-Hoffmann BL, Rooney PJ. Skin Tissue Engineering and Regenerative Medicine. In: Albanna MZ, Holmes IV JH, editors. Skin Tissue Engineering and Regenerative Medicine. Academic Press; 2016. p. 265–87.

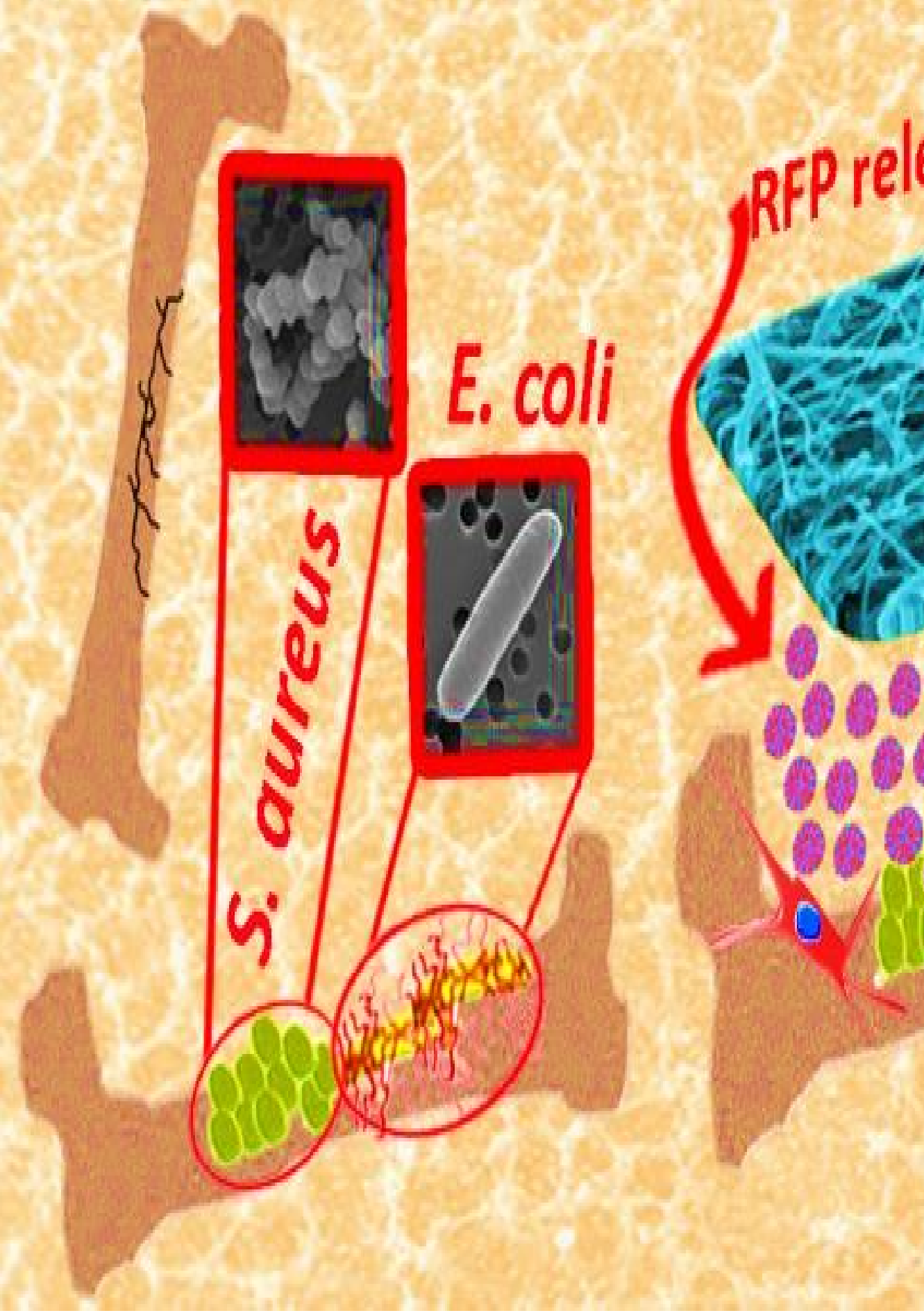
RFP rele
E. coli
S. aureus

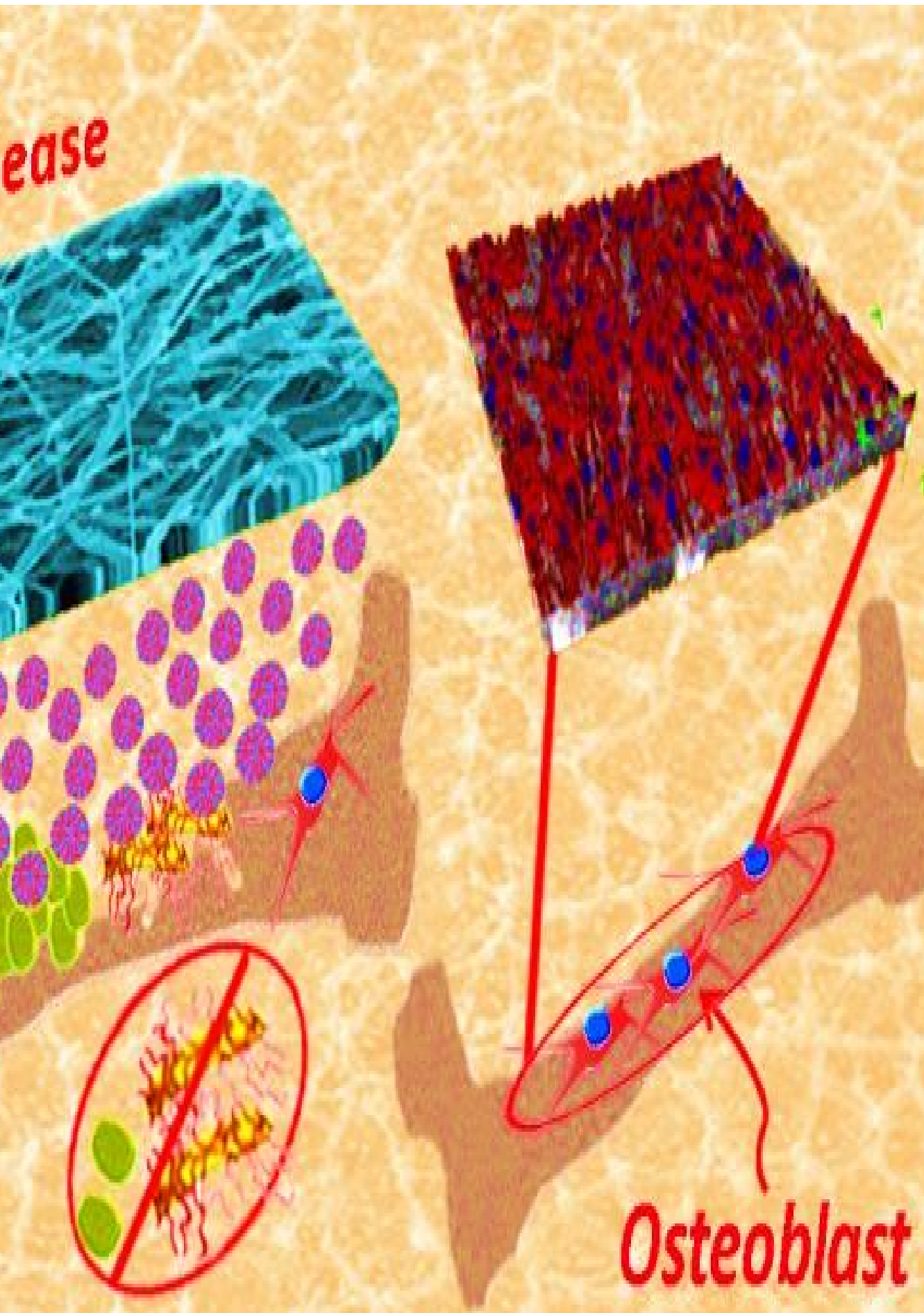
ease
Osteoblast

CHAPTER II

Composite membrane obtained by electro-hydrodynamic technique for infection prevention and treatment in bone repair

The contents of this chapter have been adapted from the following accepted work:

Composite scaffold obtained by electro-hydrodynamic technique for infection prevention and treatment in bone repair. Javier Aragón, Sergio Feoli, Silvia Irusta, Gracia Mendoza. **International Journal of Pharmaceutics** 2018.

"Bone infection is a devastating condition resulting from implant or orthopaedic surgery. Therapeutic strategies are extremely complicated and may result in serious side effects or disabilities. The development of enhanced 3D membranes, able to promote efficient bone regeneration, combined with targeted antibiotic release to prevent bacterial colonization, is a promising tool for the successful repair of bone defects. Herein, polymeric electrospun membranes composed of polycaprolactone (PCL) nanofibres coated with poly(lactic-co-glycolic acid) (PLGA) particles loaded with rifampicin were fabricated to achieve local and sustained drug release for more efficient prevention and treatment of infection. The release profile showed an initial burst of rifampicin in the first six hours, enabling complete elimination of bacteria. Sustained and long-term release was observed until the end of the experiments (28 days), facilitating a prolonged effect on the inhibition of bacterial growth, which is in agreement with the common knowledge concerning the acidic degradation of the microparticles. In addition, bactericidal effects against gram negative (Escherichia coli) and gram positive (Staphylococcus aureus) bacteria were demonstrated at concentrations of released rifampicin up to 58 ppm after 24 h, with greater efficacy against S. aureus (13 ppm vs 58 ppm for E. coli). Cell morphology and cytocompatibility studies highlighted the suitability of the fabricated membranes to support cell growth, as well as their promising clinical application for bone regeneration combined with prevention or treatment of bacterial infection."

INDEX

II.1 Introduction

Bone repair mediated by scaffold or substitute implantation such as is one of the most useful strategies in traumatology, orthopaedics, and maxillofacial surgery. Autologous bone graft implantation has been considered the main technique to successfully repair bone defects. However, in clinical practice, invasiveness at the donor site and inability to absorb large grafts are problematic (1–3).

Bone infection resulting from implantation or orthopaedic surgery is a serious complication characterized by an inflammatory reaction and bone destruction (4,5). Although implant-associated infections in orthopaedics are relatively uncommon (2-5%), implant replacement and possible resulting disabilities have a high impact on the patient's quality of life and result in economic and clinical burden (6).

Most bone infections are caused by staphylococcal species, with *Staphylococcus aureus* being the most prevalent, though other microorganisms (i.e. *Pseudomonas aeruginosa*, *Escherichia coli*) may also be involved (5,7,8). Intervention to prevent these infections is critical in the first hours after surgery, as they often originate during the surgical procedure. Rifampicin (RFP) is effective against staphylococcal infections and efficient for treatment at any bacterial growth stage (i.e. exponential, stationary, intracellular) (9–11). Furthermore, RFP is also one of the most effective first-line drugs for the treatment of tuberculosis and its bone-related effects (i.e. osteomyelitis, bone destruction) (12).

Oral and systemic administration of antibiotics for the prophylaxis or treatment of bone infections can be ineffective due to low delivery and permeation of antibiotics into bone and the possible presence of bacterial biofilms (13–15). Therefore, the need for local treatments, characterized by an initial burst of antibiotics followed by a sustained release of an adequate drug dose to prevent any further

infection, seems to be imperative to successfully treat these pathologies(4,16).

Recently, the development of novel materials as scaffolds or membranes for bone regeneration has increased to provide therapeutic options for challenging bone pathologies, such as those resulting from trauma or tumour resection (1). These scaffolds are designed as templates to mimic the extracellular matrix, providing adequate mechanical and architectural features as well as osteoconductive and osteoinductive properties. Furthermore, the addition of biologically active molecules, such as growth factors or drugs, enhances their therapeutic potential for bone regeneration (17,18).

Several materials have been reported to promote bone repair. Specially, synthetic polymers, such as polylactic acid (PLA), polyglycolic acid (PGA), poly(lactic-co-glycolic acid) (PLGA), or polycaprolactone (PCL), facilitate control of the physico-chemical and mechanical features of the synthesised scaffolds (1,17,19). In particular, electrospun PCL fibres have been previously reported as highly mimetic of the extracellular matrix and promising for bone regeneration strategies, combining the versatility and simplicity of the electrospinning technique with the biocompatibility of PCL and its degradation products (18,20–22). Conversely, PLGA, an FDA-approved polymer, is widely used in biomedical applications, mainly in drug delivery and tissue engineering, due to its high biocompatibility and hydrolytic degradation to its biocompatible constituents PLA and PGA (23).

Objective

Antibiotic-loaded membranes for the *in situ* treatment of bone infection may provide targeted drug delivery and sustained release, resulting in sustained enhancement of osteogenic properties for the successful regeneration of bone. Furthermore, membranes eliminate the need for long-term oral and intravenous systemic multidrug administration, which results

in toxic side effects, low delivery to the target site, and low patient adherence to treatment (7,24–26).

Therefore, the objective of this work was to develop a polymeric multifunctional membrane composed of electrospun PCL fibers and electrosprayed RFP-loaded PLGA microparticles combining the features of targeted and sustained drug release with the efficient regeneration of bone.

II.2 Preparation of polymeric particles and membrane

II.2.1 PLGA particles production

PLGA particles were prepared by electrospray using a Yflow 2.2.D-500 electrospinner (Electrospinning Machines/R&D Microencapsulation, Spain). The following parameter settings were investigated to obtain the microparticles: polymer concentration (5, 7.5 and 10% w/w); feeding flow rate (0.5 and 1.0 mL/h); and distance from the tip to the collector (15 and 30 cm). PLGA (0.50, 0.77, and 1.05 g) was dissolved in 10 mL of DMF to obtain final concentrations of 5, 7.5 and 10%, respectively (w/w). RFP (55, 85, and 117 mg) was added to each PLGA solution at 10% (w/w) and stirred overnight at 4 °C. The solution was loaded into a 10 mL plastic syringe and fed through a needle connected to a positive power supply. The tip of the needle was fixed 15 or 30 cm above a rotating collection drum. The negative voltage power supply was connected to the collector, which was rotated at 100 rpm. Flow rates of 0.5 and 1.0 mL/h were investigated to optimize PLGA particle production.

II.2.2 Electrospun membranes production

PCL membranes decorated with PLGA particles loaded with RFP were also produced using a Yflow 2.2.D-500 electrospinner (Electrospinning Machines/R&D Microencapsulation, Spain) following the protocol described in previous studies (27). Two needles were used to obtain the PCL fibres (needle 1) and to electrospray the PLGA-RFP particles (needle 2). Through needle 1, a 7.5% PCL (w/w) in a DCM-DMF (1:1) mixture was fed at 1.5 mL/h, while a PLGA-RFP solution was fed at 1.0 mL/h through needle 2. Both needles were connected to a positive power supply at a voltage of 18.7 kV. The tips of the needles were fixed at 18 cm (needle 1) and 15 cm (needle 2) above a rotating collection drum at 100 rpm. The negative voltage power

supply (-3.3 kV) was connected to the collector. The production process required 8 h.

The characterization techniques and different evaluation methods are described in **Appendix 1**.

II.3 Results and discussion

II.3.1 Characterization of composite membranes

Composite membranes were fabricated by electrospinning to obtain PCL fibres containing PLGA-RFP particles, which were synthesized by electrospraying.

Table II.1. Parameters assayed to optimize the PLGA particle production regarding PLGA concentration, solution flux and distance to the collector. The diameter of the particles obtained (μm) and its percentage of dispersion are also shown.

Polymer concentration %	Flow rate (mL/h)	Distance (cm)	Particle diameter (μm)	Dispersion (%)
5	0.5	15	1.1 ± 0.5	48.15
	1.0	15	1.1 ± 0.5	41.67
	0.5	30	1.5 ± 0.5	35.86
	1.0	30	0.9 ± 0.3	35.23
7.5	0.5	15	1.3 ± 0.3	35.23
	1.0	15	1.3 ± 0.4	27.82
	0.5	30	1.4 ± 0.5	38.52
	1.0	30	1.1 ± 0.4	37.72
10	0.5	15	1.3 ± 0.6	46.40
	1.0	15	1.1 ± 0.5	44.86
	0.5	30	1.6 ± 0.6	37.10
	1.0	30	2.0 ± 1.0	57.80

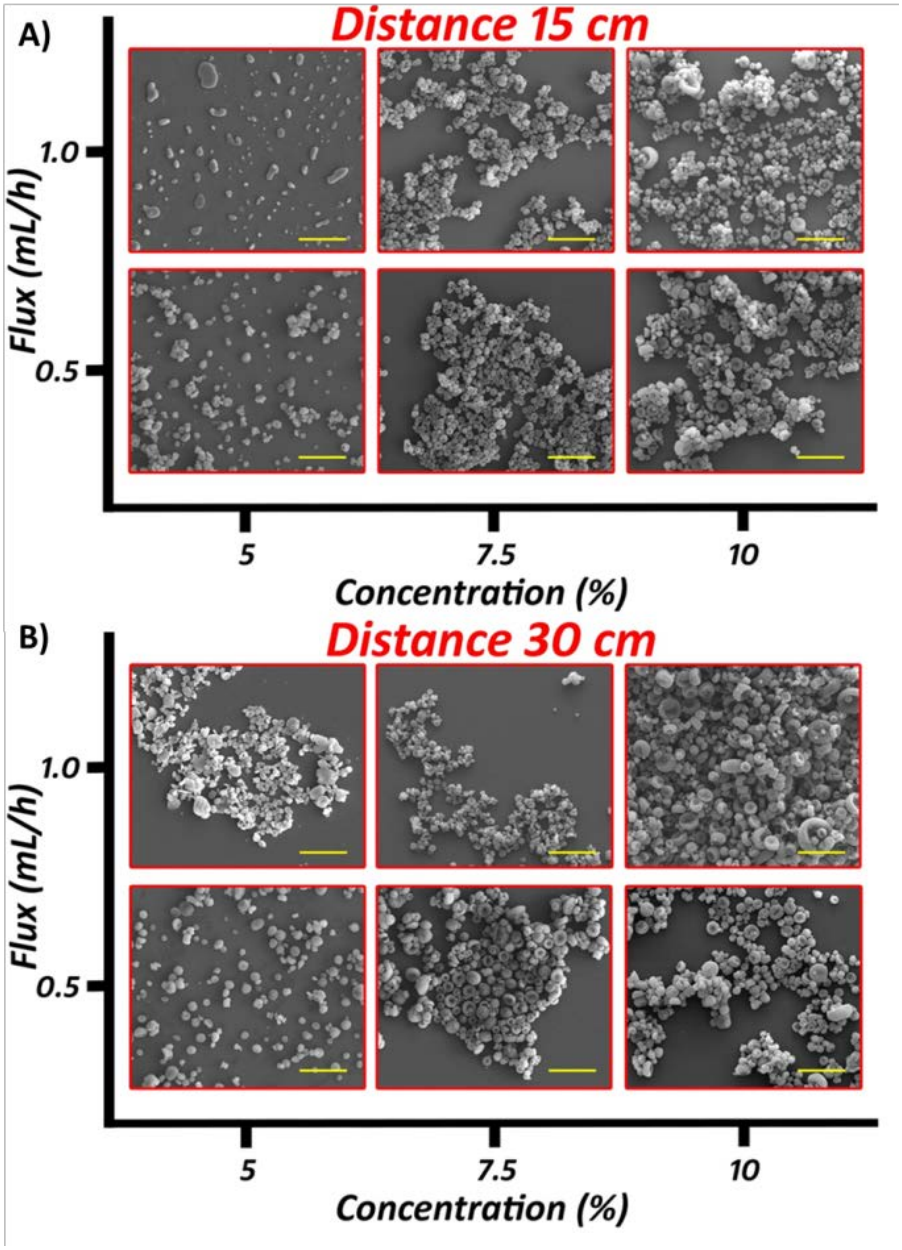

Figure II.1. SEM micrographs of PLGA particles obtained from each synthesis condition assayed: flux (mL/h), polymer concentration (% w/w) and distance from the tip to the collector (A = 15 cm; B = 30 cm). Scale bar = 10 μm.

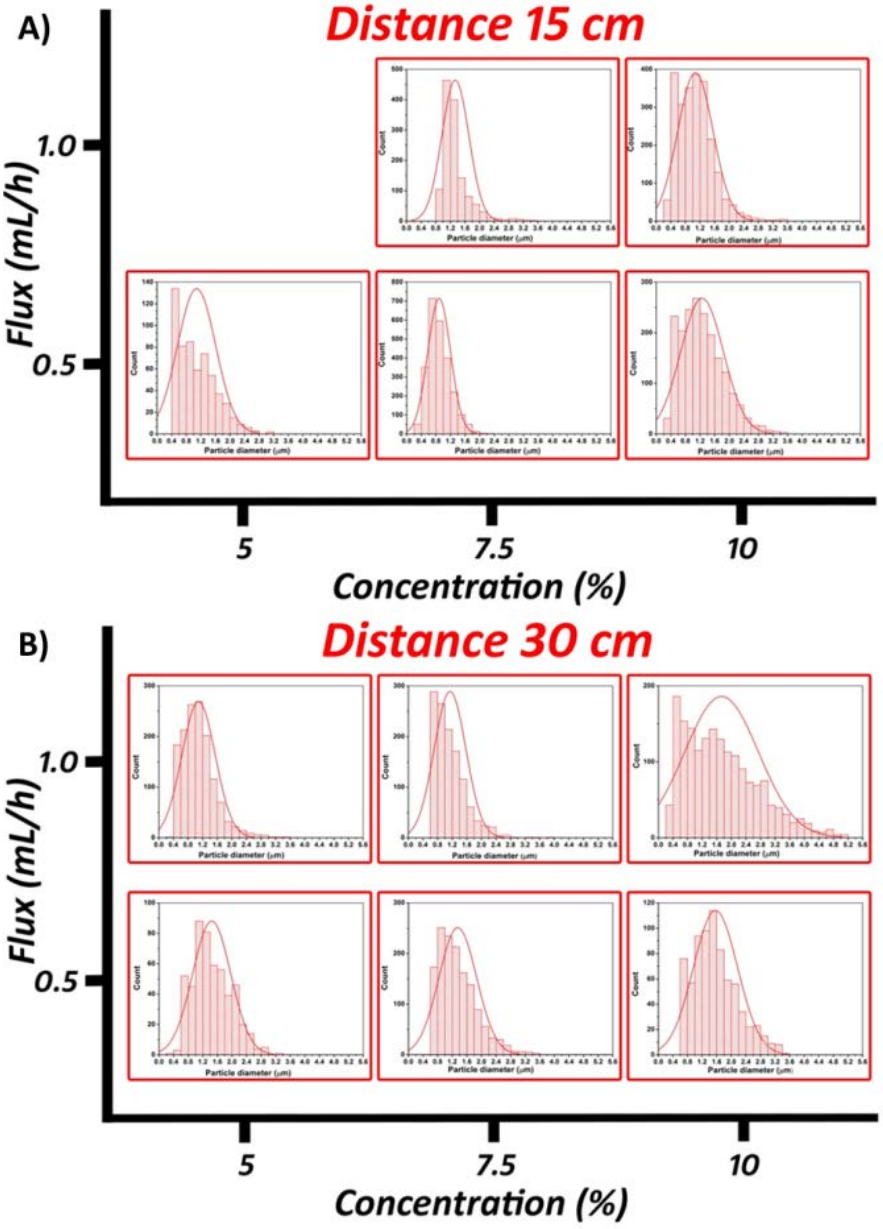

Figure II.2. Histograms of PLGA particle diameter obtained from each synthesis condition assayed: flux (mL/h), polymer concentration (% w/w) and distance from the tip to the collector (A = 15 cm; B = 30 cm).

Different conditions were evaluated to determine their effects on PLGA-RFP particle fabrication and to optimize their synthesis. These

conditions included the polymer concentration (5, 7.5 and 10% w/w), flow rate (0.5 and 1.0 mL/h), and distance from the tip to the collector (15 and 30 cm). The results obtained regarding particle diameter and morphology, and the percentage of size distribution, as functions of the different synthesis conditions evaluated, are detailed in Table II.1 and also shown in Figures II.1, II.2 and II.3.

Modification of synthesis conditions resulted in low variation of the mean particle diameter, producing microparticles with mean diameters around 1 μm. However, the highest mean diameter (2 μm) was obtained when the polymer concentration was also the highest (10%), though these particles had the highest size dispersion percentage (57.8%) (Table II.1).

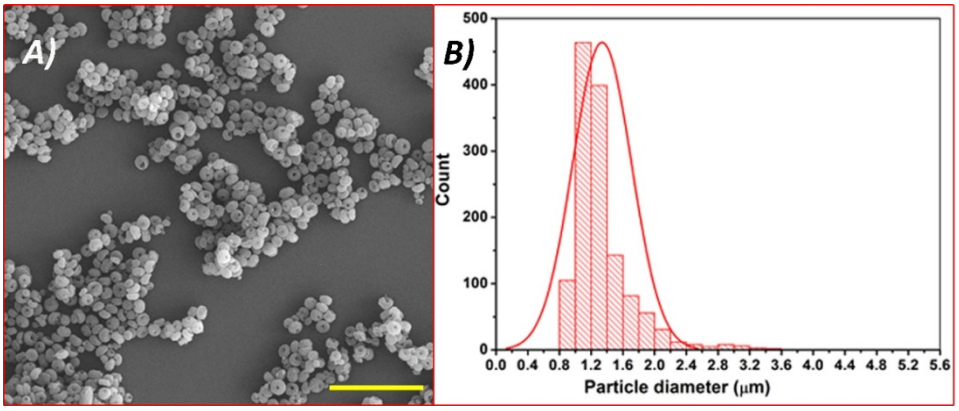

Figure II.3. SEM image of the electrosprayed PLGA-RFP particles obtained at a flux of 1.0 mL/h, 7.5% PLGA concentration, and a distance of 15 cm from the tip to the collector, scale bar = 10 μm.; b) histogram of the particle size distribution.

The best results were obtained when the polymer concentration was 7.5% (w/w), the electrospray flux was 1.0 mL/h, and the distance from the tip to the collector was 15 cm. As shown in the SEM images (Figure II.1 and II.3), PLGA-RFP particles fabricated at the optimized conditions exhibited homogeneous morphology and the lowest percentage of dispersion of mean diameter (27.82 %; Table II.1 and Figure II.2). The histogram depicted a group of particles with diameters in the range of 0.8-2.0 μm, with a mean diameter of 1.3 ± 0.4 μm, though some larger particles were present (~3 μm diameter). However, use of the same flux and tip-collector distance with the

lowest polymer concentration (5%) did not produce well-defined particles (Figure II.1) and a mean diameter could not be calculated (Figure II.2).

After particle synthesis optimization, the composite membranes were fabricated by simultaneous electrospray-electrospinning (Fig. II.4). The optimized membranes showed homogenous morphology and particle distribution. PCL nanofibres showed a mean diameter of 477 ± 246 nm (Fig. II.4A), while fibres with PLGA-RFP particles attached had a mean diameter of 678 ± 381 nm (Fig. II.4B). Attached PLGA-RFP particles had a mean diameter of 1.1 ± 0.2 μm (19% of size dispersion). The fabricated multifunctional membrane was characterized by a porous network with a large surface area-to-volume ratio, which is an essential condition for cell adhesion and proliferation and, therefore, adequate for bone regeneration. Absorbance measurements determined an RFP concentration loaded onto the synthesized membrane of 2 ± 1 wt% (encapsulation efficiency of 57 ± 26%).

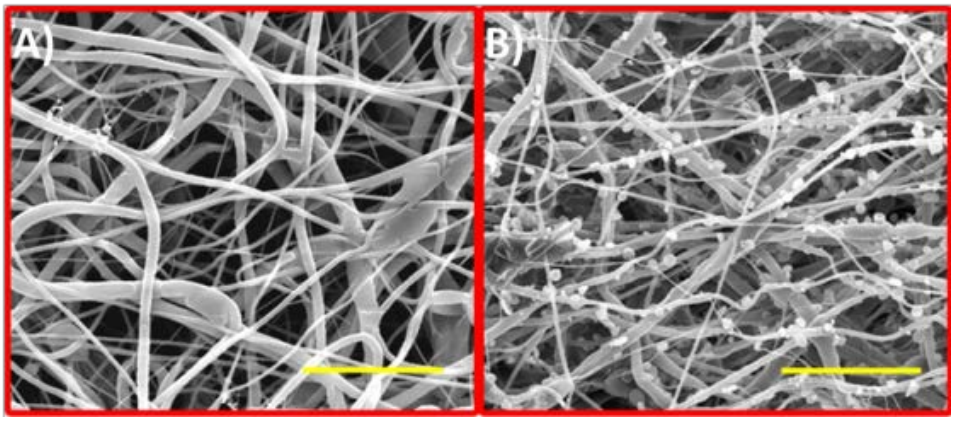

Figure II.4. SEM images of electrospun PCL fibres (A) and the PCL membranes containing electrosprayed PLGA-RFP particles (B) at a flux of 1.0 mL/h, 7.5% PLGA concentration, and a distance of 15 cm from the tip to the collector. Scale bar = 10 μm.

Bone scaffolds in shape of membranes are expected to have enough mechanical resistance to support cell expansion and tissue regeneration, and should be able to withstand manipulation. The mechanical properties of the membranes with and without RFP are described in Table II.2, showing no significant differences between the types of membranes. These results are in agreement with previous studies regarding PCL electrospun membranes for bone regeneration applications (28).

Table II.2. Mechanical properties of the electrospun membranes.

Condition	PCL/PLGA	PCL/PLGA-RFP
Tensile strength (MPa)	2.4 ± 0.6	2.6 ± 0.7
Young´s Module (MPa)	9.0 ± 4.0	8.0 ± 2.0
Strain at break (%)	140.0 ± 20.0	150.0 ± 30.0

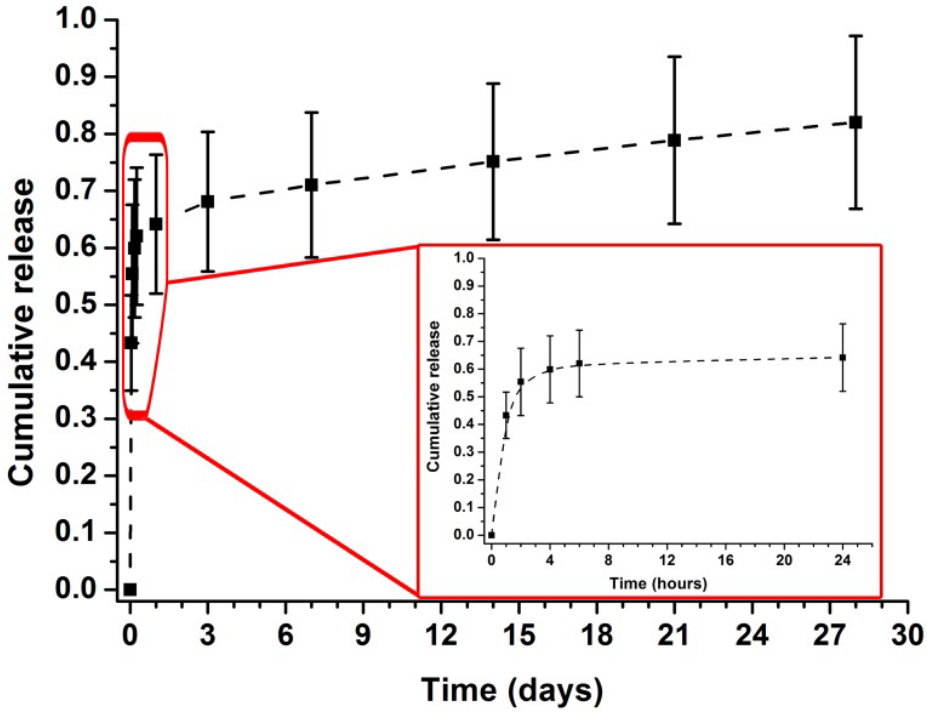

Figure II.5. Rifampicin release profile obtained from the composite membranes until the end of the experiments (28 days). The inset details the drug release for the first 24 h.

The release profile of RFP was evaluated until the end of the experiments (28 days; Fig. II.5). Antibiotic release from the composite membranes displayed a sharp initial burst within the first 6 h, with the majority released within the first hour, followed by sustained release until 28 days. In contrast, previous studies evaluating electrospun PCL membranes directly loaded with RFP showed drug release up to 8 h (29). In our study, at

the end of the experiments (28 days), the total RFP released was 82% of the loaded drug in the membranes. The initial burst and the subsequent long-term sustained release is applicable to bone infection-control, allowing adequate regeneration of bone while avoiding the impairment of bone repair (4,16).

II.3.2 MIC and MBC determination

The bactericidal effects of the fabricated composite membranes were tested against *E. coli S17* (gram negative) and *S. aureus* (gram positive). The membrane masses evaluated were calculated to evaluate RFP concentrations in the range of 0.5-90 ppm (0.5, 1, 5, 10, 15, 20, 25, 30, 45, 60, 75, and 90 ppm).

The effects observed were significantly different between gram negative and gram positive bacteria, with MIC values of 75 ppm in *E. coli* and 5 ppm in *S. aureus*, which corresponds to 48 ppm and 3 ppm of released RFP in 24 h, respectively. These differences were consistent with MBC values, in which 90 ppm of loaded RFP (58 ppm of released RFP in 24 h) was needed to completely eliminate *E. coli*, whereas 20 ppm (13 ppm of released RFP in 24 h) was enough to eradicate *S. aureus*. These values are higher than reported RFP serum levels (1-6 μg/mL) after administration of the maximum recommended therapeutic dosage (450-600 mg/day) for the treatment of bone infection and tuberculosis (30–32). Therefore, the fabricated membranes were able to successfully release a therapeutically effective amount of RFP directly into the target tissue, avoiding acid degradation and kidney and liver clearance of RFP after oral administration. Furthermore, side effects resulting from oral administration are not relevant with local administration (33). Moreover, according to our results, the required concentration of RFP to eradicate bacteria (13-58 ppm released in 24 h) was also achieved in the release assays as reported above (96-116 ppm in 24 h), highlighting the potential of these membranes to achieve their clinical purpose.

RFP is a wide antibacterial spectrum antibiotic with a bactericidal mechanism of action mediated by inhibition of bacterial RNA polymerase. Different sensitivities of gram negative and gram positive bacteria to RFP treatment have been previously demonstrated, and were not attributed to

differences in polymerases, but to the better penetrability of RFP through gram positive cell walls than through gram negative outer membranes (34).

II.3.3 *In vitro* cell studies

Human osteoblasts were seeded onto RFP-loaded composite membranes to evaluate cell adhesion, proliferation, and morphology by SEM and confocal microscopy (Figures II.6 and II.7). Both types of membranes assayed (PCL-PLGA and PCL-PLGA-RFP) showed adhesion and homogeneous distribution of HOBs on the membrane surface. Cell proliferation was also demonstrated as the surface was completely covered by HOBs at the end of the experiments (28 days), though PCL-PLGA-RFP membranes had lower cell density on their surface, pointing to possible toxicity mediated by RFP.

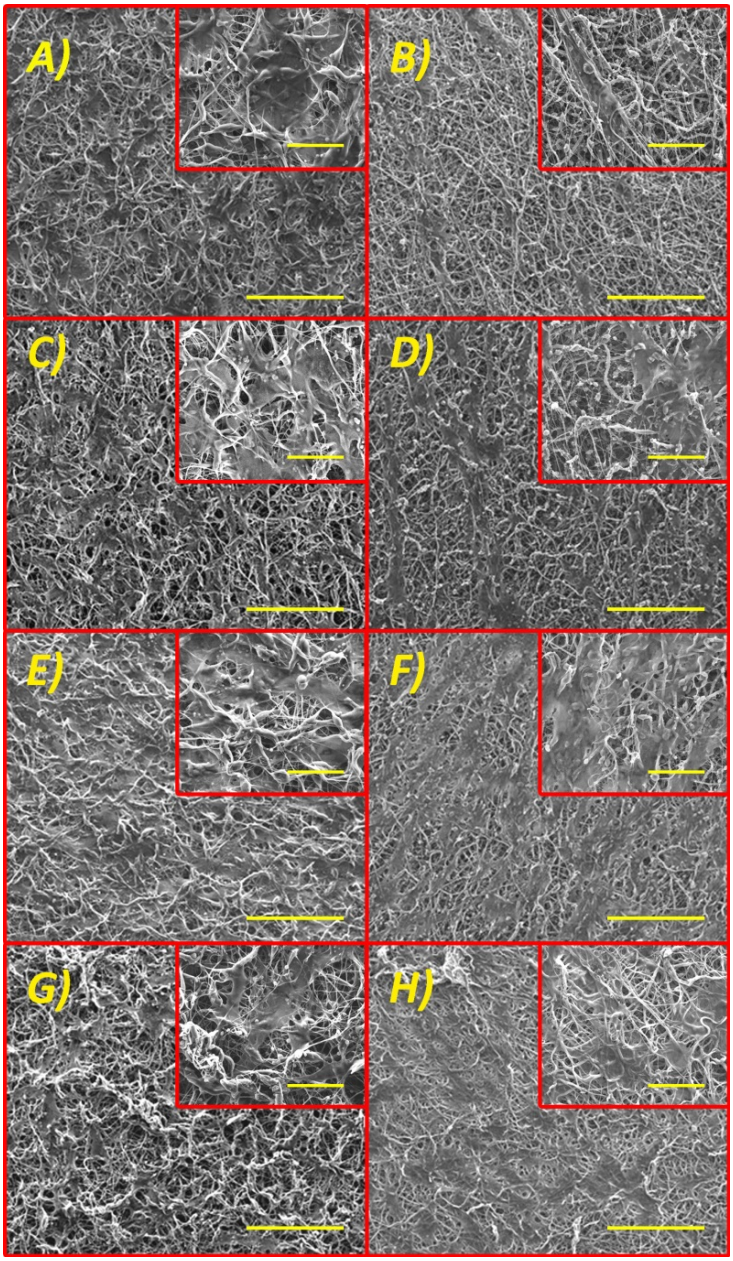

Figure II.6. Cell proliferation on rifampicin-loaded membranes (B, D, F, H) and on PCL-PLGA membranes (A, C, E, G) at different time points: 3 days (A, B), 7 days (C, D), 14 days (E, F), and 28 days (G, H). Cell structure is apparent when the fibre morphology is blurred due to cell growth on the fibres. Scale bar = 100 µm; Inset scale bar = 30 µm.

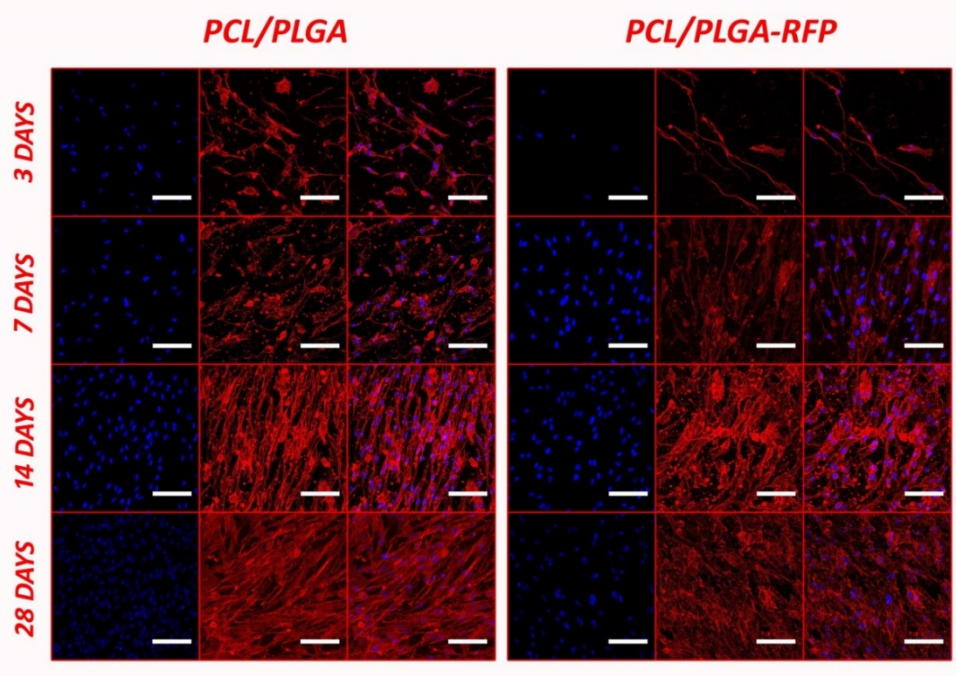

Figure II.7. Cell morphology and proliferation on PCL-PLGA membranes (left panel) and on rifampicin-loaded PCL-PLGA (RFP) membranes (right panel) at the time points studied. Nuclei are stained in blue (left column in each panel) and cytoskeleton in red (medium column in each panel). The last column in each panel displays the merge images. Scale bar = 100μm.

MTT assays (Figure II.8) confirmed the growth pattern of HOBs on RFP-loaded membranes, showing slightly lower viability when the antibiotic was present, in accordance with previous studies that reported decreased cell viability after treatment with free RFP at similar drug concentrations (≤100 μg/mL vs 96-148 μg/mL RFP released from our membranes) (26). At the end of the experiments (28 days), cell viability was not different between 2D cultures and 3D cultures on RFP-loaded membranes, whereas 3D cell cultures exerted higher viability percentages, highlighting the effect of RFP on cell proliferation and the 3D effect on cell growth. However, the effect of RFP may not be considered relevant to cell growth as the membrane surface was completely covered by HOBs after 28 days, pointing to their suitability for bone regeneration purposes.

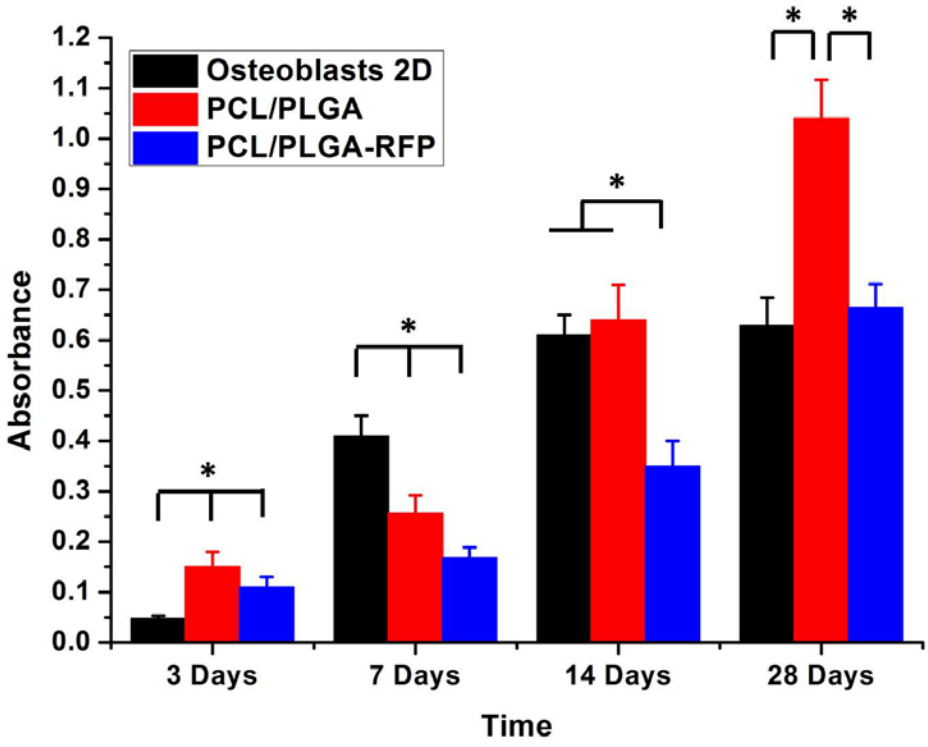

Figure II.8. Cell viability of human osteoblasts seeded on a 2D system and on the two types of membranes assayed, PCL-PLGA and rifampicin (RFP)-loaded membranes, at the time points studied. Data are represented as absorbance values (mean ± SD; n = 9). Statistically significant differences between groups were considered when $p \leq 0.01$.

II.4 Conclusions

A polymeric multifunctional membrane was developed combining electrospun PCL nanofibres with electrosprayed RFP-PLGA microparticles for bone repair and prevention or treatment of bone infection. The RFP membrane load was 2 ± 1 wt% with an encapsulation efficiency of 57%. The synthesized membrane showed a porous network with a homogeneous distribution of RFP-PLGA microparticles (around 1 μm diameter). An initial burst of RFP release was followed by sustained release until the end of the experiments, reaching 82% release of the loaded drug. This release profile is suitable for clinical application, as bone infection is initially controlled by the burst, with sustained release providing prophylaxis to avoid bone reinfection. Microbiological studies supported the potential of the fabricated membranes for bone infection treatment, as concentrations ≤58 ppm were able to eliminate *E. coli* and *S. aureus* and are in the range of the serum therapeutic dosages clinically recommended. Moreover, HOBs seeded on these membranes proliferated and completely colonized the surface. We thus have demonstrated that our membranes are potential candidates for bone repair when infection may impair regeneration of the tissue, though further studies regarding the *in vivo* efficacy of the fabricated membranes against bone infection should be conducted to fully understand their suitability for the intended clinical application.

References

1. Ghassemi T, Shahroodi A, Ebrahimzadeh MH, Mousavian A, Movaffagh J, Moradi A. Current Concepts in Scaffolding for Bone Tissue Engineering. Arch bone Jt Surg. 2018;6(2):90–9.

2. Weisz RD, Errico TJ. Spinal infections. Diagnosis and treatment. Bull Hosp Jt Dis. 2000;59(1):40–6.

3. Dong J, Zhang S, Liu H, Li X, Liu Y, Du Y. Novel alternative therapy for spinal tuberculosis during surgery: reconstructing with anti-tuberculosis bioactivity implants. Expert Opin Drug Deliv. 2014 Mar;11(3):299–305.

4. Rumian Ł, Tiainen H, Cibor U, Krok-Borkowicz M, Brzychczy-Włoch M, Haugen HJ, et al. Ceramic scaffolds enriched with gentamicin loaded poly(lactide- co -glycolide) microparticles for prevention and treatment of bone tissue infections. Mater Sci Eng C. 2016 Dec;69:856–64.

5. Arciola CR, Campoccia D, Speziale P, Montanaro L, Costerton JW. Biofilm formation in Staphylococcus implant infections. A review of molecular mechanisms and implications for biofilm-resistant materials. Biomaterials. Elsevier; 2012 Sep;33(26):5967–82.

6. Darouiche RO. Treatment of Infections Associated with Surgical Implants. N Engl J Med. Massachusetts Medical Society ; 2004 Apr;350(14):1422–9.

7. Johnson CT, García AJ. Scaffold-based anti-infection strategies in bone repair. Ann Biomed Eng. NIH Public Access; 2015 Mar;43(3):515–28.

8. Andrés NC, Sieben JM, Baldini M, Rodríguez CH, Famiglietti Á, Messina P V. Electroactive Mg2+-Hydroxyapatite Nanostructured Networks against Drug-Resistant Bone Infection Strains. ACS Appl Mater Interfaces. 2018;10(23):19534–44.

9. Frippiat F, Meunier F, Derue G. Place of newer quinolones and rifampicin in the treatment of Gram-positive bone and joint infections. J Antimicrob Chemother. Oxford University Press; 2004 Dec;54(6):1158–1158.

10. Sanz-Ruiz P, Carbó-Laso E, Del Real-Romero JC, Arán-Ais F, Ballesteros-Iglesias Y, Paz-Jiménez E, et al. Microencapsulation of rifampicin: A technique to preserve the mechanical properties of bone cement. J Orthop Res. Wiley-Blackwell; 2017 Jun;36(1):459–66.

11. Trampuz A, Widmer AF. Infections associated with orthopedic implants. Curr Opin Infect Dis. 2006 Aug;19(4):349–56.

12. Raviglione MC, Gupta R, Dye CM, Espinal MA. The burden of drug-resistant tuberculosis and mechanisms for its control. Ann N Y Acad Sci. 2001 Dec;953:88–97.

13. Flores C, Degoutin S, Chai F, Raoul G, Hornez J-C, Martel B, et al. Gentamicin-loaded poly(lactic-co-glycolic acid) microparticles for the prevention of maxillofacial and orthopedic implant infections. Mater Sci Eng C. 2016 Jul;64:108–16.

14. Furustrand Tafin U, Betrisey B, Bohner M, Ilchmann T, Trampuz A, Clauss M. Staphylococcal biofilm formation on the surface of three different calcium phosphate bone grafts: a qualitative and quantitative *in vivo* analysis. J Mater Sci Mater Med. 2015 Mar;26(3):130.

15. Zhu M, Li K, Zhu Y, Zhang J, Ye X. 3D-printed hierarchical scaffold for localized isoniazid/rifampin drug delivery and osteoarticular tuberculosis therapy. Acta Biomater. Elsevier; 2015 Apr;16:145–55.

16. Gimeno M, Pinczowski P, Pérez M, Giorello A, Martínez MÁ, Santamaría J, et al. A controlled antibiotic release system to prevent orthopedic-implant associated infections: An *In vitro* study. Eur J Pharm Biopharm. 2015 Oct;96:264–71.

17. Dorati R, DeTrizio A, Modena T, Conti B, Benazzo F, Gastaldi G, et al. Biodegradable Scaffolds for Bone Regeneration Combined with Drug-Delivery Systems in Osteomyelitis Therapy. Pharmaceuticals. 2017 Dec;10(4):96.

18. Porter JR, Ruckh TT, Popat KC. Bone tissue engineering: A review in bone biomimetics and drug delivery strategies. Biotechnol Prog. 2009;25(6):1539–60.

19. Liu X, Ma PX. Polymeric scaffolds for bone tissue engineering. Ann

Biomed Eng. 2004 Mar;32(3):477–86.

20. Aragon J, Navascues N, Mendoza G, Irusta S. Laser-treated electrospun fibers loaded with nano-hydroxyapatite for bone tissue engineering. Int J Pharm. 2017 Jun;525(1):112–22.

21. Baker SR, Banerjee S, Bonin K, Guthold M. Determining the mechanical properties of electrospun poly-ε-caprolactone (PCL) nanofibers using AFM and a novel fiber anchoring technique. Mater Sci Eng C. 2016 Feb;59:203–12.

22. Song W, Yu X, Markel DC, Shi T, Ren W. Coaxial PCL/PVA electrospun nanofibers: Osseointegration enhancer and controlled drug release device. Biofabrication. 2013 Sep;5(3):35006.

23. Makadia HK, Siegel SJ. Poly Lactic-co-Glycolic Acid (PLGA) as Biodegradable Controlled Drug Delivery Carrier. Polymers (Basel). NIH Public Access; 2011 Sep;3(3):1377–97.

24. Zhu M, Wang H, Liu J, He H, Hua X, He Q, et al. A mesoporous silica nanoparticulate/β-TCP/BG composite drug delivery system for osteoarticular tuberculosis therapy. Biomaterials. 2011 Mar;32(7):1986–95.

25. Yang Y, Yang S, Wang Y, Yu Z, Ao H, Zhang H, et al. Anti-infective efficacy, cytocompatibility and biocompatibility of a 3D-printed osteoconductive composite scaffold functionalized with quaternized chitosan. Acta Biomater. 2016 Dec;46:112–28.

26. Yuan J, Wang B, Han C, Lu X, Sun W, Wang D, et al. *In vitro* comparison of three rifampicin loading methods in a reinforced porous β-tricalcium phosphate scaffold. J Mater Sci Mater Med. Springer US; 2015 Apr;26(4):174.

27. Aragón J, Salerno S, Bartolo L De, Irusta S, Mendoza G. Polymeric electrospun scaffolds for bone morphogenetic protein 2 delivery in bone tissue engineering. J Colloid Interface Sci. 2018;

28. Heydari Z, Mohebbi-Kalhori D, Afarani MS. Engineered electrospun polycaprolactone (PCL)/octacalcium phosphate (OCP) scaffold for bone tissue engineering. Mater Sci Eng C. 2017 Dec;81:127–32.

29. Ruckh TT, Oldinski RA, Carroll DA, Mikhova K, Bryers JD, Popat KC. Antimicrobial effects of nanofiber poly(caprolactone) tissue scaffolds releasing rifampicin. J Mater Sci Mater Med. 2012 Jun;23(6):1411–20.

30. Roth B. Penetration of Parenterally Administered Rifampicin into Bone Tissue. Chemotherapy. 1984;30(6):358–65.

31. van Ingen J, Aarnoutse RE, Donald PR, Diacon AH, Dawson R, Plemper van Balen G, et al. Why Do We Use 600 mg of Rifampicin in Tuberculosis Treatment? Clin Infect Dis. Oxford University Press; 2011 May;52(9):e194–9.

32. Mehta JB, Shantaveerapa H, Byrd RP, Morton SE, Fountain F, Roy TM. Utility of rifampin blood levels in the treatment and follow-up of active pulmonary tuberculosis in patients who were slow to respond to routine directly observed therapy. Chest. 2001 Nov;120(5):1520–4.

33. Singh H, Bhandari R, Kaur IP. Encapsulation of Rifampicin in a solid lipid nanoparticulate system to limit its degradation and interaction with Isoniazid at acidic pH. Int J Pharm. 2013 Mar;446(1–2):106–11.

34. Wehrli W. Rifampin: Mechanisms of Action and Resistance. Clin Infect Dis. Oxford University Press; 1983 Jul;5(Supplement_3):S407–11.

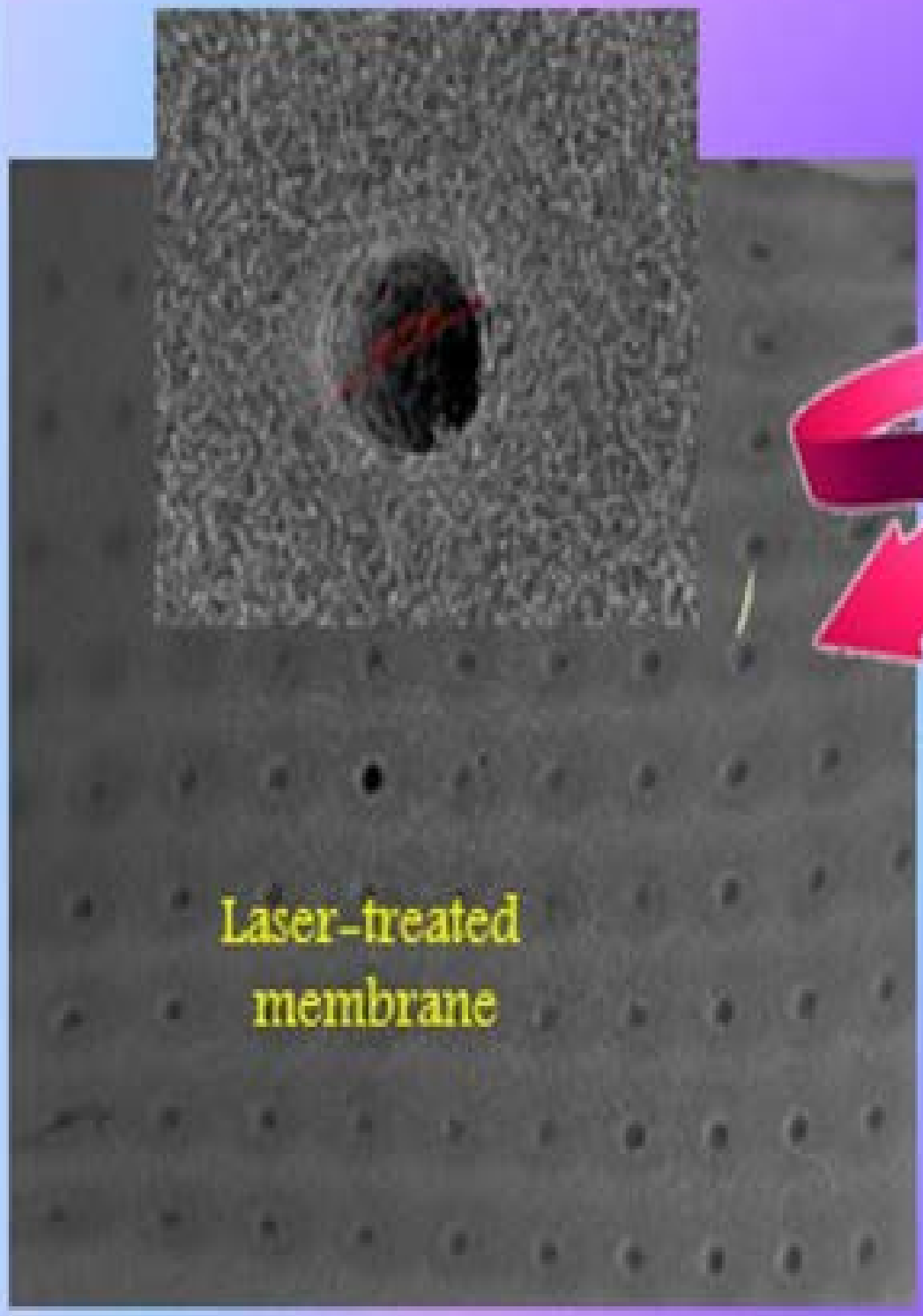
Laser-treated
membrane

eoblasts

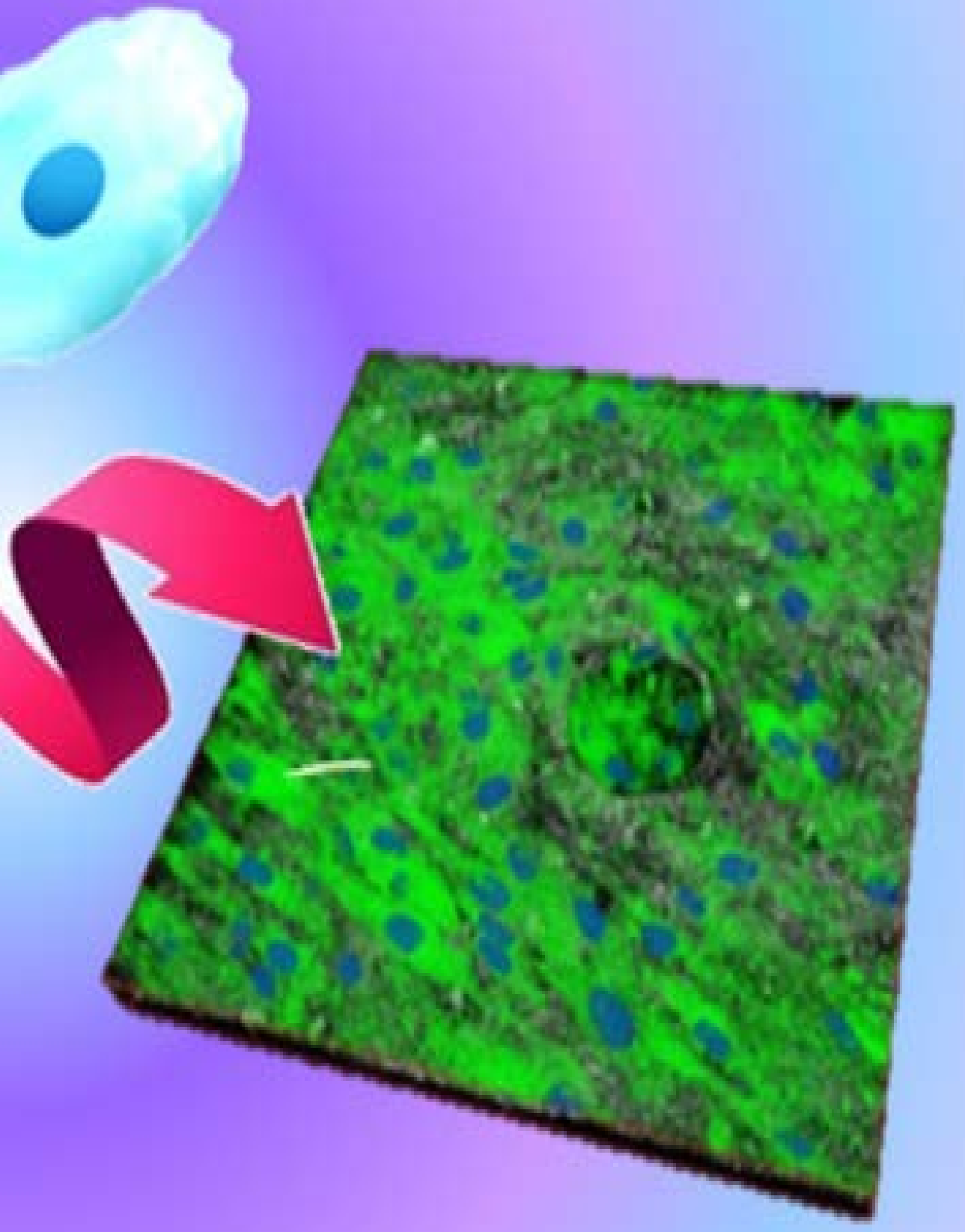

CHAPTER III

Laser-treated electrospun fibers loaded with nano-hydroxyapatite for bone tissue engineering

The contents of this chapter have been adapted from the following published work:

Laser-treated electrospun fibers loaded with nano-hydroxyapatite for bone tissue engineering. Javier Aragon, Nuria Navascues, Gracia Mendoza, Silvia Irusta. International Journal of Pharmaceutics 525,112–122, 2017.
DOI:10.1016/j.ijpharm.2017.04.022

"Core-shell polycaprolactone/polycaprolactone (PCL/PCL) and polycaprolactone/polyvinyl acetate (PCL/PVAc) electrospun fibers loaded with synthesized nanohydroxyapatite (HAn) were lased treated to create microporosity. The prepared materials were characterized by XRD, FTIR, TEM and SEM. Uniform and randomly oriented beadless fibrous structures were obtained in all cases. Fibers diameters were in the 150–300 nm range. Needle-like HAn nanoparticles with mean diameters of 20 nm and length of approximately 150 nm were mostly encase inside the fibers. Laser treated materials present micropores with diameters in the range 70–120 μm for PCL-HAn/PCL fibers and in the 50–90 μm range for PCL-HAn/PVAC material. Only samples containing HAn presented bioactivity after incubation during 30 days in simulated body fluid. All membranes presented high viability, very low mortality, and human osteoblast proliferation. Biocompatibility was increased by laser treatment due to the surface and porosity modification."

INDEX

III.1 Introduction

Scaffolds are specially designed biomaterials that provide a support for cell growth, migration and finally proliferation to allow tissue regeneration (1). In order to satisfy the required adhesion and proliferation of cells geometric factors are of great importance (2). The matrix architecture is vital for the success of bone tissue engineering which includes microstructure of scaffold, its porosity percentage and surface topography (3). Polymer nanofibers obtained by electrospinning mimic the bone extracellular matrix structure and the potential to enhance the osseointegration is very promising (4). They also exhibit high surface area to volume ratios favorable for cells and bioactive molecules attachment to the fibers surface. However, the small pore size of electrospun membranes hinders cell infiltration and ultimately reduces their use in replacing large tissues that require ample vascularization and nutrient diffusion (5). To promote cellular viability and extracellular matrix production, electrospun membranes with enhanced porosity or micro-scale pores could be beneficial since increasing porosity and pore size can provide a three-dimensional (3D) environment that not only facilitates cell seeding/diffusion but also provides better diffusion of nutrients and waste throughout the membranes (6).

Different techniques were studied to obtain electrospun materials with larger pores or higher porosity. Among them the addition of porogens during electrospinning and the posterior elimination by leaching were used (7). Collection in liquid increases the pore size but the fabrication is highly dependent on the surface tension, flow rate and weight fraction of the polymer solution (8). Another promising technique to improve electrospun materials porosity is the surface modification by laser technologies for membrane microstructuring. Laser has become an invaluable tool in processing and treating biological tissues due to its possibility of precise material processing with clean surfaces and reduced thermal damage. Pulsed laser ablation is a well-established universal tool for direct surface modification of almost all types of materials. Ultra-short laser pulses (picosecond and femtosecond) enable to obtain 3D microstructures with high precision, taking advantage of the “cold” ablation process (9). It was demonstrated that laser machining is an efficient technique to prepare patterning structures in electrospun polycaprolactone (PCL) membranes (10,11). It was found that electrospun poly(l-lactide) membranes with laser ablated holes exhibit significant better endothelial cell ingrowth (5).

McCullen et al. (12) used laser ablation on electrospun PCL membranes to favour the adhesion and growth of human adipose-derived stem cells. Electrospun PCL/β-TCP fibers were also treated by laser irradiation to obtain microsized pores (13). Beside the meaningful cellular activity the material showed enhanced compressive strength.

Naturally occurring polymers are well suited for various *in vivo* applications thanks to their ability to promote cell adhesion and growth. However, membranes fabricated by using these polymers could exhibit poor mechanical properties or fast degradation rates. Native proteins, such as collagen and fibrinogen, are also more expensive and more difficult to source than synthetic polymers (14). Among the synthetic available polymers used to fabricate three-dimensional (3D) membranes aliphatic polyesters undoubtedly represent so far the most extensive studied class, since they combine good physico-chemical and mechanical properties with assessed biocompatibility (15). Particularly PCL is a low cost, biocompatible polymer that has a slow degradation rate and distinct rheological and viscoelastic properties that make it suitable for specific long term implantation (14). Its compatibility with a wide range of drugs enables uniform drug distribution in the matrix and its long term degradation facilitates drug release up to several months (16). Polyvinyl acetate (PVAc) polymer has also been applied in many medical fields because of its strong biocompatibility. The hydrogels containing functional groups such as COOH that usually show good biocompatibility with blood, body fluids, and tissues (17). This inert polymer has the advantage that it does not induce a deleterious reaction in living tissue (18). Because of all these characteristics PVAc has been used in many medical fields, including drug and cell carries and in tissue engineering (19).

One important limitation in the use of synthetic biodegradable polymers as membrane materials is the lack of bioactivity, in particular for bone tissue applications (20). The main approach to develop bioresorbable and bioactive membranes is the addition of bioactive materials to the polymer matrix. Calcium phosphate ceramics have been extensively investigated to fabricate highly porous membranes to engineer bone due to their near similar composition of bone, including excellent biocompatibility, osteoinductive and osteoconductive properties (3). It has been found that the addition of hydroxyapatite (HA) not only enhances the tensile strength of PCL membranes but also acts as a chelating agent to accelerate the mineralization

of human fetal osteoblast cells to form bone-like apatite for bone tissue engineering (21).

Objective

The main objective of this work was to obtain a material with appropriate matrix architecture to favor cells adhesion and proliferation composed of biodegradable polymers, with mechanical resistance, good biocompatibility and high bioactivity. PCL/PVAc and PCL/PCL membranes with core-shell structure loaded with synthetic hydroxyapatite nanoparticles (HAn) to increase the bioactivity of the materials were fabricated by electrospinning. In addition, the prepared membranes were treated by laser ablation to create desired microscale topographical features in order to enhance cell adhesion and growth.

III.2 Synthesis of inorganic nanoparticles and electrospun membranes

III.2.1 Synthesis of hydroxyapatite nanoparticles

Synthesis of HA ($Ca_{10}(PO_4)_6(OH)_2$) nanoparticles was conducted as previously described (22). $CaCO_3$ was used as calcium sources, maintaining a Ca/P ratio of 1.67 during reaction in solution with 0.3 M H3PO4.

III.2.2 Preparation of electrospun membranes

Electrospun membranes were prepared using an Yflow 2.2.D-500 electrospinner (Coaxial Electrospinning Machines/R&D Microencapsulation, Malaga, Spain). PCL pellets were dissolved in DCM/DMF (1:1) and PVAc was dissolved in DMF, these solutions were stirred overnight at room temperature. To prepare PCL-HAn membranes, HAn powder was dispersed in DCM/DMF with the help of TWEEN® 80 by stirring overnight at room temperature, then this solution was added to the PCL solution and stirred overnight at room temperature. The polymers solutions were loaded into 20 mL plastic syringes. The PCL-HAn suspension was fed through the inner needle of the coaxial system and PCL or PVAc solutions were fed through the outer one. This last needle was connected to the positive voltage power supply, at a voltage ranging from 7 to 13 kV. The shell and core flow rates and the spinning distance were fixed to 0.5 mL/h (in both needles) and 19 cm respectively. The spun fibers were collected on a static plate (covered with

aluminum foil) connected to negative voltage power supply, at a voltage ranging from −2 to 4 kV for 18 h. To create macropores in the fibrous membranes structures, a pulse Nd:YAG laser (TECHNOLOGY Q-Switch) was used. Different conditions were used for each material: output power: 16 W, wavelength: 1064 nm for the PCL-HAn/PCL fibers and output power: 1 W, wavelength: 532 nm for PCL-HAn/PVAc fibers.

The characterization techniques and different evaluation methods are described in **Appendix 1**.

III.3 Results and discussion

III.3.1 Hydroxyapatite characterization

The XRD pattern for the synthesized HA nanoparticles is shown in Figure III.1a, it could be seen that all the peaks could be indexed to the hexagonal phase hydroxyapatite (JCPDS N° 09-0432). The diffractogram do not show any other peaks corresponding to secondary phases or intermediate compounds suggesting the formation of pure HAn phase. Intense diffraction peaks with broad width are indicative of the crystalline nature of the prepared material and the small crystallite size respectively (23). Inset of Figure III.1a shows the peaks corresponding to the (002) and (211) diffraction planes of hydroxyapatite. According to the JCPDS card 09-0432, the reference intensity ratio for (211), (002) is RI(211)/RI(002) = 2.61. The calculated degree of texture index (24) for the synthesized hydroxyapatite is 0.51 indicating a preferred growth orientation along the c-axis (25). These results are consistent with electronic microscope images (Figure III.1b and III.1c), which show fibrous needle-like particles with mean diameters of 20 nm and length of approximately 150 nm. The rod-like shape of the nanoparticles is more clearly seen in TEM images (Figure III.1c). The FTIR spectrum (Figure III.1.d) of the material presents the characteristic bands for PO_4^{3-} appearing at 472, 572 and 603 cm^{-1} related to the asymmetric bending, and signals assigned to symmetric and asymmetric stretching positioned in the 900-1200 cm^{-1} range (26). The broad peak around 3455 cm^{-1} is due to the adsorbed water on HAn structure and the absorption peak at 1635 cm^{-1} is attributed to the bending mode of OH^- groups (27). The absorption peak assigned to apatite hydroxyl bond is observed at 3569 cm^{-1} (28). The shoulder at 878 cm^{-1} together with the doublet at 1415 and 1458 cm^{-1} indicate the existence of CO_3^{2-} (29) probably

coming from the atmosphere carbon dioxide during sample preparation and would have been incorporated into the HAn crystal structure (30). All these results imply that the synthesis of rod-like shaped hydroxyapatite nanoparticles was successful.

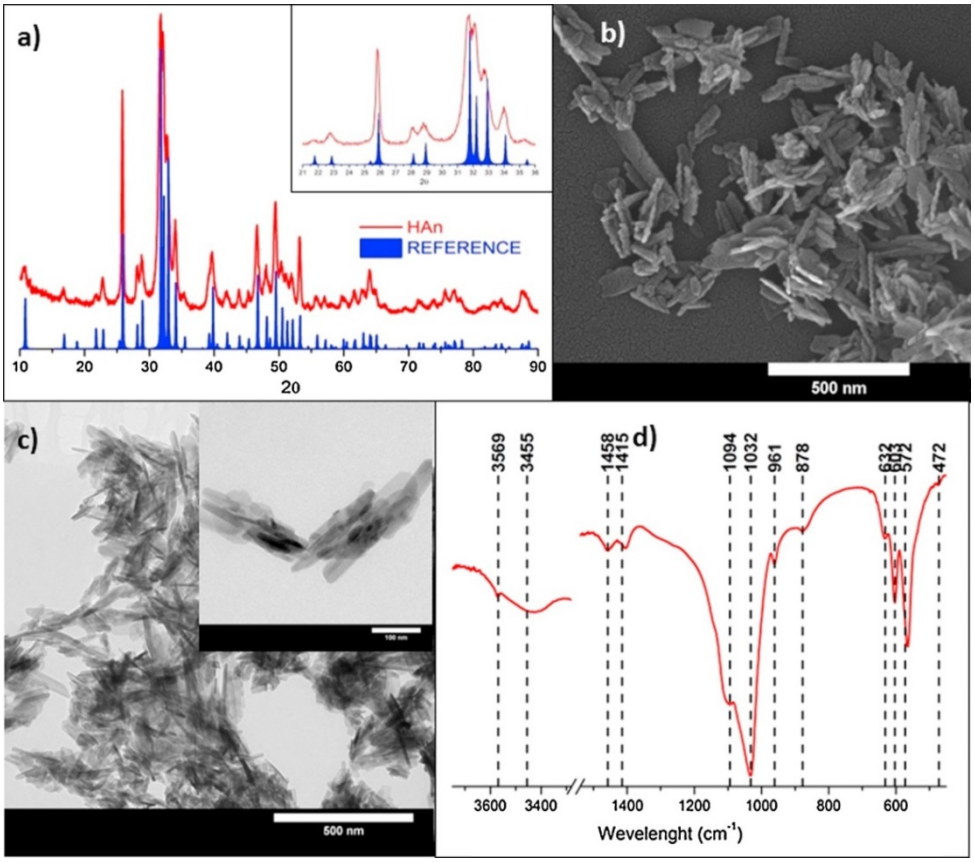

Figure III.1. Characterization of the synthesized HAn: a) XRD, b) SEM images, c) TEM micrographs, d) FTIR spectrum.

III.3.2 Membranes characterization

III.3.2.1 As spun membranes

The materials prepared by electrospinning are listed in Table III.1 together with positive and negative voltages applied. Due to the properties (viscosity, surface tension, conductivity) of the solutions the voltages

required to obtain a stable Taylor cone were higher to produce fibers containing hydroxyapatite than the voltages used for the pristine polymer fibers (Table III.1).

Table III.1. Preparations conditions and characterization results for the obtained electrospun membranes.

	Sample (Core/Shell)			
	PCL/PCL	**PCL-HAn/PCL**	**PCL/PVAc**	**PCL-HAn/PVAc**
Applied voltage -/+ (kv)	3.11/10.25	3.54/12.00	2.87/7.21	3.03/8.57
HAn load[a] (wt%)	-	(14.2) (13.8)	-	(11.9) (12.7)
Fiber diameter[b] (nm)	206±62	210±64	264±56	225±47
Porosity (%)	62.0	63.5	65.5	58.6
Pores diameter (nm)	232	210	209	188

[a] From TGA results, theoretical value between brackets.
[b] Obtained by measuring at least 100 fibers in different SEM images.

The HAn load in the fibers was measured by thermogravimetric analysis (TGA, Figure III.2) as the residue after complete polymers elimination at 600 °C (Table III.1). The experimental values of 13.8 and 12.7 wt% for PCL-HAn/PCL and PCL-HAn/PVAC respectively, were close to the theoretical ones (13.2 and 11.9 wt%). The HAn load used was the maximum possible to obtain a stable Taylor cone; higher amount of nanoparticles in the spinning solution increase excessively the viscosity and also hinder good nanoparticles dispersion.

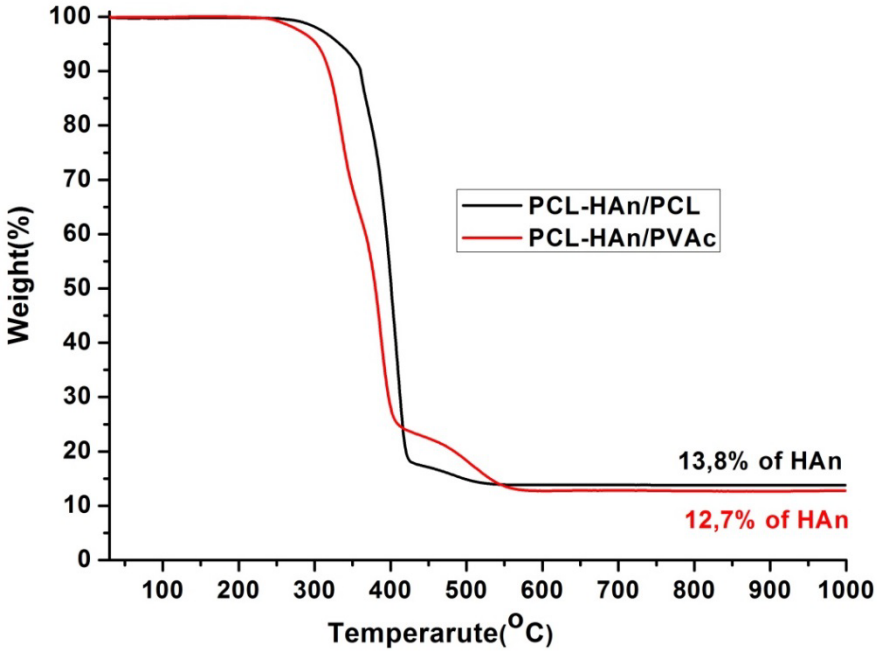

Figure III.2. TGA thermogram of PCL-HAn/PCL and PCL-HAn/PVAc fibers.

XRD patterns of fibers with HAn are shown in Figure III.3. The XRD diffractgram of PCL-Han/PCL exhibits peaks for both hydroxyapatite and PCL. Both the polymer and ceramic retain their crystalline behavior in the electrospun fibers indicating insignificant change in their crystal structure. This confirms the fact that HAn is finely and uniformly dispersed in the matrix (3). In PCL-HAn/PVAc pattern peaks at 25 and 35° establish the presence of hydroxyapatite incorporated in the membrane (inset of Figure III.3).

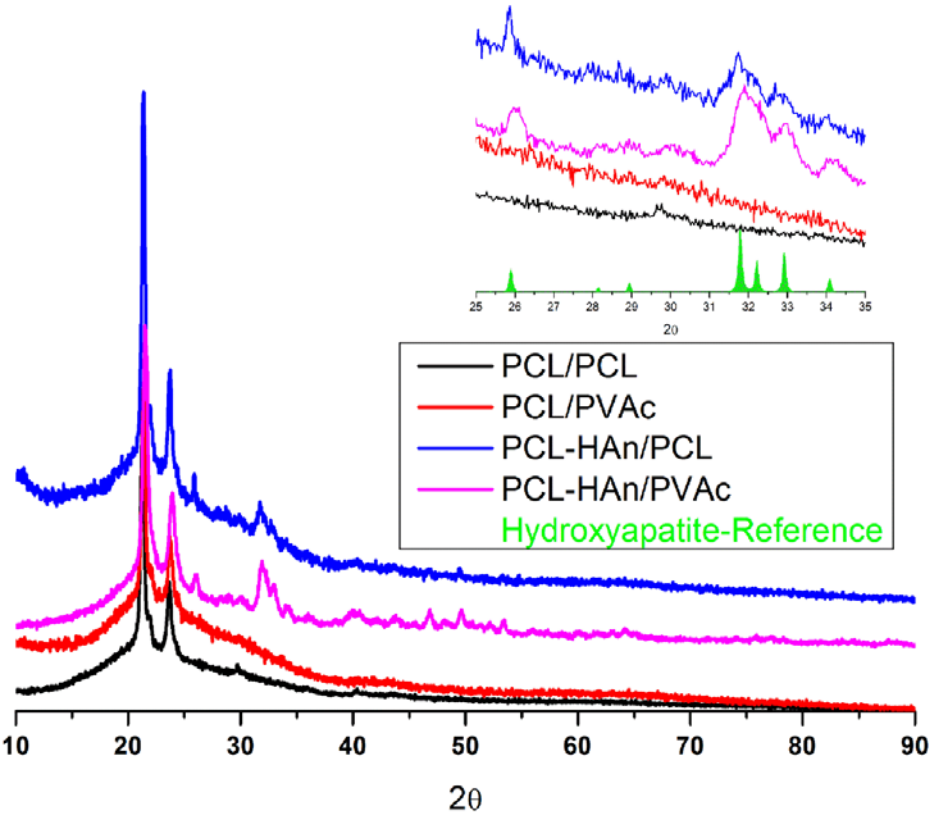

Figure III.3. XRD patterns of PCL/PCL, PCL/PVAc, PCL-HAn/PCL and PCL-HAn/PVAc fibers.

FE-SEM images of the electrospun membranes showed uniform, beadless and nano-scaled fibrous structures randomly oriented for all the prepared materials under the optimum spinning conditions utilized in each case. As an example Figure III.4a) shows SEM micrographs obtained for fibers with PCL in the core and in the shell. Hydroxyapatite nanoparticles are mostly encased inside the fibers, but some agglomerates are observed on the surface (Figure III.4b). The fibers average diameter was measured from SEM images (Table III.1). The presence of hydroxyapatite nanoparticles in the inner solution does not seem to have any effect on the PCL/PCL fiber diameter. It was previously observed for PCL fiber without defects, such as the obtained in this work, that for HA load higher than 5 wt% the average diameter was similar to the pristine fibers (31). This result for high mass fraction was attributed to the increased viscosity of the dispersion during electrospinning. For the PCL/PVAc material the presence of hydroxyapatite

leads to a slightly lower fibers mean diameter, probably due to the higher voltage needed to obtain a stable cone in the case of the hydroxyapatite loaded fibers (32).

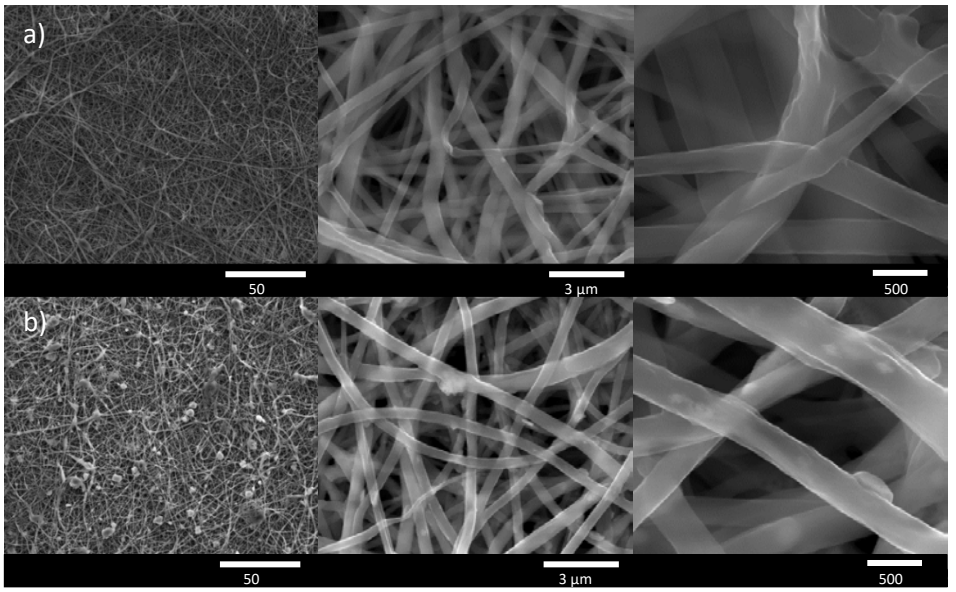

Figure III.4. SEM images of a) PCL/PCL fiber, b) PCL-HAn/PCL fibers.

The core-shell structure of the PCL/PVAc fibers was investigated by TEM microscopy as shown in Figure III.5a. The PVAc polymer (the transparent part of the outside structure of the fiber) is the shell wrapping uniformly the PCL fiber (the darker part of the inside structure of the fiber) as the core. A TEM micrograph of a PCL/PCL fiber was added in the inset for comparison purpose, as expected core and shell are indistinguishable in this case. The distribution of the HA nanoparticles inside fibers can be observed in Figure III.5b, as mentioned before most of the particles are encapsulated into the polymers.

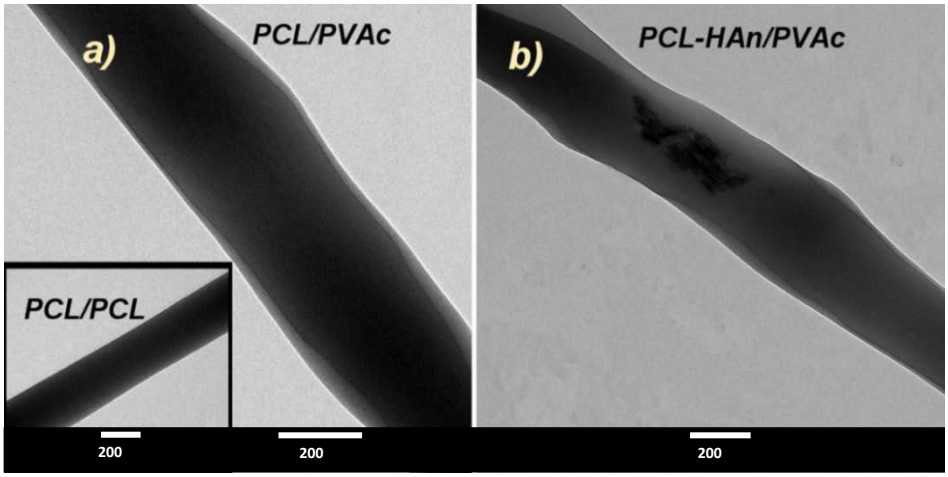

Figure III.5. TEM images of a) PCL/PVAc fiber, inset PCL/PCL fiber, b) PCL-HAn/PVAc fiber.

III.3.2.2 Laser treated membranes

After laser irradiation the membranes were analyzed by SEM microscopy (Figure III.6). For both materials the laser energy was not sufficient to machine a hole through the electrospun fibers. The images show that the membrane was not significantly affected outside the laser irradiation area. Figure III.6a shows SEM images of PCL-HAn/PCL ablated membranes, the micropores were well obtained with diameters in the range 70–120 μm. It is important to observe the morphology of the remaining fibers since the aim is to improve the porosity without any additional effect (33). Even when some melting and coalescence of the fibers can be observed around the drilled holes, the surface morphology is only slightly changed. For PCL-HAn/PVAC on the other hand, the pores diameter are in the 50–90 μm range and the change in the fibers morphology around the holes is more important. Besides, in this material not all the holes of the rectangular pattern were produced under irradiation. As mentioned in the experimental section different lasers were used in order to get the pores in each material.

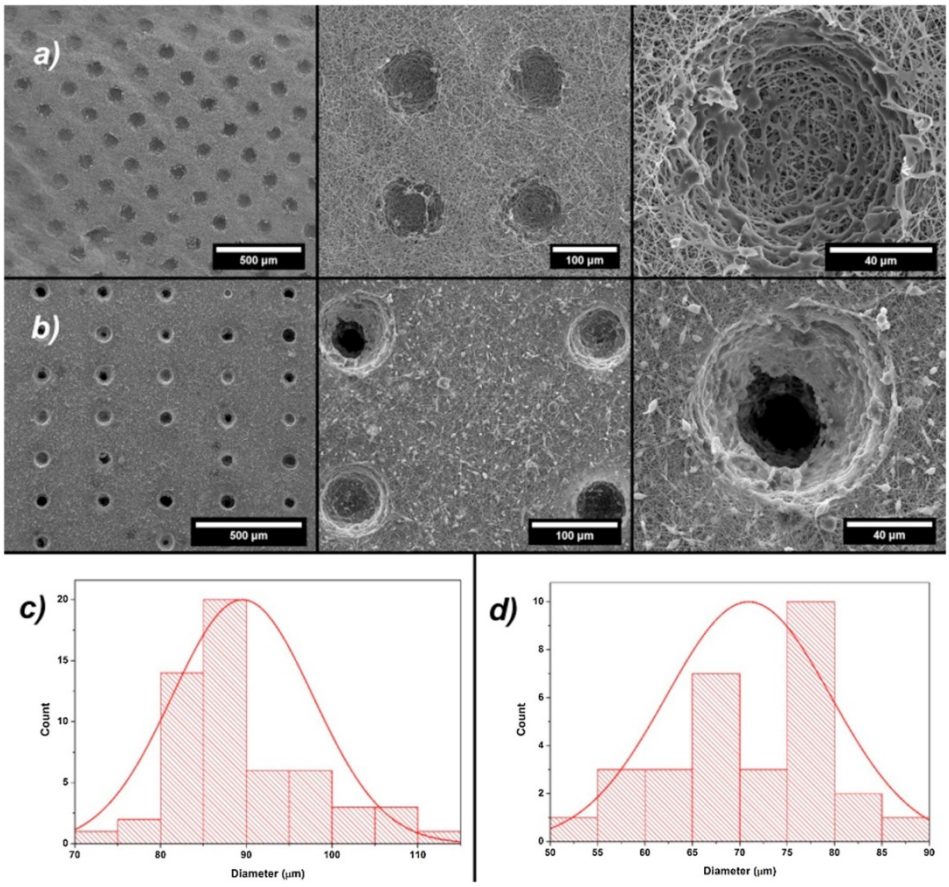

Figure III.6. SEM images and pore size distribution of laser treated a) and c) PCL-HAn/PCL and b) and d) PCL-HAn/PVAc.

III.3.3 *In vitro* bioactivity

Biomineralization method was used in order to evaluate bone binding ability of the prepared materials. The apatite formation was monitored using the fibers pad before the laser treatment since the most important factor for the bioactivity of materials is the surface nature of fibers (34). Figure III.7 shows SEM images of both kind of fibers unloaded and hydroxyapatite loaded having been soaked in SBF for various times. Hydroxyapatite precipitation can be observed after incubation during 14 and 30 days only in samples containing HAn. The apatite form aggregates that reach size of more than 3 µm. The nanoparticles on the surface of fibers would act as nucleation sites in SBF, thus the presence of HAn is necessary for the apatite formation on the nanofiber surface.

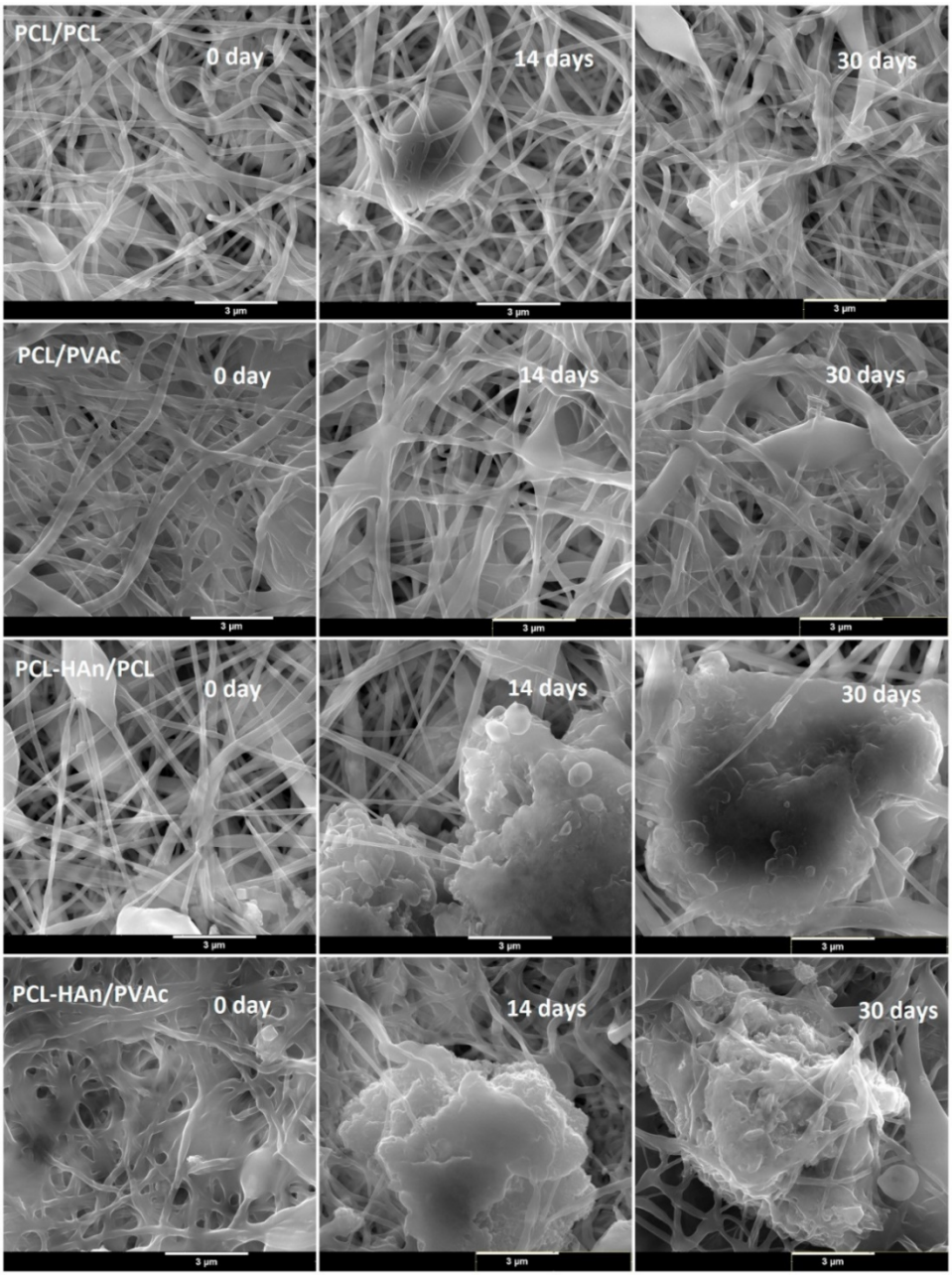

Figure III.7. SEM images of the prepared materials after immersion in SBF solution during different times.

Fibers with PVAc shell suffer some structural change due to the poor water resistance of the polymer (35), but they still exhibited a well

interconnected pore network structure, which is necessary for mineral deposition and cellular in-growth. Characteristic peaks of calcium, phosphorous and oxygen, the main components of hydroxyapatite in EDX analysis (not shown) confirm the nature of the deposited aggregates. From these analyses Ca/P atomic ratios were 1.6 for PCL-HAn/PCL and 1.7 for PCL-HAn/PVAc.

III.3.4 *In vitro* cell morphology and viability

Human osteoblasts seeded onto the different types of membranes fabricated were evaluated regarding their morphology and proliferation until 14 days in order to assess their potential as bone regeneration membranes. SEM micrographs (Figure III.8) showed cell adhesion to all the membranes and a normal morphology of cells which are homogenously distributed on the surface and with a clear higher cell density after 14 days especially in the membranes containing PVAc pointing to a good biocompatibility of the prepared materials.

To further investigate the suitability of these membranes for bone tissue engineering, the viability of the osteoblasts seeded was tested after 48 h (Figure III.9), 7 days (Figure III.10) and 14 days (Figures III.11 and III.12). It should be noted that all confocal acquisitions were performed with the same settings. Biocompatibility of our membranes is clearly shown exerting high viability, very low mortality, which is even diminished with time, and cell proliferation.

Furthermore, the laser treatment of the surfaces notably increased the membranes biocompatibility observing higher viability and cell density which could be attributed to the modification of the membranes surface and porosity (Figure III.13) even in the nanometer scale as has been described for titanium engineered surfaces due to the change in protein adsorption and thus cell adhesion and proliferation (36,37). In all the membranes assayed, cell growth was recorded mostly on the seeding surface probably due to the low pore size. In this sense, nano-porosity data of the un-treated membranes were very similar in all the different formulations assayed as described in Table III.1, pointing to this factor as the responsible of the homogeneity in the results obtained in the cell viability and proliferation studies.

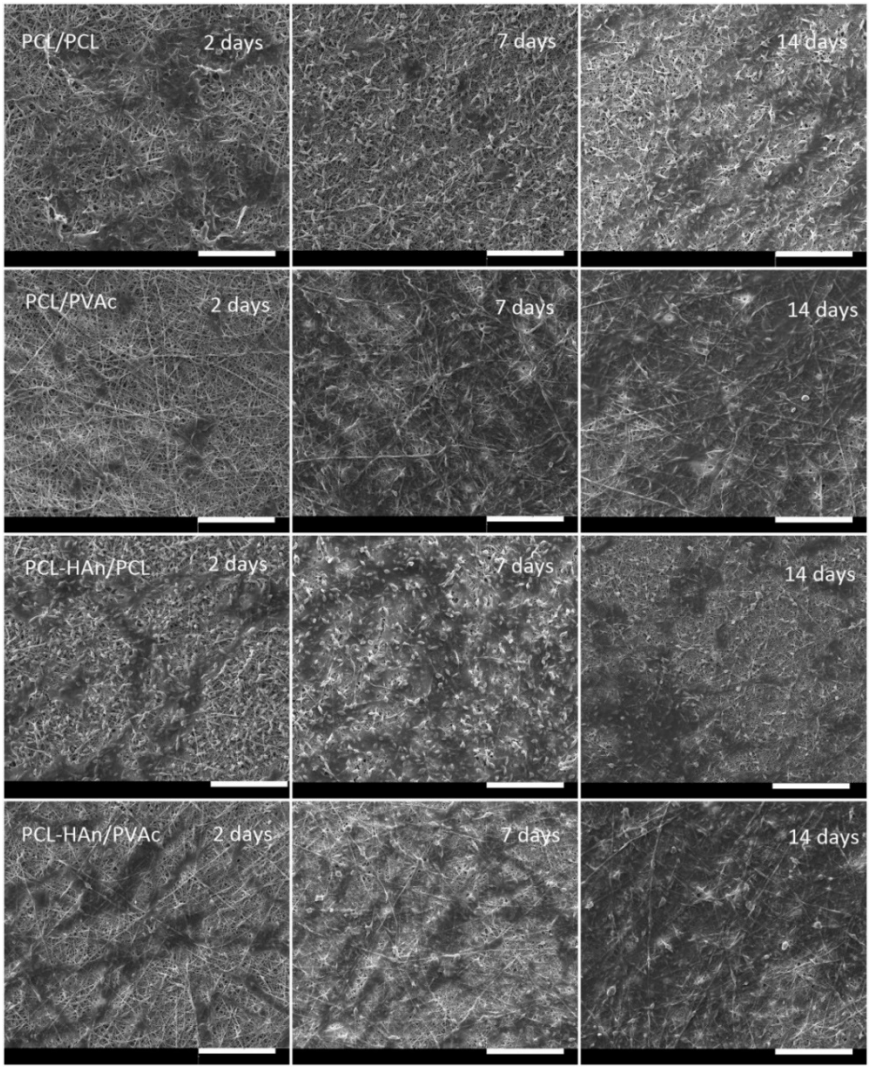

Figure III.8. SEM micrographs showing the morphology and adhesion of human osteoblasts seeded onto the different prepared materials at different time points (2, 7 and 14 days after cell seeding). Scale bars 100μm.

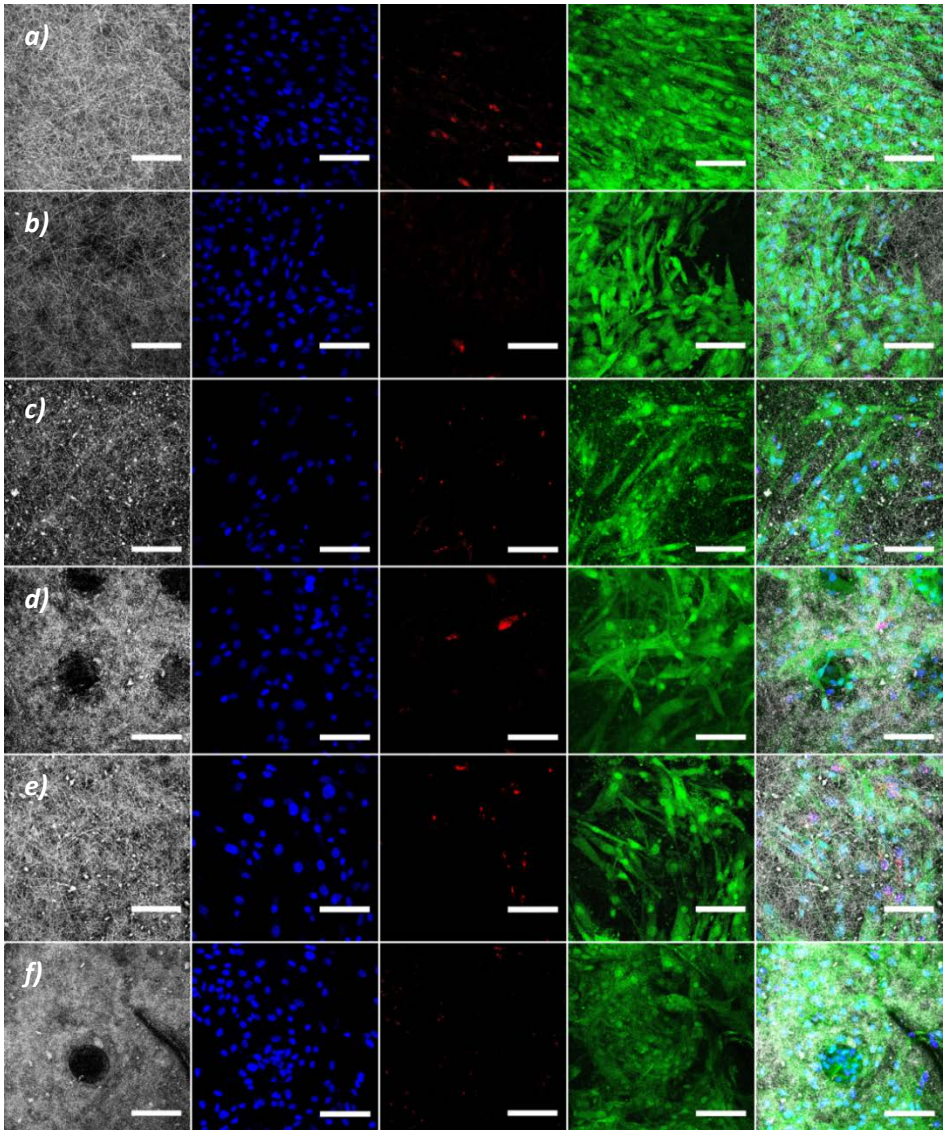

Figure III.9. Confocal laser microscope images of membranes surface and viability of osteoblasts adhered onto the materials studied after 2 days of seeding: a) PCL/PCL; b) PCL/PVAc; c) PCL-HAnP/PCL; d) PCL-HAnP/PCL (LASER); e) PCL-HAnP/PVAc; f) PCL-HAnP/PVAc (LASER). Dead cells (red) and viable (green) cells were treated with Calcein-AM and EthD-1, respectively. Nuclei (blue) were stained with DRAQ5TM. Scale bars 100μm.

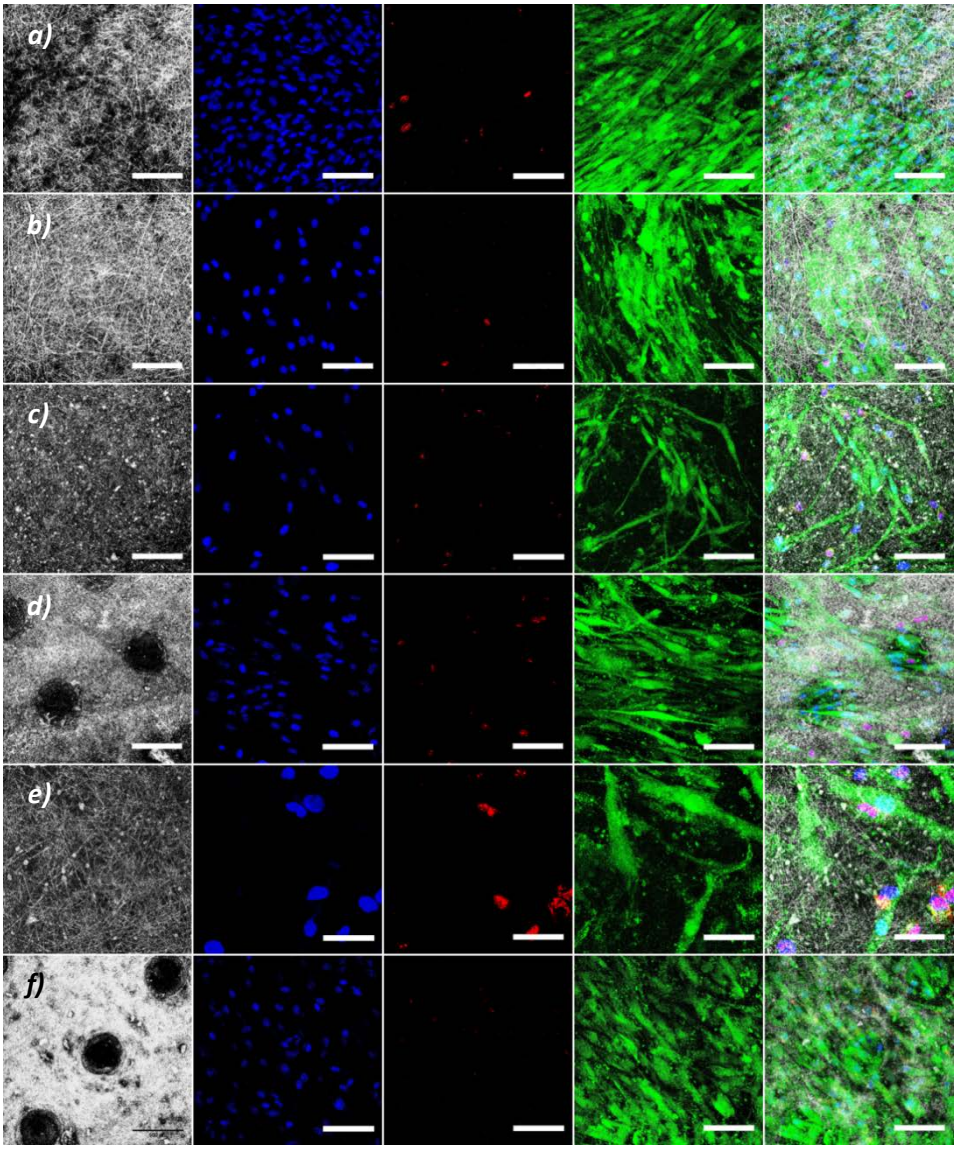

Figure III.10 Confocal laser microscope images of membranes surface and viability of osteoblasts adhered onto the materials studied after 7 days of seeding: a) PCL/PCL; b) PCL/PVAc; c) PCL-HAnP/PCL; d) PCL-HAnP/PCL (LASER); e) PCL-HAnP/PVAc; f) PCL-HAnP/PVAc (LASER). Dead cells (red) and viable (green) cells were treated with Calcein-AM and EthD-1, respectively. Nuclei (blue) were stained with DRAQ5TM. Scale bars 100μm.

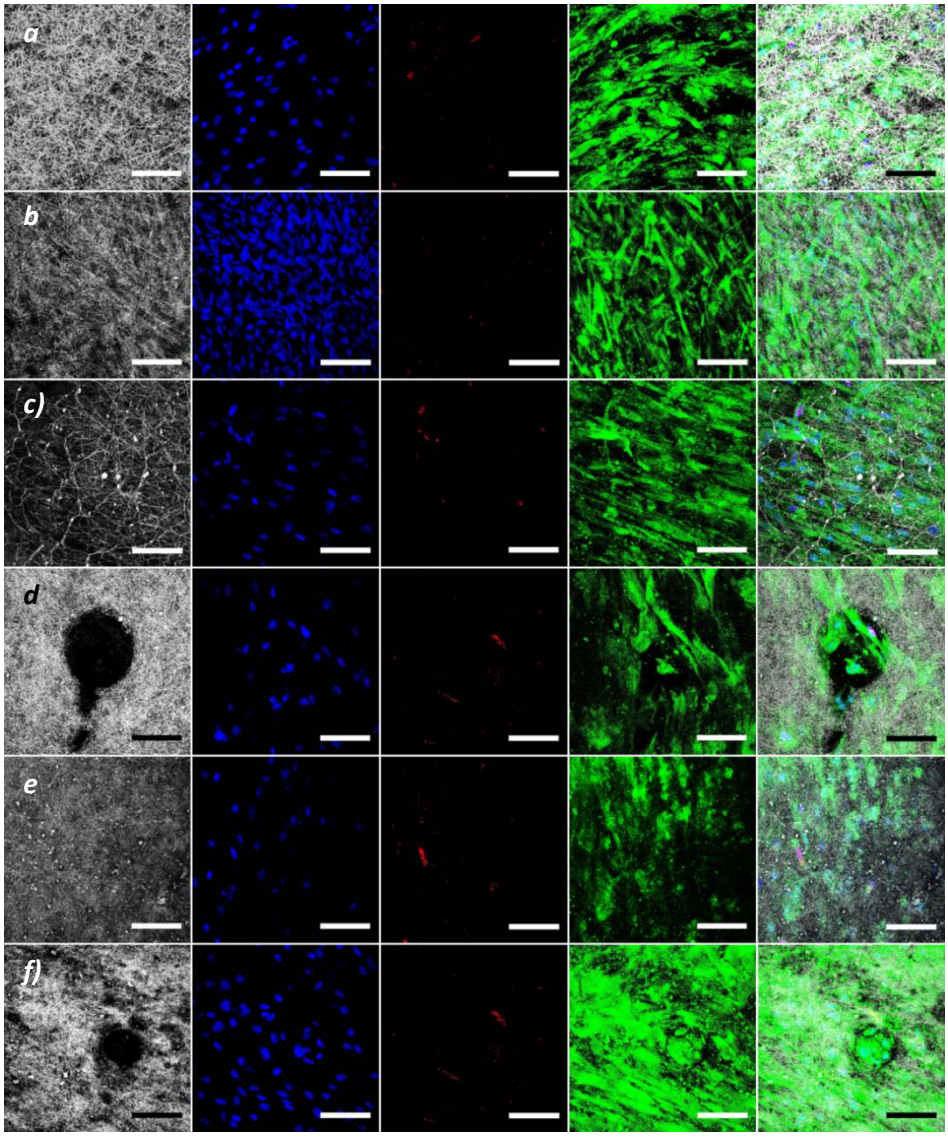

Figure III.11. Confocal laser microscope images of membranes surface and viability of osteoblasts adhered onto the materials studied after 14 days of seeding: a) PCL/PCL; b) PCL/PVAc; c) PCL-HAnP/PCL; d) PCL-HAnP/PCL (LASER); e) PCL-HAnP/PVAc; f) PCL-HAnP/PVAc (LASER). Dead cells (red) and viable (green) cells were treated with Calcein-AM and EthD-1, respectively. Nuclei (blue) were stained with DRAQ5TM. Scale bars 100μm.

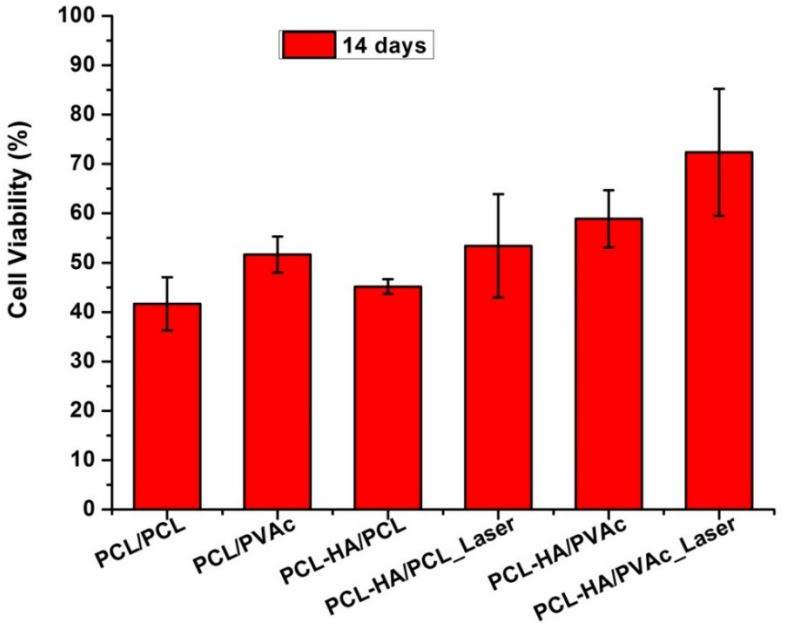

Figure III.12. Cell viability onto the different membranes assayed at the end of the experiments (14 days after seeding) calculated by image analysis (Image J software). Five different regions (at least 60 planes per region) of each sample were evaluated.

Previous studies have reported the biocompatibility of PCL electrospun 3D-membranes in a human osteoblast *In vitro* model in which the high porosity enabled cells to penetrate into the membrane (38). The grafting of collagen and chondroitin sulphate on modified surface PCL porous membranes synthesized by particulate leaching significantly increased the *In vitro* proliferation of murine chondrocytes four weeks after seeding though porosity was not altered (39) while chemically cross-linked PCL and HAn nanoparticles used to fabricate nanocomposite membranes loaded with the growth factor BMP-2 also showed very good cytocompatibility in a rabbit bone marrow stem cells *In vitro* model (40), supporting PCL suitability as biomedical material. In addition, the fabrication of PCL membranes treated with a femtosecond laser to create pores, and therefore to modify the membrane surface and porosity, has shown enhanced cellular activities compared to those membranes with the same pore size and not treated with laser (41), indicating that laser treatment may significantly improve the

potential of these types of membranes in bone regeneration as our study shows. Though it is controversy regarding the "ideal" size pore for biomedical applications, in osteoregeneration most authors have pointed to 100–400 μm as recommended to facilitate cell adhesion and growth (42). However, smaller pores are able to increase membranes surface and lead to higher cell attachment while larger pores facilitate cell migration (41). Our results showed that laser pulse on PCL-HAn/PVAc membranes implied the formation of micropores of 50–90 μm while on PCL-HAn/PCL were slightly larger (70–120 μm). These data, together with the apparently higher cell density recorded in PVAc containing membranes, suggest that smaller micropore sizes made easier cell adhesion and proliferation.

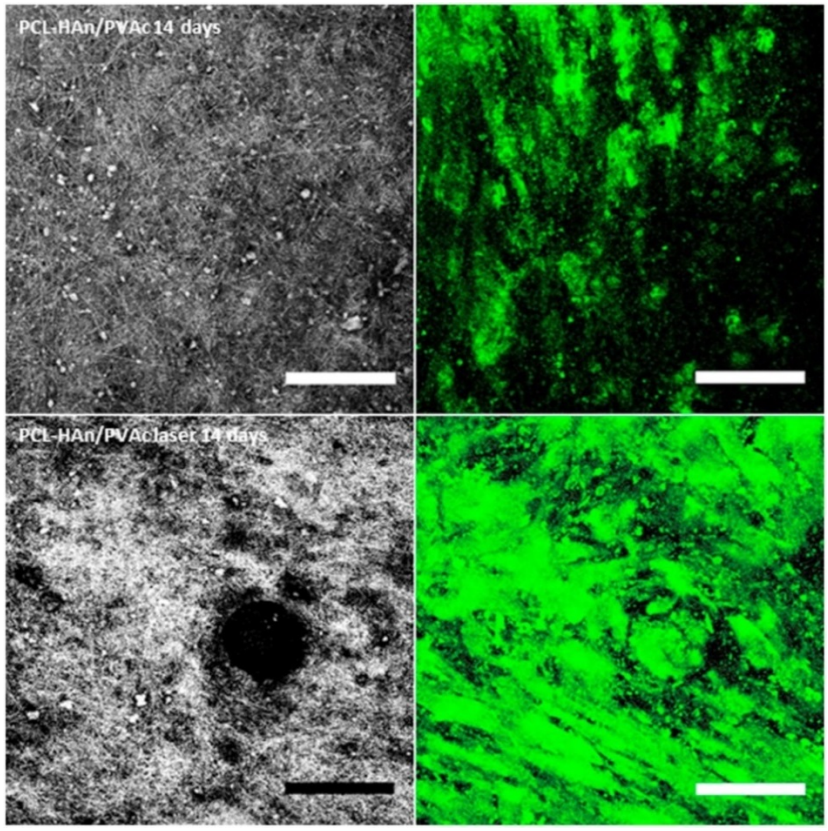

Figure III.13. Confocal laser microscope images of membranes surface (left) and viability (right) of human osteoblasts seeded in PCL-HAn/PVAc membranes not treated (above) and treated with laser (below) after 14 days of cell seeding. Scale bars 100μm.

The incorporation of HAn in the synthesis process of poly(L/DL)-lactide (43) or polylactic acid (PLA) (44) electrospun membranes for biomedical applications has been reported in order to improve cell attachment and proliferation. Since this effect is not clear in Figures III.9-III.11, the cell viability 14 days after seeding NHOst on membranes with and without HAn was measured by image quantification (Figure III.12). Results show that cell viability on samples with HAn are in the range of the ones without it. Besides, they support our observations pointing to a higher viability of cells seeded on PVAc containing membranes, exerting significant differences among PCL-HAn/PVAc group (treated and not treated with laser) vs PCL/PCL and PCL-HAn/PCL groups. Laser treated membranes also displayed higher viability percentages than the not treated ones highlighting the laser treatment as an improvement for cell attachment and viability.

To our knowledge, this is the first time that the incorporation of PVAc to PCL electrospun membranes and treated with laser to enhance their suitability in biomedical applications has been shown these promising effects regarding human osteoblasts adhesion and proliferation, pointing to its potential application in bone repair approaches.

III.4 Conclusions

Rod shaped hydroxyapatite nanoparticles were successfully synthesized and incorporated into core-shell PCL/PCL and PCL/PVAc electrospun nanofibers. Only HAn loaded fibers presented hydroxyapatite precipitation after been soaked in SBF for 14 and 30 days. The presence HAn particles would be necessary for the apatite formation on the nanofiber surface. Fibers with PVAc shell suffer some structural change but they still exhibited a well interconnected pore network structure. Even when human osteoblasts growth was observed on all seeded surface, the laser treatment of the surfaces notably increased the membranes biocompatibility observing higher viability and cell density. This effect was more important on PCL-HAn/PVAc membranes with 50–90 μm micropores than on PCL-HAn/PCL (pores of 70–120 μm) suggesting that smaller micropore sizes favor cell adhesion and proliferation.

References

1. Joshi MK, Pant HR, Tiwari AP, Maharjan B, Liao N, Kim HJ, et al. Three-dimensional cellulose sponge: Fabrication, characterization, biomimetic mineralization, and *In vitro* cell infiltration. Carbohydr Polym. 2016;136:154–62.

2. Pereira IHL, Ayres E, Averous L, Schlatter G, Hebraud A, De Paula ACC, et al. Differentiation of human adipose-derived stem cells seeded on mineralized electrospun co-axial poly(ε-caprolactone) (PCL)/gelatin nanofibers. J Mater Sci Mater Med. 2014;25(4):1137–48.

3. Uma Maheshwari S, Samuel VK, Nagiah N. Fabrication and evaluation of (PVA/HAp/PCL) bilayer composites as potential scaffolds for bone tissue regeneration application. Ceram Int. 2014;40(6):8469–77.

4. Song W, Yu X, Markel DC, Shi T, Ren W. Coaxial PCL/PVA electrospun nanofibers: Osseointegration enhancer and controlled drug release device. Biofabrication. 2013 Sep;5(3):35006.

5. Lee BL-P, Jeon H, Wang A, Yan Z, Yu J, Grigoropoulos C, et al. Femtosecond laser ablation enhances cell infiltration into three-dimensional electrospun scaffolds. Acta Biomater. 2012;8(7):2648–58.

6. Suwantong O, Pankongadisak P, Deachathai S, Supaphol P. Electrospun poly(l-lactic acid) fiber mats containing crude Garcinia mangostana extracts for use as wound dressings. Polym Bull. 2014;71(4):925–49.

7. Kim TG, Chung HJ, Park TG. Macroporous and nanofibrous hyaluronic acid/collagen hybrid scaffold fabricated by concurrent electrospinning and deposition/leaching of salt particles. Acta Biomater. 2008;4(6):1611–9.

8. Kim MS, Kim G. Electrohydrodynamic jet process for pore-structure-controlled 3D fibrous architecture as a tissue regenerative material: Fabrication and cellular activities. Langmuir. 2014;30(28):8551–7.

9. Ortiz R, Moreno-Flores S, Quintana I, Vivanco MM, Sarasua JR, Toca-Herrera JL. Ultra-fast laser microprocessing of medical polymers for

cell engineering applications. Mater Sci Eng C. 2014;37(1):241–50.

10. Wu Y, Vorobyev AY, Clark RL, Guo C. Femtosecond laser machining of electrospun membranes. Appl Surf Sci. 2011;257(7):2432–5.

11. Choi HW, Johnson JK, Nam J, Farson DF, Lannutti J. Structuring electrospun polycaprolactone nanofiber tissue scaffolds by femtosecond ablation. J Laser Appl. 2007;19(4):225–31.

12. McCullen SD, Gittard SD, Miller PR, Pourdeyhimi B, Narayan RJ, Loboa EG. Laser ablation imparts controlled micro-scale pores in electrospun scaffolds for tissue engineering applications. Ann Biomed Eng. 2011;39(12):3021–30.

13. Kim MS, Kim GH. Highly porous electrospun 3D polycaprolactone/β-TCP biocomposites for tissue regeneration. Mater Lett. 2014;120:246–50.

14. Baker SR, Banerjee S, Bonin K, Guthold M. Determining the mechanical properties of electrospun poly-ε-caprolactone (PCL) nanofibers using AFM and a novel fiber anchoring technique. Mater Sci Eng C. 2016 Feb;59:203–12.

15. Chen H, Gigli M, Gualandi C, Truckenmüller R, van Blitterswijk C, Lotti N, et al. Tailoring chemical and physical properties of fibrous scaffolds from block copolyesters containing ether and thio-ether linkages for skeletal differentiation of human mesenchymal stromal cells. Biomaterials. 2016;76:261–72.

16. Dash TK, Konkimalla VB. Poly-ε-caprolactone based formulations for drug delivery and tissue engineering: A review. J Control Release. 2012;158(1):15–33.

17. Ha Y-M, Amna T, Kim M-H, Kim H-C, Hassan MSM, Khil M-S. Novel silicificated PVAc/POSS composite nanofibrous mat via facile electrospinning technique: Potential scaffold for hard tissue engineering. Colloids Surfaces B Biointerfaces. 2013;102:795–802.

18. Sadato A, Taki W, Ikada Y, Nakahara I, Yamashita K, Matsumoto K, et al. Experimental study and clinical use of poly(vinyl acetate) emulsion as liquid embolisation material. Neuroradiology. 1994;36(8):634–41.

19. Abdal-Hay A, Hamdy AS, Khalil KA, Lim JH. A novel simple one-step air jet spinning approach for deposition of poly(vinyl acetate)/hydroxyapatite composite nanofibers on Ti implants. Mater Sci Eng C. 2015;49:681–90.

20. Aragón J, González R, Fuentes G, Palin L, Croce G, Viterbo D. Development and characterization of a novel bioresorbable and bioactive biomaterial based on polyvinyl acetate, calcium carbonate and coralline hydroxyapatite. Mater Res. 2011;14(1):25–30.

21. Jing X, Jin E, Mi H-Y, Li W-J, Peng X-F, Turng L-S. Hierarchically decorated electrospun poly(ε-caprolactone)/nanohydroxyapatite composite nanofibers for bone tissue engineering. J Mater Sci. 2015;50(12):4174–86.

22. Paz A, Guadarrama D, López M, E. González J, Brizuela N, Aragón J. A comparative study of hydroxyapatite nanoparticles synthesized by different routes. Quim Nova. 2012;35(9):1724–7.

23. Mohandes F, Salavati-Niasari M, Fathi M, Fereshteh Z. Hydroxyapatite nanocrystals: Simple preparation, characterization and formation mechanism. Mater Sci Eng C. 2014;45:29–36.

24. Núñez JD, Benito AM, González R, Aragón J, Arenal R, Maser WK. Integration and bioactivity of hydroxyapatite grown on carbon nanotubes and graphene oxide. Carbon N Y. 2014;79(1):590–604.

25. Nathanael AJ, Seo YH, Oh TH. PVP assisted synthesis of hydroxyapatite nanorods with tunable aspect ratio and bioactivity. J Nanomater. 2015;2015.

26. Taheri MM, Abdul Kadir MR, Shokuhfar T, Hamlekhan A, Assadian M, Shirdar MR, et al. Surfactant-assisted hydrothermal synthesis of Fluoridated Hydroxyapatite nanorods. Ceram Int. 2015;41(8):9867–72.

27. Mary IR, Sonia S, Viji S, Mangalaraj D, Viswanathan C, Ponpandian N. Novel multiform morphologies of hydroxyapatite: Synthesis and growth mechanism. Appl Surf Sci. 2016;361:25–32.

28. An L, Li W, Xu Y, Zeng D, Cheng Y, Wang G. Controlled additive-free

hydrothermal synthesis and characterization of uniform hydroxyapatite nanobelts. Ceram Int. 2016;42:3104–12.

29. Dai C-F, Li S-P, Li X-D. Synthesis of nanostructured methotrexate/hydroxyapatite: Morphology control, growth mechanism, and bioassay explore. Colloids Surfaces B Biointerfaces. 2015;136:262–71.

30. Verma G, Barick KC, Manoj N, Sahu AK, Hassan PA. Rod-like micelle templated synthesis of porous hydroxyapatite. Ceram Int. 2013;39(8):8995–9002.

31. Metwally HA, Ardazishvili R V, Severyukhina AN, Zaharevich AM, Skaptsov AA, Venig SB, et al. The Influence of Hydroxyapatite and Calcium Carbonate Microparticles on the Mechanical Properties of Nonwoven Composite Materials Based on Polycaprolactone. Bionanoscience. 2015;5(1):22–30.

32. Cramariuc B, Cramariuc R, Scarlet R, Manea LR, Lupu IG, Cramariuc O. Fiber diameter in electrospinning process. J Electrostat. 2013;71(3):189–98.

33. Rebollar E, Cordero D, Martins A, Chiussi S, Reis RL, Neves NM, et al. Improvement of electrospun polymer fiber meshes pore size by femtosecond laser irradiation. Appl Surf Sci. 2011;257(9):4091–5.

34. Singh RK, Jin G-Z, Mahapatra C, Patel KD, Chrzanowski W, Kim H-W. Mesoporous silica-layered biopolymer hybrid nanofibrous scaffold: A novel nanobiomatrix platform for therapeutics delivery and bone regeneration. ACS Appl Mater Interfaces. 2015;7(15):8088–98.

35. Zhang Y, Gu J, Tan H, Shi J, Di M, Zuo Y, et al. Preparation and characterization of film of poly vinyl acetate ethylene copolymer emulsion. Appl Surf Sci. 2013;276:223–8.

36. Chu S-F, Huang M-T, Ou K-L, Sugiatno E, Cheng H-Y, Huang Y-H, et al. Enhanced biocompatible and hemocompatible nano/micro porous surface as a biological scaffold for functionalizational and biointegrated implants. J Alloys Compd. 2016;684:726–32.

37. Rosales-Leal JI, Rodríguez-Valverde MA, Mazzaglia G, Ramón-

Torregrosa PJ, Díaz-Rodríguez L, García-Martínez O, et al. Effect of roughness, wettability and morphology of engineered titanium surfaces on osteoblast-like cell adhesion. Colloids Surfaces A Physicochem Eng Asp. 2010;365(1–3):222–9.

38. Wang J, Valmikinathan CM, Liu W, Laurencin CT, Yu X. Spiral-structured, nanofibrous, 3D scaffolds for bone tissue engineering. J Biomed Mater Res - Part A. 2010;93(2):753–62.

39. Chang K-Y, Hung L-H, Chu I-M, Ko C-S, Lee Y-D. The application of type II collagen and chondroitin sulfate grafted PCL porous scaffold in cartilage tissue engineering. J Biomed Mater Res - Part A. 2010;92(2):712–23.

40. Liu X, Zhao K, Gong T, Song J, Bao C, Luo E, et al. Delivery of growth factors using a smart porous nanocomposite scaffold to repair a mandibular bone defect. Biomacromolecules. 2014;15(3):1019–30.

41. Kim M, Son J, Lee H, Hwang H, Choi CH, Kim G. Highly porous 3D nanofibrous scaffolds processed with an electrospinning/laser process. Curr Appl Phys. 2014;14(1):1–7.

42. Roosa SMM, Kemppainen JM, Moffitt EN, Krebsbach PH, Hollister SJ. The pore size of polycaprolactone scaffolds has limited influence on bone regeneration in an *in vivo* model. J Biomed Mater Res - Part A. 2010;92(1):359–68.

43. Rajzer I, Menaszek E, Kwiatkowski R, Chrzanowski W. Bioactive nanocomposite PLDL/nano-hydroxyapatite electrospun membranes for bone tissue engineering. J Mater Sci Mater Med. 2014;25(5):1239–47.

44. Morelli S, Salerno S, Holopainen J, Ritala M, De Bartolo L. Osteogenic and osteoclastogenic differentiation of co-cultured cells in polylactic acid-nanohydroxyapatite fiber scaffolds. J Biotechnol. 2015;204:53–62.

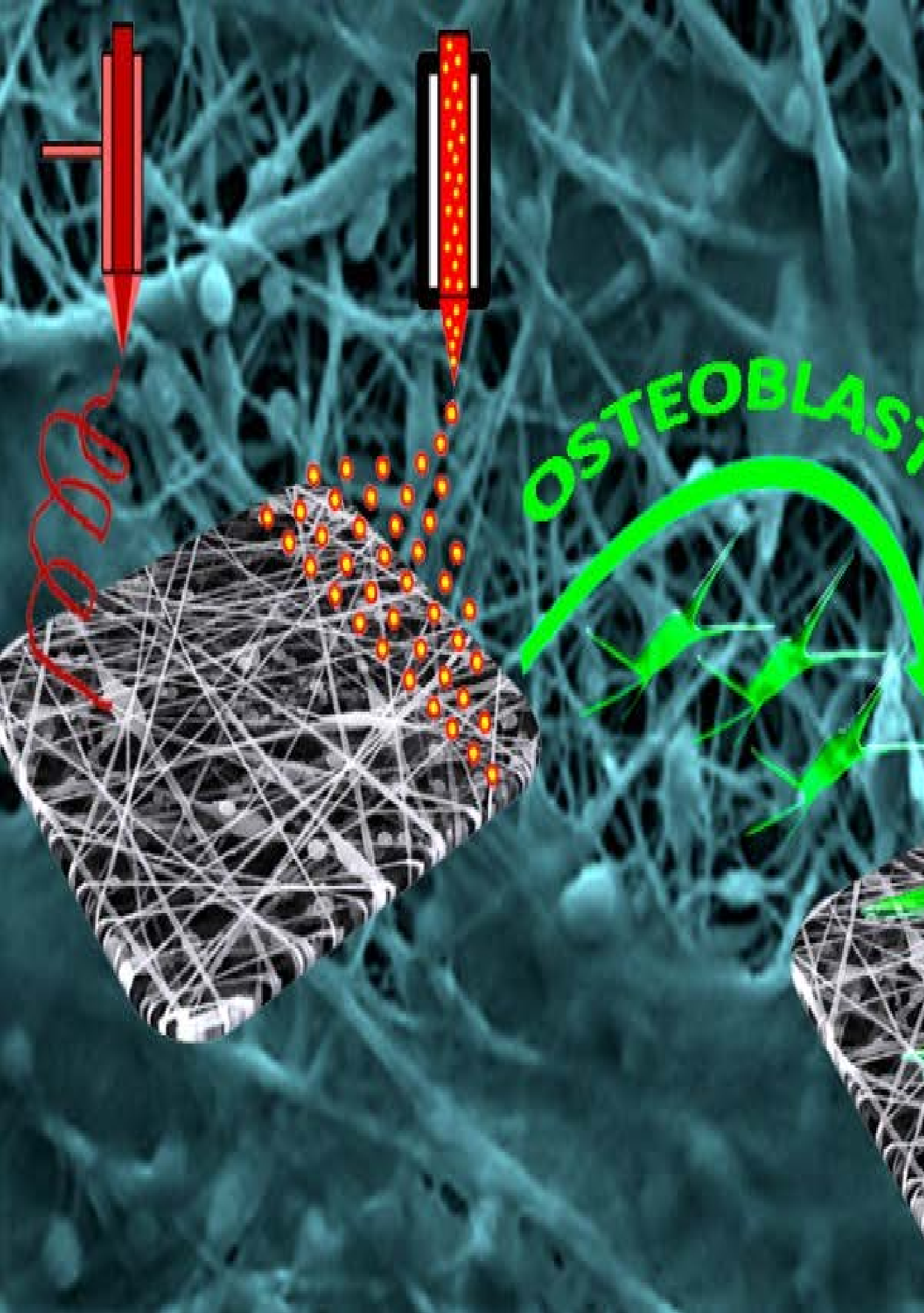
OSTEOBLAST

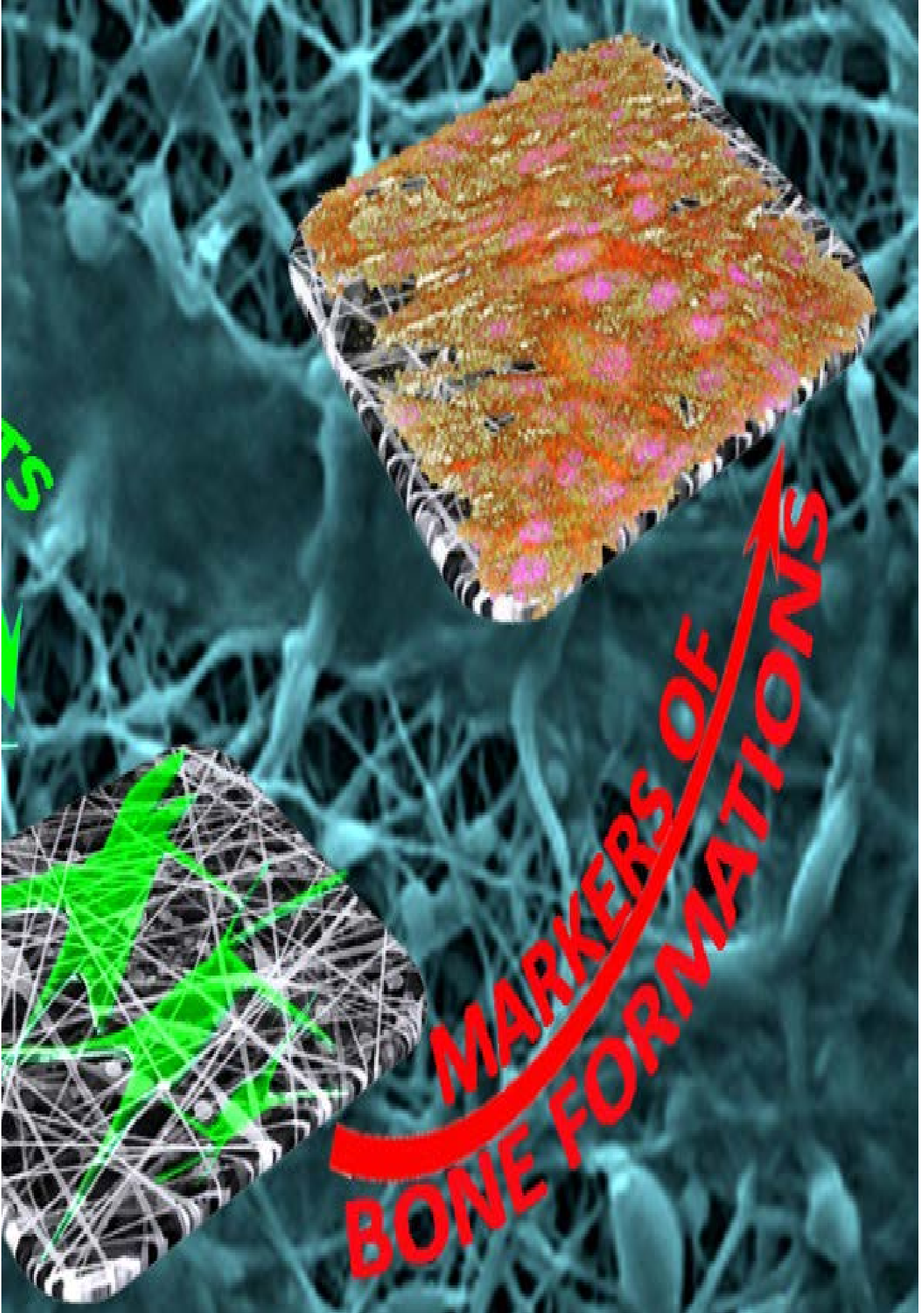
MARKERS OF
BONE FORMATIONS

CHAPTER IV

Polymeric electrospun membranes for bone morphogenetic protein 2 delivery in bone tissue engineering

The contents of this chapter have been adapted from the following published work:

Polymeric electrospun scaffolds for bone morphogenetic protein 2 delivery in bone tissue engineering. Javier Aragón, Simona Salerno, Loredana De Bartolo, Silvia Irusta and Gracia Mendoza. Journal of Colloid and Interface Science, 531 (2018) 126–137. DOI:10.1016/j.jcis.2018.07.029.

"The development of novel membranes based on biocompatible polymers is of great interest in the field of bone repair for fabrication of biodegradable membranes that mimic the extracellular matrix and have osteoconductive and osteoinductive properties for enhanced bone regeneration.

Polycaprolactone (PCL) and polycaprolactone/polyvinyl acetate (PCL/PVAc) core–shell fibers were synthesised and decorated with poly(lactic-co-glycolic acid) [PLGA] particles loaded with bone morphogenetic protein 2 (BMP2) by simultaneous electrospinning and electrospraying. Hydroxyapatite nanorods (HAn) were loaded into the core of fibers. The obtained membranes were characterized by scanning and transmission electron microscopy, Fourier-transform infrared spectroscopy, and thermogravimetric analysis. The In vitro potential of these materials for bone regeneration was assessed in biodegradation assays, osteoblast viability assays, and analyses of expression of specific bone markers, such as alkaline phosphatase (ALP), osteocalcin (OCN), and osteopontin (OPN).

PLGA particles were homogeneously distributed in the entire fiber mat. The growth factor load was 1.2–1.7 μg/g of the membrane whereas the HAn load was in the 8.8–12.6 wt% range. These membranes were able to support and enhance cell growth and proliferation facilitating the expression of osteogenic and osteoconductive markers (OCN and OPN). These observations underline the great importance of the presence of BMP2 in membranes for bone remodeling as well as the good potential of the newly developed membranes for clinical use in tissue engineering."

INDEX

IV.1 Introduction

The repair of bone defects is still a major challenge in orthopedic and maxillofacial surgery (1). Scaffolds in shape of membrane play a crucial role in bone tissue engineering by acting as a template facilitating cell growth and differentiation within bone defects (2). For these purposes, they should mimic the extracellular matrix (ECM); provide mechanical support; be biocompatible, osteoconductive, and osteoinductive; and possess high porosity provided by interconnected pores. Besides, they should be biodegradable to leave room for the new bone to grow. Fibers of mainly submicron sizes produced by electrospinning are a promising material to be used as scaffolds. These fibers resemble the ECM structure and are an excellent framework for cell adhesion, proliferation, and differentiation (3).

Among synthetic polymers, polycaprolactone (PCL) is widely used to obtain electrospun fibers because of its low cost, biocompatibility, and rheological and viscoelastic properties (4). The electrospun membranes prepared with this polymer possess flexibility, good mechanical properties, and non-toxicity (3), though its hydrophobicity and low water adsorption may impair its biomedical applications. These limitations may be solved by its association with water-soluble compounds, such as tannins (5), proteins (6), or polysaccharides (7). Furthermore, PCL osteoinduction and osteoconduction may be improved by addition of hydroxyapatite (HA) as we recently reported (4). The addition of HA nanorods (HAn) to PCL/polyvinyl acetate (PVAc) core–shell fibers yields apatite formation on the nanofiber surface while the PVAc shell increases hydrophilicity and cell viability.

Even when HAn is an important osteoconductive biomaterial, incorporation of osteogenic growth factors, such as bone morphogenetic protein 2 (BMP2), is an interesting alternative way to increase the osteogenic activity (8). Bone healing is a complex physiological process that is initiated and controlled by many growth factors such as bone morphogenetic proteins (BMPs). These proteins not only can enhance bone repair but also promote new blood vessel formation (9). BMP2 is a necessary component of the signaling cascade that governs fracture repair because BMP2 is essential for initialization of bone regeneration (10). However, this protein may lose bioactivity after a short period owing to its short half-life under physiological conditions because of rapid degradation and deactivation by enzymes and other chemical and physical reactions that limit its local delivery (11). To

achieve therapeutic efficacy, a carrier is needed to deliver BMP2 locally at a stable concentration to avoid a burst release and uncontrolled ectopic bone formation in soft tissues (12).

Poly(lactic-*co*-glycolic acid) [PLGA] has been extensively used to encapsulate osteogenic growth factors into micro- and nanoparticles for a controlled drug release (13–15). This polyester has interesting characteristics such as solubility in various solvents and approval by the US Food and Drug Administration (FDA). Several techniques have been developed for fabricating polymeric nanoparticles and for encapsulating drugs in a polymeric matrix, including emulsification. Even when this process is simple, it has multiple disadvantages, such as poor encapsulation and loading efficiency rates as well as possible denaturation of the encapsulated drug (16). To overcome these drawbacks, electrospraying or electrohydrodynamic atomization (EHDA) is a promising method for producing micro- and nanoparticles with high encapsulation efficiency of drugs (hydrophilic or hydrophobic molecules). It is a simple and inexpensive approach that enables researchers to preserve bio-functionalities of active ingredients (17). A few examples of BMP2 encapsulation in polymer nanoparticles by electrospraying found in the literature show the sustained release of the protein for 35 days, thus allowing for mesenchymal-stem-cell proliferation and differentiation (18). A stable release of BMP2 from PLGA electrosprayed spheres has been achieved, and new bone formation, accompanied by abundant in-growth of blood vessels, has been attained by *in vivo* implantation of these particles (1).

Objective

The combination of the unique properties of electrospun nanofibers with proven advantages of polymer particles for drug release can result in an innovative drug delivery system (19). This approach allows for a homogeneous distribution of the BMP2-loaded particles along the entire fiber mats, thereby ensuring a continuous release of the growth factor, in contrast to the BMP2 immobilization techniques that involve protein functionalization only on the membrane surface (20), limiting its efficiency.

For this reason, the objective of this work was to develop a core-shell electrospun membrane with HAn containing BMP2–loaded PLGA particles to provide the necessary biochemical cues for bone repair and regeneration.

The core of PCL would provide the necessary mechanical resistance while the PVAc shell increases hydrophilicity and cell viability. On the other hand HAn particles yield apatite formation on the nanofiber surface. The prepared membranes were intended to have structural, physico-chemical, and biodegradation properties required to address the architectural, biochemical, and functional features of bone tissue.

IV.2 Membrane fabrication

Different types of fibers (PCL-HAn fibers for the core, and PCL fibers and PVAc fibers for the shell) and PLGA particles loaded with BSA and BMP2, were fabricated to obtain four types of electrospun membranes (Table IV.1).

PLGA particles were prepared using an Yflow 2.2.D-500 electrospinner (Electrospinning Machines/R&D Microencapsulation, Spain). BMP2 (10 µg) was dissolved in 100 µL of a BSA aqueous solution (2 %), while PLGA (1.05 g) was dissolved in 10 mL of DMF. Then, the BSA aqueous solution was added to the PLGA solution, and the mixture was incubated with magnetic stirring for 12 h at 4 °C. The addition of a surfactant was not needed to obtain the emulsion (10 mL), which was loaded into a 10 mL plastic syringe and fed through a needle (inner diameter 0.9 mm, outer diameter 1.7 mm) connected to a positive-voltage power supply with voltage 11.65 kV. The tip of the needle was fixed 30 cm above an aluminum foil–covered flat collector. A negative-voltage power supply (-4.5 kV) was connected to the collector. The solution flow rate was 0.5 mL/h. The synthesis of HAn [$Ca_{10}(PO_4)_6(OH)_2$] nanoparticles was conducted as previously described (4). In brief, $CaCO_3$ was dissolved in a 0.3 M H_3PO_4 solution (100 mL), and we maintained a Ca/P ratio of 1.67 and pH 9 by the addition of NH_4OH during precipitation. After incubation in the stock solution for 5 days, the precipitate was washed with deionized water and dried at 110 °C for 2 h.

The aforementioned electrospinner was also used to obtain fibrous membranes (Table IV.1): 0.32 g of a HAn powder was dispersed in 5 mL of a DCM–DMF mixture (1:1) with Tween® 80 (0.5 %, v/v) by stirring overnight at room temperature. The dispersion was then added to 1.27 g of PCL dissolved in 5 mL DCM–DMF (1:1) and stirred overnight at room temperature in order to obtain a solution of PCL and HAn for the fiber core synthesis (Table IV.1). On the other hand, PCL (0.60 g) and PVAc (1.05 g) were dissolved in 10 mL of DCM–DMF (1:1) and 10 mL of DMF, respectively,

to prepare a PCL solution or PVAc solution for fabrication of the two types of shells that we developed (Table IV.1). Then, these solutions were stirred overnight at room temperature.

All the solutions were loaded into plastic syringes. A coaxial system was employed to obtain PCL-HAn/PCL or PCL-HAn/PVAc fibers; a PCL-HAn suspension was fed through the inner needle (0.5 mL/h) and PCL or PVAc solutions were fed through the outer needle at a 0.5 mL/h rate (Figure IV.1). All the needles had an inner diameter of 0.9 mm while the outer diameter was 1.7 mm.

Table IV.1. Composition of the membranes prepared in this study.

Sample	Fibers		Particles
	Core	Shell	
PCL	PCL-HAn	PCL	
PCL:PLGA-BMP2	PCL-HAn	PCL	PLGA:BSA:BMP2
PVAc	PCL-HAn	PVAc	
PVAc:PLGA-BMP2	PCL-HAn	PVAc	PLGA:BSA:BMP2

To obtain particle-decorated fibers, the coaxial needle (to produce fibers) and the one feeding the solution of PLGA, BSA, and BMP2 (to produce particles) were connected to the positive-voltage power supply (voltage range 9 to 12 kV; Figure IV.1). The tips of coaxial and single needles (inner diameter 0.9 mm, outer diameter 1.7 mm) were fixed 18 and 30 cm above a rotating collection drum (100 rpm), respectively. The collector was connected to the negative-voltage power supply (4 to −5 kV) for 8 h.

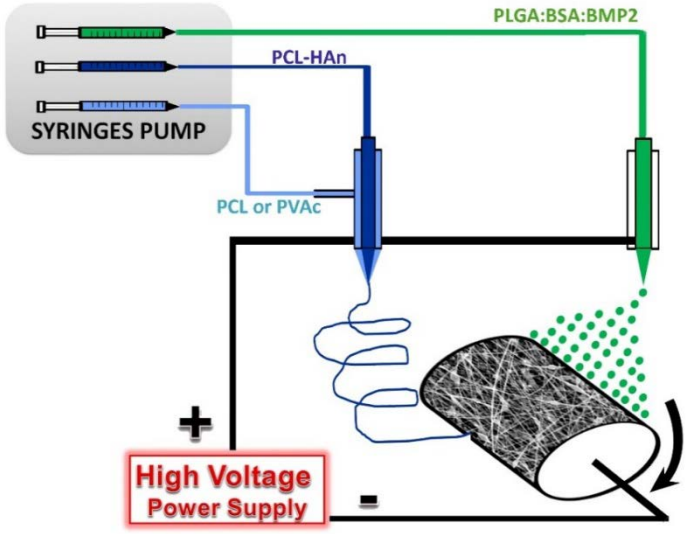

Figure IV.1. Schematic illustration of the coaxial and single electrospinning during the fabrication of PCL-HAn or PCL-HAn/PVAc fibers decorated with PLGA-BMP2 particles.

The characterization techniques and different evaluation methods are described in **Appendix 1**.

IV.3 Results and discussion

IV.3.1 Membrane characterization

Membranes were obtained by electrodynamic techniques, fibers by electrospinning, and particles by electrospraying. In the last two techniques, a polymer solution flowing out of a nozzle is forced into an electric field. Solvents evaporate on the way from the nozzle to the collector and depending on the parameters, such as solution viscosity, density, and conductivity, and polymer molecular weight, fibers or particles are obtained. Several conditions were tested to fabricate PLGA particles with a uniform size distribution: three polymer concentrations (3, 5, and 10 wt%), three flow rates (0.1, 0.5, and 1.0 mL/h), two solvents (DMF and DCM–DMF), and two tip-to-collector distances (15 and 30 cm). The best results were obtained with solutions containing 10 wt% of PLGA in DCM, a flow rate of 0.5 mL/h, and a distance of 30 cm.

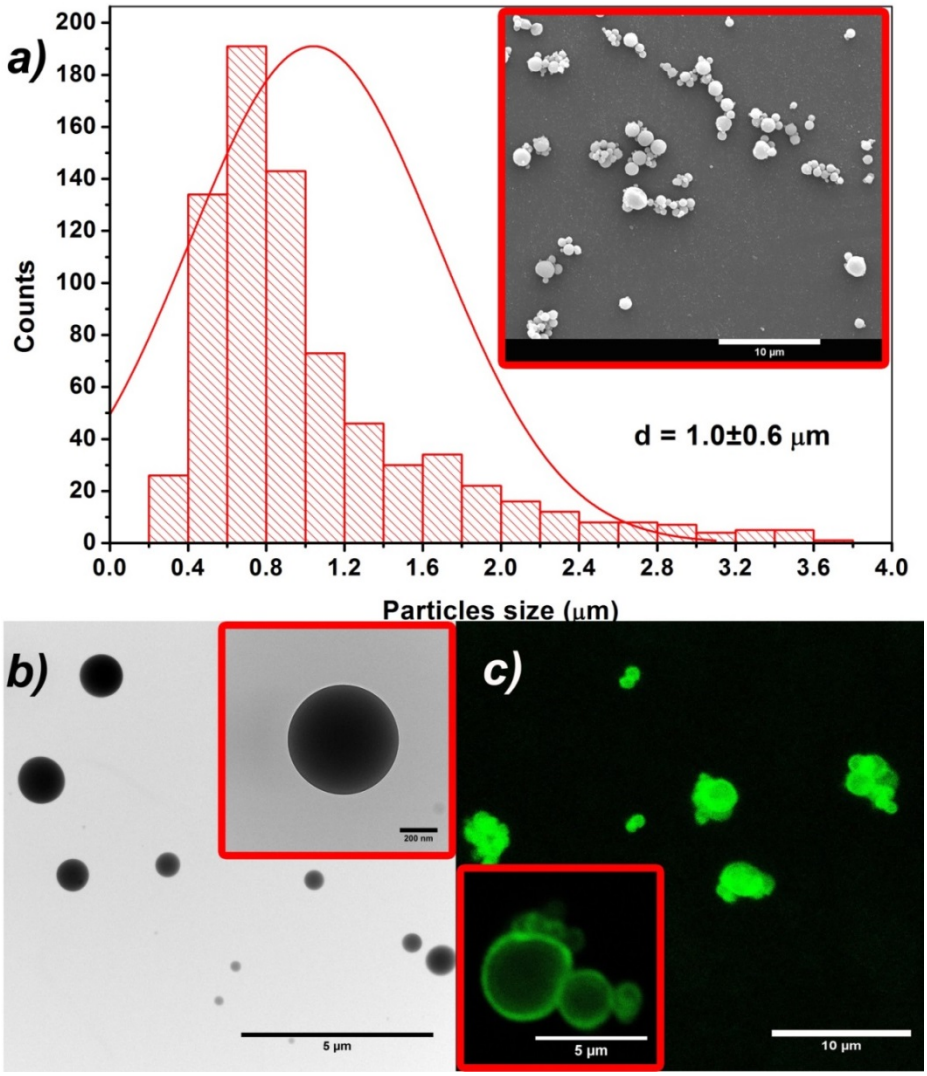

Figure IV.2. SEM (a), TEM (b), and confocal microscopy (c) images of the electrosprayed PLGA particles obtained.

The size distribution and morphology of the electrosprayed PLGA particles were investigated by means of SEM and TEM (Figures IV.2a and IV.2b), and the mean diameter was found to be 1.0 ± 0.6 μm. The histogram clearly showed the presence of a relevant type of particles in the range of 0.4–1.2 μm but also the presence of bigger particles that could be more than 3 μm in diameter. TEM images (Figure IV.2b) confirmed the spherical shape of the particles produced by electrospraying. To estimate the drug distribution

inside the synthesized particles, a BSA–fluorescein conjugate (BSA-FITC) was added to the PLGA solution. The obtained particles were examined by confocal laser scanning microscopy (Figure IV.2c), which showed that even when there was a slightly higher concentration in the shell, the fluorescent compound was almost uniformly distributed inside the microparticles. No significant phase separation of the polymer and/or drug was observed.

HAn was also characterized by means of the SEM and TEM (Figure IV.3). These images confirmed our previous results (4), in which fibrous needle-like particles with a rod-like shape were also seen (length and diameter of approximately 150 and 20 nm, respectively).

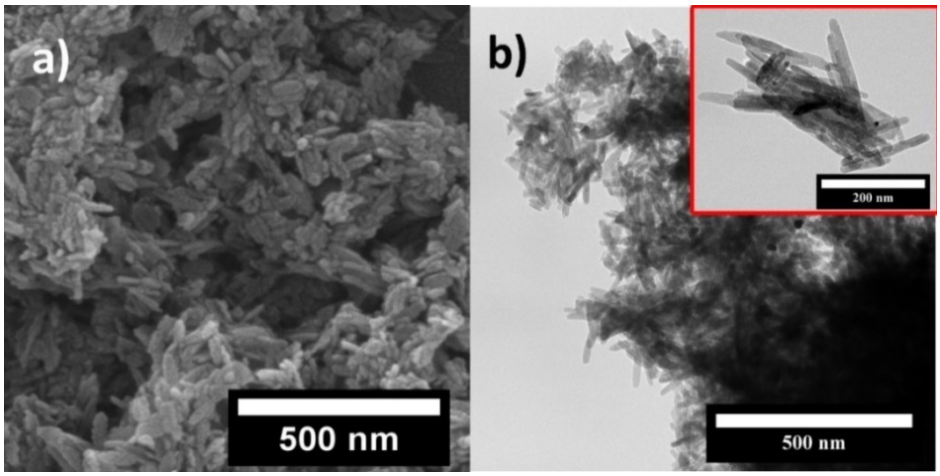

Figure IV.3. SEM (a) and TEM (b) images of synthesized HAn.

Once the particle synthesis was optimized, the simultaneous electrospray-electrospinning process was carried out to generate the final membranes of HAn-loaded PCL/PVAc fibers decorated with PLGA particles (Figure IV.4). The optimized electrospray-electrospinning process produced fibers with uniform morphology and a random distribution that led to the creation of a membrane with porosity of ≈60–64%. Because of the simultaneous synthesis, PLGA particles with a mean diameter of 1.2 ± 0.5 μm were homogeneously distributed in the entire fiber mat. It is noteworthy that the attachment of particles onto fibers did not influence fiber morphology (Figure IV.4). However, some of the particles slightly deviated from the spherical shape (Figures IV.2 and IV.4). The mean diameter of fibers (380 ± 108 nm) forming the membranes was in the range of collagen fibers (from 50

to 500 nm), mimicking the nanostructures of the natural ECM. SEM images clearly revealed the formation of membranes with an interconnected network of large pores with size between 0.9 and 2.5 μm for PCL and PVAc membranes and smaller pores ranging from 0.2 to 0.6 μm. The mean pore size was 1.14 μm for PVAc and 1.46 μm for PVAc:PLGA-BMP2 owing to the presence of a nanofibrous structure that confers microporosity on the membrane (Figure IV.4). This structure provides a large surface area-to-volume ratio for cell attachment as well as sufficient porosity for nutrient diffusion. Indeed, the measured hydraulic permeance was 8.00 ± 0.30 and 6.60 ± 0.03 L/h m^2 mbar for PVAc and PCL membranes, respectively. An increase in hydraulic permeance by 16% was observed in the PVAc:PLGA-BMP2 membranes (9.5 ± 0.4 L/h m^2 mbar) with respect to the non-loaded membrane.

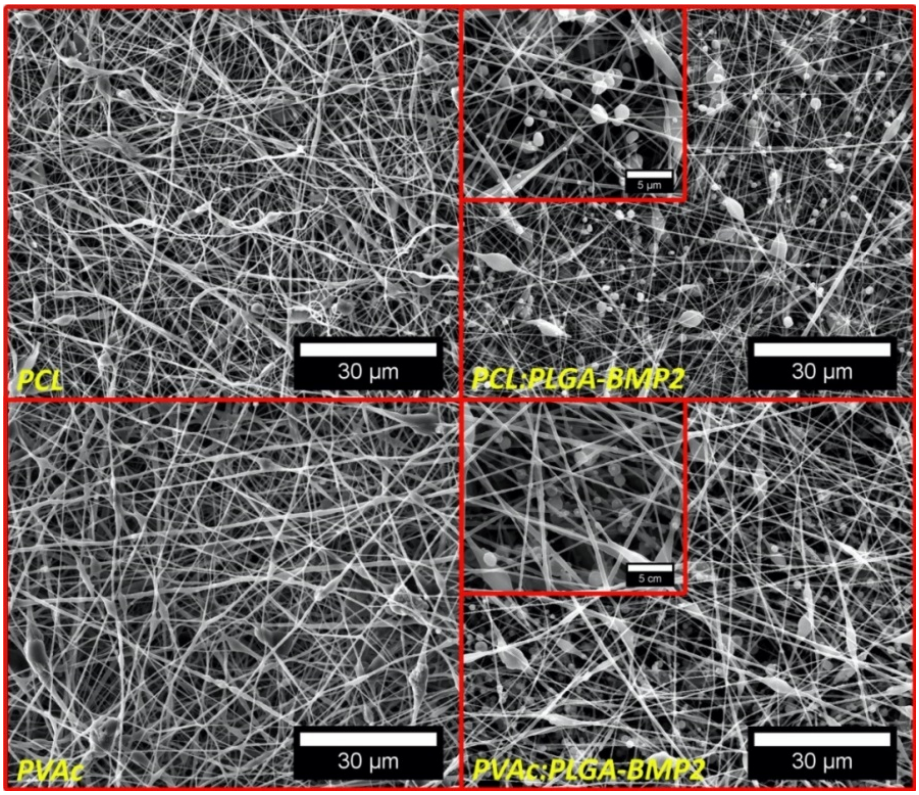

Figure IV.4. SEM images of the synthesised electrospun fibres (left) decorated with BMP2-loaded PLGA electrosprayed particles (right).

TGA analyses (Figure IV.5) confirmed HAn loads of 13.8 and 12.7 wt% for PCL and PVAc fibers, respectively, in agreement with our previous results (4). In PCL:PLGA-BMP2 and PVAc:PLGA-BMP2 membranes, owing to the presence of the PLGA polymer, the HAn load was reduced to 12.6 and 8.8 wt%, respectively. However, BMP2 encapsulation efficiency was similar between the two formulations, reaching percentages of 39% ± 5% for PCL:PLGA-BMP2 and 40% ± 11% for PVAc:PLGA-BMP2. A final BMP2 concentration of 39 and 40 μg/ml was achieved in the membranes, in line with the clinical required dose (21). These similar efficiency rates led to growth factor loads of 1.2 and 1.7 μg/g in PCL and PVAc composite fibers, respectively.

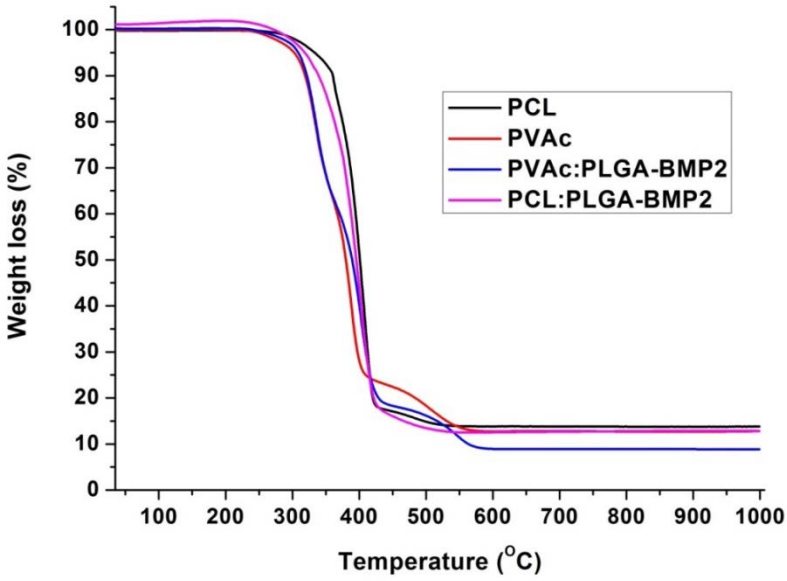

Figure IV.5. TGA thermogram of the four types of membranes synthesized: PCL, PVAc,PCL:PLGA-BMP2 and PVAc:PLGA-BMP2.

IV.3.2 *In vitro* protein release

The kinetic profile of the BMP2 release from both kinds of membranes was determined in the course of 28 days (Figure IV.6a) and the morphology of PVAc:PLGA-BMP2 membranes after the release for 28 days was also studied under the SEM (Figure IV.7).

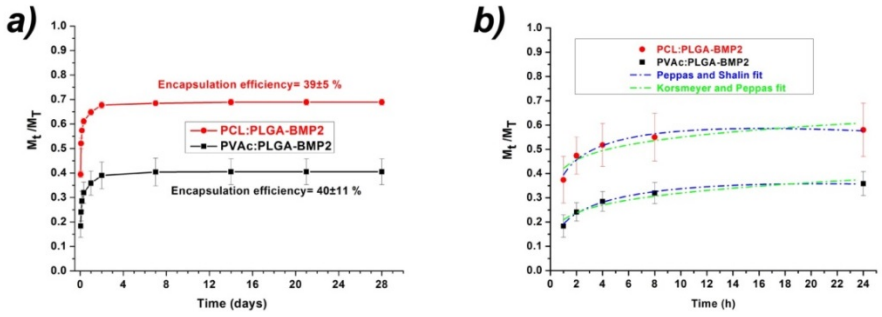

Figure IV.6. BMP2 release kinetic curves obtained for both types of membranes (a) and their mathematical adjustment (b).

The pattern of the growth factor release from both membranes showed a strong initial burst within the first 8 h, followed by a slow release until the end of the experiment. This behavior should synergistically enhance bone generation because it was suggested that the ideal BMP2 release strategy includes both an initial burst and a subsequent sustained release. The reason is that the former helps to recruit osteoprogenitor cells to the delivery system and the latter promotes osteogenic differentiation (22). The burst release reached ≈ 68 % of the BMP2 load for PCL:PLGA-BMP2 and only 40 % for PVAc:PLGA-BMP2. The difference could be due to the absorption capacity of PVAc (350 % water absorption in 24 h (23)) that may retain the protein released from the PLGA particles during the swelling process. It is important to point out that the hydrophilicity of both membranes is determined by the presence of HA, which turns both membranes into highly hydrophilic materials. SEM images of membranes (Figure IV.7) after the release (28 days) confirmed this pattern: there were no PLGA particles on the surface of the membranes or only a few damaged ones.

The kinetic mathematical models were fitted to the experimental results of the release (Table IV.2, Figure IV.6b). Preliminary calculations (not shown) indicate that the Higuchi model was not satisfactory for fitting to the experimental release data. Given that some of these models should be used only for the first 60% of the release, only the data representing the first 24 h were fitted because it was the release from PCL:PLGA-BMP2 achieved at that time (24). The best fit solution was identified by evaluating coefficient of correlation R^2. The highest values of the coefficient indicated that both samples were better described by the Peppas–Sahlin release kinetic model

(Figure IV.6b). In this model, term $k_{1P}t^n$ represents the Fickian diffusional contribution to the release (F), whereas term k_2t^{2n} is the case-II relaxational contribution (R). The negative values obtained for k_2 should be interpreted in terms of a relaxation mechanism being insignificant compared to the diffusion process (25). In accordance with the *Peppas–Sahlin* equation, the value of exponent n for the Fickian release mechanism from a polymeric system with sphere geometry should be ≈0.43 (26). The lower values found for PCL and PVAc samples may be related to the wide particle size distribution mentioned before (27).

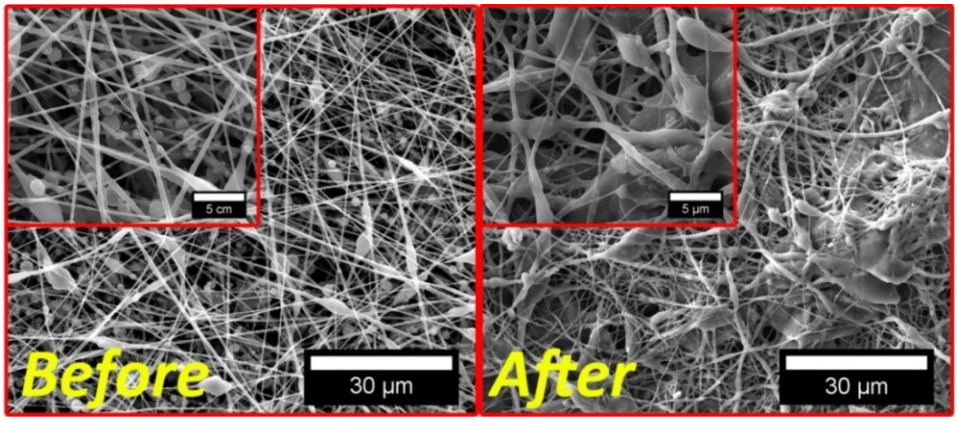

Figure IV.7. SEM images of PVAc:PLGA-BMP2 membranes before and after release for 28 days.

Table IV.2. Release modeling parameters.

Model	Parameter	PCL:PLGA-BMP2	PVAc:PLGA-BMP2
Korsmeyer-Peppas	k_{1K}	0.42	0.21
	n	0.12	0.18
	R^2	0.77	0.89
Peppas-Sahlin	k_{1P}	0.50	0.23
	k_2	-0.11	-0.04
	n	0.30	0.38
	R^2	0.91	0.98

IV.3.3 *In vitro* enzymatic degradation

An ideal membrane for bone tissue engineering should be biodegradable and bioresorbable while being able to support the growth of new bone. The degradation behavior of biomaterials in physiological environments plays an important role in the engineering process of a new tissue. The greatest advantage of degradable polymers such as PCL, PVAc, and PLGA is that they are broken down into biologically acceptable molecules that are metabolized and removed from the body via normal metabolic pathways (28). To investigate the effect of enzymes on the degradation behavior of the synthesized membranes, they were incubated in phosphate-buffered saline in the presence of lipase or lysozyme for different periods at the same concentrations as those found in human serum. The degradation was followed by gravimetric measurements (Figure IV.8). PVAc and PCL membranes manifested similar behavior in the presence of lysozyme, thus reaching degradation of 10 % ± 1 % and 13 % ± 1 %, respectively, after 60 days. This value for PCL-based fibers was higher than the one expected based on the results of Banerjee el at. (29). These authors did not find any significant PCL film degradation in the presence of lysozyme. The greater degradation observed in our PCL membranes could be explained by the fibrous structure and high porosity that increase the surface area exposed to the enzyme solution. In the presence of lipase, the degradation profile of all membranes was similar to that observed in other studies, showing a significant weight loss with time, which reached values ≈ 90 % after 60 days (29).

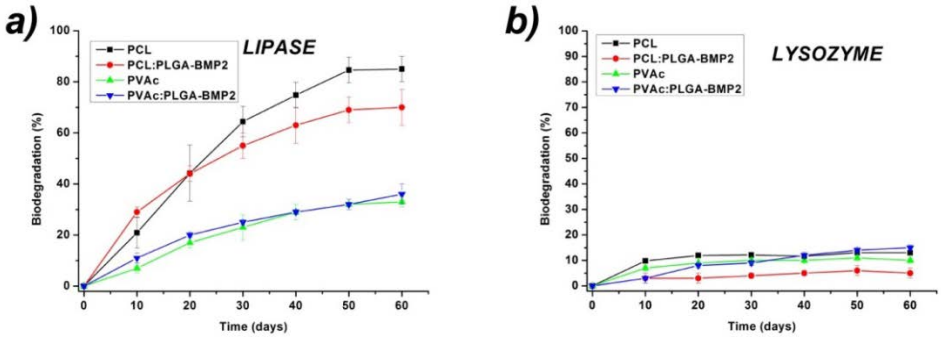

Figure IV.8. Enzymatic degradation of membranes by lipase (a) and lysozyme (b).

The effects of lipase and lysozyme on the PCL were corroborated by infrared (IR) spectroscopy (Figure IV.9). Bands at 1725 and 1240 cm^{-1}, related to C=O and C-O-C bonds, respectively, slightly changed after enzymatic degradation. Besides, the ratios between signals assigned to PO_4^{3-} (1040 cm^{-1}), owing to the presence of HAn, and the above-mentioned polymer bands indicate a minor change in sample polymer content after the enzymatic attack (Table IV.3). Even when it is known that PVAc can be degraded by microorganisms, especially filamentous fungi (30,31), to our knowledge, there is no published study about PVAc degradation by lysozyme. The mass decrease observed in the PVAc membrane may be related only to the PCL degradation.

Table IV.3. Area ratio in lipase and lysozyme degradation media.

SAMPLE	**Area ratio**	
	C=O/ PO_4^{-3}	**C-O-C/PO_4^{-3}**
PCL	2.9	0.7
PCL_LIPASE	0.5	0.2
PCL_LYSOZYME	2.2	0.6
PCL:PLGA-BMP2	2.1	0.6
PCL:PLGA-BMP2_LIPASE	0.2	0.1
PCL:PLGA-	1.9	0.6
PVAC	2.4	1.8
PVAC_LIPASE	1.7	1.7
PVAC_LYSOZYME	2.2	2.0
PVAC:PLGA-BMP2	2.1	1.4
PVAC:PLGA-BMP2_LIPASE	2.3	2.0
PVAC:PLGA-	2.2	1.6

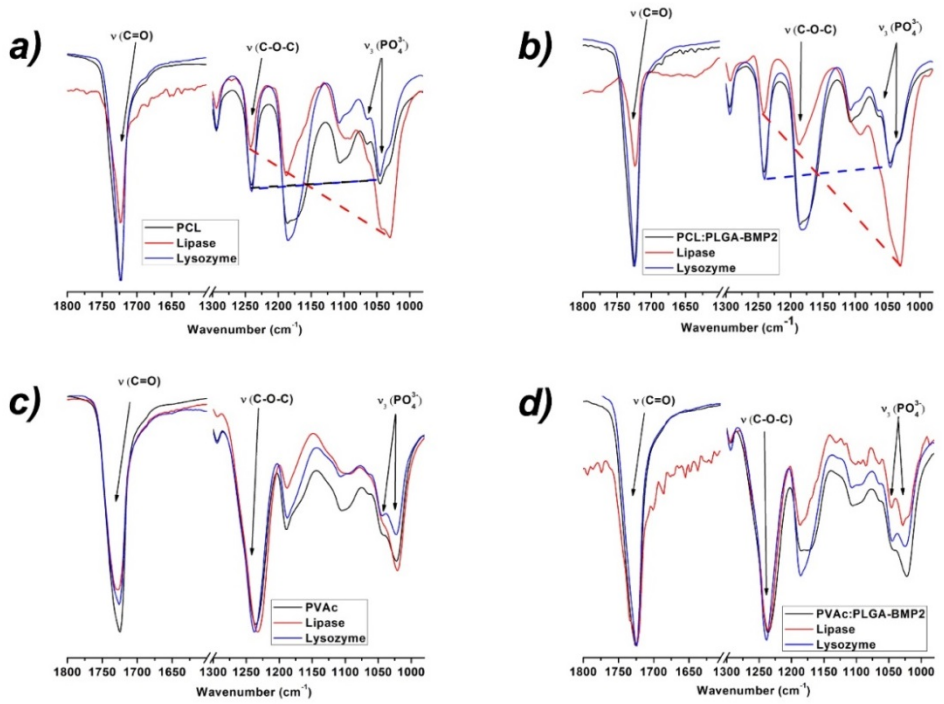

Figure IV.9. FTIR spectra of PCL (a, b) and PVAc (c, d) membranes loaded (b, d) and not loaded (a, c) with PLGA-BMP2 particles after enzymatic degradation with lipase and lysozyme.

In the presence of lipase, the fibers with PVAc in the shell showed lower degradation than did the fibers consisting only of PCL (Figure IV.8a). After 40 days, PCL lost almost 75% of the mass, while PVAc membranes lost only 29% of their mass, as expected because PCL can be hydrolytically and enzymatically degraded by lipase through hydrolysis of the ester bond (32). On the other hand, each lipase has distinct specificity towards the side chain hydrolysis of PVAc (33). The polymer backbone is not hydrolyzed, and only the side chains containing ester linkages undergo hydrolysis catalyzed by lipase. The smaller mass loss of PVAc fibers could be due not only to the smaller amount of PCL in the sample (48 and 86 wt% for PVAc and PCL samples, respectively) but also to the reported reduction in the degradation of PCL with the addition of PVAc in PCL–PVAc blends (34). PCL degradation was also confirmed by IR spectroscopy (Figure IV.5a), which revealed relative enhancement of a band at 1040 cm^{-1} associated with HAn, thereby implying a polymer mass decrease.

On the other hand, the addition of PLGA particles to the fibers slightly changed the degradation of PVAc membranes in the presence of lysozyme and did not affect the behavior with lipase. PLGA particles synthesized from different polymer formulations may possess different degradation rates because the average molecular weight and lactide:glycolide ratio affect the diffusion rate and permeability of the PLGA polymeric matrix, which consequently affect the degradation rate (35). PLGA (75:25) requires more than 56 days to lose ≈ 8 % of its mass in the presence of lysozyme (36). The polymer used in this work (50:50) is a more degradable formulation because of the preferential degradation of the glycolic acid domain owing to its higher hydrophilicity (37). However, it is frequently used to encapsulate lysozyme, and the release in PBS takes place via diffusion through pre-existing pores and channels in the polymer matrix (38). This fact suggests that the degradation of PLGA 50:50 should be very slow, and therefore the release of the remaining protein (32 % for PCL:PLGA-BMP2 and 60 % for PVAc:PLGA-BMP2) may be sustained long-term while PLGA particle degradation proceeds. This process may enable a BMP2 release in the nanogram range as reported to take place during *in vivo* normal bone regeneration (39) as well as during successful *in vivo* bone repair in an experimental model (40). As a consequence, the prepared membrane may manifest both required release types (an initial burst followed by a sustained release) to enhance bone regeneration.

It has been extensively studied and proven that biodegradation of HAn is very limited. However, due to the highly osteoconductive nature of HAn, its use in bone graft substitutes is crucial for improving the cellular response and the mineralization process (41).

IV.3.4 Cell viability and morphology

Human osteoblasts seeded onto the different types of the newly developed membranes adhered and spread, thus forming (after 2 weeks) a layer that covered the surface as a result of their proliferation (Figures IV.10, IV.11 and IV.12). The nanofibrous structure of membranes mimicking the architecture of the ECM favored adhesion and proliferation of osteoblasts as well as the maintenance of their phenotype.

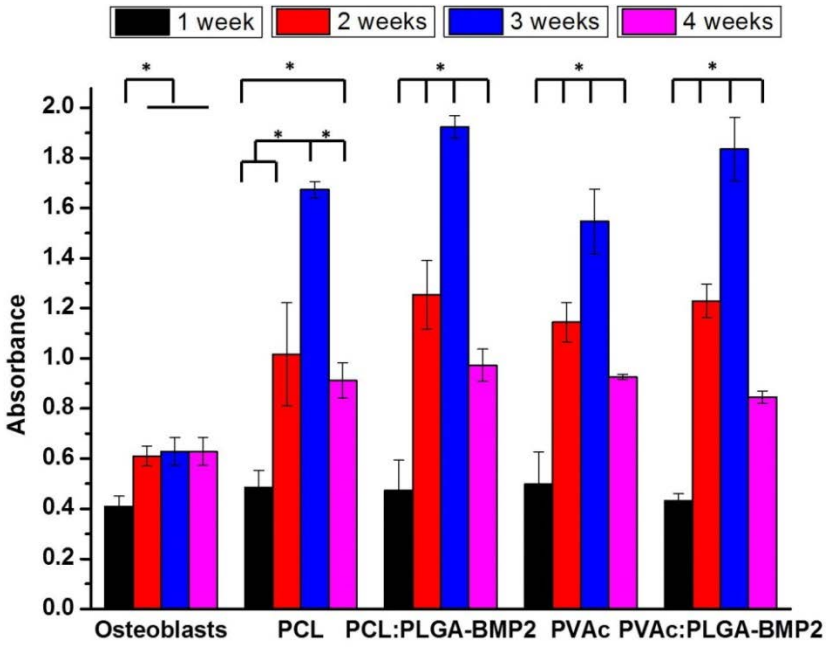

Figure IV.10. Cell viability of osteoblasts seeded in a 2D system and onto PCL and PVAc membranes, decorated and not decorated with PLGA-BMP2 particles, at different time points. Mean ± SD (9 samples). Differences between groups were considered significant when $p < 0.05$.

MTT assays (Figure IV.10) showed cell viability and proliferation during the experiments for up to 4 weeks after seeding. Osteoblast seeding in a 2D environment (directly onto a culture plate well) yielded slightly faster growth after 2 and 3 weeks, as compared to the absorbance recorded in the first week, and decreased again after 4 weeks. This decrease is consistent with saturation of the growth surface, preventing cell proliferation and decreasing cell viability. Furthermore, the results obtained clearly show the significant differences in cell viability and proliferation between 2D and 3D environments because after 2 weeks, viability significantly increased in the 3D membranes owing to the larger surface for cell proliferation. On the other hand, the 3D experiments revealed a large increase in viability until 3 weeks in all the investigated membranes, followed by a decrease after 4 weeks. This finding may be attributed to the rapid proliferation of cells during this time that led to saturation of the adhesion area as indicated in Figures IV.11 and IV.12. After 4 weeks, a decrease in viability was detected on all the membranes tested up to values that are nonetheless significantly higher with

respect to those observed after 1 week. These findings point to the membrane's ability to maintain cell viability for an extended period. Furthermore, absorbance data at the highest cell viability (3 weeks) highlighted significant differences ($p < 0.05$) among the membranes including PLGA-BMP2 particles versus non-loaded membranes, although no statistically significant differences were observed between PCL:PLGA-BMP2 and PVAc:PLGA-BMP2 membranes.

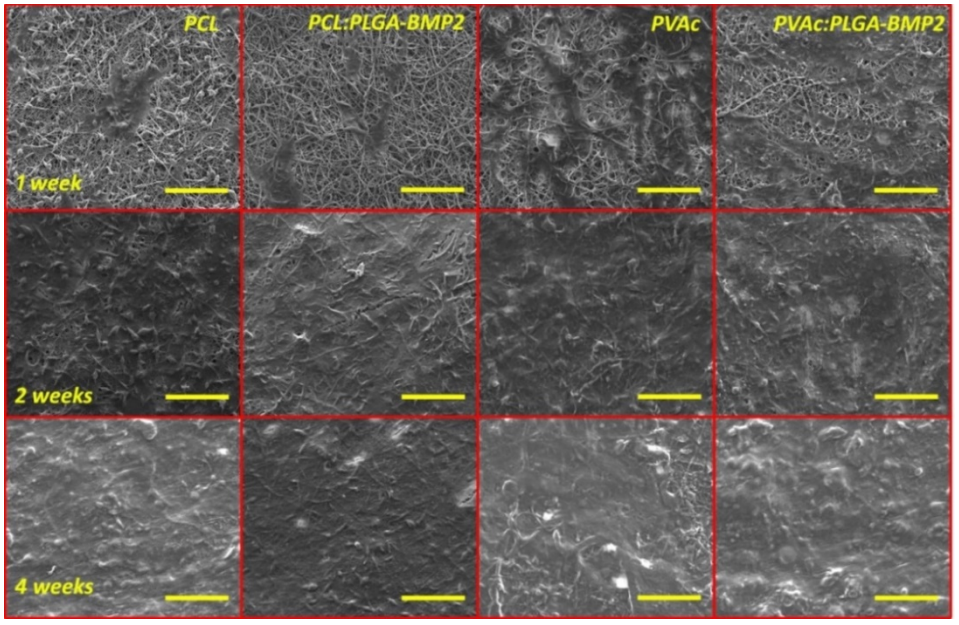

Figure IV.11. Cell proliferation at different time points on PCL and PVAc membranes loaded or not loaded with PLGA-BMP2 particles. Scale bar, 50 μm.

The presence of BMP2 in the membranes improved the cell response while promoting cell proliferation and viability. These findings are in agreement with other studies that describe the improvement of cell interactions on composite membranes that were modified by surface immobilization of collagen and BMP2 (42) or surface adsorption of BMP2 with erythropoietin (43). By contrast, in our study, BMP2 was encapsulated into PLGA particles and released with time to ensure constant exposure of the cell microenvironment to the growth factor.

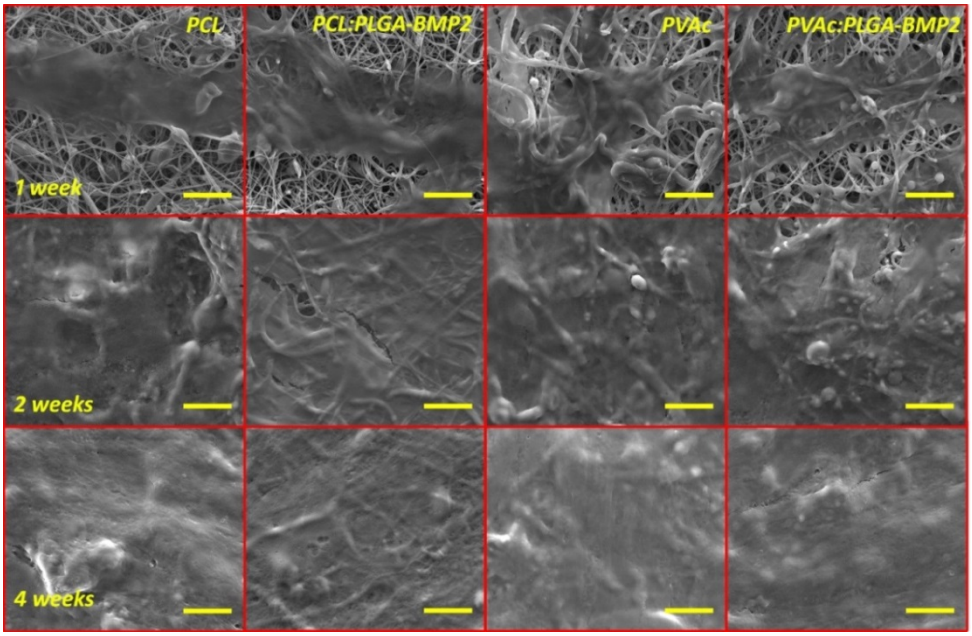

Figure IV.12. SEM images of osteoblasts proliferation onto PCL and PVAc membranes loaded or not loaded with PLGA-BMP2 particles at different time points. Scale bar 10 μm.

IV.3.5 Osteogenic, osteoinductive, and osteoconductive activities of membranes

The capability of the membranes to stimulate bone matrix formation was evaluated by investigating the expression of specific markers such as the secretion of ALP, OCN, and OPN, which perform a crucial function in bone regeneration. Given that the ALP is an early-stage marker of osteogenic differentiation (44,45), we evaluated its secretion by osteoblasts cultured on the different membranes. The ALP activity of cells increased with time, reaching a stationary phase after 3 weeks independently from the type of membrane (Figure IV.13). An improvement of the enzymatic function was observed when the cells were cultured on PCL membranes loaded with BMP2 during the first 3 weeks. These results are in agreement with data from other studies revealing the ALP activity enhancement by cells cultured on PCL membranes in a medium containing BMP2 (46). Similarly, Fu et al. (47) have found a significant increase in cellular enzymatic activity after surface immobilization of BMP2 on PLGA-HA microcarriers, for up to 14 days. In our study, the BMP2-loaded particles along the entire fiber mats ensured a

continuous release of the growth factor, thus increasing the osteogenic activity, in contrast to the BMP2 immobilized on the surface or dissolved in the culture medium.

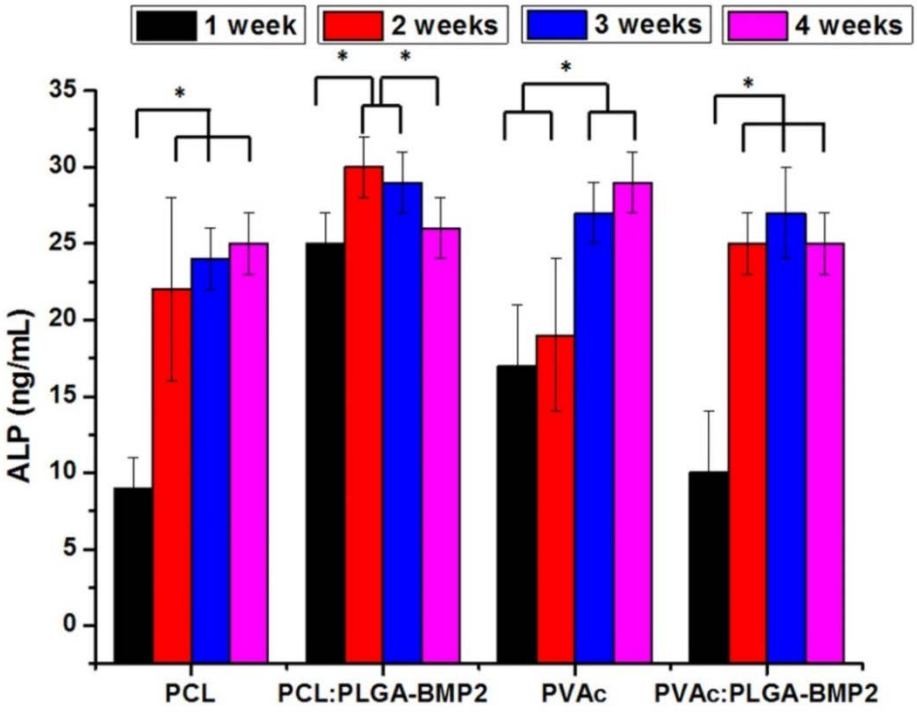

Figure IV.13. ALP concentration in osteoblast cultures seeded onto the investigated membranes at different time points. Mean ± SD (9 samples). Differences between groups were considered significant when $p < 0.05$.

The cell behavior indicated that the mineralization process occurred on all membranes within 3 weeks and then, as expected, ALP was downregulated.

ALP activity is associated with cell differentiation and precedes the secretion of other proteins such as OCN because ALP helps to prepare the ECM for the deposition before the start of mineralization.

OCN expression corresponds to the onset of mineralization, and this protein plays a pivotal role in bone formation and mineralization but also in metabolic functions of osteoblasts (48). Due to the presence of glutamic acid regions in its chemical structure, OCN has strong affinity for Ca^{2+} and HA,

whose equilibrium binding properties are involved in bone turnover and mineralization (49). In contrast to other proteins, OCN is a bone-specific protein that modulates the mineralization process.

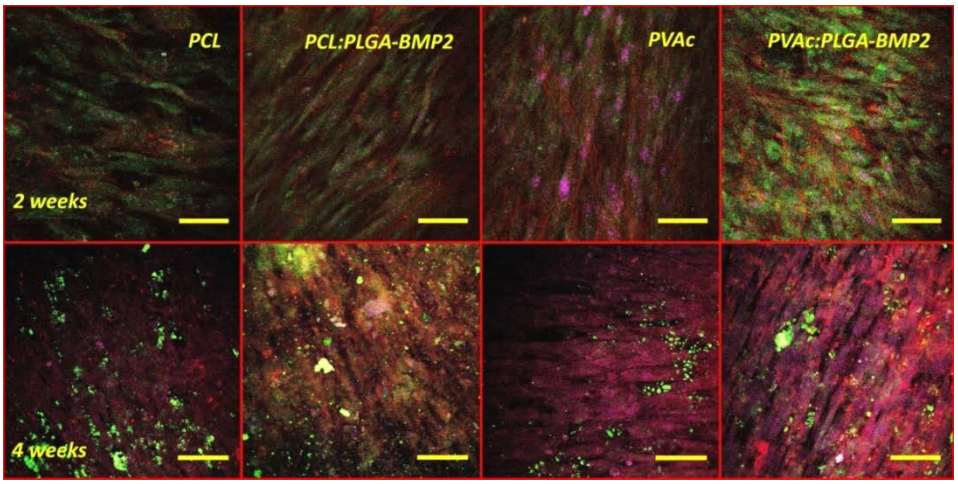

Figure IV.14. Confocal microscopy merged images of osteoblasts seeded onto the membranes after 2 weeks (upper images) and 4 weeks (lower images). The cells were stained for actin (red), osteocalcin (OCN; green), and osteopontin (OPN; purple). Scale bar, 100 μm.

OPN also participates in the ECM and bone formation although its function is more prominent in later stages of bone development, showing peaks of expression in remodeling phases because it plays a key part in supporting osteoclastic resorption (50). Figure IV.14 shows a comparison of the expression of actin (red), OCN (green), and OPN (purple) among the four types of electrospun membranes investigated at an early stage (2 weeks) and at a later stage (4 weeks) of the study. These confocal images clearly reveal the changes in OCN and OPN expression within this period, with OCN being more prevalent at 2 weeks after seeding, while OPN showed an increase in its expression after 4 weeks. The newly developed membranes were able to support the bone-related protein expression in accordance with other studies in the literature that used PCL-HA to promote the osteoconductivity of MSC-derived osteoblasts (51). Furthermore, their expression was more pronounced in BMP2-loaded membranes, especially in PVAc membranes (Figures IV.15 and IV.16). The distribution of cells in BMP2-loaded PVAc membranes is also shown, suggesting a cell distribution on the seeding surface in accordance with pore size as we previously described (4). BMP2

induced osteogenic activity as demonstrated in other works concerning BMP2 immobilized on PLGA-HA microcarriers that exerted an improved bioactivity of pre-osteoblastic cells (47).

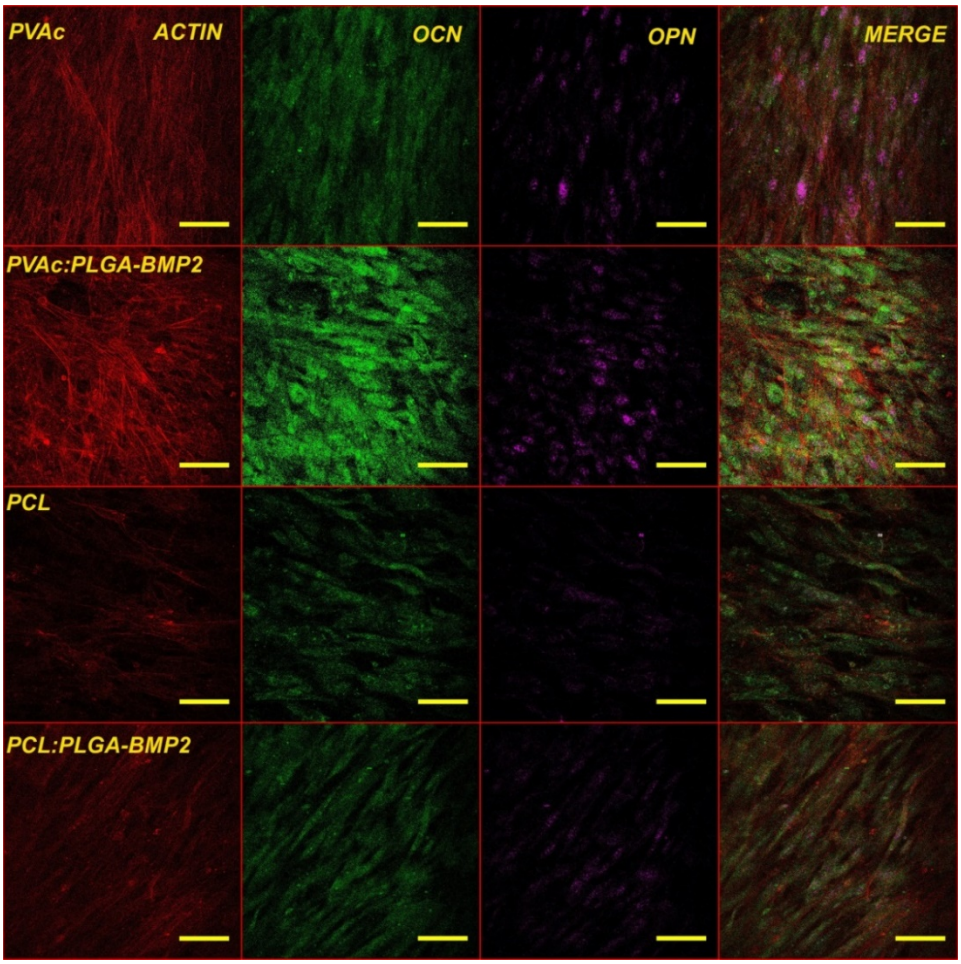

Figure IV.15. Confocal microscopy images of cells seeded onto the membranes assayed after 2 weeks. Scale bar 100 μm.

This protein is one of the most important osteogenic cytokines that regulate the transcription of *Runx2* and thus exert a direct effect on osteoblastic differentiation (44,52). Its addition to the membrane enhanced osteoblastic differentiation, as highlighted by the morphology and the prominent localization and distribution of both proteins, OCN and OPN. These results confirm our previous observations (4) and suggest that these

PCL/PVAc-loaded PLGA-BMP2 membranes are a potential therapeutic approach for bone tissue engineering.

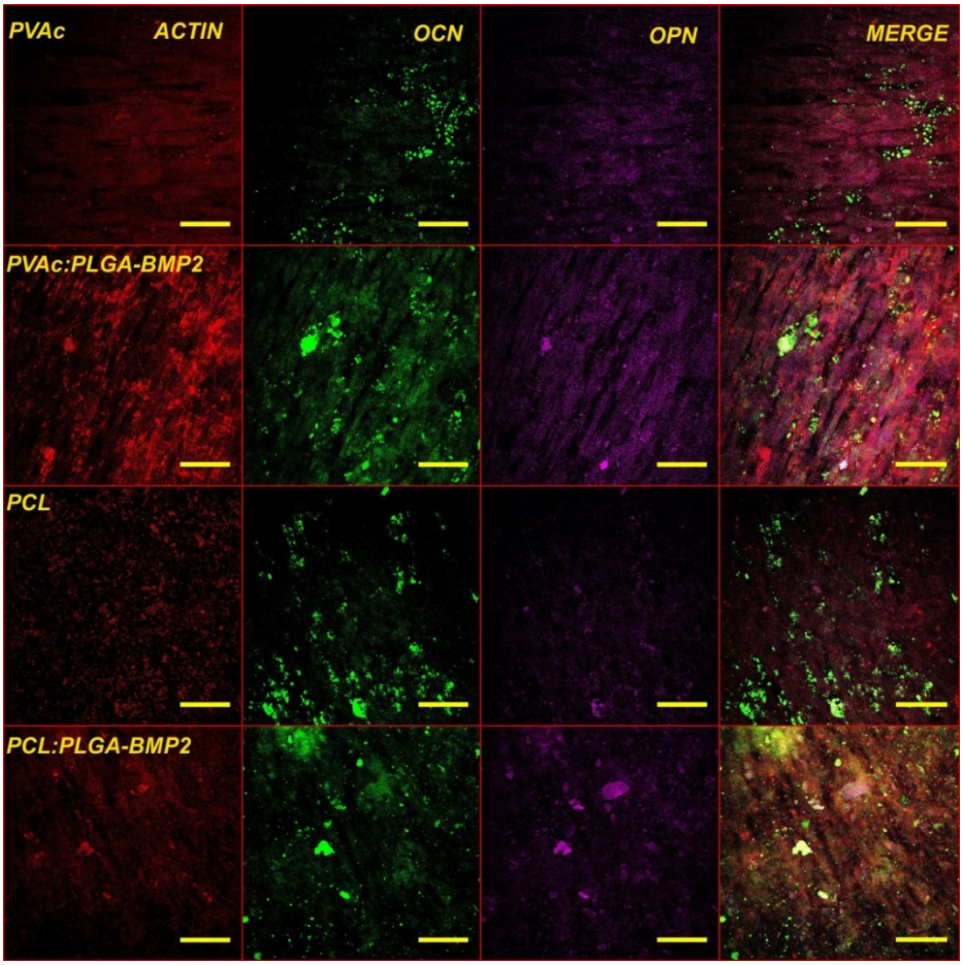

Figure IV.16. Confocal microscopy images of cells seeded onto the membranes assayed after 4 weeks. Scale bar 100 μm.

IV.4 Conclusions

It has been previously reported that electrospun PCL nanofibers loaded with HA promote apatite formation, whereas the presence of PVAc in the fiber shell increases hydrophilicity and favors osteoblast adhesion and proliferation (4). Given that BMP2 could be an alternative way to increase osteogenic activity (8), in this work, those fibers were decorated with PLGA-BMP2 particles obtained by electrospraying for osteoinductive and osteoconductive purposes in bone regeneration. Fibers and particles kept their size and structure after the particles were electrosprayed, though HAn loading was slightly lower (≤ 3.9 %) when PLGA was present in the samples. BMP2 was successfully loaded into PLGA particles, and their loading and activity after electrospraying were confirmed, yielding growth factor loads up to 1.7 μg/g in PCL:PLGA-BMP2 and PVAc:PLGA-BMP2 membranes with a final BMP2 concentration of 39 and 40 μg/mL, respectively; a mid-range concentration can fuse bone defects without adverse effects (53). The BMP2 release was 40–68 %, being lower for PVAc-containing membranes; this phenomenon may be attributed to their absorption capacity. Enzymatic degradation of the membranes highlighted their good biodegradation profile, supporting their good potential for bone regeneration. In addition, osteoblast viability and proliferation increased when the FDA-approved growth factor BMP2 was present in the membranes; the expression of bone formation and maturation markers was also improved by BMP2. Taken together, these results suggest that BMP2 is a key factor for the potential improvement of PCL/PVAc membranes. Besides, the combination of PCL, PVAc, and PLGA-BMP2 is a novel and promising therapeutic approach to bone repair.

References

1. Wang Y, Wei Y, Zhang X, Xu M, Liu F, Ma Q, et al. PLGA/PDLLA core shell submicron spheres sequential release system: Preparation, characterization and promotion of bone regeneration *In vitro* and *in vivo*. Chem Eng J. 2015;273:490–501.

2. Goonoo N, Khanbabaee B, Steuber M, Bhaw-Luximon A, Jonas U, Pietsch U, et al. κ-Carrageenan Enhances the Biomineralization and Osteogenic Differentiation of Electrospun Polyhydroxybutyrate and Polyhydroxybutyrate Valerate Fibers. Biomacromolecules. American Chemical Society; 2017 May;18(5):1563–73.

3. Tiwari AP, Joshi MK, Lee J, Maharjan B, Ko SW, Park CH, et al. Heterogeneous electrospun polycaprolactone/polyethylene glycol membranes with improved wettability, biocompatibility, and mineralization. Colloids Surfaces A Physicochem Eng Asp. Elsevier; 2017 May;520:105–13.

4. Aragon J, Navascues N, Mendoza G, Irusta S. Laser-treated electrospun fibers loaded with nano-hydroxyapatite for bone tissue engineering. Int J Pharm. 2017 Jun;525(1):112–22.

5. Martins AF, Facchi SP, da Câmara PCF, Camargo SEA, Camargo CHR, Popat KC, et al. Novel poly(ε-caprolactone)/amino-functionalized tannin electrospun membranes as scaffolds for tissue engineering. J Colloid Interface Sci. 2018 Sep;525:21–30.

6. Ren K, Wang Y, Sun T, Yue W, Zhang H. Electrospun PCL/gelatin composite nanofiber structures for effective guided bone regeneration membranes. Mater Sci Eng C. Elsevier; 2017 Sep;78:324–32.

7. Hong S, Kim G. Fabrication of electrospun polycaprolactone biocomposites reinforced with chitosan for the proliferation of mesenchymal stem cells. Carbohydr Polym. Elsevier; 2011 Jan;83(2):940–6.

8. Cao L, Yu Y, Wang J, Werkmeister JA, McLean KM, Liu C. 2- N , 6- O - sulfated chitosan-assisted BMP-2 immobilization of PCL scaffolds for enhanced osteoinduction. Mater Sci Eng C. 2017 May;74:298–306.

9. Bezemer JM, Radersma R, Grijpma DW, Dijkstra PJ, van Blitterswijk CA, Feijen J. Microspheres for protein delivery prepared from amphiphilic multiblock copolymers. 1. Influence of preparation techniques on particle characteristics and protein delivery. J Control Release. 2000 Jul;67(2–3):233–48.

10. Tsuji K, Bandyopadhyay A, Harfe BD, Cox K, Kakar S, Gerstenfeld L, et al. BMP2 activity, although dispensable for bone formation, is required for the initiation of fracture healing. Nat Genet. 2006 Dec;38(12):1424–9.

11. Li L, Zhou G, Wang Y, Yang G, Ding S, Zhou S. Controlled dual delivery of BMP-2 and dexamethasone by nanoparticle-embedded electrospun nanofibers for the efficient repair of critical-sized rat calvarial defect. Biomaterials. 2015 Jan;37:218–29.

12. Li X, Min S, Zhao X, Lu Z, Jin A. Optimization of entrapping conditions to improve the release of BMP-2 from PELA carriers by response surface methodology. Biomed Mater. 2014 Dec;10(1):15002.

13. Crecente-Campo J, Borrajo E, Vidal A, Garcia-Fuentes M. New scaffolds encapsulating TGF-β3/BMP-7 combinations driving strong chondrogenic differentiation. Eur J Pharm Biopharm. 2017 May;114:69–78.

14. Hassan A, Hosny K, Murshid Z, Alhadlaq A, Yamani A, Naguib G. Depot injectable biodegradable nanoparticles loaded with recombinant human bone morphogenetic protein-2: preparation, characterization, and *in vivo* evaluation. Drug Des Devel Ther. Dove Press; 2015 Jul;9:3599.

15. Zhang H-X, Zhang X-P, Xiao G-Y, Hou Y, Cheng L, Si M, et al. *In vitro* and *in vivo* evaluation of calcium phosphate composite scaffolds containing BMP-VEGF loaded PLGA microspheres for the treatment of avascular necrosis of the femoral head. Mater Sci Eng C. 2016 Mar;60:298–307.

16. Zhang L, Si T, Fischer AJ, Letson A, Yuan S, Roberts CJ, et al. Coaxial Electrospray of Ranibizumab-Loaded Microparticles for Sustained Release of Anti-VEGF Therapies. Jablonski MM, editor. PLoS One.

Public Library of Science; 2015 Aug;10(8):e0135608.

17. Karimi Zarchi AA, Abbasi S, Faramarzi MA, Gilani K, Ghazi-Khansari M, Amani A. Development and optimization of N-Acetylcysteine-loaded poly (lactic-co-glycolic acid) nanoparticles by electrospray. Int J Biol Macromol. 2015 Jan;72:764–70.

18. Yoo S-Y, Kim S-K, Heo S-J, Koak J-Y, Lee J-H, Park J-M. Biochemical Responses of Anodized Titanium Implants with a Poly(lactide-co-glycolide)/Bone Morphogenic Protein-2 Submicron Particle Coating. Part 1: An *In vitro* Study. Int J Oral Maxillofac Implants. 30(3):512–8.

19. Lavielle N, Hébraud A, Schlatter G, Thöny-Meyer L, Rossi RM, Popa A-M. Simultaneous Electrospinning and Electrospraying: A Straightforward Approach for Fabricating Hierarchically Structured Composite Membranes. ACS Appl Mater Interfaces. American Chemical Society; 2013 Oct;5(20):10090–7.

20. Kim SE, Yun Y-P, Han Y-K, Lee D-W, Ohe J-Y, Lee B-S, et al. Osteogenesis induction of periodontal ligament cells onto bone morphogenic protein-2 immobilized PCL fibers. Carbohydr Polym. 2014 Jan;99:700–9.

21. Zara JN, Siu RK, Zhang X, Shen J, Ngo R, Lee M, et al. High Doses of Bone Morphogenetic Protein 2 Induce Structurally Abnormal Bone and Inflammation *In vivo*. Tissue Eng Part A. 2011 May;17(9–10):1389–99.

22. Lee HJ, Koh W-G. Hydrogel Micropattern-Incorporated Fibrous Scaffolds Capable of Sequential Growth Factor Delivery for Enhanced Osteogenesis of hMSCs. ACS Appl Mater Interfaces. American Chemical Society; 2014 Jun;6(12):9338–48.

23. Gupta SC, Baheti G., Gupta B. Application of hydrogel system for neutron attenuation. Radiat Phys Chem. Pergamon; 2000 Jul;59(1):103–7.

24. Kannan R, Muthuvijayan V, Prasad E. *In vitro* study of a glucose attached poly(aryl ether) dendron based gel as a drug carrier for a local anaesthetic. New J Chem. The Royal Society of Chemistry; 2017 Jul;41(15):7453–62.

25. SIMONI RC, LEMES GF, FIALHO S, GONÇALVES OH, GOZZO AM, CHIARADIA V, et al. Effect of drying method on mechanical, thermal and water absorption properties of enzymatically crosslinked gelatin hydrogels. An Acad Bras Cienc. 2017 May;89(1 suppl):745–55.

26. Siepmann J, Peppas NA. Higuchi equation: Derivation, applications, use and misuse. Int J Pharm. 2011 Oct;418(1):6–12.

27. Ritger PL, Peppas NA. A simple equation for description of solute release I. Fickian and non-fickian release from non-swellable devices in the form of slabs, spheres, cylinders or discs. J Control Release. Elsevier; 1987 Jun;5(1):23–36.

28. Chaerunisaa M, Chaerunisaa AY. Polymer combination for parenteral drug delivery. Int J Pharm Sci Res. 2017;8(5):1993–2002.

29. Banerjee A, Chatterjee K, Madras G. Enzymatic degradation of polycaprolactone–gelatin blend. Mater Res Express. IOP Publishing; 2015;2(4):45303.

30. Cappitelli F, Sorlini C. Microorganisms attack synthetic polymers in items representing our cultural heritage. Appl Environ Microbiol. American Society for Microbiology (ASM); 2008 Feb;74(3):564–9.

31. Takasu A, Baba M, Hirabayashi T. Preparation and Biodegradation of Sugar-Containing Poly(vinyl acetate) Emulsions. Macromol Biosci. 2008 Feb;8(2):193–8.

32. Gámiz-González MA, Vidaurre A, Gómez Ribelles JL. Biodegradable chitosan-poly(Ɛ-caprolactone) dialdehyde copolymer networks for soft tissue engineering. Polym Degrad Stab. 2017 Apr;138(138):47–54.

33. Chattopadhyay S, Sivalingam G, Madras G. Lipase specificity for the hydrolysis of poly (vinyl acetate). Polym Degrad Stab. Elsevier; 2003 Jan;80(3):477–83.

34. Sivalingam G, Chattopadhyay S, Madras G. Enzymatic degradation of poly (ε-caprolactone), poly (vinyl acetate) and their blends by lipases. Chem Eng Sci. Pergamon; 2003 Jul;58(13):2911–9.

35. Qodratnama R, Serino LP, Cox HC, Qutachi O, White LJ. Formulations for modulation of protein release from large-size PLGA microparticles for tissue engineering. Mater Sci Eng C. 2015 Feb;47:230–6.

36. Zhou X, Cai Q, Yan N, Deng X, Yang X. *In vitro* hydrolytic and enzymatic degradation of nestlike-patterned electrospun poly(D,L-lactide-co-glycolide) scaffolds. J Biomed Mater Res Part A. 2010 Dec;95A(3):755–65.

37. Makadia HK, Siegel SJ. Poly Lactic-co-Glycolic Acid (PLGA) as Biodegradable Controlled Drug Delivery Carrier. Polymers (Basel). NIH Public Access; 2011 Sep;3(3):1377–97.

38. Jiang G, Woo BH, Kang F, Singh J, DeLuca PP. Assessment of protein release kinetics, stability and protein polymer interaction of lysozyme encapsulated poly(D,L-lactide-co-glycolide) microspheres. J Control Release. 2002 Feb;79(1–3):137–45.

39. Gamradt SC, Lieberman JR. Genetic modification of stem cells to enhance bone repair. Ann Biomed Eng. 2004 Jan;32(1):136–47.

40. Huber E, Pobloth A-M, Bormann N, Kolarczik N, Schmidt-Bleek K, Schell H, et al. * Demineralized Bone Matrix as a Carrier for Bone Morphogenetic Protein-2: Burst Release Combined with Long-Term Binding and Osteoinductive Activity Evaluated *In vitro* and *In vivo*. Tissue Eng Part A. 2017 Dec;23(23–24):1321–30.

41. Venkatesan J, Pallela R, Bhatnagar I, Kim S-K. Chitosan–amylopectin/hydroxyapatite and chitosan–chondroitin sulphate/hydroxyapatite composite scaffolds for bone tissue engineering. Int J Biol Macromol. 2012 Dec;51(5):1033–42.

42. Song M-J, Amirian J, Linh NTB, Lee B-T. Bone morphogenetic protein-2 immobilization on porous PCL-BCP-Col composite scaffolds for bone tissue engineering. J Appl Polym Sci. 2017 Sep;134(33):45186.

43. Patel JJ, Modes JE, Flanagan CL, Krebsbach PH, Edwards SP, Hollister SJ. Dual Delivery of EPO and BMP2 from a Novel Modular Poly-ε-Caprolactone Construct to Increase the Bone Formation in Prefabricated Bone Flaps. Tissue Eng Part C Methods. 2015 Sep;21(9):889–97.

44. Rutkovskiy A, Stensløkken K-O, Vaage IJ. Osteoblast Differentiation at a Glance. Med Sci Monit Basic Res. International Scientific Literature, Inc.; 2016 Sep;22:95–106.

45. Jensen ED, Gopalakrishnan R, Westendorf JJ. Regulation of gene expression in osteoblasts. Biofactors. NIH Public Access; 2010;36(1):25–32.

46. Yilgor P, Sousa RA, Reis RL, Hasirci N, Hasirci V. Effect of scaffold architecture and BMP-2/BMP-7 delivery on *In vitro* bone regeneration. J Mater Sci Mater Med. 2010 Nov;21(11):2999–3008.

47. Fu C, Yang X, Tan S, Song L. Enhancing Cell Proliferation and Osteogenic Differentiation of MC3T3-E1 Pre-osteoblasts by BMP-2 Delivery in Graphene Oxide-Incorporated PLGA/HA Biodegradable Microcarriers. Sci Rep. 2017 Dec;7(1):12549.

48. Wei J, Karsenty G. An overview of the metabolic functions of osteocalcin. Rev Endocr Metab Disord. NIH Public Access; 2015 Jun;16(2):93–8.

49. Hauschka P V., Wians FH. Osteocalcin-hydroxyapatite interaction in the extracellular organic matrix of bone. Anat Rec. 1989 Jun;224(2):180–8.

50. Chen J, Singh K, Mukherjee BB, Sodek J. Developmental expression of osteopontin (OPN) mRNA in rat tissues: evidence for a role for OPN in bone formation and resorption. Matrix. 1993 Mar;13(2):113–23.

51. Morelli S, Facciolo D, Messina A, Piscioneri A, Salerno S, Drioli E, et al. Polycaprolactone-Hydroxyapatite Composite Membrane Scaffolds for Bone Tissue Engineering. MRS Proc. Cambridge University Press; 2013 Jan;1502:mrsf12-1502-t01-09.

52. Chen D, Harris MA, Rossini G, Dunstan CR, Dallas SL, Feng JQ, et al. Bone morphogenetic protein 2 (BMP-2) enhances BMP-3, BMP-4, and bone cell differentiation marker gene expression during the induction of mineralized bone matrix formation in cultures of fetal rat calvarial osteoblasts. Calcif Tissue Int. 1997 Mar;60(3):283–90.

53. Halling Linder C, Ek-Rylander B, Krumpel M, Norgård M, Narisawa S,

Millán JL, et al. Bone Alkaline Phosphatase and Tartrate-Resistant Acid Phosphatase: Potential Co-regulators of Bone Mineralization. Calcif Tissue Int. Springer US; 2017 Jul;101(1):92–101.

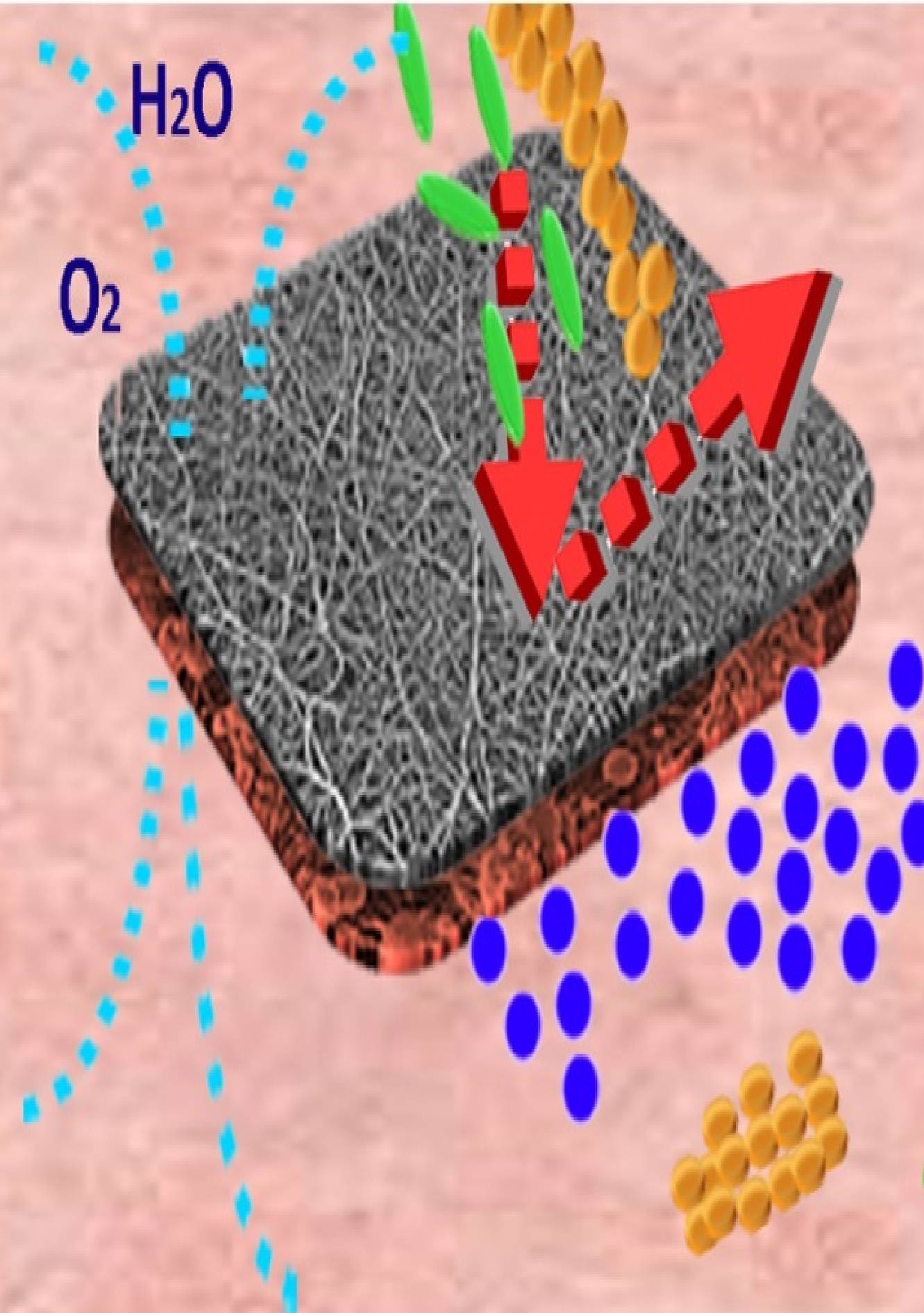
H2O
O2

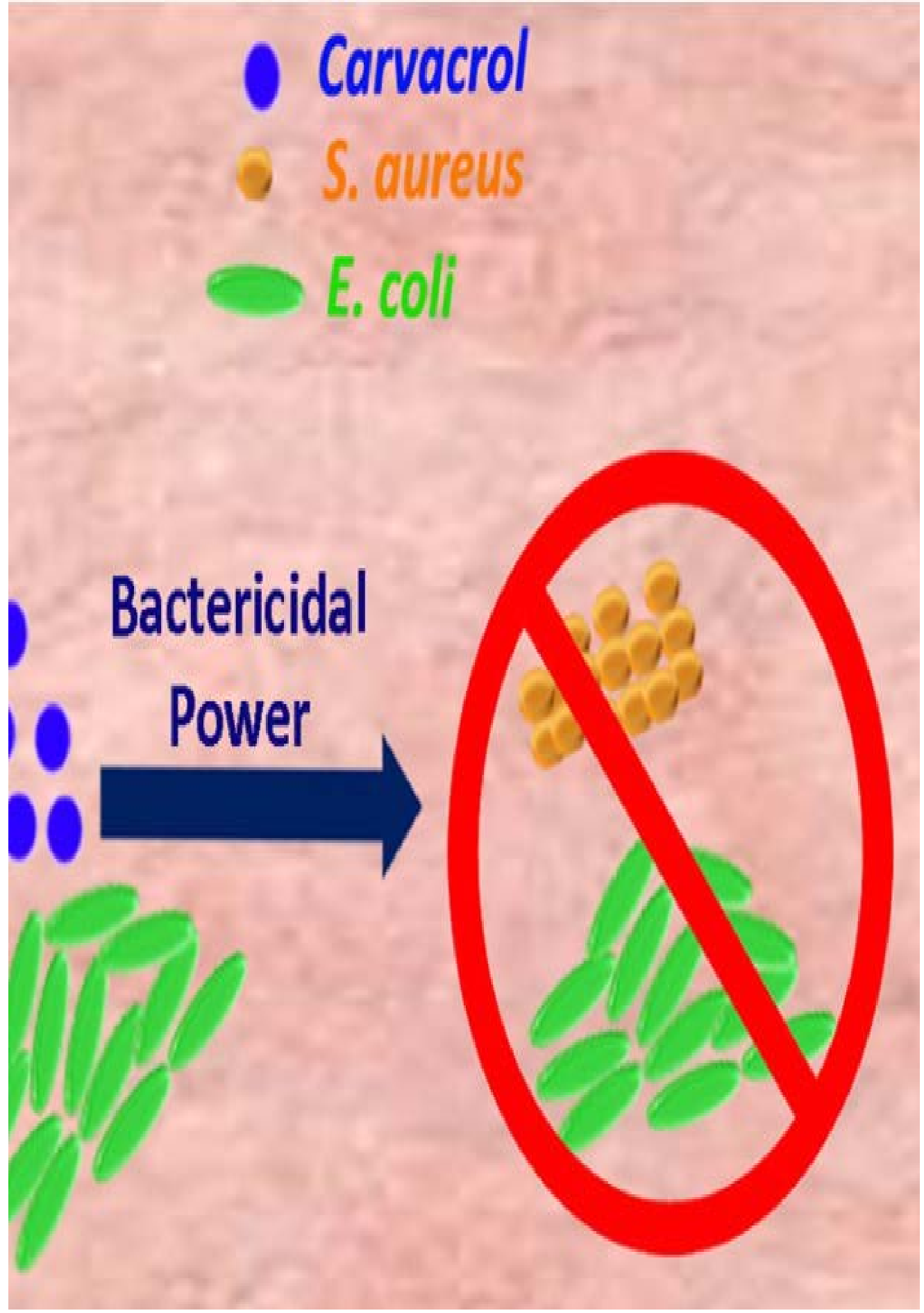
Carvacrol
S. aureus
E. coli
Bactericidal
Power

CHAPTER V

Electrospun asymmetric membranes for wound dressing applications

The contents of this chapter have been adapted from the following submitted work (under review):

Electrospun asymmetric membranes for wound dressing applications. Javier Aragón, Clarinda Costa, Isabel Coelhoso, Gracia Mendoza, Ana Aguiar-Ricardo and Silvia Irusta. **Materials Science and Engineering C (MSEC_2018_3013)**

"To accomplish a rapid wound healing it is necessary to develop an asymmetric membrane with interconnected pores consisting of a top layer that prevents rapid dehydration of the wound and bacteria penetration and a sub-layer with high absorption capacity and bactericidal properties. Polycaprolactone (PCL)/polyvinyl acetate (PVAc) asymmetric membranes loaded with the bactericidal monoterpene carvacrol (CRV) were synthesized and characterized by scanning electron microscopy and Fourier transform infrared spectroscopy. Mechanical properties in dry and wet conditions and fluid handling behavior were also assessed. In addition, biological studies regarding their bactericidal effects, cytocompatibility and wound closure properties were also developed. Loading efficiencies of 40-50 % were achieved in the prepared samples and 85-100 % of the loaded CRV was released in simulated wound pH evolution medium. The significant inhibition of gram negative (Escherichia coli S17) and gram positive (Staphylococcus aureus ATCC 25923) bacteria growth clearly showed the suitability of the fabricated membranes for wound healing applications. Furthermore, cytocompatibility of the loaded membranes was demonstrated both in 2D and 3D human dermal fibroblast cultures, as well as cell migration was not impaired by released carvacrol from the membranes. These results highlight the potential of these polymeric electrospun membranes for wound healing."

INDEX

V.1 Introduction

Wound healing is a complex physiological process which requires the action in consonance of cells and matrix components. This process consists of three dynamic and overlapping phases: inflammation, proliferation and tissue remodeling (1). An ideal wound dressing should establish an optimal environment over the wound to accelerate the healing. Among the properties required, the first one is acting as barrier against elements as well as invasion of pathogenic organism. It should also be able to absorb wound exudates to prevent tissue maceration or pyo-inflammatory complications (2). Given the need of a physiologically moist environment for reepithelialization, it is equally important that wound dressing materials have moisture vapor transmission rate (MVTR) to manage fluid equilibrium avoiding either desiccation or exudate accumulation. In addition, gaseous exchange is needed to allow cellular respiration (3). Furthermore, the materials should not be toxic or allergenic to the human body.

Polymeric nanofiber membranes have drawn the attention in the wound dressing development field since they can mimic a natural nanometer dimension of the tissue they are healing (4). Polymeric meshes produced by electrospinning consist of ultra-fine fibers with diameters ranging from several micrometers down to few nanometers. The high surface area and nanoporosity make these structures particularly interesting for wound healing applications because these properties have been shown to promote homeostasis of injured tissues (5). The high surface area also favors fluid absorption and enhances loaded antimicrobial delivery. The porous nature of electrospun mats not only works against bacterial infection due to a small pores size but it also maintains a high gas permeation, which protects against tissue dehydration (4).

In order to accomplish all the requirements for rapid wound healing, an asymmetric membrane with interconnected pores consisting of a top layer able to prevent rapid dehydration of the wound surface and bacteria penetration and a sub-layer with high absorption capacity appear as an ideal candidate (6). Electrospun synthetic polymer mats are commonly used as wound dressings because the mechanical stiffness and slow degradation rate (3). Polycaprolactone (PCL) is a biodegradable and biocompatible poly(α-ester) and is one of the polymers that has been extensively used for wound healing applications because it promotes faster healing and reduced

inflammatory infiltrate. PCL physico-chemical properties, such as hydrophobic characteristics, excellent spinnability, favorable mechanical properties, and slow degradation make this polymer a good candidate for wound dressing top layer (7). On the other hand, poly(vinyl acetate) (PVAc), a biocompatible and biodegradable polymer (owing to the hydrolysable groups in the side chain), has also been used in biomedical applications, including drug and cell carriers, and tissue engineering (8). It is an inert polymer with the advantage that it does not induce a deleterious reaction in living tissue. Hydrogels such as PVAc containing functional groups, i.e. the ester group COOR, usually show good biocompatibility in contact with body fluids, and tissues. Most important, the swelling ratio of PVAc capsules was found to be around 140 % after 15 h in water medium which makes this polymer an interesting material for the sub-layer with high absorption capacity (9).

The infection under dressing caused by burns, split skin graft donor sites, pressure, sores, and diabetic ulcers can lead to prolonged healing time; consequently, wounds often require treatment with antibiotics. Sustained local delivery for about a week is preferred to systemic administration because of the advantages of these delivery systems. Local delivery improves the effectiveness of drug therapy, decreases the side effects on a tissue, and reduces the frequency of dressing replacements to increase patient compliance (8). Unlike common techniques, electrospinning is more convenient for incorporating bioactive compounds, including antiseptics, antibiotics and antifungals into the polymeric fibers. Electrospun drug-loaded membranes have recently received a great attention due to their optimal high drug-encapsulation efficiency and high surface area-to-volume ratio (10).

However, antibiotic resistance is an important problem in infected wounds; colonization by resistant microorganisms leads to a complicated and expensive management of the wound due to restricted therapeutic choice. Different state-of-the-art strategies involving natural products have been used in ulcers or related wounds treatments. Among these natural products, extracts from herbal medicinal plants have been used to accelerate the wound healing process since ancient times (7). Essential oils have been shown to possess antibacterial, antifungal, antiviral, insecticidal and antioxidant properties due to their biologically active compounds such as carvacrol, eugenol, and thymol (11). Thyme essential oil, rich in thymol and

carvacrol, loaded into chitosan films showed high antimicrobial properties and, in a concentration of 1.2 % (v/v), the highest antioxidant activity due mainly to carvacrol. Carvacrol (CRV) loaded clays and incorporated into poly(vinylalcohol), poly (vinylpyrrolidone) and chitosan glutamate membranes maintain antioxidant properties and increase its antimicrobial properties (12).

The pH value within a wound is an important parameter because it reflects and influences numerous fundamental physiological and biochemical processes evolved in wound healing (13). Intact skin is naturally acidic (pH ranging from 4 to 6) due to organic acid secretion by keratinocytes in the epidermis. In a wound, the skin is destroyed and the pH of the wound surface increases due to leakage from the microvessels and approximate a pH of 7.4 or even 8.5 in the case of burned patients (14). During the healing process the wound environment may become alkaline due to non-healing wound, but as the healing process progresses, it becomes acidic again (15). It is important that wound dressing materials keep their properties in the environment found in each wound stage.

Objective

The purpose of this work was to obtain an antimicrobial wound dressing material, with appropriate mechanical resistance avoiding rapid dehydration and absorbing exudates in conditions found in all wound healing stages. PCL/PVAc asymmetric membranes, loaded with carvacrol as antimicrobial agent, were prepared by electrospinning technique in order to obtain potential candidates to be used for wound dressing applications. The PCL layer would provide a hydrophobic surface able to act as a waterproof layer and avoid invasion of exogenous microorganisms while the carvacrol loaded PVAc layer would absorb the exudates generated by the wound and release carvacrol as a bactericidal agent. The entire membrane must provide good oxygen permeability and prevent dehydration of the wound.

V.2 Membrane preparation

Asymmetric membranes were prepared in 3 steps (Table V.1) using an Yflow 2.2.D-500 electrospinner (Electrospinning Machines/R&D Microencapsulation, Spain). Two single needles were used; through needle 1 a PCL 7.5 (w/w)% in DCM/DMF (1:1) mixture was fed at 1.5 mL/h, through needle 2 a PVAc-CRV 10 (w/w)% in DMF or 12 (w/w)% in DMF/ETOH (1:1) mixture were fed at 1.5 mL/h. CRV to PVAc ratio in the solutions was 1:10 (w/w). Both needles were connected to the positive power supply at a voltage of 12.4 kV. The tips of the needles were fixed 18 cm above a rotating collection drum. The negative voltage power supply (-2.6 kV) was connected to the collector. The steps followed to obtain Sample I and Sample II are summarized in Table V.1.

Table V.1. Development of asymmetric membranes

Steps		Sample I	Sample II
Step 1 (3 hours)	**Needle 1**	PCL	PCL
	Needle 2	---	---
Step 2 (1.5 hours)	**Needle 1**	PCL	PCL
	Needle 2	PVAc*-CRV	PVAc**-CRV
Step 3 (3 hours)	**Needle 1**	---	---
	Needle 2	PVAc*-CRV	PVAc**-CRV

* 12 (w/w)% PVAc in DMF/ETOH (1/1) ** 10 (w/w)% PVAc in DMF

The characterization techniques and different evaluation methods are described in **Appendix 1**.

V.3 Results and discussion

V.3.1 Membranes characterization by SEM and FTIR

The morphology of the prepared membranes was studied by SEM (Figure V.1). The hydrophobic PCL layer has a thickness of around 100-120 μm in both types of samples and SEM images show fibers with an average diameter of 360 ± 68 nm. As can be seen in the cross section images, because of the synthesis process, there is an intermediate layer composed of both kind of materials that assure the integrity of the membrane. The PVAc layer

is different depending on the preparation conditions, for Sample I a closed net of fibers were obtained (mean diameter 0.6 ± 0.1 μm) while for Sample II microparticles (average size 3 ± 1 μm) were distributed and retained in a loose spiderweb ultrathin fiber structure. Histograms of PCL and PVAc fibers and PVAc particles size were obtained from SEM images (Figure V.2).

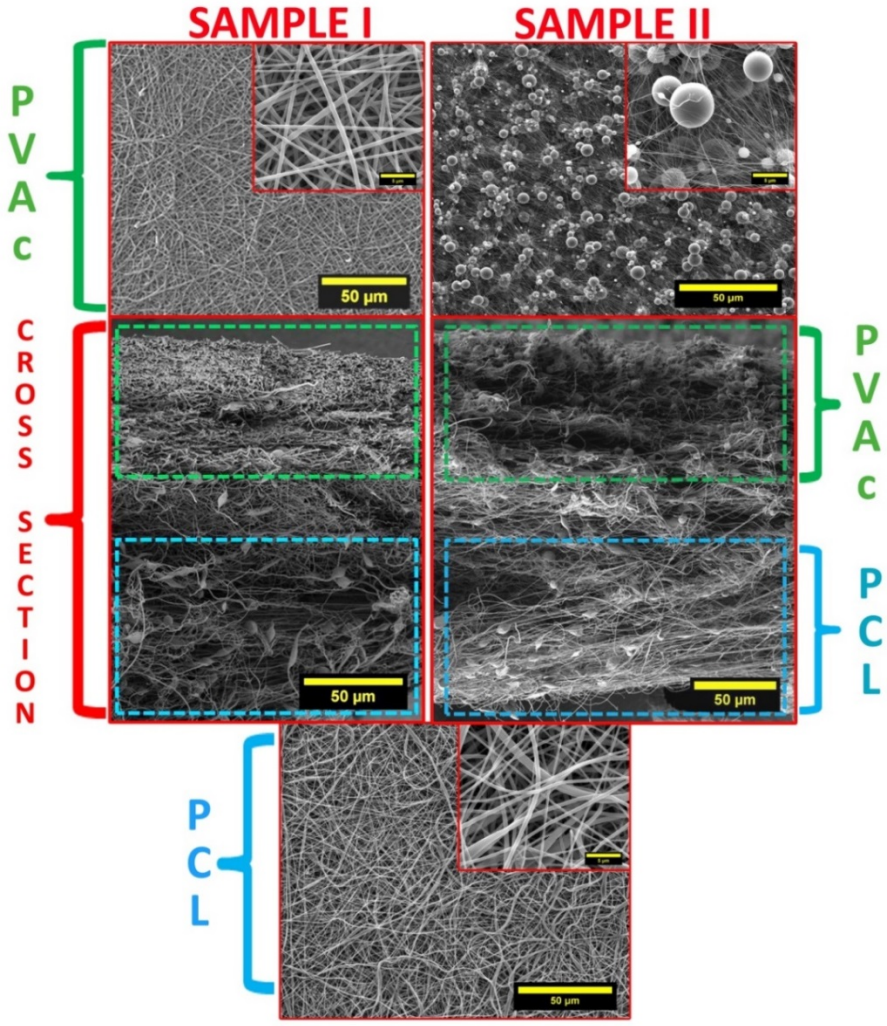

Figure V.1. SEM images of PVAc and PCL faces and cross section of Sample I and Sample II.

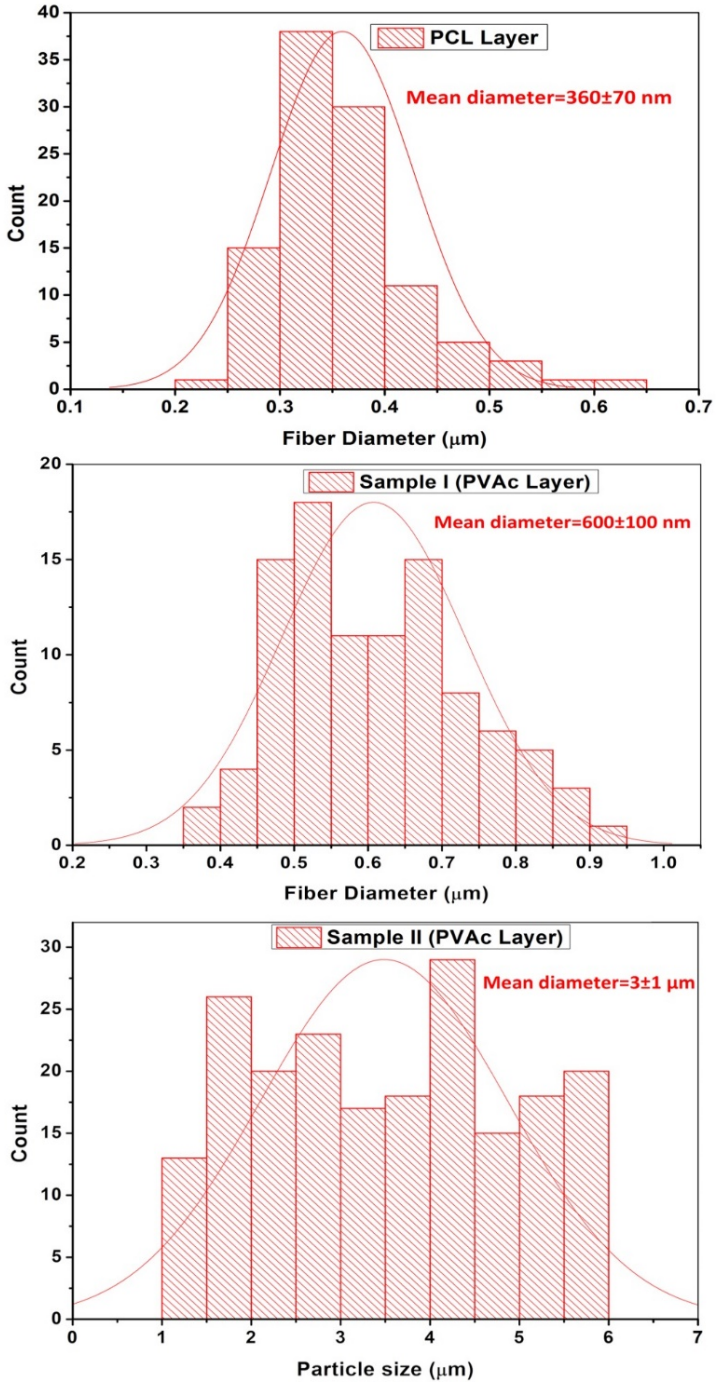

Figure V.2. Size distribution histograms of PCL layer and PVAc layers in Sample I and II.

In order to confirm external faces composition of the prepared membranes, they were analyzed by FTIR and results for Sample II are shown in Figure V.3 (results for Sample I are very similar). The PCL layer spectrum shows all the characteristic peaks of the polymer. The peak at 1724 cm^{-1} is related to the C=O stretching of the ester group. The band in the region 1130 cm^{-1} - 1215 cm^{-1} consists of three overlapping peaks, one at 1188 cm^{-1}, which could be assigned to O-C-O stretching, the second at 1168 cm^{-1} due to symmetrical COC stretching, and the last one at 1155 cm^{-1} to C-O and C-C stretching in the amorphous phase (16). The PVAc face spectrum also exhibit the C=O stretching vibration peak of acetate groups at 1730 cm^{-1}. The prominent band observed at 1225 cm^{-1} can be attributed to C-O-C symmetric stretching vibration on PVAc (17) while the band at 1240 cm^{-1} in PCL spectrum is related to C-O-C asymmetric stretching (18). Comparison of both spectra confirms the asymmetry of the prepared membranes.

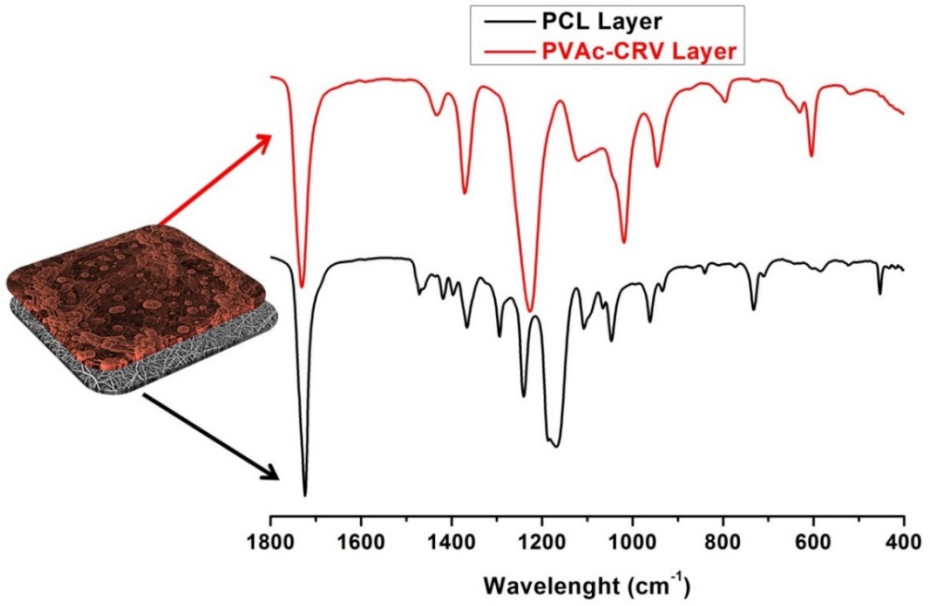

Figure V.3. FTIR analysis of both membrane faces of Sample II.

V.3.2 Mechanical properties

For wound dressing materials the tensile strength and strain are of particular interest because they should not break with regard to load or deformation. Moreover, considering that wound management will involve the use of dressings to keep a moist environment in the wound bed, it is important to measure the mechanical properties in wet conditions. Table V.2 shows the tensile strength results obtained for Sample I and Sample II as prepared and after 1 week at pH 8, the second week at pH 7.4 and last week at pH 5. This protocol was followed due to the results obtained from a clinical trial that studied the skin pH variation in burn patients (19). Maximum tensile strengths are similar for both as-spun samples and are close to values reported for PCL and PCL/collagen electrospun membranes (20). The range of maximum tensile strength for human skin is in the range of 2.5-16 MPa and considering the role of a wound dressing of covering and protection the native skin, values in the range of 6-12 MPa would be high enough to meet the practical requirements (21). The ultimate tensile strengths (UTS) obtained for samples immersed for 1 week at pH 8 were similar to values obtained for the spun membranes. However, after 1 week at pH 7.4 an important decrease in the maximum strength was observed in Sample I. However, since the pH change is very low (0.6 points) the phenomena would be more related to the fluid absorption process during two weeks (22). The continuous water uptake would lead to fibers network re-orientation and fiber hydration would be responsible for the reduction of the ultimate tensile strength. The predominance of particles in Sample II would avoid this change even after three weeks in aqueous medium. There was no further change in UTS after the third week, even when acid media were used for immersing the samples, probably because the equilibrium was reached after this time in contact with water.

Elongation at break of human skin are in the 17-207 % range (23). Both kinds of samples have strain to failure values higher than 100 %, showing their flexible nature that would make these membranes adequate for being deposited over a wound surface (Figure V.4a). The higher Young´s modulus exhibited for Sample II (Figure V.4b) could be related to the small diameter of the ultrafine fibers 49 ± 26 nm) that join PVAc microparticles together, since higher modulus values were reported for fibers with lower diameters (24). However, the elongation at break is higher also for Sample II indicating that it is the best morphology from the mechanical properties point of view.

It is known that water uptake makes the materials more flexible (23) and according to that elasticity of both membranes was increased after being 1 week immerse in TRIS. The elongation at break was higher and the Young´s Modulus was lower for wet samples than for the dry ones.

Table V.2. Samples tensile strength (MPa) after immersion in solutions at different pHs.

Condition	Sample I	Sample II
Dry	11.0 ± 3.0	8.0 ± 2.0
1st week: pH 8	8.6 ± 0.3	6.6 ± 0.3
2nd week: pH 7.4	3.3 ± 0.3	6.3 ± 0.2
3rd week: pH 5	3.2 ± 0.3	8.0 ± 2.0

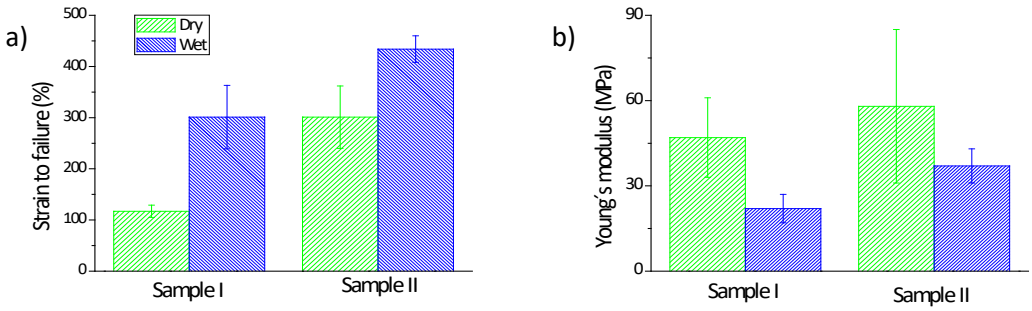

Figure V.4. a) Strain to failure and b) Young´s modulus at dry and wet conditions.

V.3.3 Fluids handling properties

Because of the need of absorbing the excess exudates, high water uptake capacity is an important parameter to consider in wound dressing materials. In order to mimic wound pH evolution, the swelling behavior of membranes was measured at the pH of chronic and infected wounds (pH = 8) during 24 h and then they were immersed in a solution at the pH of a healed wound (pH = 5) (Figure V.5). Important swellings of around 350 and 400 % were observed for Sample II and Sample I, respectively, during the first 2 h at pH 8.

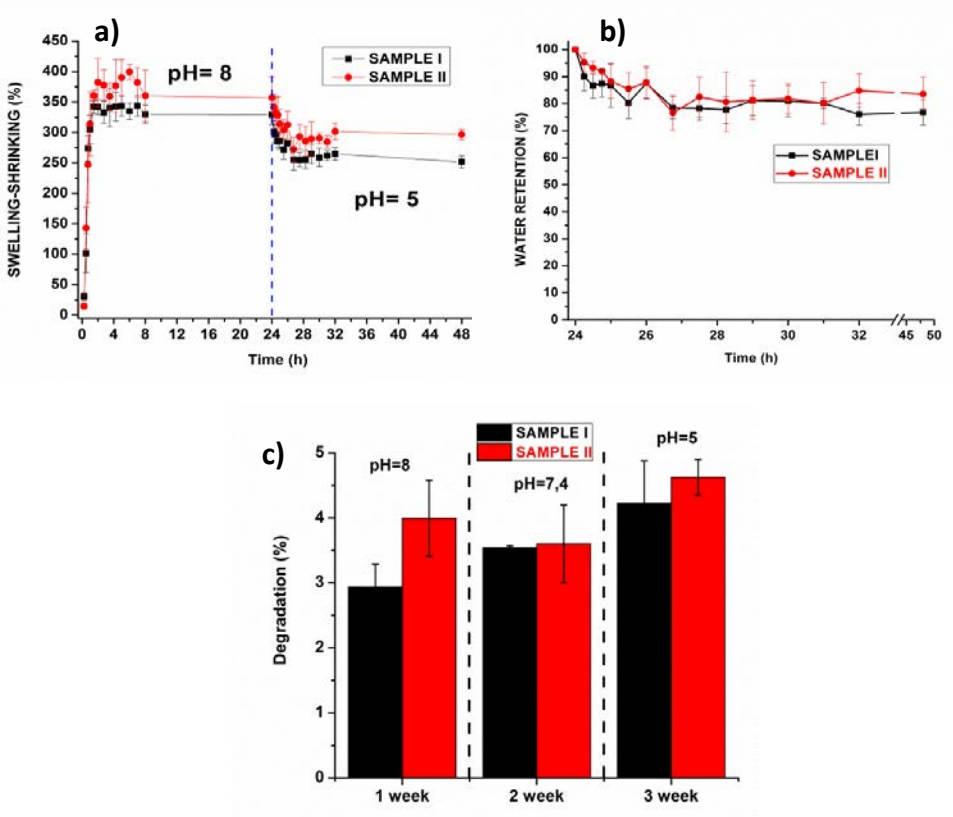

Figure V.5. Fluid uptake characteristics of the membranes: a) Swelling behavior of membranes at pH = 8 and pH = 5; b) Water retention at pH 5 after being 24 h at pH 8; c) Membranes weight loss in media mimicking wound pH values at different time points.

These swelling degrees stabilized and were maintained during 24 h. Then, at pH 5, the samples suffered a slight shrinkage (to 250-300 % swelling values); after that time, membranes got into equilibrium and around 80 % of the absorbed water was retained for 50 h (Figure V.5b). The higher swelling degree at higher pH was previously observed for hydrogels (25,26) and was attributed to the ionization of oxygen containing groups that cause high anion-anion electrostatic repulsion and thus high swelling of the polymer matrix. On the contrary, at pH 5 the acidic groups would be protonated and the anion-anion repulsion force was minimized causing the observed shrinkage (27). The degree of swelling found in our membranes is sufficient enough to be used as wound dressing according to the literature (28).

The swelling values are in agreement with the contact angle measurements (Table V.3) that showed lower values for Sample II compared to Sample I. Besides, the contact angle for Sample II PVAc face decreases dramatically with the increasing of the contact time (from 76 to 20 º) while the decrease for Sample I was less important (120 to 111 º). On the other hand, the PCL face of the membrane showed a clear hydrophobic character but lower for Sample II, probably because of the swelling effect of PVAc layer. The higher water absorption of Sample II could be associated to the high aspect ratio of the ultrathin spiderweb structure that connect microparticles in the PVAc layer which can increase absorption (29).

Table V.3. Contact angle results of prepared membranes.

Membrane	Contact time (min)	Contact angle	
		PCL face	PVAc face
Sample I	0	135 º 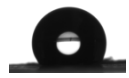	120 º 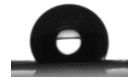
	20	135 º 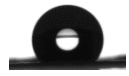	111 º 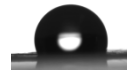
Sample II	0	120 º 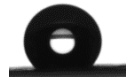	76 º 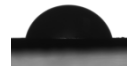
	20	119 º 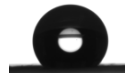	27 º 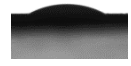

The water permeability of wound dressing materials is an important factor for the skin repairing process in order to create the appropriate moisture in the wound area and favoring cells migration to close the wound (30). The water vapor transmission rate (WVTR) values measured at different relative humidity for both samples are shown in Table V.4. As expected from swelling results, WVTR is higher for Sample II and increases with the humidity gradient, while for Sample I the values increase when the gradient goes from 38 % to 53 % RH, but remain constant for further increase. It was reported that the water evaporating from injured skin is in the range of 279-5130 $g.m^{-2}.day^{-1}$ (30). With WVTR values in the required

range (2100-4600 $g.m^{-2}.day^{-1}$) both samples are good candidates to keep good moisture balance with water loss from the wound at the optimal rate.

Table V.4. Water vapor transmission rate of the prepared membranes ($g.\ m^{-2}.day^{-1}$).

Membrane	Relative humidity gradient (%RH)		
	38	53	72
Sample I	2280 ± 153	2992 ± 72	2843 ± 344
Sample II	2506 ± 42	3649 ± 65	4552 ± 82

In spite of the high swelling degree, the membranes weight loss at the three pH values tested (Figure V) is lower than 5 %, showing that the polymers hydrolytic degradation was quantitatively negligible. It is in agreement with the literature since it is known that PCL degradation is very slow (more than 2 years *in vivo*) (31). PVAc also undergoes biodegradation slowly, some weight loss was observed after 120 days when buried in soil but the presence of fungi is required for complete degradation (32).

V.3.4 Carvacrol release

Analysis of samples according to section A.1.7.3 showed that CRV load in Sample I was 3.0 ± 0.4 wt% and 2.3 ± 0.5 wt% in Sample II, values slightly lower than the theoretical one (5.54 wt%). The difference could be attributed to some essential oil evaporation during the electrospinning process. With these loading values the calculated encapsulation efficiencies were 55 ± 5 and 43 ± 9 % for Sample I and Sample II, respectively. Figures V.6a and V.6b show the CRV release profiles for both samples at basic and acid pHs. As expected from swelling results, the increase of swelling capability with pH promotes faster drug release (33).

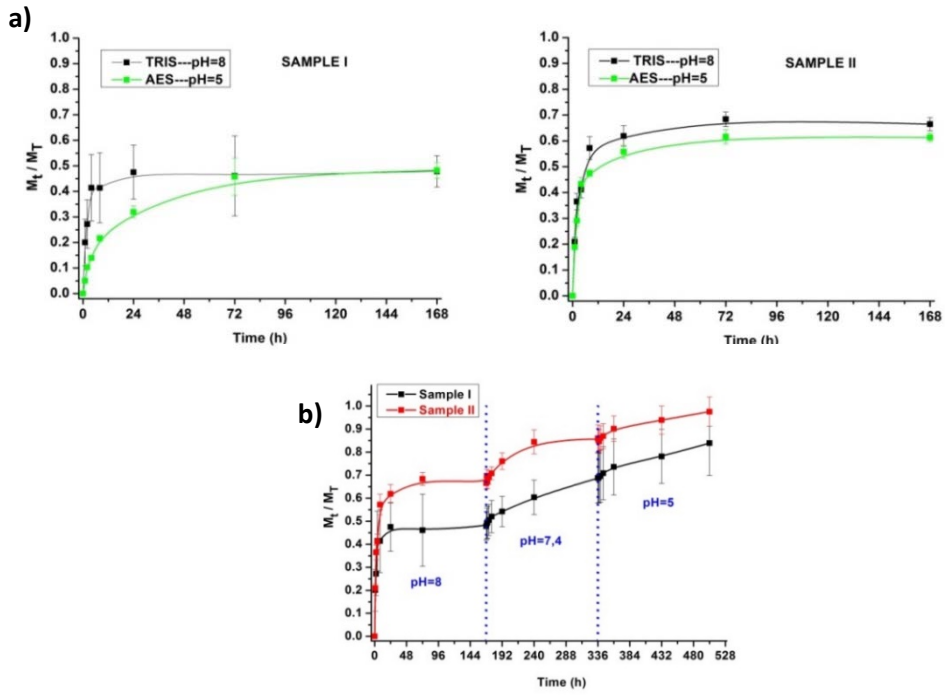

Figure V.6. Carvacrol release from the membranes: a) CRV release profile from Sample I and Sample II at pH 5 and pH 8; b) CRV release following a simulated wound pH evolution.

The higher swelling degree reached by Sample II would explain the release of about 60 % of the loaded CRV, while for Sample I only 45 % of the total drug was released. Besides, from theoretical prediction and experimental data, it is known that polymeric fiber exhibits slower and less efficient release of a drug in comparison with polymeric particles (34). Samples were also subjected to a simulated wound pH evolution (Figure V.6c) and after 7 days in basic pH they were transferred to PBS. After the change of medium, an increase in the release was observed due to the higher concentration gradient in the fresh PBS solution. The CRV release in this medium reached 60 % and 85 % of the loaded drug for Sample I and Sample II, respectively. After 14 days, the samples were removed and put in an acidic medium where after one week Sample II released around 100 % of the CRV and Sample I only 85 %.

The mechanism of drug release from both samples was evaluated by fitting release data into different kinetic models, i.e., Higuchi, Korsmeyer-

Peppas and Peppas-Sahlin (Table V.5). Peppas-Sahlin model was better for describing the release mechanism for all cases based on the statistically higher R^2 correlation coefficient indicating that Fickian diffusion and diffusion due to polymer relaxation occur concurrently with CRV release (35). The purely Fickian diffusion exponent (n) varied between 0.51-0.65 indicating an anomalous transport mechanism (36).

Table V.5. Fitting of drug release data with various kinetic models.

Membrane	Medium pH	Higuchi	Korsmeyer and Peppas		Peppas and Sahlin	
		R^2	n	R^2	n	R^2
Sample I	8	-0.009	0.240	0.817	0.510	0.910
	5	0.778	0.750	0.981	0.600	0.992
Sample II	8	0.567	0.320	0.851	0.590	0.949
	5	0.969	0.480	0.962	0.650	0.973

V.3.5 Antimicrobial properties

Bactericidal activity of carvacrol loaded membranes was tested against *Staphylococcus aureus* and *Escherichia coli*. The membrane sample used in each assay was calculated to release the same amount of CRV during the 24 h incubation. All samples exhibited an inhibition on the growth of both *E. coli* and *S. aureus* with inhibition zone diameters in the range of 14.3-15.8 mm. *E. coli* growth was reduced 2 logs by Sample I and 3 logs by Sample II (Figure V.7). The same trend was observed in *S. aureus* (Figure V.7), but for this bacterium strain the growth inhibition was more important than for *E. coli*, exerting Sample I a decrease of 3 logs while Sample II diminished *S. aureus* growth in 4 logs compared to the control sample. These results were expected since it is known that Gram-positive bacteria are more sensitive to terpenes than Gram-negative (37). The higher bactericidal effect of Sample II against both bacteria could be related to the PVAc layer morphology (Figure V.1). The more open structure would allow a better contact of bacteria with the membrane and consequently with the released CRV increasing the bactericidal effect.

In addition, these data point to the accomplishment of a significant inhibition of bacteria growth by both types of membranes after bacteria

contact with the loaded membranes for 24 h (Figure V.6). The inhibitory effects between Sample I and Sample II displayed only 1 log of difference, which is consistent with the close CRV release levels obtained from both membranes after 24 h.

CRV has been reported as an efficient bactericidal essential oil, present in oregano and thyme oil, which is able to exert its activity against both Gram negative and Gram positive microorganisms through bacteria membrane disruption (38,39). However, its encapsulation has been demonstrated as an efficient tool to improve its bactericidal efficiency, achieving an extended release profile compared to the free compound, together with the ability of loaded nanomaterials to diminish CRV evaporation avoiding its loss (12), and to deliver CRV to target areas, such as the mucus environment of biofilm (40). These results are in agreement with our microbiological assays and point to the relevance of CRV encapsulation to preserve and prolong its bactericidal effects.

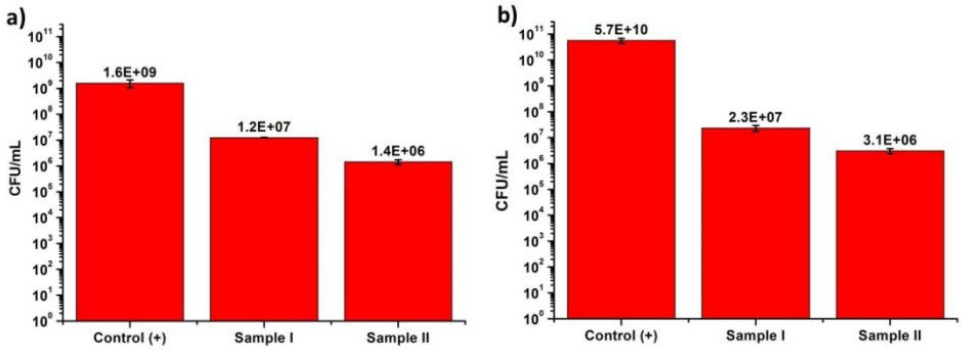

Figure V.7. Bactericidal activity of asymmetric membranes against: a) *E. coli* and b) *S. aureus.*

V.3.6 Cytocompatibility

MTT assay was performed to assess the toxicity of the prepared membranes on human dermal fibroblasts at different time points up to 3 days (Figure V.8). Compared to the positive control (membrane without CRV) both Sample I and II showed viabilities higher than 70 %, so it could be considered non-toxic (Figure V.8) according to ISO 10993-5 (41) which reports that a reduction in viability larger than 30 % should be considered a cytotoxic effect. On the other hand, Sample II not only did not show any toxic effects

but even increased the cells viability. Similar results were found by Matluobi et al. (42), who also reported that CRV at low concentrations not only did not induce cytotoxicity but also increased cell survival rate in mesenchymal stem cells over a period of 48 h. In this line, Tenci et al. (12) described high viability percentages of normal human dermal fibroblasts from foreskin when treated with CRV or CRV loaded polymer films during 24h at concentrations up to 50 μg/mL or higher, respectively.

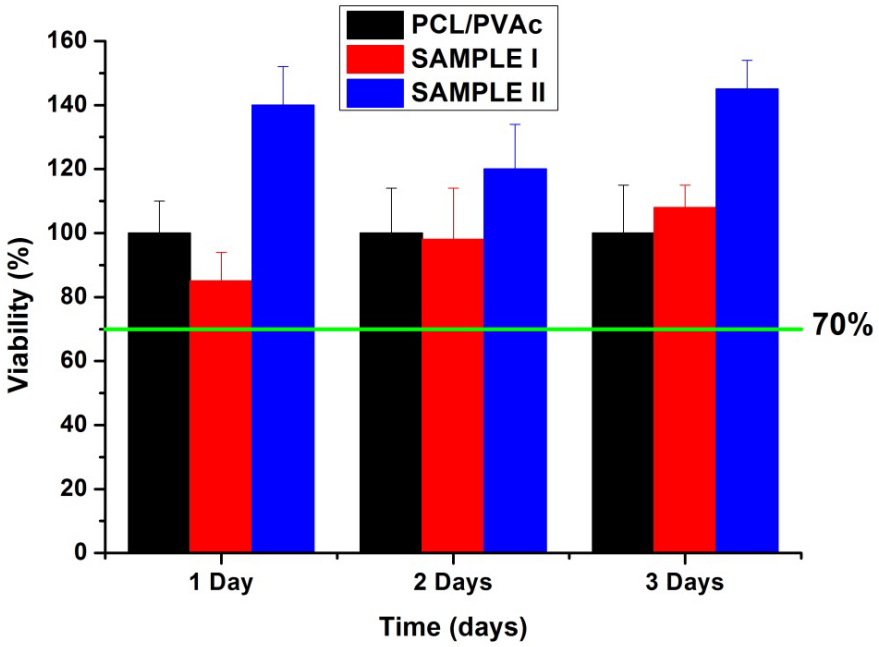

Figure V.8. Cell viability after exposure to the asymmetric membranes at different time points.

Cytocompatibility of the prepared samples was also evaluated by seeding HDFs on CRV loaded PVAc layer as a 3D culture and visualized under SEM (Figure V.9) and confocal microscopy (Figure V.10). After 3 days, cells properly adhered and homogenously spread on nanofibers and particles with flattened morphology could be observed (Figure V.9) indicating that the presence of CRV did not affect HDFs viability and proliferation on both types of fabricated membranes, pointing to their suitability for biomedical applications with bactericidal purposes in wound healing.

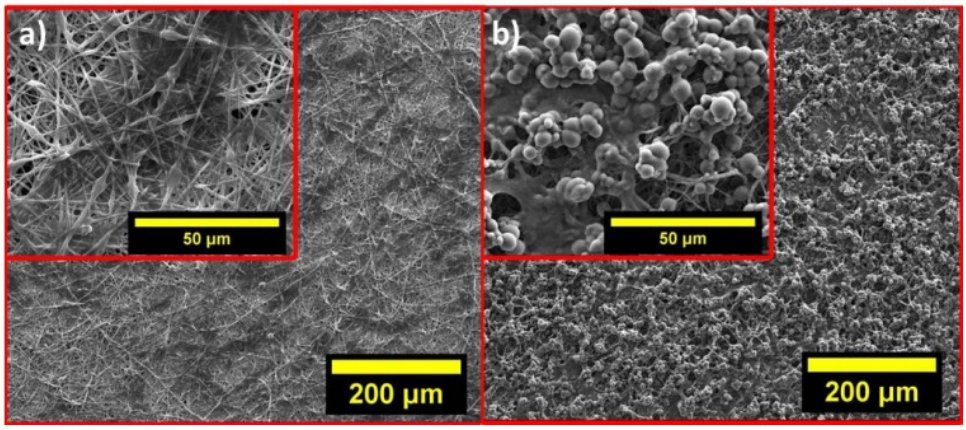

Figure V.9. SEM images of human dermal fibroblast proliferation onto Sample I and II after three days.

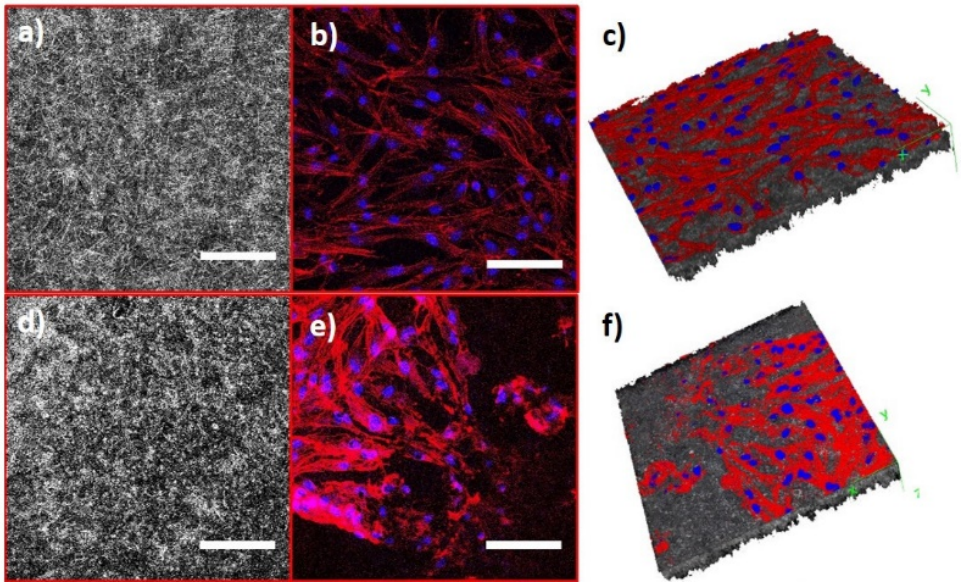

Figure V.10. Confocal microscopy images of human dermal fibroblasts seeded onto the asymmetric membranes assayed after three days: a-c) Sample I: membrane (a), fibroblasts stained for actin (red) and nuclei (blue) (b), merged image in 3D (c); d-f) Sample II: membrane (d), fibroblasts stained for actin (red) and nuclei (blue) (e), merged image in 3D (f). Scale bar, 500 µm.

V.3.7 Cell scratch assay

Wound healing is mainly based on cell migration capacity in order to efficiently close the wound to avoid bacterial infections, and properly regenerate the tissues. To evaluate the effect of CRV on cell migration, scratch assays were performed and the effect of CRV released from both types of synthesized membranes was studied (Figure V.11). The qualitative analysis of the images acquired up to 3 days after the scratch was performed in the cultures revealed no differences between the control sample (not treated) and the treated ones (Sample I and Sample II). Therefore, released CRV from both membranes did not display significant effects on cell migration which implies that the release of the compound did not favor nor impair cell migration in *In vitro* wound closure assays. Our results are not related to those previously reported by other authors, who have shown the CRV-induced inhibition of cell proliferation and migration in tumor cells (43).

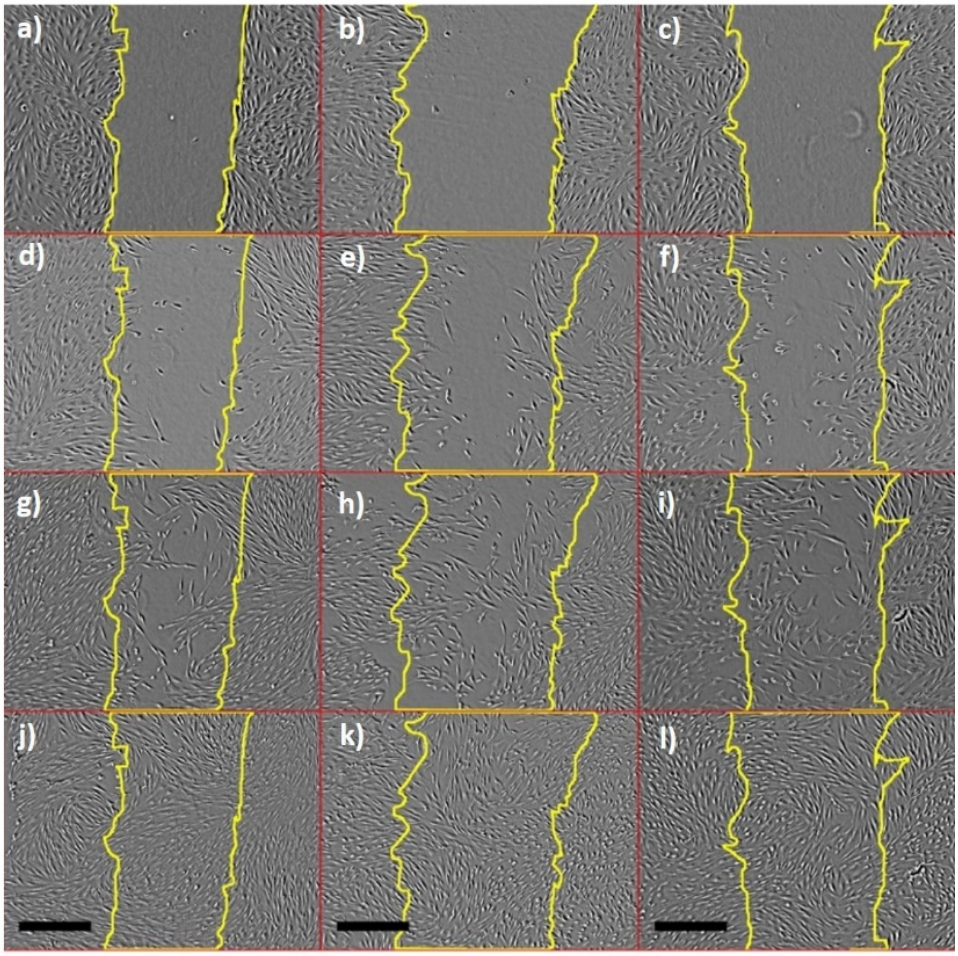

Figure V.11. Evaluation of cell migration under the effect of carvacrol release by the wound healing assay in human dermal fibroblasts incubated without membrane (control; a, d, g, j), with Sample I (b, e, h, k) or with Sample II (c, f, i, l) at the different time points studied: 0 h (a-c), 24 h (d-f), 48 h (g-i) and 72 h (j-l). Scale bar, 500 μm.

V.4 Conclusions

Asymmetric membranes with a polycaprolactone (PCL) layer, a carvacrol (CRV) loaded polyvinyl acetate (PVAc) layer and an intermediate layer composed of both kind of polymers were obtained by electrospinning. The use of dimethylformamide/ethanol (DMF/ETOH) or just DMF as solvent results in different morphologies for the PVAc-CRV layer. In Sample I (DMF/ETOH) it was composed of fibers with fibers (607± 124 nm diameter) while for Sample II (DMF) the PVAc layer consists of microparticles (3 ± 1 μm diameter) in a spiderweb ultrathin fiber structure. Both kinds of samples have strain to failure values higher than 100 % in the range of human skin, being adequate to be deposited over a wound surface. However, the dissimilar morphologies lead to different membranes behavior. The Young´s modulus and elongation at break are higher for Sample II (58 and 37 MPa and 301 and 434 % in dry and wet conditions respectively). On the other hand, WVTR values are in the required range (2100-4600 $g.m^{-2}.day^{-1}$) for both samples to keep good moisture balance with water loss from the wound at the optimal rate.

CRV load in Sample I was 3.0 ± 0.4 wt% and 2.3 ± 0.5 wt% in Sample II, and encapsulation efficiencies were 55 ± 5 and 43 ± 9 % for Sample I and Sample II, respectively. After one week 60% and 85 % of the loaded drug were released from Sample I and Sample II respectively while after three weeks Sample II released around 100% of the CRV and Sample I only 85%. Fickian diffusion and diffusion due to polymer relaxation occur concurrently with CRV release in both kinds of samples.

Both types of membranes showed inhibition effects against *S. aureus* and *E. coli* being Sample II slightly more active for both strains reducing CFU/mL up to 4 log with just 28-36 μg of CRV released. Both types of asymmetric membranes did not induce cytotoxicity to human dermal fibroblasts. Cells properly adhered and homogenously spread on both types of materials. Besides, the presence of the membranes didn't have any effect on cell migration in *In vitro* cell migration assay.

The mechanical properties, fluid handling capacity, antimicrobial properties and non-cytotoxicity to human dermal fibroblasts (HDFs) point to the potential of these asymmetric membranes, especially Sample II, for wound dressing applications.

References

1. Andreu V, Mendoza G, Arruebo M, Irusta S. Smart Dressings Based on Nanostructured Fibers Containing Natural Origin Antimicrobial, Anti-Inflammatory, and Regenerative Compounds. Materials (Basel). 2015;8(8):5154–93.

2. Xu H, Chang J, Chen Y, Fan H, Shi B. Asymmetric polyurethane membrane with inflammation-responsive antibacterial activity for potential wound dressing application. J Mater Sci. 2013;48(19):6625–39.

3. Georgescu M, C. Chifiriuc M, Marutescu L, Gheorghe I, Lazar V, Bolocan A, et al. Bioactive Wound Dressings for the Management of Chronic Wounds. Curr Org Chem. 2017;21(1):53–63.

4. Hassiba AJ, El Zowalaty ME, Nasrallah GK, Webster TJ, Luyt AS, Abdullah AM, et al. Review of recent research on biomedical applications of electrospun polymer nanofibers for improved wound healing. Nanomedicine. 2016;11(6):715–37.

5. Abrigo M, McArthur SL, Kingshott P. Electrospun Nanofibers as Dressings for Chronic Wound Care: Advances, Challenges, and Future Prospects. Macromol Biosci. 2014;14(6):772–92.

6. Morgado PI, Aguiar-Ricardo A, Correia IJ. Asymmetric membranes as ideal wound dressings: An overview on production methods, structure, properties and performance relationship. J Memb Sci. 2015;490:139–51.

7. Pinzon-Garcia AD, Cassini-Vieira P, Ribeiro CC, Jensen CED, Barcelos LS, Cortes ME, et al. Efficient cutaneous wound healing using bixin-loaded PCL nanofibers in diabetic mice. J Biomed Mater Res Part B-Applied Biomater. 2017;105(7):1938–49.

8. Jannesari M, Varshosaz J, Morshed M, Zamani M. Composite poly(vinyl alcohol)/poly(vinyl acetate) electrospun nanofibrous mats as a novel wound dressing matrix for controlled release of drugs. Int J Nanomedicine. 2011;6.

9. Riyajan SA, Sakdapipanich JT. Encapsulated neem extract containing

Azadiractin-A within hydrolyzed poly(vinyl acetate) for controlling its release and photodegradation stability. Chem Eng J. 2009;152(2–3):591–7.

10. Basar AO, Castro S, Torres-Giner S, Lagaron JM, Sasmazel HT. Novel poly(epsilon-caprolactone)/gelatin wound dressings prepared by emulsion electrospinning with controlled release capacity of Ketoprofen anti-inflammatory drug. Mater Sci Eng C-Materials Biol Appl. 2017;81:459–68.

11. Altiok D, Altiok E, Tihminlioglu F. Physical, antibacterial and antioxidant properties of chitosan films incorporated with thyme oil for potential wound healing applications. J Mater Sci Med. 2010;21(7):2227–36.

12. Tenci M, Rossi S, Aguzzi C, Carazo E, Sandri G, Bonferoni MC, et al. Carvacrol/clay hybrids loaded into in situ gelling films. Int J Pharm. 2017;531(2):676–88.

13. Liu L, Li X, Nagao M, Elias AL, Narain R, Chung HJ. A pH-Indicating Colorimetric Tough Hydrogel Patch towards Applications in a Substrate for Smart Wound Dressings. Polymers (Basel). 2017;9(11).

14. Osti E. Skin Ph Variations from the Acute Phase to Re-Epithelialization in Burn Patients Treated with New Materials (Burnshield®, Semipermeable Adhesive Film, Dermasilk®, and Hyalomatrix®). Non-Invasive Preliminary Experimental Clinical Trial. Ann Burns Fire Disasters. Mediterranean Council for Burns and Fire Disasters; 2008;21(2):73–7.

15. Kruse CR, Singh M, Targosinski S, Sinha I, Sorensen JA, Eriksson E, et al. The effect of pH on cell viability, cell migration, cell proliferation, wound closure, and wound reepithelialization: *In vitro* and *in vivo* study. Wound Repair Regen. 2017;25(2):260–9.

16. Rychter M, Baranowska-Korczyc A, Milanowski B, Jarek M, Maciejewska BM, Coy EL, et al. Cilostazol-Loaded Poly(epsilon-Caprolactone) Electrospun Drug Delivery System for Cardiovascular Applications. Pharm Res. 2018;35(2).

17. Wang F, Chandler P, Oszust R, Sowell E, Graham Z, Ardito W, et al.

Thermal and structural analysis of silk-polyvinyl acetate blends. J Therm Anal Calorim. 2017;127(1):923–9.

18. Gorodzha SN, Muslimov AR, Syromotina DS, Timin AS, Tcvetkov NY, Lepik K V, et al. A comparison study between electrospun polycaprolactone and piezoelectric poly(3-hydroxybutyrate-co-3-hydroxyvalerate) scaffolds for bone tissue engineering. Colloids and Surfaces B-Biointerfaces. 2017;160:48–59.

19. Morgado PI, Lisboa PF, Ribeiro MP, Migue SP, Simoes PC, Correia IJ, et al. Poly(vinyl alcohol)/chitosan asymmetrical membranes: Highly controlled morphology toward the ideal wound dressing. J Memb Sci. 2014;469:262–71.

20. Gumusderelioglu M, Dalkiranoglu S, Aydin RST, Cakmak S. A novel dermal substitute based on biofunctionalized electrospun PCL nanofibrous matrix. J Biomed Mater Res Part A. 2011;98A(3):461–72.

21. Wei QL, Xu FY, Xu XJ, Geng X, Ye L, Zhang AY, et al. The multifunctional wound dressing with core-shell structured fibers prepared by coaxial electrospinning. Front Mater Sci. 2016;10(2):113–21.

22. Reis TC, Castleberry S, Rego AMB, Aguiar-Ricardo A, Hammond PT. Three-dimensional multilayered fibrous constructs for wound healing applications. Biomater Sci. 2016;4(2):319–30.

23. Dias JR, Baptista-Silva S, de Oliveira CMT, Sousa A, Oliveira AL, Bartolo PJ, et al. In situ crosslinked electrospun gelatin nanofibers for skin regeneration. Eur Polym J. 2017;95:161–73.

24. Park JH, Rutledge GC. Ultrafine high performance polyethylene fibers. J Mater Sci. 2018;53(4):3049–63.

25. Demirdirek B, Uhrich KE. Novel salicylic acid-based chemically crosslinked pH-sensitive hydrogels as potential drug delivery systems. Int J Pharm. 2017;528(1–2):406–15.

26. Rojas-Oviedo I, Rodriguez-Hernandez S, Cardenas J, Rivas-Ojeda JC, Gavino R. Synthesis, characterization and *In vitro* application of pH/temperature sensitive superabsorbent hydrogel of phosphated co-polymer of methacrylic acid and methyl methacrylate ester. J

Porous Mater. 2016;23(6):1495–505.

27. Elvira C, Abraham GA, Gallardo A, Román JS. Smart Biodegradable Hydrogels with Applications in Drug Delivery and Tissue Engineering. In: Reis RL, Román JS, editors. Biodegradable Systems in Tissue Engineering and Regenerative Medicine. Boca Raton: CRC Press.; 2005.

28. Pal DB, Srivastava P, Mishra A, Giri DD, Srivastava KR, Singh P, et al. Synthesis and characterization of bio-composite nanofiber for controlled drug release. J Environ Chem Eng. 2017;5(6):5843–9.

29. Zhao J, Dehbari N, Han W, Huang L, Tang Y. Electrospun multi-scale hybrid nanofiber/net with enhanced water swelling ability in rubber composites. Mater Des. 2015;86:14–21.

30. Mary SA, Dev VRG. *In vivo* bioactivity of herbal-drug-incorporated nanofibrous matrixes. J Appl Polym Sci. 2015;132(26).

31. Aleman-Dominguez ME, Ortega Z, Benitez AN, Vilarino-Feltrer G, Gomez-Tejedor JA, Valles-Lluch A. Tunability of polycaprolactone hydrophilicity by carboxymethyl cellulose loading. J Appl Polym Sci. 2018;135(14).

32. Cooke TF. BIODEGRADABILITY OF POLYMERS AND FIBERS - A REVIEW OF THE LITERATURE. J Polym Eng. 1990;9(3):171–211.

33. Laha A, Sharma CS, Majumdar S. Sustained drug release from multi-layered sequentially crosslinked electrospun gelatin nanofiber mesh. Mater Sci Eng C. 2017;76:782–6.

34. Kyzioł A, Michna J, Moreno I, Gamez E, Irusta S. Preparation and characterization of electrospun alginate nanofibers loaded with ciprofloxacin hydrochloride. Eur Polym J. 2017;96(Supplement C):350–60.

35. Yadav I, Shaw GS, Nayak SK, Banerjee I, Shaikh H, Al-Zahrani SM, et al. Gelatin and amylopectin-based phase-separated hydrogels: An in-depth analysis of the swelling, mechanical, electrical and drug release properties. Iran Polym J. 2016;25(9):799–810.

36. Peppas NA, Sahlin JJ. A simple equation for the description of solute release. III. Coupling of diffusion and relaxation. Int J Pharm. Elsevier; 1989 Dec;57(2):169–72.

37. Zengin H, Baysal AH. Antibacterial and Antioxidant Activity of Essential Oil Terpenes against Pathogenic and Spoilage-Forming Bacteria and Cell Structure-Activity Relationships Evaluated by SEM Microscopy. Molecules. 2014;19(11):17773–98.

38. Garcia-Salinas S, Elizondo-Castillo H, Arruebo M, Mendoza G, Irusta S. Evaluation of the Antimicrobial Activity and Cytotoxicity of Different Components of Natural Origin Present in Essential Oils. Molecules. 2018;23(6).

39. Nazzaro F, Fratianni F, De Martino L, Coppola R, De Feo V. Effect of Essential Oils on Pathogenic Bacteria. Pharmaceuticals. MDPI; 2013;6(12):1451–74.

40. Iannitelli A, Grande R, Di Stefano A, Di Giulio M, Sozio P, Bessa LJ, et al. Potential Antibacterial Activity of Carvacrol-Loaded Poly(DL-lactide-co-glycolide) (PLGA) Nanoparticles against Microbial Biofilm. Int J Mol Sci. 2011;12(8):5039–51.

41. ISO 10993-5:2009(E). Biological evaluation of medical devices — Part 5: Tests for *In vitro* cytotoxicity. INTERNATIONAL STANDARD. 2009.

42. Matluobi D, Araghi A, Maragheh BFA, Rezabakhsh A, Soltani S, Khaksar M, et al. Carvacrol promotes angiogenic paracrine potential and endothelial differentiation of human mesenchymal stem cells at low concentrations. Microvasc Res. 2018;115:20–7.

43. Jung CY, Kim SY, Lee C. Carvacrol Targets AXL to Inhibit Cell Proliferation and Migration in Non-small Cell Lung Cancer Cells. Anticancer Res. 2018;38(1):279–86.

General Conclusions

In this work biomimetic membranes for bone and wound tissue engineering were developed by using an innovative electrodynamic technique. The most relevant conclusions of the prepared materials are summarized in this chapter.

Three polymeric multifunctional membranes were developed by using electrospinning and electrospraying for bone repair and the prevention or treatment of bone infection. In particular, PCL and PCL/PVAc core/shell fibers obtained by electrospinning can be decorated with rifampicin or BMP2 loaded PLGA microparticles using the electrospraying technique. The incorporation of nano-hydroxyapatite particles in the polymer fibers favors the apatite formation on nanofiber surface.

All the synthesized membranes show a porous network providing a large surface area-to-volume ratio for cell attachment as well as sufficient porosity for diffusive nutrient transport. It is important to highlight that surface laser treatment notably increases the membranes cytocompatibility resulting in higher cell viability and proliferation.

PCL and PCL/PVAc core/shell fibers decorated with rifampicin loaded into PLGA microparticles present a homogeneous distribution of RFP-PLGA microparticles along the entire membranes, thereby ensuring a continuous rifampicin release. The drug release is initially pronounced to be followed by a sustained stage until the end of the experiments. The release profile obtained from the membrane loaded with rifampicin is suitable for the clinical application, as bone infection is initially controlled to maintain later the prophylaxis in order to avoid bone reinfection.

Indeed the microbiological studies support the potential of the fabricated membranes loaded with rifampicin for the treatment of bone infection. The membranes loaded with RFP-PLGA microparticles are able to eliminate *E. coli* and *S. aureus* using rifampicin levels that could be adjusted to the range of rifampicin reported in serum for the therapeutic dose clinically recommended.

Furthermore, *In vitro* studies demonstrate that human osteoblasts seeded on the membranes decorated with RFP-PLGA microparticles display cell adhesion and proliferation, which at 28 days have completely covered the material surface. These findings suggest that the membranes decorated with RFP-PLGA microparticles could be a potential candidate for bone repair when infection may impair the regeneration of the tissue.

The combination of PCL, PVAc, and PLGA-BMP2 is a novel and promising therapeutic approach for bone repair. BMP2 could be an alternative to increase osteogenic activity, while the PVAc fiber shell increases hydrophilicity and favors osteoblast adhesion and proliferation.

Osteoblast viability and proliferation, as well as the expression of bone formation and maturation markers, increase significantly when the growth factor (BMP2) is included in the PCL/PVAc membranes, as result of the relevant role played by this protein in bone regeneration. The developed membranes (PCL-HAn/PCL and PCL-HAn/PVAc with and without PLGA:BSA:BMP2 microparticles) show enzymatic degradation, highlighting their biodegradation and therefore their suitability to be used in biomedical approaches.

For wound dressing applications, asymmetric membranes loaded with carvacrol are produced by electrospinning and electrospraying. These membranes exhibit suitable mechanical properties, fluid handling capacity, antimicrobial properties and non-cytotoxic effects to human dermal fibroblasts.

In particular, the membrane strain to failure values are in the range of those observed in human skin, highlighting the potential of the fabricated membranes as dressings to be placed over a wound surface. The water vapor transmission rate values are in the required range to keep good moisture balance with water loss from the wound at the optimal rate.

Finally, carvacrol release produces inhibitory effects against *S. aureus* and *E. coli* growth without inducing cytotoxicity to human dermal fibroblasts nor impair cell migration. These characteristics evidence the membranes suitability for their clinical application.

The studies discussed in this Doctoral thesis have demonstrated that electrospun membranes are attractive candidates for generating bone tissue substitute and wound dressing. Electrospinning technique provides desirable membrane properties and the necessary potential to fabricate biomaterials with the morphology and the physico-chemical properties comparable to the extracellular matrix, favoring their biomedical application. In addition, the combination of electrospinning and electrospraying provides a step forward for the fabrication of novel multifunctional biomedical materials, such as novel tissue engineered membranes loaded with active biomolecules for their successful clinical application in bone defects or skin wounds.

Conclusiones Generales

En este trabajo se han desarrollado membranas biomiméticas para ingeniería de tejido óseo y de heridas utilizando una técnica electrodinámica innovadora. En este capítulo se resumen las conclusiones más relevantes de los materiales preparados.

Se desarrollaron tres membranas poliméricas multifuncionales utilizando el electrohilado y electropulverización para ser utilizadas en reparaciones óseas y en la prevención o tratamiento de infecciones óseas. En particular, las fibras de PCL y PCL/PVAc con estructura núcleo/corona obtenidas mediante electrohilado se pueden decorar con partículas de PLGA cargadas con rifampicina o BMP2 utilizando la técnica de electropulverización. La incorporación de nano-partículas de hidroxiapatita en las fibras poliméricas favorece la formación de apatita biológica sobre la superficie de las nano-fibras.

Todas las membranas sintetizadas presentan un enrejado poroso con una alta relación área superficial/volumen que facilita la adhesión celular así como la difusión de nutrientes a través de él. Es importante destacar que el tratamiento láser en la superficie aumenta notablemente la citocompatibilidad, provocando una mayor proliferación y viabilidad celular.

Las fibras de PCL y PPL/PVAc con estructura de núcleo/corona decoradas con micropartículas de PLGA cargadas con rifampicina presentan una distribución homogénea de las micropartículas a lo largo de toda la membrana, que proporciona una liberación continua de rifampicina. Inicialmente se libera una gran cantidad de fármaco seguida de una liberación sostenida hasta el final del experimento. EL perfil de liberación de rifampicina obtenido desde las membranas cargadas es adecuado para su uso en aplicaciones clínicas, debido a que la infección ósea es inicialmente controlada, manteniendo después la profilaxis con el objetivo de evitar la reinfección ósea.

Los estudios microbiológicos realizados respaldan el potencial que presentan las membranas fabricadas cargadas con rifampicina para el tratamiento de infecciones óseas. Las membranas cargadas con micropartículas de PLGA-RFP son capaces de eliminar bacterias como la *E. coli* y el *S. aureus* utilizando niveles de rifampicina que podrían ajustarse al

rango de rifampicina reportado en suero para la dosis terapéutica clínicamente recomendada.

Por otra parte, los estudios *In vitro* demuestran que las células de osteoblastos humanos sembrados sobre la membranas cargadas con micropartículas de PLGA-RFP se adhieren y proliferan, cubriendo completamente la superficie del material a los 28 días. Estos resultados sugieren que las membranas cargadas con micropartículas de PLGA-RFP puede ser un candidato potencial en reparaciones óseas cuando la infección puede comprometer la regeneración del tejido.

La combinación de PCL, PVAc y PLGA-BMP2 proporciona un enfoque terapéutico novedoso y prometedor en la reparación ósea. Debido a que la BMP2 podría ser una alternativa para aumentar la actividad osteogénica, mientras que el PVAc que recubre las fibras aumenta la hidrofilicidad y favorece la adhesión y proliferación de osteoblastos.

La inclusión del factor de crecimiento (BMP2) en las membranas de PCL/PVAc provoca un incremento significativo en la viabilidad y proliferación celular, así como en la expresión de marcadores de maduración y formación ósea, como resultado del papel relevante que juega esta proteína en la regeneración ósea. La degradación enzimática que muestran las membranas desarrolladas (PCL-HAn/PCL y PCL-HAn/PVAc con o sin micropartículas de PLGA:BSA:BMP2) destaca su biodegradación y por tanto su idoneidad para su uso en enfoques biomédicos.

Se obtuvieron membranas asimétricas cargadas con carvacrol mediante electrohilado y electrospulverización para aplicaciones como apósitos para heridas. Estas membranas presentan adecuadas propiedades mecánicas, capacidad de manejo de fluidos, propiedades antimicrobianas y no presenta efectos citotóxicos frente a fibroblastos dérmicos humanos.

Los valores obtenidos de deformación antes de la rotura, están en el rango de los valores reportados en la piel humana, destacando el potencial de las membranas desarrolladas como apósitos que pueden ser colocados sobre la superficie de una herida. La tasa de transmisión de vapor de agua está en el rango óptimo requerido para mantener un adecuado balance entre la humedad y la pérdida de agua de la herida.

Por último, la liberación de carvacrol produce efectos inhibitorios frente al *S. aureus* y la *E. coli* sin inducir citotoxicidad en los fibroblastos dérmicos humanos ni altera la migración celular. Estas características evidencian la idoneidad de las membranas para su aplicación clínica.

Los estudios discutidos en esta tesis doctoral han demostrado que las membranas electrohiladas son candidatos atractivos para desarrollar sustituto de tejido óseo y vendaje para heridas. La técnica de electrospinning proporciona el desarrollo de membranas con propiedades específicas y el potencial necesario como biomateriales con morfología y propiedades físico-químicas comparables a la matriz extracelular, favoreciendo su aplicación biomédica. Por otra parte, la combinación de electrohilado y electropulverización proporciona un paso de avance en la fabricación de nuevos materiales biomédicos multifuncionales, como nuevas membranas para ingeniería de tejido cargadas con biomoléculas activas para su aplicación clínica exitosa en defectos óseos o heridas en la piel.

Conclusioni Generali

In questo lavoro di tesi, sono state sviluppate membrane biomimetiche per l'ingegneria del tissuto osseo e della pelle impiegando una tecnica elettrodinamica altamente innovativa. Le conclusioni più rilevanti riguardanti i dei materiali realizzati sono riassunte in questo capitolo.

Tre membrane polimeriche multifunzionali sono stati sviluppate utilizzando elettrofilatura ed elettrospraying per la riparazione ossea e la prevenzione o per il trattamento dell'infezione ossea. In particolare, sono state realizzate mediante elettrofilatura membrane costituite da fibre core/shell PCL e PCL/PVAc, che sono state decorate con microparticelle PLGA caricate con RFP o BMP2 utilizzando la tecnica dell'elettrospray. L'inclusione di particelle di HAn nelle fibre polimeriche favorisce la formazione di apatite sulla superficie di nanofibre.

Le membrane sintetizzate mostrano una struttura porosa che fornisce un ampio rapporto superficie-volume per l'adesione cellulare ed una porosità sufficiente per il trasporto diffusivo dei nutrienti. Il trattamento laser delle superfici delle membrane ha comportato un notevole aumento della loro citocompatibilità ottenendo così una vitalità e proliferazione cellulare più elevata.

Le membrane di PCL e PCL/PVAc decorate con microparticelle PLGA contenenti RFP presentano una distribuzione omogenea delle microparticelle lungo l'intera struttura, garantendo in tal modo un rilascio continuo del farmaco. Il rilascio della molecola è stato inizialmente elevato per poi essere seguito da una fase di rilascio prolungato fino al termine degli esperimenti. I risultati mettono in evidenza che il profilo di rilascio ottenuto dalle membrane caricate con RFP è adeguato per l'applicazione clinica, poiché l'infezione ossea deve essere inizialmente controllata per poi mantenere in seguito la profilassi al fine di evitare la reinfezione del tessuto.

Infatti, studi microbiologici confermano il potenziale uso delle membrane caricathe con RFP per il trattamento delle infezioni ossee. Le membrane sviluppate sono in grado di eliminare ceppi come E. coli e S. aureus utilizzando livelli di RFP che sono nell'intervallo dei dosaggi terapeutici sierici raccomandati clinicamente.

Inoltre, studi *In vitro* hanno messo in evidenza che osteoblasti umani posti in coltura su queste membrane decorate con microparticelle RFP-PLGA aderiscono e proliferano ricoprendo completamente la loro superficie. Questi dati dimostrano che le membrane realizzate fungono da potenziali candidati per la riparazione ossea quando l'infezione può compromettere la rigenerazione del tessuto.

La combinazione di PCL, PVAc e PLGA-BMP2 è un approccio terapeutico innovativo e promettente per la riparazione dell'osso danneggiato oppure mancante. Le microparticelle rilasciano BMP2 nella parte interna delle fibre allo scopo di aumentare l'attività osteogenica delle membrane mentre la parte esterna della fibre di PVAc conferiscono maggiore idrofilicità, che favorisce l'adesione e la proliferazione degli osteoblasti.

La vitalità e la proliferazione degli osteoblasti, così come l'espressione di markers specifici della formazione e di maturazione dell'osso sono aumentati significativamente quando il fattore di crescita (BMP2) era presente negli membrane di PCL/PVAc, come risultato del ruolo rilevante svolto da questa proteina nella rigenerazione ossea.. Inoltre, tutte le membrane (PCL-HAn/PCL e PCL-HAn/PVAc con e senza PLGA:BSA:BMP2 microparticelle) mostrano degradazione enzimatica, evidenziando la loro biodegradazione e quindi la loro idoneità ad essere utilizzate in approcci biomedici.

Per il trattamento delle ferite della pelle sono state sviluppate membrane asimmetriche caricate con carvacrolo adoperando le tecniche di elettrofilatura ed elettrospray. Le membrane esibiscono proprietà meccaniche, capacità di gestione dei fluidi, proprietà antimicrobiche e caratteristiche di non citotossicità testate con fibroblasti dermici umani (HDF).

Le membrane hanno dei valori di deformazione fino a rottura che sono nel range di quelli osservati nella pelle umana, pertanto possono essere potenzialmente adoperate nel trattamento delle ferite. I valori della velocità di trasmissione del vapore acqueo sono nell'intervallo necessario per mantenere un buon equilibrio di umidità con una perdita d'acqua dalla ferita ad una velocità ottimale.

Infine, il rilascio di carvacrolo ha inibito la crescita batterica dei ceppi S. aureus e E. coli senza causare citotossicità nei confronti di fibroblasti umani dermici e senza compromettere la migrazione cellulare,. Tali caratteristiche evidenziano l'idoneità delle membrane in applicazioni cliniche.

Lo studio presentato in questa tesi di dottorato ha dimostrato che le membrane elettrofilate sono candidati attraenti per la generazione del sostituto del tessuto osseo e della medicazione delle ferite. La tecnica di elettrofilatura fornisce proprietà desiderabili alle membrane e il potenziale necessario per fabbricare biomateriali con la morfologia e le proprietà fisico-chimiche paragonabili alla matrice extracellulare, favorendo la loro applicazione in campo biomedico. Inoltre, la combinazione di elettrofilatura e elettrospray fornisce un'innovazione per la fabbricazione di nuovi materiali biomedici multifunzionali, come nuove membrane di ingegneria tissutale caricate con biomolecole attive per la loro efficace applicazione clinica in difetti ossei o ferite della pelle.

Conclusões Gerais

Neste trabalho foram desenvolvidas membranas biomiméticas para engenharia óssea e tecidual de feridas utilizando uma técnica eletrodinâmica inovadora. As conclusões mais relevantes dos materiais preparados estão resumidas neste capítulo.

Três membranas poliméricas multifuncionais foram desenvolvidas usando eletrofiação e eletropulverização para reparo ósseo e prevenção ou tratamento de infecção óssea. Em particular, fibras de nucleo PCL e PCL / PVAc obtidas por electrospinning podem ser decoradas com rifampicina ou micropartículas de PLGA carregadas com BMP2 utilizando a técnica de electropulverização. A incorporação de partículas de nano-hidroxiapatita nas fibras poliméricas favorece a formação de apatita na superfície da nanofibra.

Todas as membranas sintetizadas mostram uma rede porosa que proporciona uma razão elevada entre a área superficial e o volume para a ligação celular, bem como uma porosidade suficiente para o transporte difusivo de nutrientes. É importante ressaltar que o tratamento com laser de superfície aumenta notavelmente a citocompatibilidade das membranas, resultando numa maior viabilidade e proliferação celular.

As fibras de núcleo/casca PCL e PCL / PVAc decoradas com rifampicina carregada nas micropartículas de PLGA apresentam uma distribuição homogênea de micropartículas de RFP-PLGA ao longo de todas as membranas, garantindo assim uma libertação contínua de rifampicina. A libertação do fármaco é inicialmente pronunciada sendo seguida por um estágio sustentado até ao final dos experimentos. O perfil de libertação obtido da membrana carregada com rifampicina é adequado para a aplicação clínica, uma vez que a infecção óssea é inicialmente controlada para manter a profilaxia posteriormente, para evitar a reinfecção óssea.

De facto, os estudos microbiológicos suportam o potencial das membranas fabricadas carregadas com rifampicina para o tratamento da infecção óssea. As membranas carregadas com micropartículas de RFP-PLGA são capazes de eliminar E. coli e S. aureus usando níveis de rifampicina que poderiam ser ajustados para a faixa de rifampicina relatada no soro para a dose terapêutica clinicamente recomendada.

Além disso, estudos in vitro demonstram que os osteoblastos humanos semeados nas membranas decoradas com micropartículas de RFP-PLGA exibem adesão e proliferação celular, que aos 28 dias cobriram completamente a superfície do material. Esses achados sugerem que as membranas decoradas com micropartículas de RFP-PLGA podem ser um potencial candidato para reparo ósseo quando a infecção pode prejudicar a regeneração do tecido.

A combinação de PCL, PVAc e PLGA-BMP2 é uma abordagem terapêutica inovadora e promissora para o reparo ósseo. A BMP2 pode ser uma alternativa para aumentar a atividade osteogênica, enquanto a casca de fibra de PVAc aumenta a hidrofilicidade e favorece a adesão e proliferação de osteoblastos.

A viabilidade e proliferação de osteoblastos, assim como a expressão de marcadores de maturação e formação óssea, aumentam significativamente quando o fator de crescimento (BMP2) é incluído nas membranas PCL / PVAc, como resultado da relevante função desempenhada por esta proteína na regeneração óssea. As membranas desenvolvidas (PCL-HAn / PCL e PCL-HAn / PVAc com e sem micropartículas de PLGA: BSA: BMP2) apresentam degradação enzimática, destacando a sua biodegradação e, portanto, a sua adequação para o uso em abordagens biomédicas.

Para aplicações como curativos de feridas, as membranas assimétricas carregadas com carvacrol são produzidas por eletrofiação e eletropulverização. Estas membranas exibem propriedades mecânicas adequadas, capacidade de manuseamento de fluidos, propriedades antimicrobianas e efeitos não citotóxicos para fibroblastos dermicos humanos.

Os valores de tensão de ruptura da membrana estão na gama dos observados na pele humana, evidenciando o potencial das membranas fabricadas como curativos a serem colocados sobre uma superfície da ferida. Os valores da taxa de transmissão de vapor de água estão na faixa necessária para manter um bom equilíbrio de humidade com a perda de água da ferida na taxa ideal.

Finalmente, a libertação de carvacrol produz efeitos inibitórios contra o crescimento de S. aureus e E. coli, sem induzir citotoxicidade aos fibroblastos dérmicos humanos, nem prejudicar a migração celular. Estas características evidenciam a adequabilidade das membranas para a sua aplicação clínica.

Os estudos discutidos nesta tese de Doutoramento demonstraram que as membranas eletrofuncionais são candidatos atrativos para a geração de substituto do tecido ósseo e como curativos de feridas. A técnica de eletrofiação proporciona propriedades desejáveis de membrana e o potencial necessário para fabricar biomateriais com a morfologia e propriedades físico-químicas comparáveis à matriz extracelular, favorecendo a sua aplicação biomédica. Além disso, a combinação de electrospinning e electropulverização fornece um passo em frente para o fabrico de novos materiais biomédicos multifuncionais, tais como novas membranas de engenharia de tecidos carregadas com biomoléculas activas para a sua aplicação clínica com sucesso em defeitos ósseos ou feridas da pele.

APPENDIX 1

Materials and Methods

INDEX

A.1.1 Materials

Polycaprolactone (PCL) with an average molecular weight of 80,000 Da, polyvinyl acetate (PVAc) with an average molecular weight of 140,000 Da RFP (≥97%), N,N-dimethylformamide (DMF; ≥99.8%), dichloromethane (DCM; ≥99.8%), acetic acid (≥99%), dimethyl sulfoxide (DMSO; ≥99.8%), ethanol absolute (ETOH; ≥ 99.5 %), calcium carbonate ($CaCO_3$; ≥95%), phosphoric acid (H_3PO_4; ≥85%), ammonium hydroxide solution (NH_4OH; 28–30%), sodium chloride (NaCl; ≥99%), calcium chloride dihydrate ($CaCl_2.2H_2O$; ≥99%), phosphate-buffered saline (PBS), tris(hydroxymethyl)aminomethane (Tris; ≥99.8%), ammonium sulfate ($(NH_4)_2SO_4$; ≥99%), sodium nitrate ($NaNO_2$; ≥97%), sodium hydroxide (NaOH; ≥98%), potassium acetate (CH_3COOK; (≥99%)), carvacrol (CRV; ≥99%), naproxen sodium (≥98-102%), TWEEN® 80, bovine serum albumin (BSA; ≥98%), albumin–fluorescein isothiocyanate conjugate (BSA-FITC), 3-(3,4-dimethylthiazol-2-yl)-2,5-diphenyltetrazoliumbromide (MTT; ≥98%), human lysozyme (≥100,000 U/mg protein, lyophilised powder; ≥90%), lipase from *Aspergillus oryzae* (50 U/mg), and CellCrown™ inserts (24 well plate inserts) were purchased from Sigma-Aldrich (Spain).

Poly(D,L-lactide-co-glycolide)lactide:glycolide 50:50 (PLGA) ester terminated at molecular weight 38,000–54,000 Da was purchased from Evonik Industries (Spain), and bone morphogenetic protein 2 (BMP2; ≥95%) is from R&D Systems (US). Sodium dodecyl sulfate (SDS) and Triton X-100 were obtained from Bio-Rad (USA). Trypticasein soy broth (TSB) and trypticasein soy agar (TSA) were acquired from Conda-Pronadisa (Spain). Trypsin-EDTA, Dulbecco's phosphate-buffered saline (DPBS) high-glucose DMEM (DMEM w/stable glutamine) and antibiotic-antimycotic (60 µg/mL penicillin, 100 µg/mL streptomycin and 0.25 µg/mL amphotericin B) were obtained from Biowest (France).

Escherichia coli S17 was kindly gifted by Professor J. A. Aínsa Claver from Department of Microbiology, Preventive Medicine, and Public Health, University of Zaragoza, while *Staphylococcus aureus* (ATCC®25923) was purchased from Ielab (Spain). Human dermal fibroblasts (HDFs) were obtained from Lonza (US) and fetal bovine serum (FBS) was purchased from Gibco (UK). Osteoblast cells were provided by two companies; human osteoblasts (HOBs) and osteoblast growth medium (OGM) were obtained from PromoCell (Germany), and Clonetics™ normal human osteoblasts

(NHOst) and Clonetics™ OGM™ osteoblast growth medium (OGM) were purchased from Lonza (Belgium).

A.1.2 Physico-chemical characterization

The morphology of HAn and PLGA particles and electrospun membranes was analyzed using a Transmission Electron Microscope (TEM) operated at 300 kV (Tecnai F30, FEI, USA) and two Scanning Electron *Microscope* (SEM; Field Emission Scanning Electron Microscope CSEM-FEG INSPECT 50, FEI, USA and Field Emission SEM, by Nova 200 NanoLab Dual Beam-SEM/FIB, FEI, equipped with a cryogenic module, Quorum Technologies PP200T). Particles and fibers diameter was measured by Image J software (Version 1.48f, NIH, US). The size distribution statistics was obtained by measuring at least 100 fibers or particles in different images.

Fourier transform infrared (FTIR) spectrum and X-ray diffraction (XRD) were used to evaluate the molecular structure and to identify the crystallographic phases in the case of the HAn. Fourier-transform infrared (FTIR) spectra were recorded on a Vertex-70 FTIR spectrophotometer (Bruker, US) and a Spectrum 1000, Perkin Elmer to evaluate the molecular structure. The powder diffraction pattern was measured in a diffractometer (Rigaku RINT 2000) with a monochromatic Cu Kα radiation. Thermal analyses of membranes were conducted with a thermogravimetric analyzer (TGA) from METTLER TOLEDO (TGA/SDTA 851e; US).

The mean pore size and pore size distribution were determined by means of a Capillary Flow Porometer CFP 1500 AEXL (Porous Materials Inc. PMI, Ithaca, New York, US). Porosity of membranes was also measured by mercury intrusion using a mercury porosimeter (Poremaster, Quantachrome and Micromeritics' AutoPore IV 9500 Series). At least five samples were tested for each type of membrane.

Contact angle of each face of the prepared membranes was evaluated with water droplets (6 µL) using a Dataphysics OCA-Series equipment (Dataphysics instruments GmbH, Germany) at room temperature.

A.1.3 *In vitro* studies in simulated body fluid (SBF) on "Laser-treated electrospun fibers loaded with nano-hydroxyapatite" (Chapter III)

In vitro studies in simulated body fluid (SBF) were carried out using the SBF composition and the standard procedures described by Kokubo and Takadama (1). Electrospun membranes were immersed in 10 mL of SBF for 30 days at 37 °C and, every 72 h in the first 15 days and every week in the last 15 days, the liquid phase was replaced with 10 mL of fresh SBF. After immersion in SBF the samples were characterized by SEM to verify whether HAn was formed on the surfaces of the membranes.

A.1.4 Mechanical properties

A.1.4.1 Mechanical properties of "Composite membrane loaded with RFP" (Chapter II)

Mechanical properties of the RFP loaded membranes were determined at room temperature through a Uniaxial Instron test machine (Instron, US) with video extensometer 5548 (1 KN load cell, 1 mm/min). Five samples per membrane were cut into 50 mm x 5 mm strips and subjected to a tensile test. A full-scale load of 20 N and maximum extension of 100 mm were used.

A.1.4.2 Mechanical properties on "Electrospun asymmetric membranes" (Chapter V)

In order to mimic a real wound environment, asymmetric membranes were soaked in 3 different pH solutions and tested during 3 weeks at 37 ºC: 1st week in 0.1M TRIS solution at pH 8; 2nd week in 0.1M PBS solution at pH 7.4; 3rd week in artificial exudates solutions (AES) at pH 5 (142 mmol of Na^{+} and 2.5 mmol of Ca^{+2}). In this case mechanical properties were evaluated at room temperature with a tensile testing machine (MINIMAT firm-ware v.3.1). Five samples per membrane in dried and wet conditions (soaked during 3 weeks) were cut into 30 mm x 10 mm strips and subjected to a tensile test. A full-scale load of 20 N and maximum extension of 50 mm were used.

A.1.5 Membranes permeability in "Polymeric electrospun membranes for bone morphogenetic protein" (Chapter IV)

To test membranes permeability, pure water was used to determine flux values at different levels of trans-membrane pressure (ΔP^{TM}, mbar). Hydraulic permeance Lp, expressed in units of flux per pressure, $L/m^2\,h\,mbar$, was estimated by applying the following equation [Eq. A.1] in which a linear dependence between water flux (J, L/m^2h) and the convective driving force is expressed:

$$L_p = \left(\frac{J_{Solvent}}{\Delta P^{TM}}\right)_{\Delta C=0} \qquad \text{[Eq. A.1]}$$

A.1.6 Encapsulation efficiency

Encapsulation efficiency (EE) of RFP, CRV and BMP2 was analyzed by different technique.

EE was calculated with the following equation [Eq. A.2]:

$$EE = \frac{Experimental\ amount}{Theoretical\ amount} \times 100 \qquad \text{[Eq. A.2]}$$

The theoretical amount was calculated based on the amount of drug added to the solution.

A.1.6.1 Encapsulation efficiency in "Composite membrane loaded with RFP" (Chapter II)

In samples containing rifampicin (RFP) the EE was evaluated by absorbance measurement at 334 nm using a calibration curve prepared from a RFP standard at 50 ppm in DMF using a microplate reader (Multimode Synergy HT Microplate Reader; Biotek, US). Approximately 10-20 mg of PCL-PLGA-RFP membrane (five replicas were analyzed) was placed in 1 mL of DMF with constant agitation during 3 h at 4 ºC to extract the loaded RFP. RFP calibration curves in DMF was prepared in the range of 0-50 ppm and measured in triplicate.

A.1.6.2 Encapsulation efficiency in "Polymeric electrospun membranes for bone morphogenetic protein" (Chapter IV)

A solvent extraction technique was used to measure the EE of BMP2. Approximately 15 mg of each membrane were dissolved in 1 mL of DCM at 37 °C. After 6 h, BMP2 was extracted by adding 5 mL of DPBS (pH 7.4) and keeping the mixture for 24 h at 37 °C. The resultant emulsion was centrifuged at 150 × g for 10 min. The water phase was carefully collected and kept at -20 °C. The protein amount in collected solutions was measured with the BMP2 Quantikine ELISA Kit (R&D Systems, US). Absorbance of samples was measured at 450 nm on a microplate reader (Multimode Synergy HT Microplate Reader; BioTek, US), and the concentration was determined by interpolation of the absorbance data obtained from the samples on a standard calibration curve (0-2,000 pg/mL) provided by the manufacturer.

A.1.6.3 Encapsulation efficiency in "Electrospun asymmetric membranes" (Chapter V)

In case of CRV gas chromatography mass spectrometry (GC-MS), GCMS-QP2010 SE (Shimadzu, Japan) equipped with an AOC 20i auto-injector was used to determine EE of CRV. Approximately 15-20 mg of each asymmetric membrane was dissolved in DCM/Acetonitrile (1:1) to extract the loaded CRV.

A.1.7 *In vitro* release study and kinetic modeling

A.1.7.1 *In vitro* release study and kinetic modeling of "Composite membrane loaded with RFP" (Chapter II)

The *In vitro* release of RFP from loaded electrospun membranes (15-20 mg) was performed at 37 ºC (Heater Memmert, Germany) in DPBS (1.5 mL; n = 5). At scheduled time intervals (from 1 h to 28 days), all DPBS were harvested and an equal volume of fresh DPBS was added back to the vessels. The collected samples (five replicates per time point) were stored at -20 °C until analysis.

To determine RFP concentration, three aliquots (150 µL) per sample were added to a 96-well plate to measure the absorbance. The RFP calibration curve in DPBS was prepared across the range of 0-50 ppm and measured in triplicate.

A.1.7.2 *In vitro* release study and kinetic modeling of "Polymeric electrospun membranes for bone morphogenetic protein" (Chapter IV)

An *In vitro* release of BMP2 from loaded membranes was carried out at 37 °C in a heater (Memmert, Germany) in DPBS (1.5 mL; n = 5). According to scheduled time intervals (from 30 min to 28 days), all DPBS was collected and replaced with an equal volume of fresh DPBS. The collected samples were stored at -20 °C until analysis and measured BMP2 Quantikine ELISA Kit as described above in section A.1.6.2.

A.1.7.3 *In vitro* release study and kinetic modeling of "Electrospun asymmetric membranes" (Chapter V)

In vitro CRV release from asymmetric membranes was carried out during 7 days in TRIS and AES solutions. On the other hand, in order to mimic real wound healing process, the release was also measured during 3 weeks: 1st week in 0.1 M TRIS solution at pH 8; 2nd week in 0.1 M PBS solution at pH 7.4; 3rd week in AES at pH 5 (142 mmol of Na^+ and 2.5 mmol of Ca^{+2}). According to scheduled time intervals (from 1, 2, 4, 8, 24, 72 and 168 hours), 1 mL of each solution was collected and replaced with equal volume of fresh solutions. The collected samples were stored at -20 ºC until analysis by high-performance liquid chromatography (HPLC) using a Agilent 1100 series chromatography system coupled with a UV-vis multiwavelength detector. The monitoring wavelength was 275 nm. The column used was a Phenomenex Kinetex 2.6 µm XB-C18 100A 100x4.6 mm. The mobile phase was an isocratic combination of acetonitrile (ACN):H_2O (50:50) with a flow rate of 0.4 ml/min. Injection volume for all samples and standard solutions was 25 µl. The carvacrol calibration curve (0-50 ppm) was made with naproxen sodium as internal standard.

A.1.8 Drug release kinetics

Release kinetics from each membranes was evaluated using the Higuchi (2), Korsmeyer-Peppas (3), Peppas-Sahlin (4)and Lindner-Lippold's (5) models. Experimental data were analyzed by a linear and a non-linear least-squares regression. The Higuchi, Korsmeyer-Peppas and Peppas-Sahlin models are valid only for the first 60% of the drug release, while the Lindner-

Lippold's model is valid for the first 80% (4,5). The equations [Eq. A.3-A.6] for these kinetic models were as follows:

Higuchi model: $\frac{M_t}{M_T} = k\, t^{1/2}$ [Eq. A.3]

Korsmeyer-Peppas model: $\frac{M_t}{M_T} = k_{1K}\, t^n$ [Eq. A.4]

Peppas-Sahlin model: $\frac{M_t}{M_T} = k_{1P}\, t^n + k_2\, t^{2n}$ [Eq. A.5]

Lindner-Lippold's model: $\frac{M_t}{M_T} = k_{1L}\, t^n + b$ [Eq. A.6]

Where M_t/M_T is the drug release fraction at time t, k is the Higuchi rate constant, k_{1K}, k_{1L} are kinetic constants incorporating structural and geometric features of the system and the term b describes the burst effect (fast release from surface). In the Peppas and Sahlin model, k_{1P} and k_2 are constants, and the first term on the right hand side represents the Fickian diffusional contribution (F), whereas the second term represents the case-II relaxation contribution (R). The ratio of both contributions can be calculated as follows: $R/F = (k_2/k_1)\, t^n$ (4). In all of them, n is the diffusional exponent that can be related to the drug transport mechanism. For a spherical sample, when n = 0.43, the drug release mechanism follows a Fickian diffusion and when n = 0.85, the case II transport occurs, leading to zero-order release (polymer chains swelling or relaxing). When n value is between 0.43 and 0.85, an anomalous transport is observed (6).

Correlation coefficient (R^2) values obtained were calculated and compared. Besides the coefficient of determination (R^2), the smaller value of sum of the squared residuals (SSR) and the Akaike Information Criterion (AIC) [Eq. A.7] were applied to discriminate the model that best described the drug release mechanism (7).

$AIC = N\,(\ln SSR) + 2p$ [Eq. A.7]

Where N is the number of experimental data points and p is the number of parameters. When comparing several models, the one associated with the smallest value of AIC is given the best fit for the given data set. Additionally, the fit of the predicted curve to the experimental data was also evaluated.

A.1.9 Swelling studies of "Electrospun asymmetric membranes" (Chapter V)

The swelling was measured via gravimetric method by immersing dry membranes with initial weight W_d in a TRIS solution, after 24 h the medium was changed for AES. Membranes were removed from solutions at a prescribed time interval and weighed after wiping the excess water from the surface to get its final weight, W_t. Membranes swelling was calculated using the following equation:

$$Swelling = \frac{W_t - W_d}{W_d} \times 100\% \qquad \text{[Eq. A.8]}$$

Water retention of membranes was calculated as follows:

$$Water\ retention = \frac{W_t - W_d}{W_s - W_d} \times 100\% \qquad \text{[Eq. A.9]}$$

Where W_s is the weight of the membrane removed from TRIS solution, when the swelling equilibrium is reached.

A.1.10 Water vapor transmission of "Electrospun asymmetric membranes" (Chapter V)

The water vapor transmission rate (WVTR) was measured according to ASTM Standard E96/E96M-10 (8). Three different driving forces were imposed to determine the water vapor permeability of the asymmetric membranes. Square pieces of the membrane (2x2 cm) were conditioned at room temperature and relative humidity of 81 % overnight. Then they were mounted on a glass dish with a diameter of 5 cm and placed on a top of a cup with 15 mL of a solution with a specific relative humidity. The device was introduced in a desiccator containing a saturated salt solution (CH_3COOK solution with RH = 28 %) and equipped with a fan to promote air circulation, in order to minimize the mass transfer resistance in the air boundary layer above the membrane. Room temperature and relative humidity (RH) inside the desiccator were monitored using a thermohygrometer HM40 (Vaisala, Finland). The WVTR was determined by measuring the rate of change of mass in regular time intervals for 24 h at three different driving forces of RH: 100 %, 81 % ($(NH_4)_2SO_4$ solution) and 65 % ($NaNO_2$ solution) to 28 % (CH_3COOK solution), following this equation:

$$WVTR\ (^{g}/_{m^2\ h}) = \frac{mass}{t \times area} \qquad \text{[Eq. A.10]}$$

Three independent runs were performed.

A.1.11 Biodegradation studies

The biodegradation percentage was calculated by the following equation [Eq. A.11]:

$$Biodegradation\ (\%) = \frac{M_t - M_i}{M_i} \times 100 \qquad \text{[Eq. A.11]}$$

Where M_i is the initial mass and M_t *is* the dry mass at time t after incubation.

A.1.11.1 Enzymatic degradation in "Polymeric electrospun membranes for bone morphogenetic protein" (Chapter IV)

Enzymatic degradation experiments were carried out at 37 °C in DPBS to mimic biodegradation conditions. Square samples (2.5 × 2.5 × 0.2 mm) of the fabricated membranes were cut out and placed in 6-well culture plates containing 1 mL of DPBS with 0.12 U/mL lipase from *Aspergillus oryzae* or 1 mL of DPBS containing 1300 U/mL human lysozyme, to emulate the enzymatic activities of human serum (9). Every 10 days until 60 days, three membranes per sample and enzyme were withdrawn from the degradation medium. Then, they were dried at 37 °C for 4 h to be weighed. After weighing, the enzymatic solution (1 mL) was refreshed, and the membranes were immersed again until the next weight measurement (every 10 days up to 60 days).

A.1.11.2 Biodegradability in a mimic real wound environment of "Electrospun asymmetric membranes" (Chapter V)

The biodegradability of asymmetric membranes was studied *In vitro* over 3 weeks at 32 ºC. Five samples per membrane were soaked in the 3 different pH solutions (one per week) with the same order described before for the samples in wet conditions. Samples were taken out from the solutions every week, washed with distilled water, freeze-dried and placed in the

solution at different pH. The weight was measured before and after lyophilization.

A.1.12 Bactericidal tests

A.1.12.1 Bactericidal tests in "Composite membrane loaded with RFP" (Chapter II)

To evaluate the antimicrobial efficiency of the fabricated materials, the minimum inhibitory concentration (MIC) and minimum bactericidal concentration (MBC) of the PCL-PLGA-RFP electrospun membranes were determined against *E. coli S17* as a gram negative model, and *S. aureus* as a gram positive infective model.

Antibacterial activities of the RFP-loaded electrospun membranes against *E. coli* and *S. aureus* were studied using ASTM E-2180 ("ASTM E2180 - 18 Standard Test Method for Determining the Activity of Incorporated Antimicrobial Agent(s) In Polymeric or Hydrophobic Materials," n.d.) (10). Briefly, an overnight stationary growth phase of bacteria in TSB was diluted in sterile TSA solution at 40 °C to obtain a starting bacterial concentration of 10^5 colony forming units per milliliter (CFU/mL). The inoculated TSA was placed in a 12-well plate (2 mL per well). The electrospun membranes were sterilized on both sides by UV-irradiation for 1 h and weighed to obtain RFP concentrations ranging from 0.5 to 90 ppm, considering the total amount of RFP loaded in the membranes. Then, these membranes were placed in the 12-well plate on the bacteria-inoculated TSA. After incubation (37 °C, 24 h), the samples were collected in 10 mL of sterile TSB, sonicated in an ultrasonic bath (50 kHz) for 1 min, then vortex-mixed for 1 min to accurately determine the bacterial growth. Subsequently, the samples were serially diluted in PBS and spot-plated on TSA plates (four replicates per sample). Viable bacterial colonies were counted after overnight incubation at 37 °C and compared to those obtained from the control sample (PCL-PLGA electrospun membranes without RFP). Each experiment was performed in triplicate and the results are reported as mean ± S.D.

A.1.12.2 Bactericidal tests in "Asymmetric membranes loaded with CRV" (Chapter V)

Asymmetric membranes antibacterial activity loaded with CRV against *E. coli* and *S. aureus* was studied using the Antimicrobial Disk Susceptibility

Tests of the US Clinical and Laboratory Standards Institute (CLSI) (11). Briefly, TSA plates were inoculated with 0.2 mL of a bacterial suspension containing 10^7 CFU/mL. Membrane discs (14 mm diameter) were placed on the top of the agar plate (with the PVAc-CRV layer in contact with the agar) and incubated at 37 °C for 24 h. After incubation, agar discs (10 mm in diameter) were obtained from the inhibition zone, cut and aseptically placed in a tube with TSB These tubes were sonicated 1 min and stirred 1 min to assure the bacteria release. Then, bacterial suspensions were diluted in PBS, plated on TSA and viable colonies counted after incubation (37 ºC, 24 h). Control samples (untreated bacteria) were also run. Each experiment was done in triplicate and the results are reported as mean ± S.D.

A.1.13 Cell attachment, morphology, viability, and immunohistochemistry

A.1.13.1 Cell culture on "Composite membrane loaded with RFP" (Chapter II)

Electrospun membranes (15 mm diameter, surface area 1.54 cm^2) were sterilized on both sides by UV-irradiation for 1 h and successively soaked with an OGM culture medium for 1 h to avoid floating. HOBs were grown in the OGM culture medium in a 5% CO_2 atmosphere at 37 °C. The culture medium was removed and 10 µL of cell suspension (3.2 x 10^6 cells/mL) was seeded on the top region of the membranes. To promote cell adhesion to the membrane, the samples were incubated for 1 h (5% CO_2, 37 °C) followed by addition of 500 µL of OGM. The seeded membranes were cultured for 3, 7, 14, and 28 days, renewing the culture medium every 2-3 days. In addition, 2D cultures (HOBs seeded on 24-well plates) were also run as cell growth and proliferation control samples.

A.1.13.2 Cell morphology on "Composite membrane loaded with RFP" (Chapter II)

SEM was used to observe the morphology of the attached cells to the electrospun membranes. At the time points indicated above, the seeded membranes were washed with DPBS and fixed in a 4% paraformaldehyde solution (Affymetrix, US) for 30 min at room temperature. After fixation, the samples were washed with DPBS and distilled water, air-dried, and sputter-

coated with a thin platinum layer prior to visualization by SEM (Field Emission Scanning Electron Microscope CSEM-FEG INSPECT 50, FEI, US).

A.1.13.3 Confocal analysis on "Composite membrane loaded with RFP" (Chapter II)

Confocal analysis was performed to observe the cytoskeleton protein distribution of actin (Alexa Fluor™ 546 Phalloidin; Molecular Probes, US) after 3, 7, 14, and 28 days of cell culture. Seeded membranes were rinsed with DPBS and fixed with 4% paraformaldehyde solution for 15 min. Then, samples were permeabilized in ice-cold acetone (-20 °C, 5 min), air-dried, and rinsed with DPBS. Triton X-100 (0.5%) was added to the samples for blocking (30 min) with 5% normal donkey serum (NDS; Jackson ImmunoResearch Europe Ltd, UK). After blocking, actin staining (1:200; Alexa Fluor™ 546 Phalloidin; Molecular Probes, US) was performed for 30 min at room temperature. The membranes were then washed with DPBS and incubated with 8 µM anthraquinone dye (DRAQ5; eBiocence, US) for 30 min at room temperature to stain the cellular nuclei. Finally, samples were washed, mounted, and visualized under a confocal laser scanning microscope (Leica TCS SP2, Leica, Germany).

A.1.13.4 *In vitro* cytotoxicity studies of "Composite membrane loaded with RFP" (Chapter II)

The cytotoxicity of the seeded electrospun membranes with and without RFP was determined by the 3-(3,4-dimethylthiazol-2-yl)-2,5-diphenyltetrazoliumbromide (MTT) test at the time points described above (3-28 days) (12). In brief, an MTT solution (5 mg/mL in DPBS) was diluted in OGM (final concentration 0.5 mg/mL), added to the seeded membranes at the time points described above, and incubated for 4 h at 37 °C and 5% CO_2. The cell medium was discarded and the insoluble formazan crystals obtained were dissolved by addition of SDS (sodium dodecyl sulfate; Bio-Rad, US) solution (100 mg/mL in DMSO and 0.6% of acetic acid). Aliquots (100 µL) were transferred to a 96-well plate and the absorbance was read at 570 nm in a Synergy HT microplate reader (Biotek, US). Results were expressed as mean ± SD of the total absorbance of the samples analyzed in triplicate.

A.1.13.5 Cell culture on "Laser-treated electrospun fibers loaded with nano-hydroxyapatite" (Chapter III)

Electrospun membranes were fixed in CellCrown™, sterilized by UV-irradiation for 30 min on both sides and rinsed overnight with OGM. Normal human osteoblasts (NHOst, Lonza, Belgium) were grown in OGM culture medium, supplemented with 10% FBS, ascorbic acid and 5% solution of gentamicin and amphotericin-B (OGM BulletKit, Lonza, USA) as the manufacturer indicates in an atmosphere containing 5 % CO_2 at 37 °C. Electrospun membranes fixed in CellCrown™ were incubated for 12-18 h in OGM. Then, culture medium was removed and NHOst at passages between 5 and 6 were seeded on the membranes at a density of 3.2×10^6 cells/mL suspended in 10 µL of medium on the membranes center. Samples were incubated for 1 h and then more OGM was added to each well. Next, the cells were cultured up to 2, 7 and 14 days, renewing the culture medium every 2 days.

A.1.13.6 Cell viability of "Laser-treated electrospun fibers loaded with nano-hydroxyapatite" (Chapter III)

A Live/Dead® Viability/Cytotoxicity Kit *for mammalian cells* (Molecular Probes, UK) was used to determine cell viability after 48 h, 7 and 14 days of cultivation, according to the manufacturer's protocol. Calcein-AM was used as a marker of esterase activity in living cells, EthD-1 penetrates into dead cells through their damaged membrane and produces red fluorescence and cellular nuclei were stained with an anthraquinone dye (DRAQ5TM). The membranes were washed with DPBS five times for five minutes every time and incubated in 0.5 mL of Live/Dead® working solution and 8 µM of DRAQ5. Staining was performed under dark conditions for 30 min at room temperature. Imaging the sample surfaces and cellular morphology were obtained on a confocal laser scanning microscope (Leica TCS SP2).

A.1.13.7 Image processing for cell viability quantification on "Laser-treated electrospun fibers loaded with nano-hydroxyapatite" (Chapter III)

Image J software (Version 1.48f, NIH, US) was used to quantify the viability of NHOst seeded onto the different membranes described above.

Confocal images were analyzed through a step-by-step procedure on the green channel as it recorded the live cells, setting up the scale and the threshold in this channel. Cell viability was determined by the ratio of green pixel area to the total area of pixels. Five different regions of each sample were evaluated and the maximum projection of at least 60 planes per region was quantified (total area analyzed per region ≈ 0.14 cm^2). Semiautomatic measurement was developed to calculate the percentage of the covered area by live cells stained with calcein.

A.1.13.8 Cell morphology on "Laser-treated electrospun fibers loaded with nano-hydroxyapatite" (Chapter III)

SEM was performed to observe cell morphology and attachment on electrospun membranes. After 48 h, 7 and 14 days of cultivation samples were washed with DPBS, fixed in a 4% paraformaldehyde solution at room temperature for 30 min. The samples were sputter-coated with platinum and characterized by SEM microscopy (Field Emission Scanning Electron Microscope CSEM-FEG INSPECT 50, FEI, USA).

A.1.13.9 Cell culture on "Polymeric electrospun membranes for bone morphogenetic protein" (Chapter IV)

Human osteoblasts were grown in the OGM culture medium in a 5 % CO_2 atmosphere at 37 °C. Electrospun membranes of 15 mm diameter were placed in CellCrown™ inserts and sterilised on both sides by ultraviolet (UV) irradiation for 60 min. After that, the membranes were placed into 24-well plates to be successively conditioned with the OGM culture medium for 1 h to soak them and avoid floating. Next, the culture medium was removed, and cells at passage 6 (3.2×10^6 cells/mL) were resuspended in 10 µL of the medium and were seeded onto the middle top region of the membranes (surface area 1.54 cm^2). Samples were incubated for 1 h (5 % CO_2, 37 °C) to facilitate cell adhesion to the membrane and then, 500 µL of OGM were added into each well for subsequent growth and proliferation. The seeded membranes were cultured for 1, 2, 3, or 4 weeks, and the culture medium was refreshed every 2-3 days.

A.1.13.10 Cell viability of "Polymeric electrospun membranes for bone morphogenetic protein" (Chapter IV)

Cell viability was determined by examination of the cultured membranes in a 3-(3,4-dimethylthiazol-2-yl)-2,5-diphenyltetrazolium bromide (MTT) assay (12). Briefly, an MTT solution (5 mg/mL in DPBS) was diluted in OGM to a final concentration of 0.5 mg/mL and added to the seeded membranes at the time points described above. After incubation for 4 h (37 °C, 5% CO_2), the cell medium was discarded and an SDS (Sodium Dodecyl Sulfate; Bio-Rad, US) solution (100 mg/mL in 0.6 % acetic acid in DMSO) was added to the samples to dissolve the insoluble formazan obtained. Aliquots (100 µL) of each sample were transferred to 96-well plates in triplicate, and absorbance was recorded at 570 nm on a Synergy HT microplate reader (BioTek, US). The results were expressed as total absorbance of the samples.

A.1.13.11 Cell morphology on "Polymeric electrospun membranes for bone morphogenetic protein" (Chapter IV)

The morphology of the cells attached to the membranes at the time points indicated above was visualized under an SEM (Field Emission Scanning Electron Microscope CSEM-FEG INSPECT 50, FEI, US). HOBs that were seeded onto the membranes, as described in the previous section, and were incubated for 1, 2, 3, or 4 weeks, were washed with DPBS and fixed in a 4% paraformaldehyde solution (Affymetrix, US) for 15 min. Then, the fixed samples were washed with DPBS, dried, and sputter-coated with a thin platinum layer prior to visualization under the SEM.

A.1.13.12 Alkaline phosphatase assay in "Polymeric electrospun membranes for bone morphogenetic protein" (Chapter IV)

ALP concentration was determined to elucidate the potential of the seeded cells for bone turnover and mineralization, as previously described (13), by means of the SensoLyte® pNPP Alkaline Phosphatase Assay Kit (Anaspec, US). At different time points (1–4 weeks), membranes with and without (control samples) seeded cells were washed with assay buffer, rinsed with a Triton X-100 solution and scraped to release the enzyme through cell membrane leakage. Finally, the membranes were discarded, and the samples were collected to be next stirred (250 rpm, 10 min, 4 °C) and

centrifuged (10,000 × *g*, 10 min, 4 °C). Then, the supernatants were collected, and aliquots (100 µL) were transferred to 96-well plates in triplicate. The absorbance of the samples was measured at 570 nm on the Synergy HT microplate reader (Biotek, US). The results were expressed as total absorbance of the samples.

A.1.13.13 Immunohistochemistry in "Polymeric electrospun membranes for bone morphogenetic protein" (Chapter IV)

The expression of specific osteogenic markers, such as OCN (anti-osteocalcin antibody [G-5] conjugated with Alexa Fluor® 488, Santa Cruz Biotechnology, US) and OPN (anti-OPN antibody [AKm2A1] conjugated with Alexa Fluor® 647, Santa Cruz Biotechnology, US), together with the evaluation of the cytoskeleton protein distribution and actin (Alexa Fluor™ 546–conjugated phalloidin, Molecular Probes, US) in HOBs seeded onto the different types of membranes, was analyzed by immunohistochemistry.

Seeded membranes at an early (2 weeks) and at a later (4 weeks) time point were rinsed with DPBS and fixed with a 4 % paraformaldehyde solution (Affymetrix, US) for 15 min. After that, paraformaldehyde was discarded, and the samples were permeabilized by incubation in ice-cold acetone (-20 °C, 5 min). Then, acetone was discarded and the membranes were air-dried and rinsed with DPBS. Triton X-100 (0.5 %) was then added to the samples for blocking (30 min) with 5 % normal donkey serum (Jackson ImmunoResearch Europe Ltd., UK). After incubation, anti-OCN (G-5) Alexa Fluor® 488 (1:100) and anti-OPN (AKm2A1) Alexa Fluor® 647 (1:200) mouse monoclonal conjugated antibodies (Santa Cruz Biotechnology, US) diluted in 2.5 % normal donkey serum in DPBS were added to the membranes and incubated overnight at 4 °C. Subsequent actin staining (1:200; Alexa Fluor™ 546-conjugated phalloidin) was developed for 30 min at room temperature. Finally, the samples were washed, mounted, and observed by confocal laser scanning microscopy (Leica TCS SP2, Leica, Germany).

A.1.13.14 *In vitro* cytotoxicity studies of "Electrospun asymmetric membranes" (Chapter V)

HDFs were used for the cell viability experiments as cell line model for wound healing. Both 2D and 3D experiments were developed to address cytocompatibility of the target cells for the clinical application.

2D cell viability studies were developed by seeding cells in 24-well plates at a density of 6×10^4 cells/mL and asymmetric membranes previously sterilized with UV were then added to the cell cultures for 1, 2, 3 and 7 days at 37 ºC in a 5 % CO_2 atmosphere in high glucose DMEM supplemented with 10 % v/v FBS and 1% antibiotic-antimycotic. Cytotoxicity of CRV released from asymmetric membranes loaded with and without (control sample) CRV was determined by the 3-(3,4-dimethylthiazol-2-yl)-2,5-diphenyltetrazoliumbromide (MTT) test, as previously described (12). In brief, MTT solution in supplemented medium (0.5 mg/mL) was added to the cells at the time points previously specified. Cells were further incubated (4 h; 37 ºC, 5 % CO_2) and then, the cell medium was discarded to add SDS solution (100 mg/mL in a 0.6 % acetic acid in DMSO) to solubilize the insoluble formazan yielded. Finally, absorbance was recorded in triplicate at 570 nm in a Synergy HT microplate reader (Biotek, US). Results were expressed as viability percentage of the samples related to the control sample (PCL/PVAc not loaded with CRV; 100 % viability).

A.1.13.15 Cell morphology and confocal analysis on "Electrospun asymmetric membranes" (Chapter V)

3D cell morphology and cytocompatibility assays were developed by seeding HDFs onto the asymmetric membrane in contact with the PVAc-CRV layer. First, sterilized membranes were conditioned with DMEM for 1 h to soak them and avoid floating. Then, the culture medium was removed and cells were seeded onto the middle region of the PVAc-CRV layer of the membranes at a density of $6x\ 10^4$ cells/mL in a volume of 20 µL of supplemented culture medium. Samples were incubated for 1 h (5 % CO_2, 37 ºC) to promote cell adhesion to the membrane and then 500 µL of supplemented DMEM were added to each well to enable cell proliferation. Culture medium was renewed every 2 days in all samples. After 3 days, membranes were washed with DPBS, fixed in a 4 % paraformaldehyde solution in PBS (Affymetrix, US) at room temperature for 30 min. The samples were sputter-coated with platinum and characterized by SEM. Confocal analysis of 3D cell cultures was also achieved to observe the expression of cytoskeleton protein F-actin (Alexa Fluor™ 546 Phalloidin; Molecular Probes, US) after 3 days of cell culture onto the membranes in order to further evaluate cell proliferation and cytocompatibility of the membranes. Cells were fixed with 4% paraformaldehyde solution (Affymetrix, US) for 15 min and permeabilized with 0.5 % Triton X-100 for

30 min, to be then blocked (30 min) with 5 % normal donkey serum (NDS; Jackson ImmunoResearch Europe Ltd, UK). After blocking, the membranes were incubated with Alexa Fluor™ 546 Phalloidin (1:200; Molecular Probes, US) for 30 min at room temperature and then washed three times in DPBS and incubated with 8 µM anthraquinone dye (DRAQ5; eBioscience, US) for 30 min at room temperature for nuclei staining. Finally, stained membranes were washed three times in DPBS and milli-Q water to be then mounted on glass slides and examined under confocal microscopy (Leica TCS SP2, Germany).

A.1.14 Cell scratch model on "Electrospun asymmetric membranes" (Chapter V)

HDFs were seeded in 24-well plates at 1.2×10^5 cells/mL and grown until a confluence. Then, cells were washed with DPBS and a manual scratch of 1 mm wide straight-line was made with a 1000 µL sterile pipette tip to emulate a wound. Cells were washed again with DPBS in order to remove cell debris and added fresh DMEM. Membranes were then added to the cultures to evaluate the effect of released CRV from Sample I and Sample II on cell migration. Control samples (not treated) were also run to compare cell migration. Scratch closure was qualitative analyzed under an Olympus motorized inverted research microscope model IX81, Japan, by acquiring images at time 0 (immediately after scratching) and after 1, 2 and 3 days in culture.

A.1.15 Statistical analysis

All the data are reported as mean ± standard deviation (SD). For fiber and particle diameter at least n = 100 were studied. Measurements of porosity, mechanical properties and swelling study were made by quintuplicate (n = 5). Water vapor transmission rate, biodegradations studies, permeability, antibacterial activity, encapsulation efficiency and *In vitro* release of RFP, BMP2, and CRV were measured in triplicate and quintuplicate according to the specific case. For confocal analysis, more than 50 planes per region and three regions per sample were evaluated. MTT and ALP determinations were performed in triplicate and three measurements were performed per experiment (9 sets of data). Statistical analysis of data was performed using the Student-Newman-Keuls t-test and ANOVA or U-Mann-Whitney analysis (Statgraphics® Centurion XV statistical software,

StatPoint Technologies, Inc., US). Statistically significant differences were considered when $p \leq 0.05$.

References

1. Kokubo T, Takadama H. How useful is SBF in predicting *in vivo* bone bioactivity? Biomaterials. 2006;27(15):2907–15.

2. Higuchi T. Mechanism of sustained-action medication. Theoretical analysis of rate of release of solid drugs dispersed in solid matrices. J Pharm Sci. Wiley-Blackwell; 1963 Dec;52(12):1145–9.

3. Korsmeyer RW, Gurny R, Doelker E, Buri P, Peppas NA. Mechanisms of solute release from porous hydrophilic polymers. Int J Pharm. Elsevier; 1983 May;15(1):25–35.

4. Peppas NA, Sahlin JJ. A simple equation for the description of solute release. III. Coupling of diffusion and relaxation. Int J Pharm. Elsevier; 1989 Dec;57(2):169–72.

5. Lindner WD, Lippold BC. Drug release from hydrocolloid embeddings with high or low susceptibility to hydrodynamic stress. Pharm Res. 1995 Nov;12(11):1781–5.

6. Ritger PL, Peppas NA. A simple equation for description of solute release II. Fickian and anomalous release from swellable devices. J Control Release. Elsevier; 1987 Jun;5(1):37–42.

7. Yamaoka K, Nakagawa T, Uno T. Application of Akaike's information criterion (AIC) in the evaluation of linear pharmacokinetic equations. J Pharmacokinet Biopharm. Kluwer Academic Publishers-Plenum Publishers; 1978 Apr;6(2):165–75.

8. ASTM E96 / E96M-16, Standard Test Methods for Water Vapor Transmission of Materials. ASTM International. West Conshohocken, PA; 2016.

9. Azevedo H, Reis RL. Understanding the Enzymatic Degradation of Biodegradable Polymers and Strategies to Control Their Degradation Rate. In: Biodegradable Systems in Tissue Engineering and Regenerative Medicine. 2005.

10. ASTM E2180-18, Standard Test Method for Determining the Activity of Incorporated Antimicrobial Agent(s) In Polymeric or Hydrophobic

Materials. ASTM International. 2018.

11. Bauer AW, Kirby WMM, Sherris JC, Turck M. ANTIBIOTIC SUSCEPTIBILITY TESTING BY A STANDARDIZED SINGLE DISK METHOD. Am J Clin Pathol. 1966;45(4):493–6.

12. Morelli S, Piscioneri A, Salerno S, Al-Fageeh MB, Drioli E, De Bartolo L. Neuroprotective effect of didymin on hydrogen peroxide-induced injury in the neuronal membrane system. Cells Tissues Organs. 2014;199:184–200.

13. Halling Linder C, Ek-Rylander B, Krumpel M, Norgård M, Narisawa S, Millán JL, et al. Bone Alkaline Phosphatase and Tartrate-Resistant Acid Phosphatase: Potential Co-regulators of Bone Mineralization. Calcif Tissue Int. Springer US; 2017 Jul;101(1):92–101.

APPENDIX 2

Articles published and participation in scientific forums

Publications

- Electrospun asymmetric membranes for wound dressing applications. Javier Aragón, Clarinda Costa, Isabel Coelhoso, Gracia Mendoza, Ana Aguiar-Ricardo and Silvia Irusta. Materials Science and Engineering C. **Submitted work (under review, MSEC_2018_3013).**

- Composite scaffold obtained by electro-hydrodynamic technique for infection prevention and treatment in bone repair. Javier Aragón, Sergio Feoli, Silvia Irusta, Gracia Mendoza. International Journal of Pharmaceutics. **Accepted work, 2018**.

- Polymeric electrospun scaffolds for bone morphogenetic protein 2 delivery in bone tissue engineering. Javier Aragón; Simona Salerno, Loredana De Bartolo, Silvia Irusta and Gracia Mendoza. Journal of Colloid and Interface Science, 531 (2018) 126–137. DOI:10.1016/j.jcis.2018.07.029.

- Synthesis of a Novel Electrospun Polycaprolactone Scaffold Functionalized with Ibuprofen for Periodontal Regeneration: An *In vitro* and *In vivo* Study. Fareeha Batool, David-Nicolas Morand, Lionel Thomas, Isaac Maximiliano Bugueno, Javier Aragon, Silvia Irusta, Laetitia Keller, Nadia Benkirane-Jessel, Henri Tenenbaum and Olivier Huck. Materials 11, 580, 2018. DOI:10.3390/ma11040580.

- Production, characterization and testing of antibacterial PVA membranes loaded with HA-Ag3PO4 nanoparticles, produced by SC-CO2 phase inversion. Lucia Baldino, Javier Aragon, Gracia Mendoza, Silvia Irusta, Stefano Cardea, Ernesto Reverchon1. Journal of Chemical Technology & Biotechnology. 2018. DOI:10.1002/jctb.5749.

- Laser-treated electrospun fibers loaded with nano-hydroxyapatite for bone

tissue engineering. Javier Aragon, Nuria Navascues, Gracia Mendoza, Silvia Irusta. International Journal of Pharmaceutics 525,112–122, 2017. DOI:10.1016/j.ijpharm.2017.04.022.

- Integration and bioactivity of hydroxyapatite grown on carbon nanotubes and graphene oxide. J. David Núñez, Ana M. Benito, Ramón González, Javier Aragón, Raul Arenal, Wolfgang K. Maser. CARBON, Vol. 79: 590-604, 2014. DOI: 10.1016/j.carbon.2014.08.020.

Presentations at scientific meetings

- 2017. 2nd International Caparica Christmas Congress on Translational Chemistry. Multilayer membrane obtained by electrospinning technique for wound dressing applications.

- 2017. 4th Congress University Nova de Lisboa-University of Yamaguchi-Univesity of Zaragoza: "Engineering at the service of our society: From nanotechnology to megastructures". Polymeric electrospun membrane for tissue engineering applications.

- 2017. 28th European Conference on Biomaterials, Athens, Greece, 4th – 8th September 2017. POLYMERIC NANOFIBROUS MEMBRANES OBTAINED BY ELECTROSPINNING FOR BIOMEDICAL APPLICATIONS

- 2014. XXXII Annual Congress of the Spanish Society of Biomedical Engineering (CASEIB 2014). Core-shell fibers of biocompatible polymers loaded with Hydroxyapatite and Ibuprofen.

- 2014. 6 th Journey of young researchers of Aragon. Development of fibers with biomedical applications by electrospinning technology.

Postgraduate courses

2015. International training school on advanced characterization techniques for electrospun nanofibers: hands -on experience. Ankara, Turkey.